The palladium-catalysed aerobic oxidative homocoupling reaction of arylboronic acids in aqueous micellar medium

kinetic and mechanistic studies

MAZIN A. OTHMAN

A thesis submitted for Degree of Doctor of Philosophy

School of Chemistry

Cardiff University

CARDIFF
UNIVERSITY

PRIFYSGOL
CAERDYⱭD

May 2011

DECLARATION

This work has not previously been accepted in substance for any degree and is not concurrently submitted in candidature for any degree.

Signed .... (candidate)   Date ...27/05/2011...

STATEMENT 1

This thesis is being submitted in partial fulfillment of the requirements for the degree of PhD

Signed .... (candidate)   Date ...27/05/2011...

STATEMENT 2
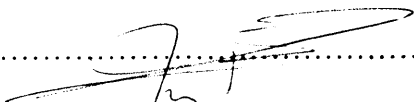
This thesis is the result of my own independent work/investigation, except where otherwise stated.
Other sources are acknowledged by explicit references.

Signed .... (candidate)   Date ...27/05/2011...

STATEMENT 3

I hereby give consent for my thesis, if accepted, to be available for photocopying and for inter-library loan, and for the title and summary to be made available to outside organisations.

Signed .... (candidate)   Date ...27/05/2011...

Acknowledgements

Summary

This thesis is divided into five Chapters.

The *first* Chapter introduces water and micellar solutions as reaction medium, catalysis, palladium catalysts, the Suzuki cross-coupling and the oxidative homocoupling of arylboronic acids.

The *second* Chapter describes studies of the aerobic oxidative homocoupling reaction of arylboronic acids in aqueous micellar media using Pd(bimsulfide)Cl$_2$ as a (pre) catalyst. Our results, in particular a bell-shaped pH-rate profile, favour a reaction mechanism where the rate-determining step is transmetalation involving a palladium-hydroxo complex and the acidic form of the arylboronic acid, although an alternative mechanism involving a palladium-aqua complex reacting with the arylboronate cannot be excluded.

The *third* Chapter presents the synthesis of Pd^0-CTAB nanoparticles and their use as catalysts for the aerobic oxidative homocoupling of phenylboronic acid in aqueous micellar solutions. Again, a bell-shaped pH dependence of observed rate constant (k_{obs}) was observed which, together with our other results, suggests that the reaction again involves pH-dependent Pd-hydroxo and Pd-aqua species. We cannot confirm whether catalysis occurs on the surface of the nanoparticles or through leached Pd atoms/ions.

The *fourth* Chapter embraces bimetallic core-shell Au-Pd nanoparticles encapsulated in a shell of poly(*N*-isopropylacrylamide) (pNIPAM) of different sizes and morphologies, as well as Pd-pNIPAM nanocomposites. Both systems were used to catalyse the aerobic oxidative homocoupling reaction of PBA in aqueous micellar medium. Our kinetic studies gave similar results as observed for the Pd-complex described in Chapter 2 and the nanoparticles described in Chapter 3. Hence, an analogous mechanism was proposed. The observed rate constant

showed non-Eyring-like behaviour, highlighting the dependence of k_{obs} on the state (swollen or collapsed) of the pNIPAM shell surrounding the nanoparticles.

Finally, the *fifth* Chapter describes preliminary studies exploring aerobic oxidative cross-coupling reactions of arylboronic acids and their derivatives in aqueous micellar solutions. Conclusions, future outlooks, remarks and suggestions finish Chapter 5 and the thesis.

List of abbreviations and symbols

ArBA	Arylboronic acid
PBA	Phenylboronic acid
CTAB	Cetyltrimethylammonium bromide
SDS	Sodium dodecylsulfate
cmc	critical micelle concentration
NPs	Nanoparticles
Ncomp	Nanocomposite
NIPAM	N-isopropylacrylamide
pNIPAM	poly(N-isopropylacrylamide)
BIS	N,N'-methylenebisacrylamide
AAPH	2,2`-azobis(2-methylpropionamidine) dihydrochloride
PVP	poly(N-vinyl-2-pyrrolidone)
SPB	Spherical polyelectrolyte brushes
LCST	Lower critical solution temperature
k_{obs}	Observed rate constant
$k_{obs(max)}$	Maximum observed rate constant
K_a	Acid dissociation constant
pK_a	$-\log K_a$
pH	$-\log [H^+]$
pH_{opt}	Optimum pH
k_a	Second order rate constant for the reaction of acidic catalyst with basic

ArBA

k_b Second order rate constant for the reaction of basic catalyst with acidic

ArBA

UV-Vis NIR Ultra Violet – Visible - Near Infra Red

ε extinction coefficient (or Molar absorptivity)

A Absorbance

λ Wavelength

HPLC High-performance (pressure) liquid chromatography

t Time

TEM Transmission electron microscopy

DLS Dynamic light scattering

PCS Photon correlation spectroscopy

T Temperature

σ (Hammett) substituent constant

ρ (Hammett) reaction constant

nm Nanometer

M Molar

mM Milimolar

μM Micromolar

L Liter

mL Milliliter

μL Microliter

°C	Degree Celsius
K	Kelvin
fcc	face-centred-cubic
SAED	Selected area electron diffraction
XRD	X-ray diffraction
NMR	Nuclear Magnetic Resonance
PEG	polyethylene glycol
Te-Dps	DNA binding protein from starved cells of a thermophilic bacterium "*Thermosynechoccus elongatus*"
K_m	Micellar pseudophase equilibrium constant
K_c	Equilibrium constant for the collapse-swelling process
PIE	Pseudophase Ion Exchange
T_c	Collapse temperature
a.u.	arbitrary units
PEPPSI-iPr	Pyridine-Enhanced Precatalyst Preparation, Stabilisation and Initiation-isoPropyl

Contents

Chapter 1

General introduction

Chapter 2

Homocoupling of arylboronic acids using molecular Pd-catalyst in aqueous micellar media (kinetic and mechanistic studies)

Chapter 3

Homocoupling or phenylboronic acid using Pd-CTAB NPs

Chapter 4

Homocoupling of phenylboronic acid using Au@Pd@pNIPAM nanoparticles and Pd-pNIPAM nanocomposites

Chapter 5

Epilogue

Exploring the possibility of aerobic oxidative cross-coupling reactions of arylboronic acids and their derivatives

Outlook and challenges for the future mechanistic studies of aqueous (cross) coupling reactions

Chapter 1

General introduction

1. General introduction

1.1. Water, "the Unique Reaction Medium"

Water plays a pivotal role in life processes on our planet. It has been called the "molecule of life", the "matrix of life", and "life's natural habitat", as one cannot imagine life in the absence of water or take away any of water's features without destroying life "as we know it".[1] Water as a molecule has no peculiar properties apart from being very small and polar. Nevertheless, liquid water, which has the ability to form strong three-dimensional (3-D) hydrogen bond (H-bond) networks, has an enormous number of anomalous properties *e.g.* high melting and boiling points, the floating of ice on water, the temperature of highest density at 4 °C, the relatively high specific heat capacity, and the high proton and hydroxide mobilities.[2,3]

The hydrogen bonds in water are highly dynamic, they exchange on a time scale of few picoseconds and these dynamics have been described beautifully by Phil Ball as the "dance of water molecules".[4] Water is amphoteric: it can act as a Brønsted acid and base through donating or accepting protons, it can also act as Lewis a acid and base through the lone pair of electrons on its oxygen atom or through its ability to form hydrogen bonds with electron donors. Water can adapt its H-bond structure to the presence of a solute, either polar or apolar.[2]

Water is a preferable solvent to be used for reactions, because of its characteristic behaviour as a liquid, and because it is the cheapest, most abundant solvent available, while it is also non-toxic and nonflammable.[2] Furthermore, additives such as salts, surfactants and cyclodextrins can be added, the pH can be varied, and cosolvents or biphasic reaction systems can be utilised.[5]

Despite the fact that water has unique properties, it has not conventionally been the solvent of choice in which to perform organic reactions. One reason has been the very limited solubility of typical organic molecules in water. In addition, organic synthesis strategies often involve the use of water-sensitive reagents, catalysts, or intermediates. Also, problems can be encountered in isolating water soluble products.[2, 5]

In the last few decades, an increase and diversification of the use of aqueous reaction media for organic reactions have occurred, regardless of whether reactants are soluble in water or not. For example, Michael additions, pericyclic reactions, and organometallic reactions have all been carried out in water and, in some cases, water has increased the rate and the selectivity of the reaction.[2, 6-9] For instance, Breslow and co-workers demonstrated an increase in the rate for a Diels-Alder reaction "in water",[10, 11] while Sharpless and co-workers have shown substantial increases in the reaction rate when the reactants are not soluble in the aqueous phase, describing their reactions as occurring "on water".[12] Moreover, there are several examples of reactions "in the presence of water" *e.g.* catalytic asymmetric aldol reactions, in which the presence of water has been reported to increase the reactivity and stereoselectivity.[13-15]

As there is confusion about the terminology "in water" and "in the presence of water", Yujiro Hayashi[16] has proposed to define a reaction "in water" as one in which the reactants are dissolved homogenously in water (or buffer, for controlling pH), whereas a reaction "in the presence of water" is one in which reactants are dissolved in an organic phase with water being a secondary phase (or dissolved water in the organic phase) that influences the reaction in the organic phase. Sharpless' "on water" reactions are then covered by the more broad terminology of reactions "in the presence of water".[12]

Generally, calling organic reactions performed in water either "green" or "environmentally friendly" is not always correct, as the workup of the products of some reactions from the aqueous phase requires significant amounts of organic solvents. Thus, not only the reaction medium describes the "greenness" of a reaction, but the workup also must be taken into consideration.[17]

1.2. Micelles

Micelles are aggregates of surfactant molecules dispersed in a liquid solvent. A surfactant "monomer" consists of a hydrophilic (ionic or non-ionic) headgroup and a long chain or hydrophobic hydrocarbon tail. Micelles only form when the concentration of surfactant is greater than the critical micelle concentration (cmc), and the temperature of the system is greater than the so-called "Krafft temperature" (also called the critical micelle temperature, where the solubility of the surfactant becomes equal to the cmc, or "Krafft point"). Surfactant monomers can aggregate to form different morphologies including spherical micelles, wormlike micelles, bilayers, vesicles and inverted micelles.[18] Scheme 1.1, shows some typical examples of micelle-forming surfactants.

$$—(CH_2)_{15}—N^{\oplus}— \qquad Br^{\ominus}$$

Cetyltrimethylammomium bromide
CTAB

$$—(CH_2)_{11}—O—\overset{\overset{O}{\|}}{\underset{\underset{O}{\|}}{S}}—O^{\ominus}\ Na^{\oplus}$$

Sodium dodecyl sulfate
SDS

$$—(CH_2)_{11}—(OCH_2CH_2)_8—OH$$

Octaethylene glycol monododecyl ether
$C_{12}E_7$

$$—(CH_2)_{10}—(CONH)—(CH_2)_2—N^{\oplus}—$$

Cocamidopropyl betaine
CAPB
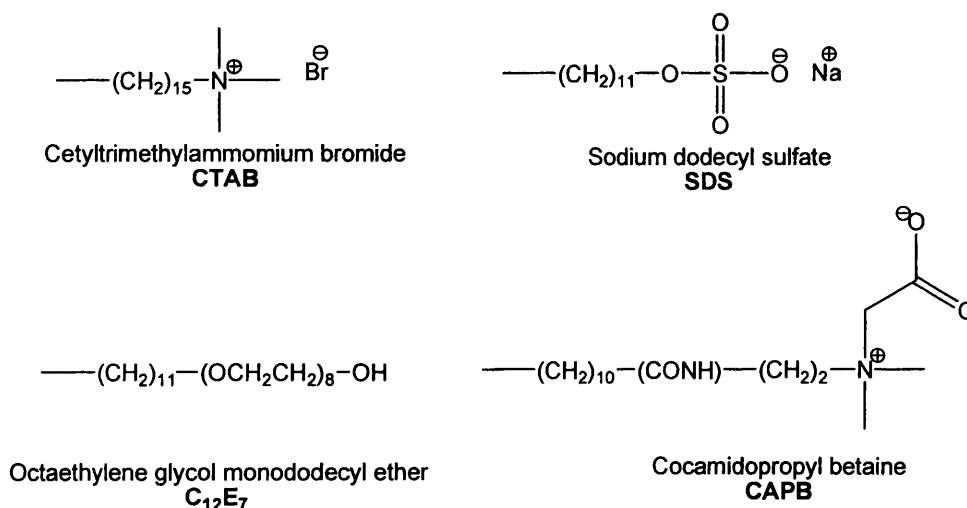
Scheme 1.1 Typical examples of micelle-forming surfactants

Ninham and Israelachvili[19] have developed a dimensionless packing parameter P (equation 1.1) to describe the morphology of different micelles, depending on the shape of surfactants.

$$P = \frac{V}{a_o.l_c}$$ (1.1)

Where V is the volume of the hydrocarbon chain(s) of the surfactant, a_o the mean cross-sectional (effective) headgroup surface area and l_c is the length of the hydrocarbon tail in the all-trans configuration. Surfactants with $P<1/3$ are cone-shaped and form spherical micelles. For $1/3<P<1/2$, surfactants are truncated-cone-shaped resulting in wormlike micelles.[20]

For spherical micelles the interface between the dry hydrophobic hydrocarbon core of the micelle and bulk water contains the hydrophilic headgroups, part of the counter ions and water. This interfacial region is typically called the "Stern region" (Figure 1.1).[21, 22] Micelles can provide several binding sites for apolar molecules. These include the hydrophobic core and rather flexible (in terms of the balance between hydrophobicity and polarity) binding sites located in the Stern region.[22, 23]
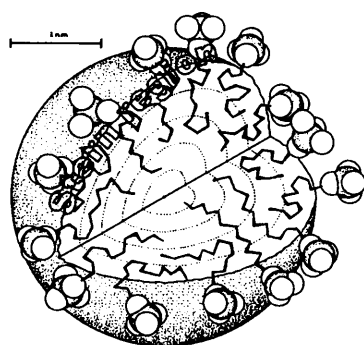
Figure 1.1 Picture of a micelle (taken from ref[10])

Furthermore, micelles are highly dynamic structures. For example the typical lifetime of a micelle is 10^{-3}-10^{-2} seconds, whereas individual surfactant molecules exchange on a 10^{-6}-

10^{-5} seconds time scale.[18] In addition, the rather delicate balance in forces (headgroup repulsion and attraction between hydrophobic tails of micelles) is responsible for micellar structures being sensitive to temperature and additives, *etc.*[20]

1.2.1. Solubilisation in micelles

One of the important properties of micelles is the ability of micellar solutions to solubilise materials. Solubilisation forms the basis for the extensive uses of surfactants and micellar solutions in industrial, biological, and synthetic chemical/catalytic applications.[20, 22-24]

In order to understand the effects of micelles on (organic) reactions, it is pivotal to specify where reactants are located in the "micellar pseudophase" (the term pseudophase is used because micelles are transparent to UV-visible radiation and they do not form a real separate phase[18]), and the nature of this region in terms of reaction medium.[20]

Solubilisation by micellar solutions is known to occur at a number of different sites in the micelle: (1) in the Stern region and (2) in the inner hydrophobic core of the micelle. Apolar aliphatic hydrocarbons are typically located in the hydrophobic micellar core. For aromatic compounds it is more difficult to specify the solubilisation site because binding sites are frequently concentration dependent.[23, 25]

Different (fluorescence and NMR)[26-29] techniques have been utilised to study the binding locations of organic solubilisates. It is now commonly assumed that the preferable binding site for most organic molecule is the Stern region.[30-32]

1.2.2. Reactivity in micellar medium

Ideally, micelles bring together all reactants and the catalyst involved in a reaction. Provided that transport of reactants and catalyst between bulk water and micelles (or the "micellar pseudophase") is faster than the chemical reaction, the observed rate effects exerted by micelles are the result of (typically) high local reactant concentrations in

combination with local reaction medium effects affecting local rate constants.[20, 33] For

example, reactions of ionic reagents with non-ionic substrates are accelerated by counter-

ionic (the micelle's counter ions have the same charge as the ionic reactant molecules) and

inhibited by co-ionic (micellar counter ions have different charge from the ionic reactant

molecule) micelles.[33]

Compared to bulk water, the local reaction medium offered by the micellar Stern region

has the following key features which could affect the reaction rate constants: (1) lower

local water concentration, (2) high ionic strength (in the case of ionic surfactants), (3)

reduced polarity, and (4) local charge (again for ionic surfactants).[20] In a related project,

we develop quantitative descriptions of the micellar medium in order to understand

micellar effects on reaction rates of various reactions.

In principle, organic reactions involving more than one reactant in aqueous micelles often

proceed faster when reactants (and the catalyst if required) share the same binding site.

Although higher or lower local reaction rate constants compared to those in bulk water

may be observed, lower rate constants in micelles will be balanced by the increase in local

reactant and catalyst concentrations. The combination then typically gives a positive

micellar rate effect. In the case of reactants and catalyst not sharing the same binding site,

the effect of the reduced local concentrations leads to reduced reaction rates. However, if

appropriate surfactants can be identified, local rate constants in micelles can be

significantly higher than those in bulk aqueous solution. In summary, the variation of the

observed reaction rates (increase or decrease) in aqueous micellar solutions compared to

the same reaction in bulk water is not straightforward and depends on the above-

mentioned factors.[20]

1.2.3. Kinetic models describing micellar rate effects

Micellar reactivity can be described using different kinetic models, based on the type of the reaction and the nature of the reactants. Herein, we review a few common models which have been used to describe micellar rate effects.

1.2.3.1. (Pseudo) unimolecular reactions

The Menger-Portnoy kinetic model is the most straightforward model describing micellar kinetics for (pseudo) unimolecular reactions.[34] The model assumes rapid equilibrium of the reactant of interest over the bulk water and micellar pseudophase with an equilibrium constant K_m. The reaction proceeds with rate constants k_w and k_m in the bulk water and micellar pseudophase, respectively (Scheme 2).

$$P \xleftarrow{k_w} R_w \rightleftharpoons R_m \xrightarrow{k_m} P$$
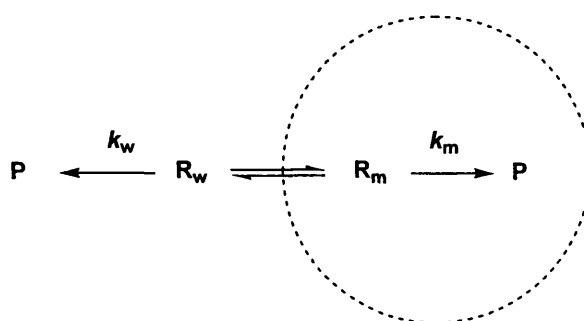
Scheme 1.2. Taken from ref[20]

The Menger-Portnoy model leads to equation 1.2 in which the observed rate constant k_{obs} is described as a function of surfactant concentration [S], cmc, and aggregation number N; ([S]-cmc)/N thus corresponds to the concentration of micelles.

$$k_{obs} = \frac{k_w + k_m \cdot K_m \cdot ([S] - cmc)/N}{1 + K_m \cdot ([S] - cmc)/N} \tag{1.2}$$

A related model has been developed by Berezin et al.[35] in which partition coefficients have been used instead of equilibrium constants. The partitioning of the reactants is given by the partition coefficient P_m, considering two pseudophases (bulk water and micelle).

The observed rate constant as a function of surfactant concentration is given by equation 1.3.

$$k_{obs} = \frac{k_w \cdot \left(1 - [S]_m \cdot V_{m,S}\right) + k_m \cdot P_m \cdot [S]_m \cdot V_{m,S}}{1 + P_m \cdot [S]_m \cdot V_{m,S}}$$

(1.3)

Where k_{obs}, k_w and k_m are defined as before, $[S]_m$ is the concentration of micellised surfactant and $V_{m,S}$ is the molar volume of the surfactant.

Analysis of data using both Menger-Portnoy and Berezin models results in micellar rate constants and micellar binding or partitioning constants.[20] For uncharged reactants, the micellar binding (or partitioning) constants are often believed to be determined mainly by hydrophobic interactions.[36]

In terms of transition state theory, (the change in) Gibbs energy of activation for a reaction within the micelle is directly related to the micellar rate constant.[20] Moreover, in combination with the micellar binding constant, the change in the activation Gibbs energies upon going from water to the micellar pseudophase can be used to calculate the binding constant of the transition state $K_{m,TS}$.[37-39] $K_{m,TS}$ is then interpreted in terms of stabilisation or destabilisation of the activated complex by the micelle. Whereas this approach is valuable for certain reactions, it is crucial to bear in mind that the transition state in bulk water can be very different from the transition state (or even rate-determining step) in the micellar Stern region (Cf. enzyme catalysis, see ref. [40]). In fact, this approach rapidly loses its appeal when reactions are pseudo-unimolecular or second order and higher, rather than truly unimolecular.[20]

Both the Menger-Portnoy model and the Berezin model assume the existence of two pseudophases in a bulk micellar solution, viz. bulk water and the micellar pseudophase. Nevertheless, both models could be expanded. For instance, one could consider the micellar pseudophase itself as consisting of two separate pseudophases, viz. a pseudophase

corresponding to the Stern region and one corresponding to the hydrophobic core.[22, 41, 42]

Assuming a reaction occurs in the Stern region and not in the micellar core (but the reactant still partitions into the micellar core), the micellar rate constant k_m would be expressed by the product of the local reaction rate constant in the Stern region k_s and the distribution of the reactant between different micellar pseudophase (equation 1.4).[22]

$$k_m = k_s \cdot \left\{ \frac{V_{Stern} \cdot P_{wS}}{V_{mic} \cdot P_m} \right\} \qquad (1.4)$$

Where k_s is the rate constant in the Stern region, V_{Stern} and V_{mic} are the volumes of the Stern region and of the micelle, respectively, P_{wS} and P_m are the water-to-Stern-region and water-to-micelle partition coefficients, respectively. Additional partitioning of micellar pseudophase is (mathematically) possible,[43, 44] but is unlikely to yield meaningful parameters.

1.2.3.2. (Pseudo) bimolecular reactions

For bimolecular reactions, data analysis of micellar rate effects becomes considerably more complicated than analysis for (pseudo) unimolecular reactions. Kinetic models quickly become unwieldy and parameter correlation starts to play a role. Nevertheless, two general models merit a more detailed discussion:[20] (1) one of the reactants is also a counter-ion to the (ionic) surfactant and (2) both reactants are neutral molecules.

1.2.3.3. The pseudophase ion exchange model (PIE)

For bimolecular reactions of an ionic reagent with non-ionic substrates in ionic micelles, the reaction rate can be accelerated by counter-ionic (and inhibited by co-ionic) micelles.[33] The so-called pseudophase ion exchange "PIE" model can be used to explain the effect of counter-ionic micelles on the reaction rate (first case, *vide supra*).[41, 45-49] The PIE model is based on the Menger-Portnoy model for unimolecular reactions, but it includes ion

exchange in the micellar Stern region where there is a competition between reactive and non-reactive counter-ions (Scheme 1.3).
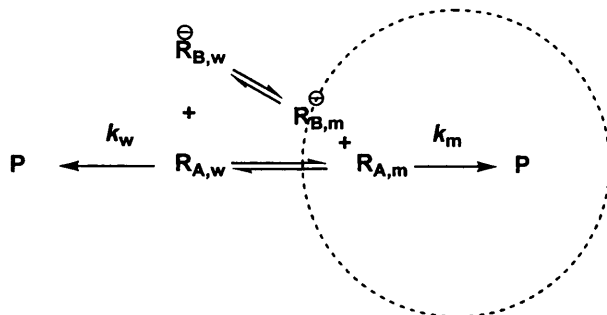
Scheme 1.3 Taken from ref[20]

The additional assumptions underpinning the PIE model compared to the Menger-Portnoy model are: (1) the micellar Stern region behaves as an ion-exchange resin, and (2) counter-ion exchange occurs strictly 1:1, *i.e.* the degree of counter-ion binding (β) remains constant.[18, 20] The local reactive counter-ion concentration can be calculated on the basis of the above-mentioned assumptions, provided that the equilibrium constant for counter-ion exchange is known. Consequently, the second-order rate constant for bimolecular reactions of interest can be calculated from the local reactive counter-ion concentration and the pseudophase model.

Typically, for this type of bimolecular reaction, the effect of surfactant concentration [surfactant] on the observed first-order rate constants, k_{obs}, with respect to substrate goes through a maximum (if the total concentration of reactive ions is kept constant). This behaviour results from substrate incorporation at low [surfactant] which increases the reaction rate. However, with increasing [surfactant], competition between the reactive ions and the surfactant counter-ions results in dilution of the reagent in the micelles and a decrease in local concentration of the reactive ions, decreasing k_{obs}. These rate maxima

disappear when there is no inert counter-ion in the solution, or when its concentration, relative to that of the reactive ion, is kept constant.[33]

The hydrophilicity (or hydration energy) of counter-ions reflects the competing forces of their binding to the Stern region. Typically, more hydrated counter-ions bind weakly and *vice versa*. However, for organic counter-ions, hydrophobic interactions should be taken into account as well.[20] Despite the fact that the assumption of strict 1:1 counter-ion exchange breaks down for some systems (especially for highly hydrophilic counter-ions),[33, 50-52] the PIE model is still regarded favourably for analysis of micellar kinetic effects for bimolecular reactions involving reactive counter-ions.

1.2.3.4. The pseudophase model for non-ionic bimolecular reactions

Further expansion of the pseudophase kinetic model is required for a bimolecular reaction involving two uncharged reactants A and B (second case, *vide supra*). The simplest of the possible extensions is when reactant A in the aqueous pseudophase reacts only with reactant B in the aqueous pseudophase, and the same is true in the micellar pseudophase, without any reactions "crossing" between the two pseudophases (Scheme 1.4).[20]
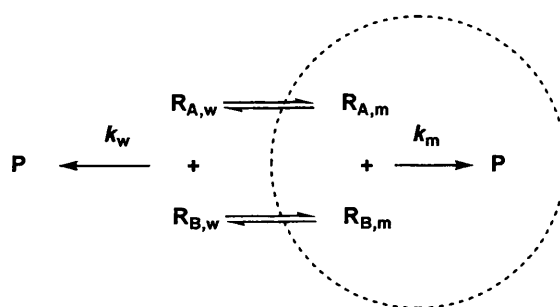
Scheme 1.4. Taken from ref[20]

The overall observed rate of the reaction depends on the local concentration of the reactants and the local reaction rate constant in both pseudophases. Ideally, rate-enhancing effects by the added surfactant are observed for this kind of reactions. However, any rate-

enhancing effect diminishes at high surfactant concentration. This behaviour is related to the high local concentration of the reactants in the micellar pseudophase at low [surfactant], *i.e.* reactants are fully bound in the micellar pseudophase. However, at high [surfactant], the observed reaction rate decreases with [surfactant], due to the increase of the micellar pseudophase volume, which leads to dilution of the reactants. The observed second-order rate constant $k_{obs,2}$ as a function of surfactant concentration describing these types of reactions is given in equation 1.5.

$$k_{obs,2} = \frac{k_{w,2} \cdot (1 - [S]_m \cdot V_{m,S}) + k_{m,2} \cdot P_{m,A} \cdot P_{m,B} \cdot [S]_m \cdot V_{m,S}}{(1 + (P_{m,A} - 1) \cdot [S] \cdot V_{m,S}) \cdot (1 + (P_{m,B} - 1) \cdot [S] \cdot V_{m,S})}$$ (1.5)

Where variables are defined as before, $k_{w,2}$ and $k_{m,2}$ are the (second-order) rate constants in water and in the micellar pseudophase, respectively, $P_{m,A}$ and $P_{m,B}$ are the partition coefficients for reactants A and B, respectively.

In general, the possibility of having cross-interface reactions occurring between the reactants in the micellar pseudophase and bulk water exists. However, including such possibilities makes the kinetic model too complicated to be used to reliably analyse data. There are a few reports that show apparent failure of bimolecular reactions to obey these pseudo-bimolecular models. This failure is attributed to various factors, including the possibility of cross-interface reactions.[53-60]

Finally, to test the validity of the above-mentioned models for a reaction under investigation requires a set of experimental kinetic data showing the effect of surfactant concentration on the observed reaction rate constant. Refinement of the mechanism (and hence the kinetic model) for the reaction under study is suggested when the model fails to fit the kinetic data.[18] Unfortunately, while extension and combination of these models might in principle allow the interpretation of micellar effects on reaction rates, typically the number of variables becomes so large that they become difficult to interpret. Also, in

extended models the different variables often show strong correlation, making the model difficult to validate. Nevertheless, the above-mentioned models help us to at least qualitatively understand micellar effects on the observed rate constant for a reaction under study. As Menger suggested "models are to be used not believed"[61] and Khan extended "models are to be used, but not to be believed in a sense to give the ultimate truth".[18]

1.3. Catalysts and Catalysis

Catalysis lies at the heart of myriad chemical protocols, from those used in academic laboratories to the chemical industry. The feasibility of the synthesis of many industrial and pharmaceutical products is a result of the use of catalysts.[62] Manufacturing protocols can be made more economic, green, and sustainable by the design and vigilant use of catalysts.[63] Berzelius in 1835 was the first to use the word catalysis (*katalyse*) and he defined catalysts as "substances which by their mere presence evoke chemical reactions that would not otherwise take place".[62] Wilhelm Ostwald in 1895 was the first to describe the effect of a catalyst on the rate of chemical reactions,[64] defining catalysts as "substances which change the velocity of a reaction without modification of the energy factors of the reaction". According to Ostwald, and based on the first-law of thermodynamics, catalysts must not change the magnitude of the equilibrium constant for reactions in equilibrium because forward and backward rate constants must change by the same ratio in the presence of the catalyst.

Nowadays, there is a general perception to define a catalyst as a "chemical species (atom(s) or molecule(s)), a molecular segment, or a molecular aggregate that changes the rate of a reaction without being consumed during the course of the reaction, and capable to be reused until the reaction is ceased or over".[18] The reusability of the catalyst makes small quantities (a so-called "catalytic amount") sufficient to accomplish a reaction.

Substances which increase the activity of a catalyst are called promoters, while compounds which decrease the activity of a catalyst are called inhibitors or catalyst poisons. The presence of a catalyst may cause the reaction to follow different elementary steps (different mechanism) compared to the reaction in its absence. In terms of Gibbs-energy of activation, a catalyst provides an alternative route for the reaction (rate-limiting step) with a lower activation energy (compared to the absence of the catalyst), resulting in an increased reaction rate.

The efficiency, productivity or activity of a catalyst is typically measured by its turnover number (TON) which is the number of moles of reactants converted (or moles of product formed) by one mole of catalyst. Similarly, turnover frequency (TOF), which is defined as the TON per unit of time, is used as a measure of the catalyst efficiency.[65] In biochemistry the term "katal" ($mol.s^{-1}$) is sometimes used to represent the enzyme catalytic activities.[66]

Catalytic processes are divided into two main categories. The first category is homogeneous catalysis in which the substrate(s) and the catalyst are in the same phase, usually the liquid phase. The second category is heterogeneous catalysis in which the catalyst has a different phase from the substrate(s) and usually is a solid. In general, activity and selectivity in homogeneous catalysis is higher than in heterogeneous catalysis. Also mechanistic understanding is more (typically, but not always) advanced in homogeneous catalysis. The latter is the case principally because mechanistic studies in heterogeneous catalysis can be very difficult. However, separation of the products and recycling of the catalyst are much easier in heterogeneous catalysis.[67]

1.3.1. Palladium reagents and catalysts

Palladium (Pd) is a rare, precious, transition metal discovered in 1803 by William Hyde Wallaston.[68] It belongs to the platinum group metals in the periodic table, which share

some unique properties that account for their widespread use. Palladium is used in many fields, including catalysis,[69] dentistry,[70] manufacturing of biomedical devices,[71] pharmaceutical industry.[72] In fact, palladium is considered the most versatile and widely used transition metal in catalysis.[69] The toxicity of Pd as a metal has caused no serious problems so far.[73] The common oxidation states of palladium are 0 and +2, however, higher oxidation states such as +4 (rare)[74] and +6 (discovered in 2002)[75] exist.[76]

In organic synthesis two kinds of Pd compounds are used viz. Pd^{II} salts and Pd^0 complexes. Pd^{II} compounds are usually electrophilic and mainly used as oxidising agents; they are catalysts for some reactions, or precursors for Pd^0 complexes.[77, 78] The majority of Pd^0 complexes are used as catalysts.[79, 80] Pd^0-complexes are typically nucleophilic 18-electron species and have tetrahedral geometry, whereas Pd^{II}-complexes are typically electrophilic 16-electron species and have square planar geometry.

Nowadays, there are many commercially available Pd^0 and Pd^{II} complexes which can be purchased for reasonable prices from known chemical producing companies. In addition, many methods have been developed to synthesise a variety of Pd^0 and Pd^{II} complexes starting from commercially-available Pd-compounds. There is frequently a stability problem concerning Pd^0 compounds, because they normally are air, light or moisture sensitive. This is true in particular for Pd^0-complexes bearing phosphine ligands. The stability of Pd-complexes depends on the nature and the structure of the ligand(s) attached. Furthermore, the solubility of Pd complexes is also typically controlled by bound ligands and counterions.

1.3.2. Palladium aqua complexes

Palladium(II) complexes can exchange their weakly coordinated ligands for water molecules when they are placed in hydrous or aqueous media.[81-84] As a result, they form

aqua complexes which are more soluble in water and undergo an acid/base equilibrium.

The direct synthesis of aqua palladium complexes occurs by the reaction of halo palladium

complexes with silver or thallium or other salts of weakly coordinating anions (*e.g.* ClO_4^-,

BF_4^-, SbF_6^-, BPh_4^-, SO_4^{2-}, TfO^-, and TsO^-) in solvents with poor donor abilities (*e.g.*

chlorocarbons). In some of these reactions, the synthesis of the aqua complexes proceeds

through species such as $[L_nPd-Y]$ (Y = anion) or an intermediate solvent complex

$[L_nPd(solv)]Y$, depending on the coordination ability of Y^- or on the solvent competing

with water for the acid moiety L_nPd^+ (Schemes 1.5a and b).[81]
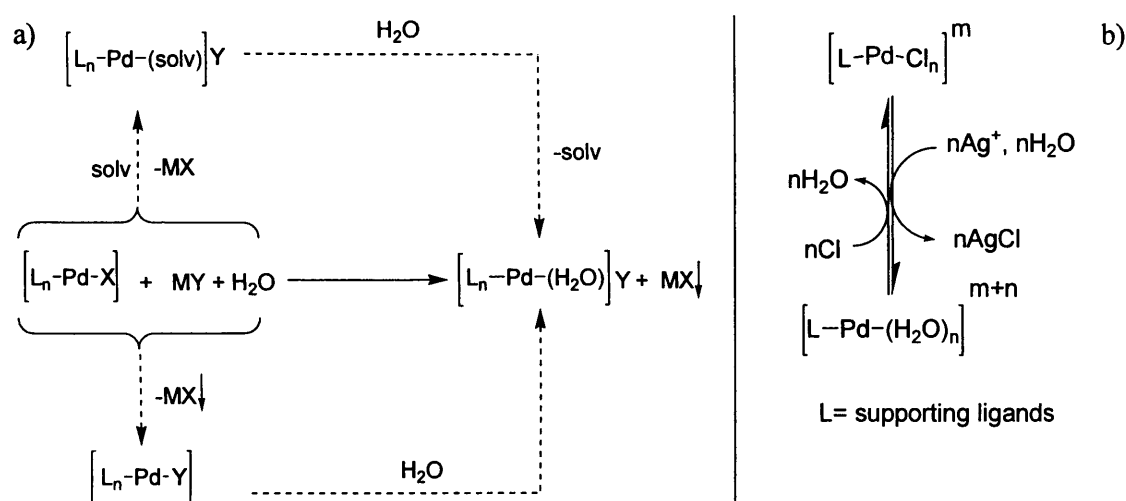
Scheme 1.5 a) taken from ref[47] and b) taken from ref[83]

Hohmann and Van Eldik[85] have reported that $Pd(en)Cl_2$ (en = ethylenediamine) undergoes

spontaneous solvolysis in aqueous solution to produce $Pd(en)(H_2O)Cl^+$ and

$Pd(en)(H_2O)_2^{2+}$. They have employed spectrophotometric and potentiometric techniques to

determine the equilibrium constants for the replacement of the first and second H_2O

molecules by Cl^-, *viz.* $K_1 = 4000$ and $K_2 = 137$ M^{-1}, respectively, at 25 °C and 0.1 M ionic

strength. The acid dissociation constant for the di-aqua complex $Pd(en)(H_2O)_2^{2+}$ (pK_{a1})

was found to be 5.6. The same authors found a pK_a of 7.3 ± 0.2 for the $Pd(en)(H_2O)Cl^+$

complex. In another publication, Hohmann *et al.*[84] found $Pd(R_4en)$ $(H_2O)_2^{2+}$ to have

pK_{a1}=5.6 ± 0.2, 5.4 ± 0.2 and 5.8 ± 0.2, and Pd(R_4en) (H_2O)Cl$^+$ to have pK_{a2}=7.3 ± 0.2, 7.0

± 0.2 and 7.7 ± 0.2 for R=H, Me and Et, respectively, at 25 °C and 0.1 M ionic strength.

These data exhibit a general decrease in pK_{a1} and pK_{a2} on going from the unsubstituted to

the Me$_4$en complexes, followed by an increase in these values on going to the Et$_4$en

complexes. In addition, Berger and co-workers[86] have determined pK_{a1} values of 7.19 ±

0.03 and 7.53 ± 0.09 for the [Pd(Me$_5$dien)H_2O]$^{2+}$ and [Pd(Et$_5$dien)H_2O]$^{2+}$ (where Me =

methyl, Et= ethyl and dien = diethylenetriamine) species, respectively, from the pH

dependence of the ^{13}C and ^{1}H chemical shifts of both complexes. Wimmer and co-

workers[87] have reported pK_{a1} and pK_{a2} values of 6.8 and 7.6 for Pd(AMP)(H_2O)$_2$$^{+2}$

[where, AMP = 2- (aminomethyl)pyridine], and one pK_a value of 7.1 for [Pd(2,4`-

bpyMe-H)(H_2O)$_2$]$^{+2}$ (where, 2,4`-bpyMe-H = N-methyl-2,4`-bipyridin-3-ylium), in

aqueous solution of 0.1 M ionic strength. Both complexes have the ability to form

aqua/hydroxo dimers with dimerisation logK_D values of 7.0 and 5.4, respectively.

Recently, Jaganyi et al.[88] have synthesised [Pd(bpma)(H_2O)]$^{2+}$, where bpma = bis(2-

yridylmethyl)amine. The pK_a of 6.67 ± 0.07 of the coordinated water molecule in

[Pd(bpma)(H_2O)]$^{2+}$ was determined from the plot of absorbance at a wavelength of 249

nm against pH, at 25 °C and 0.1 M ionic strength.

1.3.3. Palladium nanoparticles

Nanoparticle (NP) catalysis forms a frontier between homogeneous and heterogeneous

catalysis and has been referred to as "semi-heterogeneous catalysis".[89] Usually NP

catalysts are prepared from a metal salt, a reducing agent and a stabiliser, such as

dendrimers, specific ligands, ionic liquids, surfactants, proteins, membranes, carbon

nanotubes, polymers and a variety of oxides.[90-92] Pd-nanoparticles (Pd NPs) are of great

interest because of the popularity of Pd chemistry, especially in catalysis. Colloidal Pd^0

nanoparticles protected by different stabilising agents have been developed with variety of morphologies and sizes using different stabilising agents and synthetic protocols.[93-104] These NPs have been deployed as catalytic systems for many chemical transformations (especially C-C coupling reactions).[105-111] These systems will be discussed in more details in Chapter 3 and 4. Furthermore, a brief description of Au nanoparticles, their synthesis and use in catalysis (especially in C-C coupling reactions), together with the synthesis of bimetallic Au-Pd core-shell NPs are discussed in Chapter 4.

1.4. Palladium catalysts in C-C bond formation (with a focus on the Suzuki-Miyaura cross-coupling reaction and oxidative homocoupling of arylboronic acids)

The importance of carbon-carbon bond formation in organic synthesis needs no explanation. Palladium, among many other transition metals, offers an abundance of versatile methods for C-C bond formation. The importance of Pd catalysis in C-C bond formation has recently been reflected through the award of the Nobel Prize in chemistry 2010 to Richard F. Heck, Ei Ichi Negishi and Akira Suzuki for their pioneering contributions in "Palladium-catalysed cross-couplings in organic chemistry". An interesting feature of Pd reagents is their tolerance of many functional groups such as carbonyl and hydroxyl groups, consequently Pd-catalysed reactions require no protection of these groups. However, one of the drawbacks of using Pd reagents in chemical reactions is that many Pd reagents are sensitive to oxygen (air), moisture, and sometimes even light. Therefore, immense efforts have been deployed for the synthesis of Pd-catalysts with ligands that are resistant to air and/or moisture[112-114] or using supporting ligands on functional support (e.g. synthesising stable Pd nanoparticles).[115-117] The stability, solubility and reactivity of Pd-catalysts are hugely dependent on the nature and structure of the ligands.[118]

The era of Pd-catalysed C-C bond formation started in 1972 through the publication of the

Pd-catalysed vinylic substitution reaction with aryl halides by Richard Heck (one of the

Nobel Laureates in 2010)[119] even though nearly one year before Heck's publication,

Mizoroki already reported the same reaction under different conditions.[120] Further

examples of C-C coupling reactions continued to appear throughout the 1970s.

Sonogashira used a copper and Pd catalyst pair for the coupling reaction of aryl halides

and alkynes rather than alkenes.[121] Stille explored tin reagents in coupling chemistry.[122]

The coupling of organometallic derivatives of zinc and magnesium was first reported by

Negishi and Murahashi, respectively.[123-125]

In 1979[126] Suzuki (Nobel Laureate in 2010) and Miyaura published their pioneering work

on a cross-coupling reaction employing aryl/vinyl boronic acids or esters with aryl/vinyl

halides. This reaction has found a wide acceptance by pharmaceutical chemists, especially

for the production of biaryl derivatives which are the building blocks of many

pharmaceutical compounds. The original paper published in 1979 described the reaction of

alkenyl boronates and alkenyl halides, whereas the reaction of phenylboronic acid and aryl

halides was first reported in 1981.[127] The mechanism of the Suzuki-Miyaura cross-

coupling reaction is believed to proceed through a catalytic cycle involving three basic

steps:[128, 129](1) the oxidative addition of the aryl/vinyl halide (or triflate) to a

coordinatively unsaturated Pd^0-complex (Pd^0L or Pd^0L_2), (2) the transmetalation of the

aryl/vinyl boronic acid to $RPd^{II}XL_2$ with the assistance of base, and (3) the relatively rapid

reductive elimination (Scheme 1.6).

L = mono or bi dentate ligand

Pd^0L_n

RR`

Reductive elimination

Oxidative addition

RX

$R`RPd^{II}L_n$

$RPd^{II}L_nX$

Transmetalation

$B(OH)_2(base)$
or
$^{\ominus}B(OH)_2(base)X$

$R`B(OH)_2$ + Base

Scheme 1.6. adapted from ref [129]

The catalytic cycle summarised in Scheme 1.6 is a highly complex process. Nevertheless, the oxidative addition and reductive elimination steps have been extensively studied and their detailed mechanistic steps have been explained theoretically and experimentally.[130-134] However, the reaction mechanism o f the transmetalation step still remains under discussion, especially the role of the base which is believed to be crucial in this step.[128, 129, 135, 136] Base is crucial for the Suzuki-Miyaura cross coupling reaction. For example, both computational and experimental studies have shown that the transmetalation between $Ar`B(OH)_2$ and halopalladium intermediate $ArPdL_2X$ does not take place in the absence of base (path A scheme 1.7).[137, 138]

Several roles for the added base have been proposed based on experimental and theoretical studies. Firstly, the reaction of the base (OR`) with $Ar`(B(OH)_2$ could be required to form the boronate adduct $Ar`B(OH)_2OR^-$ which is more nucleophilic and hence more reactive

towards transmetalation with $ArPdL_2X$ to form the $ArPdArL_2$ species than the parent

boronic acid (path C in scheme 1.7).[135-139]

Path A

$$Ar-\overset{\overset{L}{|}}{\underset{\underset{L}{|}}{Pd}}-X + Ar'-B\overset{OH}{\underset{OH}{\diagdown}} \xrightarrow{\quad\quad} \text{No reaction or unfavoured}$$

No base

Path B

$$Ar-\overset{\overset{L}{|}}{\underset{\underset{L}{|}}{Pd}}-X + RO^- \rightleftharpoons Ar-\overset{\overset{L}{|}}{\underset{\underset{L}{|}}{Pd}}-OR + X^-$$

$Ar'B(OH)_2$

$^\ominus B(OH)_2OR$

$$Ar-\overset{\overset{L}{|}}{\underset{\underset{L}{|}}{Pd}}-X$$

$$Ar-\overset{\overset{L}{|}}{\underset{\underset{L}{|}}{Pd}}-Ar'$$

PathC

$$Ar'-B\overset{OH}{\underset{OH}{\diagdown}} + RO^- \rightleftharpoons Ar'-\overset{OH}{\underset{OR}{\overset{|\ominus}{B}}}-OH$$

$^\ominus B(OH)_3X$

Path D

$$Ar-\overset{\overset{L}{|}}{\underset{\underset{L}{|}}{Pd}}-X + Ar'-B\overset{OH}{\underset{OH}{\diagdown}} + 2RO^- \rightleftharpoons Ar'-\overset{OH}{\underset{OH}{\overset{|\ominus}{B}}}-OH + Ar-\overset{\overset{L}{|}}{\underset{\underset{L}{|}}{Pd}}-OR + X^-$$

unfavoured

Scheme 1.7. Possible pathways for the transmetalation step in Suzuki-Miyaura reaction.

Secondly, the direct replacement of the halide (X) in $ArPdL_2X$ by the base (OR^-) is

proposed to form a $ArPdL_2OR$ species which reacts with the oxophilic $Ar`B(OH)_2$ to form

$ArPdArL_2$ (Path B scheme 1.7).[136, 140, 141] Thirdly, the presence of base could lead to the

formation of both $Ar`B(OH)_3^-$ and $ArPdL_2OR$. However, the reaction between these two

species is unfavourable presumably because of the difficult transfer of OR^- to a negatively

charged species (Path D scheme 1.7).[138, 141] Recently, Jutand *et al.*[138] have proposed

another role of the added base which is to enhance the reductive elimination step from the

intermediate *trans*-[ArPdAr`L_2] via the formation of a transient penta-coordinated Pd-

22

complex *viz. cis*-[ArPdAr`(OH) (PPh₃)₂] allowing facile reductive elimination (Scheme 1.8).

$$Ar-\underset{L}{\overset{L}{Pd^{II}}}-Ar` + \quad HO^- \quad \rightleftharpoons \quad \left[ Ar-\underset{OH}{\overset{Ar`}{Pd}}\overset{L}{\underset{L}{\diagdown}} \right]^{-} \quad \xrightarrow[\text{elimination}]{\text{reductive}} \quad Ar-Ar` + \underset{L}{\overset{L}{Pd^0}} + \quad {}^-OH$$

Scheme 1.8

Symmetrical biaryls Ar`Ar` generated from Ar`B(OH)₂ are often a side product in Suzuki-Miyaura reactions.[142, 143] Moreno-Mañas *et al.* in 1996 have turned this side reaction, for the first time, to a main catalytic reaction in the presence of Pd^0 and Pd^{II} as catalysts in the presence of air and/or dioxygen.[144, 145] Koza and Carita have shown that using $Cu(NO_3)_2$ as an oxidant enhances the rate and the yield of the production of symmetrical biaryls from arylboronic acids using $Pd(PPh_3)_2$ as a catalyst and ethanol as a solvent.[146] In addition, Yoshida *et al.*[147] have demonstrated a base-free oxidative homocoupling reaction of arylboronic esters using a catalytic amount of a $Pd(OAc)_2$ and [1,3-bis(diphenylphosphino) propane] (DPPP) complex as a catalyst and DMSO as a solvent, under an oxygen atmosphere, affording a variety of biaryls in modest to excellent yields.

The first proposed mechanism for the oxidative homocoupling reaction was published by Moreno-Mañas *et al.*[144, 145] using Pd^0 and Pd^{II} complexes as catalysts and toluene as the solvent. They showed that the catalytic cycle includes an acid-base reaction between ArB(OH)₂ and Pd^0 or Pd^{II} through the pair of electrons of the coordinatively unsaturated (14-electrons) species PdL₂ to form intermediate *trans*-[Ar-Pd-B(OH)₂(L₂)] in a step they call "oxidative addition/transmetalation". This intermediate [Ar-Pd-B(OH)₂(L₂)] loses a ligand L, and subsequently the formed [Ar-Pd-B(OH)₂(L)] reacts with another molecule of ArB(OH)₂ in a similar step to the first one to form *trans*-[Ar-Pd-Ar(B(OH)₂)₂]. Reductive

elimination of trans-$[Ar\text{-}Pd\text{-}Ar(B(OH)_2)_2]$ produces the biaryl (ArAr) and $(OH)_2B\text{-}Pd\text{-}B(OH)_2$. Finally, the authors proposed formation of PdH_2 and [O=B-OH] from $(OH)_2B\text{-}Pd\text{-}B(OH)_2$, Pd^0L_2 forms again by return of the previously liberated ligands. The authors proposed that H_2 is liberated and reacts with oxygen. In our opinion, there are several problems with this mechanism, including limiting the role of oxygen to the final step, the suggested formation of H_2, and also mixing an oxidative addition and transmetalation steps in one step.

Yoshida et al.[147] have demonstrated that oxygen reacts readily with Pd^0-complexes $[Pd^0\text{-}L]$ (where, L = bidentate ligand (DPPP)) to form a three-membered peroxo-Pd^{II}-complex [PdOO(L)] in an oxidative addition step. Subsequent double transmetalation of the arylboronic esters with the peroxo-Pd^{II}-complex occurs without the aid of a base to give diarylpalladium $[ArPdAr(L_2)]$ and boron peroxide [B-OO-B] through intermediate complex [ArPdOOB(L)]. Reductive elimination of the homocoupling product [ArAr] from [ArPdAr(L)] follows with regeneration of the $[Pd^0\text{-}L]$ complex.

Recently, Adamo et al.[148, 149] demonstrated that a reactive $Pd^{II}\text{-}\eta^2$-peroxo species **1a** is generated and can be isolated from the direct stoichiometric reaction of O_2 with Pd^0L_4 (where, L = PPh_3) in chloroform (Scheme 1.9). The catalytic cycle could be initiated by **1a** and the possibility of **1a** being a true reactive intermediate was confirmed by subsequent detailed kinetic and NMR studies. The authors further showed that the reaction followed second-order kinetics in **2a** and first-order kinetics in **1a**. The kinetic studies in combination with ^1H and ^{31}P NMR studies, led the authors to propose a fast equilibrium involving initial binding of **2a** to one of the oxygen atoms of the $Pd^{II}\text{-}\eta^2$-peroxo species **1a** to generate intermediate **1b**. This intermediate (**1b**) is proposed to be activated by the initial binding of **2a** for transmetalation with a second equivalent of **2a** to produce

intermediate **1c**. Pd[II]-hydroxide species **1d** is then generated through addition of H_2O to

1c, followed by *cis–trans* isomerisation to form **1e**.

Scheme 1.9

Moreover, the authors were able to isolate complex **1e** and subsequently added another

equivalent of **2a**. ^{31}P NMR spectroscopy was used to monitor the reaction and trans-Pd[II]-

biaryl intermediate **1f** was observed. Finally, the catalytic cycle was completed by

isomerisation of intermediate **1f** to the cis-Pd[II]-biaryl complex **1g**. Subsequent reductive

elimination liberates the product and reforms Pd^0L_2 complex.

Furthermore, Adamo *et al.* have investigated the origin of the undesired formation of the

phenol (ArOH) by-product.The y showed that in the absence of Pd-catalyst, the stability of

2a was not affected by the direct exposure to O_2 for 3 days. However, in the presence of a

Pd-catalyst, phenol was formed and the authors propose that H_2O_2 generated from the

peroxo boronic species released during the catalysed homocoupling reaction reacts with

the organoboronic acid to generate the phenol (Scheme 1.10). They have found that adding

H_2O_2 to **2a** also leads to phenol formation.

$$HOOB(OH)_2 \; + \; H_2O \longrightarrow B(OH)_3 \; + \; H_2O_2$$

$$ArB(OH)_2 \quad + \; H_2O_2 \longrightarrow B(OH)_3 \; + \; ArOH$$
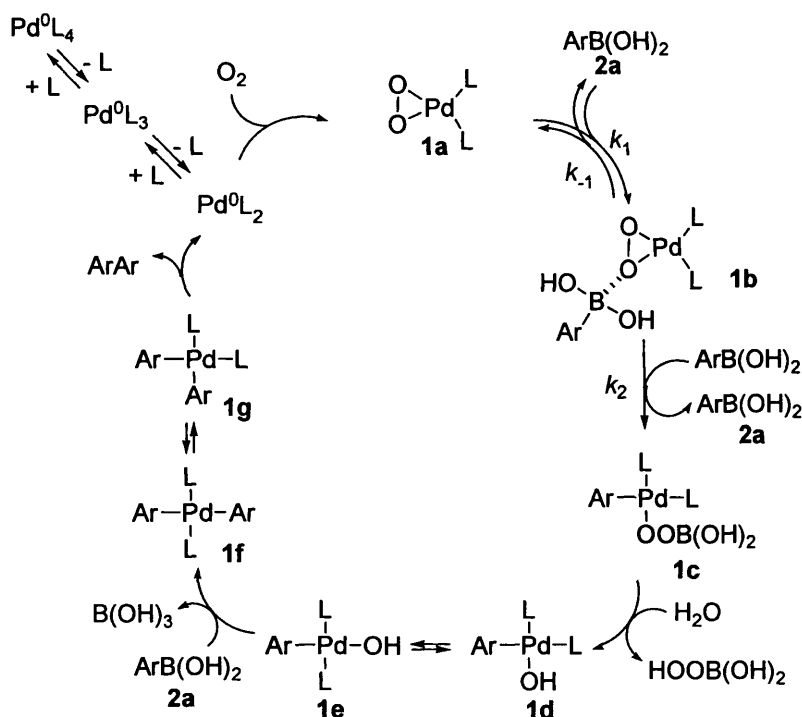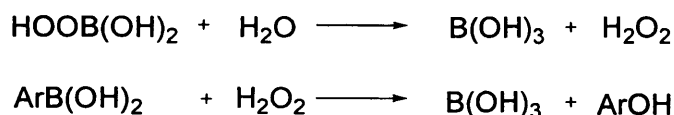
Scheme 1.10

The detailed mechanistic analysis above demonstrates the complexity of the Pd-catalysed

oxidative homocoupling of organoboronic acids and shows the pivotal role of molecular

O_2.

1.5. Arylboronic acids

The use of arylboronic acids, $ArB(OH)_2$, in organic chemistry has been a matter of great

interest in the last years. Arylboronic acids can be easily prepared using different synthetic

protocols,[150-156] varieties of structurally different $Ar(OH)_2$ reagents are now commercial

available and most of them are reasonably stable (with some exceptions including several

heterocyclic boronic acids[156]) upon storage.[118] Also, most arylboronic acids are considered

as environmentally friendly reagents and have posed no serious toxicity problems.[157]

However, there are some drawbacks accompanying the use of $ArB(OH)_2$ in organic

transformations. Firstly, under anhydrous conditions, $ArB(OH)_2$ mainly exists as a dimer

or cyclic trimer (Scheme 1.11). These dimers a nd/or trimers easily hydrolyse to the

corresponding $ArB(OH)_2$ under aqueous conditions.[158, 159]

Scheme 1.11

26
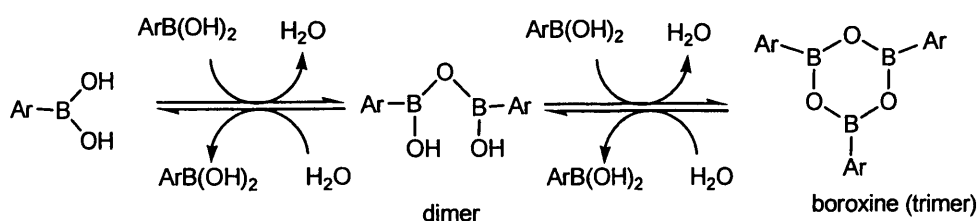
Secondly, substituted arylboronic acids X-ArB(OH)$_2$ undergo protodeboronation in highly acidic[160, 161] (especially when X is an electron-donating group) or basic (especially when X is an electron-withdrawing group) solutions which leads to the formation of the corresponding X-Ar-H compound.[157] Finally, the boronic acid functional group is sensitive to several common organic reagents, so that it is not normally carried over through sequential synthetic protocols.[118]

The acidity of arylboronic acids arises from the Lewis acid character of the boron atom which has a vacant p orbital which can be used for the formation of a dative bond with a ligand offering a lone pair to form a tetrahedral boronate ion (the conjugate base of the boronic acid) (Scheme 1.12a).[162] The acidic character of substituted ArB(OH)$_2$ increases with the presence of electron-withdrawing groups on the aryl ring and decreases with the presence of electron-donating groups. For example, the acidity constant (pK_a) of phenylboronic acid is 8.8, while the pK_as for 4-methoxyphenylboronic acid and 2-methoxyphenylboronic acids are 9.4 and 9.0, respectively. More electron-poor 4-nitrophenylboronic acid and N-methyl-3-pyridineboronic acid have pK_as of 7.1 and 4.4, respectively (all in water and at room temperature).[157, 162] Also, bulky substituents close to the boron centre lead to decreased acidity due to steric effects that resist the formation of the tetrahedral boronate ion. For example, ortho-tolylboronic acid is less acidic than the para isomer (pK_a 9.7 vs. 9.3). Exceptionally, ortho-nitrophenylboronic acid is less acidic than the para isomer (pK_a 9.2 vs. 7.1),[157, 163] which might be attributed to the internal coordination of one of the oxygen atoms in the nitro group of the ortho isomer to the boron centre.

Ar—B(OH)$_2$ + 2H$_2$O $\rightleftharpoons$ Ar—B$^-$(OH)$_3$ + H$_3$O$^+$ a) Lewis acid behaviour

Ar—B(OH)$_2$ + H$_2$O $\underset{\text{rare}}{\rightleftharpoons}$ Ar—B(O$^-$)(OH) + H$_3$O$^+$ b) Brønsted acid behaviour
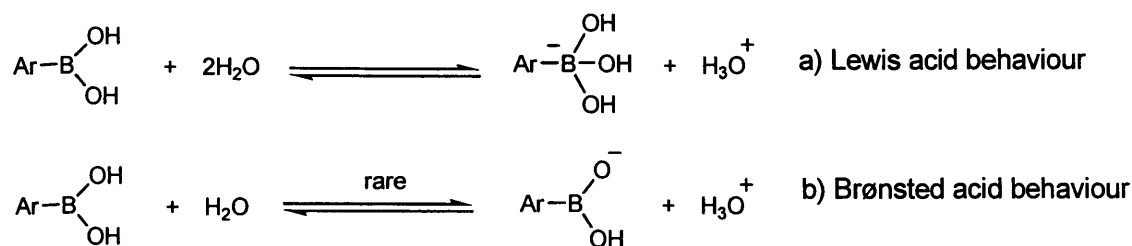
Scheme 1.12

There are a few exceptional cases in which ArB(OH)$_2$ shows Brønsted acid behaviour (scheme 1.12b) rather than Lewis acid behaviour, in particular when the formation of the tetrahedral boronate ion is thermodynamically unfavourable, Scheme 1.13 shows an example of this case .[157,164]
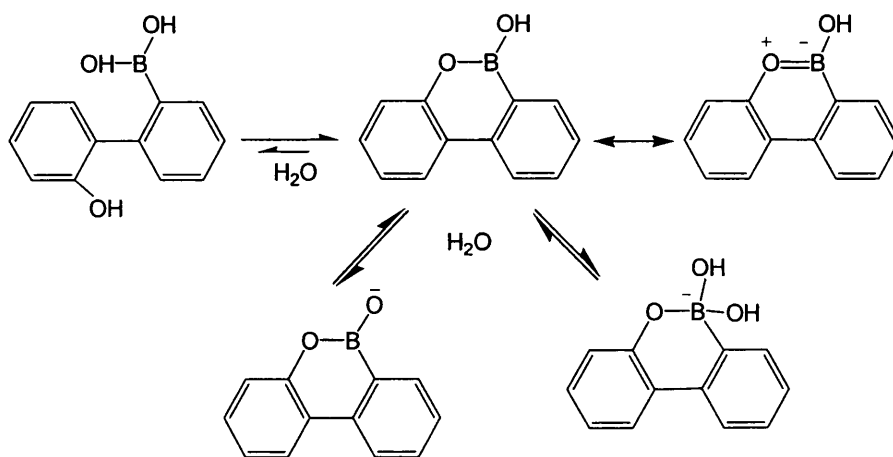
Scheme 1.13 adopted from ref [157]

The ease of handling, low toxicity, and unique Lewis acidity and reactivity of arylboronic acids make them of great interest in many fields e.g. organic synthesis (Suzuki-Miyaura cross coupling, oxidative dimerisation, etc.), pharmaceutical industry, and medicine. Moreover, the affinity of boronic acids to bind to diols made boronic acids interesting candidates for sensors for saccharide recognition, nucleotide and carbohydrate transporters, and even as antibody mimics targeting cell-surface carbohydrates.[157]

1.6. Aims and objectives of the project

The key aim of this project is to explore the kinetics of the aerobic oxidative homocoupling reaction of arylboronic acids in aqueous micellar medium under environmentally benign conditions (water as a solvent, micelle to help solubilise hydrophobic adducts and near room temperature). The reaction is palladium-catalysed and therefore our first challenge is to find a suitable catalyst in order to get reliable and reproducible kinetic results. For that reason we explore the use of a molecular Pd-catalyst, of Pd-CTAB nanoparticles, and of bimetallic core-shell Au-Pd nanoparticles encapsulated in thermoresponsive poly-(N-isopropylacrylamide). The synthesis and characterisation of the nanoparticles is in collaboration with University of Vigo in Spain. We hope that our kinetic studies lead to some insights into the possible mechanism(s) for the reactions using each of the catalytic systems mentioned above. We further note that an improved understanding of the oxidative homocoupling reaction of arylboronic acids is likely beneficial for our understanding of the Suzuki-Miyaura (SM) cross-coupling reaction as well, because transmetalation is frequently the rate-determining step in the SM reaction.

References

1. Finney, J. L., *Philosophical Transactions of the Royal Society B-Biological Sciences* **2004,** *359* (1448), 1145-1163.

2. Lindström, U. M., *Organic reactions in water : principles, strategies and applications.* Blackwell Pub.: Oxford ; Ames, Iowa, **2007;** 405 p.

3. Chaplin, M. F., *Biophysical Chemistry* **2000,** *83* (3), 211-221.

4. Ball, P., *H2O : a biography of water.* Weidenfeld & Nicolson: London, **1999;** 387 p.

5. Hailes, H. C., *Organic Process Research & Development* **2007,** *11* (1), 114-120.

6. Cornils, B., *Organic Process Research & Development* **1998,** *2* (2), 121-127.

7. Li, C. J.; Chen, L., *Chemical Society Reviews* **2006,** *35* (1), 68-82.

8. Sinou, D., *Advanced Synthesis & Catalysis* **2002,** *344* (3-4), 221-237.

9. Li, C. J., *Chemical Reviews* **2005,** *105* (8), 3095-3165.

10. Rideout, D. C.; Breslow, R., *Journal of the American Chemical Society* **1980,** *102* (26), 7816-7817.

11. Breslow, R., *Accounts of Chemical Research* **1991,** *24* (6), 159-164.

12. Narayan, S.; Muldoon, J.; Finn, M. G.; Fokin, V. V.; Kolb, H. C.; Sharpless, K. B., *Angewandte Chemie-International Edition* **2005,** *44* (21), 3275-3279.

13. Kobayashi, S.; Mori, Y.; Nagayama, S.; Manabe, K., *Green Chemistry* **1999,** *1* (4), 175-177.

14. Darbre, T.; Machuqueiro, M., *Chemical Communications* **2003,** (9), 1090-1091.

15. Torii, H.; Nakadai, M.; Ishihara, K.; Saito, S.; Yamamoto, H., *Angewandte Chemie-International Edition* **2004,** *43* (15), 1983-1986.

16. Hayashi, Y., *Angewandte Chemie-International Edition (English)* **2006,** *45* (48), 8103-4.

17. Blackmond, D. G.; Armstrong, A.; Coombe, V.; Wells, A., *Angewandte Chemie-International Edition* **2007,** *46* (21), 3798-3800.

18. Khan, M. N., *Micellar catalysis.* Taylor & Francis: Boca Raton, **2006;** p 482 p.

19. Israelachvili, J. N.; Mitchell, D. J.; Ninham, B. W., *Journal of the Chemical Society-Faraday Transactions Ii* **1976,** *72,* 1525-1568.

20. Buurma, N. J., *Advances in Physical Organic Chemistry,* **2009,** *43,* 1-37.

21. Gruen, D. W. R., *Progress in Colloid and Polymer Science* **1985,** *70,* 6-16.

22. Buurma, N. J.; Herranz, A. M.; Engberts, J. B. F. N., *Journal of the Chemical Society-Perkin Transactions 2* **1999,** (1), 113-119.

23. Buurma, N. J.; Serena, P.; Blandamer, M. J.; Engberts, J. B. F. N., *Journal of Organic Chemistry* **2004,** *69* (11), 3899-3906.

24.   Carregal-Romero, S.; Buurma, N. J.; Perez-Juste, J.; Liz-Marzan, L. M.; Herves, P., *Chemistry of Materials* **2010**, *22* (10), 3051-3059.

25.   Suratkar, V. V.; Mahapatra, S., *Journal of Colloid Interface Science* **2000**, *225* (1), 32-38.

26.   Bunton, C. A.; Cowell, C. P., *Journal of Colloid and Interface Science* **1988**, *122* (1), 154-162.

27.   Ranganathan, R.; Vautier-Giongo, C.; Bales, B. L., *Journal of Physical Chemistry B* **2003**, *107* (37), 10312-10318.

28.   Lebedeva, N.; Bales, B. L., *Journal of Physical Chemistry B* **2006**, *110* (20), 9791-9799.

29.   Cang, H.; Brace, D. D.; Fayer, M. D., *Journal of Physical Chemistry B* **2001**, *105* (41), 10007-10015.

30.   Lebedeva, N.; Ranganathan, R.; Bales, B. L., *Journal of Physical Chemistry B* **2007**, *111* (21), 5781-5793.

31.   Gallivan, J. P.; Dougherty, D. A., *Proceedings of the National Academy of Sciences of the United States of America* **1999**, *96* (17), 9459-9464.

32.   Fendler, J. H.; Liu, L. J., *Journal of the American Chemical Society* **1975**, *97* (5), 999-1003.

33.   Bunton, C. A., *Advances in Colloid and Interface Science* **2006**, *123*, 333-343.

34.   Menger, F. M.; Portnoy, C. E., *Journal of the American Chemical Society* **1967**, *89* (18), 4698-4703.

35.   Mittal, K. L., *Micellization, solubilization and microemulsions*. Plenum: New York ; London, **1977**; p 2v.(xv,945p.).

36.   Blokzijl, W.; Engberts, J. B. F. N., *Angewandte Chemie-International Edition* **1993**, *32* (11), 1545-1579.

37.   Kurz, J. L., *Journal of the American Chemical Society* **1963**, *85* (7), 987-989.

38.   Tee, O. S.; Fedortchenko, A. A., *Canadian Journal of Chemistry-Revue Canadienne De Chimie* **1997**, *75* (10), 1434-1438.

39.   Tee, O. S.; Yazbeck, O. J., *Canadian Journal of Chemistry-Revue Canadienne De Chimie* **2000**, *78* (8), 1100-1108.

40.   Allemann, R. K.; Scrutton, N. S., *Quantum tunnelling in enzyme-catalysed reactions*. RSC Pub.: Cambridge, **2009**; 385 p.

41.   Pereira, R. D.; Zanette, D.; Nome, F., *Journal of Physical Chemistry* **1990**, *94* (1), 356-361.

42.   Minero, C.; Pramauro, E.; Pelizzetti, E., *Journal of Physical Chemistry* **1988**, *92* (16), 4670-4676.

43.   Davies, D. M.; Gillitt, N. D.; Paradis, P. M., *Journal of the Chemical Society-Perkin Transactions 2* **1996**, (4), 659-666.

44.   Davies, D. M.; Foggo, S. J.; Paradis, P. R., *Journal of the Chemical Society-Perkin Transactions 2* **1998**, (7), 1597-1602.

45.   Quina, F. H.; Chaimovich, H., *Journal of Physical Chemistry* **1979**, *83* (14), 1844-1850.

46.   Chaimovich, H.; Bonilha, J. B. S.; Politi, M. J.; Quina, F. H., *Journal of Physical Chemistry* **1979**, *83* (14), 1851-1854.

47.   Biresaw, G.; Bunton, C. A., *Journal of Organic Chemistry* **1986**, *51* (14), 2771-2777.

48.   Cheong, M. Y.; Ariffin, A.; Khan, M. N., *Bulletin of the Korean Chemical Society* **2007**, *28* (7), 1135-1140.

49.   Khan, M. N.; Ismail, E., *Journal of the Chemical Society-Perkin Transactions 2* **2001**, (8), 1346-1350.

50.   Bunton, C. A.; Debuzzaccarini, F., *Journal of Physical Chemistry* **1981**, *85* (21), 3142-3145.

51.   Bunton, C. A.; Nelson, S. E.; Quan, C., *Journal of Organic Chemistry* **1982**, *47* (7), 1157-1160.

52.   Neves, M. D. S.; Zanette, D.; Quina, F.; Moretti, M. T.; Nome, F., *Journal of Physical Chemistry* **1989**, *93* (4), 1502-1505.

53.   Bunton, C. A.; Romsted, L. S.; Savelli, G., *Journal of the American Chemical Society* **1979**, *101* (5), 1253-1259.

54.   Nome, F.; Rubira, A. F.; Franco, C.; Ionescu, L. G., *Journal of Physical Chemistry* **1982**, *86* (10), 1881-1885.

55.   Stadler, E.; Zanette, D.; Rezende, M. C.; Nome, F., *Journal of Physical Chemistry* **1984**, *88* (9), 1892-1896.

56.   Rodenas, E.; Vera, S., *Journal of Physical Chemistry* **1985**, *89* (3), 513-516.

57.   Vera, S.; Rodenas, E., *Tetrahedron* **1986**, *42* (1), 143-149.

58.   Bunton, C. A.; Moffatt, J. R., *Journal of Physical Chemistry* **1986**, *90* (4), 538-541.

59.   Ortega, F.; Rodenas, E., *Journal of Physical Chemistry* **1987**, *91* (4), 837-840.

60.   Ferreira, L. C. M.; Zucco, C.; Zanette, D.; Nome, F., *Journal of Physical Chemistry* **1992**, *96* (22), 9058-9061.

61.   Menger, F. M., *Accounts of Chemical Research* **1979**, *12* (4), 111-114.

62.   Ertl, G., *Handbook of heterogeneous catalysis*. 2nd, completely rev. and enl. ed. / edited by Gerhard Ertl ... [et al.]. ed.; Wiley-VCH ; [Chichester : John Wiley, distributor]: Weinheim, **2008**; 3963 p.

63.   Polshettiwar, V.; Varma, R. S., *Green Chemistry* **2010**, *12* (5), 743-754.

64.   Chorkendorff, I.; Niemantsverdriet, J. W., *Concepts of modern catalysis and kinetics.* Wiley-VCH: Weinheim ; [Cambridge], 2003; 452 p.

65.   Kurosawa, H.; Yamamoto, A., *Fundamentals of molecular catalysis.* Elsevier: Amsterdam ; London, 2003; 522 p.

66.   Dybkaer, R., *Pure and Applied Chemistry* 2001, *73* (6), 927-931.

67.   Cornils, B.; Herrmann, W. A., *Aqueous-phase organometallic catalysis : concepts and applications.* 2nd, completely rev. and enl. ed. ed.; Weinheim ; Chichester : Wiley-VCH ; 2004; 750 p.

68.   Griffith, W. P., *Platinum Metals Review* 2003, *47* (4), 175-183.

69.   Tsuji, J., *Palladium reagents and catalysts : new perspectives for the 21st century.* John Wiley & Sons: Chichester, 2004; 656 p.

70.   Rushforth, R., *Platinum Metals Review* 2004, *48* (1), 30-31.

71.   Wataha, J. C.; Shor, K., *Expert Rev Med Devices* 2010, *7* (4), 489-501.

72.   Garrett, C. E.; Prasad, K., *Advanced Synthesis and Catalysis* 2004, *346* (8), 889-900.

73.   Kielhorn, J.; Melber, C.; Keller, D.; Mangelsdorf, I., *Int J Hyg Environ Health* 2002, *205* (6), 417-32.

74.   Canty, A. J., *Accounts of Chemical Research* 1992, *25* (2), 83-90.

75.   Chen, W.; Shimada, S.; Tanaka, M., *Science* 2002, *295* (5553), 308-10.

76.   Crabtree, R. H., *Science* 2002, *295* (5553), 288-9.

77.   Ozawa, F.; Kubo, A.; Hayashi, T., *Chemistry Letters* 1992, (11), 2177-2180.

78.   Hayashi, T.; Kubo, A.; Ozawa, F., *Pure and Applied Chemistry* 1992, *64* (3), 421-427.

79.   Otsuka, S.; Yoshida, T.; Matsumoto, M.; Nakatsu, K., *Journal of the American Chemical Society* 1976, *98* (19), 5850-5858.

80.   Dai, C.; Fu, G. C., *J Am Chem Soc* 2001, *123* (12), 2719-24.

81.   Vicente, J.; Arcas, A., *Coordination Chemistry Reviews* 2005, *249* (11-12), 1135-1154.

82.   Wimmer, S.; Castan, P.; Wimmer, F. L.; Johnson, N. P., *Inorganica Chimica Acta* 1988, *142* (1), 13-15.

83.   Ogo, S.; Takebe, Y.; Uehara, K.; Yamazaki, T.; Nakai, H.; Watanabe, Y.; Fukuzumi, S., *Organometallics* 2006, *25* (2), 331-338.

84.   Hohmann, H.; Hellquist, B.; Vaneldik, R., *Inorganica Chimica Acta* 1991, *188* (1), 25-32.

85.   Hohmann, H.; Van Eldik, R., *Inorganica Chimica Acta* 1990, *174* (1), 87-92.

86.   Berger, J.; Kotowski, M.; Van Eldik, R.; Frey, U.; Helm, L.; Merbach, A. E., *Inorganic Chemistry* 1989, *28* (19), 3759-3765.

87.   Wimmer, F. L.; Wimmer, S.; Afcharian, A.; Castan, P.; Fabre, P. L., *Journal of Chemical Research - Part S* 1999, (3), 194-195.

88.   Jaganyi, D.; Tiba, F.; Munro, O. Q.; Petrovic, B.; Bugarcic, Z. D., *Dalton Transaction* **2006**, (24), 2943-9.

89.   Astruc, D.; Lu, F.; Aranzaes, J. R., *Angewandte Chemie - International Edition* **2005**, *44* (48), 7852-7872.

90.   Bonnemann, H.; Brijoux, W.; Joussen, T., *Angewandte Chemie - International Edition in English* **1990**, *29* (3), 273-275.

91.   Bonnemann, H.; Brijoux, W.; Brinkmann, R.; Dinjus, E.; Fretzen, R.; JouÃŸen, T.; Korall, B., *Journal of Molecular Catalysis* **1992**, *74* (1-3), 323-333.

92.   Ozkar, S.; Finke, R. G., *Journal of the American Chemical Society* **2002**, *124* (20), 5796-5810.

93.   Gittins, D. I.; Caruso, F., *Angew Chem Int Ed Engl* **2001**, *40* (16), 3001-3004.

94.   Ley, S. V.; Mitchell, C.; Pears, D.; Ramarao, C.; Yu, J. Q.; Zhou, W., *Org Lett* **2003**, *5* (24), 4665-8.

95.   Kidambi, S.; Dai, J.; Li, J.; Bruening, M. L., *J Am Chem Soc* **2004**, *126* (9), 2658-9.

96.   Demir, M. M.; Gulgun, M. A.; Menceloglu, Y. Z.; Erman, B.; Abramchuk, S. S.; Makhaeva, E. E.; Khokhlov, A. R.; Matveeva, V. G.; Sulman, M. G., *Macromolecules* **2004**, *37* (5), 1787-1792.

97.   Chauhan, B. P. S.; Rathore, J. S.; Bandoo, T., *Journal of the American Chemical Society* **2004**, *126* (27), 8493-8500.

98.   Sanji, T.; Ogawa, Y.; Nakatsuka, Y.; Tanaka, M.; Sakurai, H., *Chemistry Letters* **2003**, *32* (10), 980-981.

99.   Sawoo, S.; Srimani, D.; Dutta, P.; Lahiri, R.; Sarkar, A., *Tetrahedron* **2009**, *65* (22), 4367-4374.

100.   Ornelas, C.; Boisselier, E.; Martinez, V.; Pianet, I.; Ruiz Aranzaes, J.; Astruc, D., *Chemical Communications (Cambridge)* **2007**, (47), 5093-5.

101.   Ornelas, C.; Salmon, L.; Aranzaes, J. R.; Astruc, D., *Chemical Communication (Cambridge)* **2007**, (46), 4946-8.

102.   Yang, C. C.; Wan, C. C.; Wang, Y. Y., *Journal of Colloid and Interface Science* **2004**, *279* (2), 433-439.

103.   Tan, H.; Zhan, T.; Fan, W. Y., *Chemical Physics Letters* **2006**, *428* (4-6), 352-355.

104.   Fan, F. R.; Adel, A.; Sur, U. K.; Chen, J. B.; Xie, Z. X.; Li, J. F.; Bin, R.; Tian, Z. Q., *Crystal Growth and Design* **2009**, *9* (5), 2335-2340.

105.   Han, W.; Liu, C.; Jin, Z., *Advanced Synthesis and Catalysis* **2008**, *350* (3), 501-508.

106.   Han, W.; Liu, C.; Jin, Z. L., *Organic Letters* **2007**, *9* (20), 4005-4007.

107.   Desmarets, C.; Omar-Amrani, R.; Walcarius, A.; Lambert, J.; Champagne, B.; Fort, Y.; Schneider, R., *Tetrahedron* **2008**, *64* (2), 372-381.

108.   Gallon, B. J.; Kojima, R. W.; Kaner, R. B.; Diaconescu, P. L., *Angewandte Chemie-International Edition* **2007**, *46* (38), 7251-7254.

109.   Diallo, A. K.; Ornelas, C.; Salmon, L.; Aranzaes, J. R.; Astruc, D., *Angewandte Chemie-International Edition* **2007**, *46* (45), 8644-8648.

110.   Saha, D.; Chattopadhyay, K.; Ranu, B. C., *Tetrahedron Letters* **2009**, *50* (9), 1003-1006.

111.   Prastaro, A.; Ceci, P.; Chiancone, E.; Boffi, A.; Cirilli, R.; Colone, M.; Fabrizi, G.; Stringaro, A.; Cacchi, S., *Green Chemistry* **2009**, *11* (12), 1929-1932.

112.   Wang, S.; Zhang, Z.; Hu, Z.; Wang, Y.; Lei, P.; Chi, H., *Journal of Environmental Sciences* **2009**, *21* (Supplement 1), S124-S126.

113.   Yilmaz, U.; Şireci, N.; Deniz, S.; Küçükbay, H., *Applied Organometallic Chemistry* **2010**, *24* (5), 414-420.

114.   Borhade, S. R.; Waghmode, S. B., *Indian Journal of Chemistry - Section B Organic and Medicinal Chemistry* **2010**, *49* (5), 565-572.

115.   Astruc, D., *Inorg Chem* **2007**, *46* (6), 1884-94.

116.   Durap, F.; Rakap, M.; Aydemir, M.; Özkar, S., *Applied Catalysis A: General* **2010**, *382* (2), 339-344.

117.   Søbjerg, L. S.; Gauthier, D.; Lindhardt, A. T.; Bunge, M.; Finster, K.; Meyer, R. L.; Skrydstrup, T., *Green Chemistry* **2009**, *11* (12), 2041-2046.

118.   Molander, G. A.; Canturk, B., *Angewandte Chemie-International Edition in English* **2009**, *48* (49), 9240-61.

119.   Heck, R. F.; Nolley, J. P., *Journal of Organic Chemistry* **1972**, *37* (14), 2320-&.

120.   Mizoroki, T.; Mori, K.; Ozaki, A., *Bulletin of the Chemical Society of Japan* **1971**, *44* (2), 581-&.

121.   Sonogashira, K.; Tohda, Y.; Hagihara, N., *Tetrahedron Letters* **1975**, (50), 4467-4470.

122.   Stille, J. K., *Angewandte Chemie-International Edition in English* **1986**, *25* (6), 508-523.

123.   Negishi, E.; King, A. O.; Okukado, N., *Journal of Organic Chemistry* **1977**, *42* (10), 1821-1823.

124.   King, A. O.; Negishi, E. I.; Villani, F. J.; Silveira, A., *Journal of Organic Chemistry* **1978**, *43* (2), 358-360.

125.   Yamamura, M.; Moritani, I.; Murahashi, S. I., *Journal of Organometallic Chemistry* **1975**, *91* (2), C39-C42.

126.   Suzuki, A.; Miyaura, N., *Abstracts of Papers of the American Chemical Society* **1979**, (Apr), 260-260.

127.   Miyaura, N.; Yanagi, T.; Suzuki, A., *Synthetic Communications* **1981**, *11* (7), 513-519.

128.   Suzuki, A., *Journal of Organometallic Chemistry* **1999**, *576* (1-2), 147-168.

129.   Sicre, C.; Braga, A. A. C.; Maseras, F.; Cid, M. M., *Tetrahedron* **2008**, *64* (30-31), 7437-7443.

130.   Casado, A. L.; Espinet, P., *Organometallics* **1998**, *17* (5), 954-959.

131.   Goossen, L. J.; Koley, D.; Hermann, H.; Thiel, W., *Chemical Communication (Cambridge)* **2004**, (19), 2141-3.

132.   Senn, H. M.; Ziegler, T., *Organometallics* **2004**, *23* (12), 2980-2988.

133.   Zuidema, E.; Van Leeuwen, P. W. N. M.; Bo, C., *Organometallics* **2005**, *24* (15), 3703-3710.

134.   Ahlquist, M.; Norrby, P. O., *Organometallics* **2007**, *26* (3), 550-553.

135.   Smith, G. B.; Dezeny, G. C.; Hughes, D. L.; King, A. O.; Verhoeven, T. R., *Journal of Organic Chemistry* **1994**, *59* (26), 8151-8156.

136.   Matos, K.; Soderquist, J. A., *Journal of Organic Chemistry* **1998**, *63* (3), 461-470.

137.   Braga, A. A. C.; Morgon, N. H.; Ujaque, G.; Lledós, A.; Maseras, F., *Journal of Organometallic Chemistry* **2006**, *691* (21), 4459-4466.

138.   Amatore, C.; Jutand, A.; Le Duc, G., *Chemistry* **2011**.

139.   Jover, J.; Fey, N.; Purdie, M.; Lloyd-Jones, G. C.; Harvey, J. N., *Journal of Molecular Catalysis A: Chemical* **2010**, *324* (1-2), 39-47.

140.   Miyaura, N.; Suzuki, A., *Chemical Reviews* **1995**, *95* (7), 2457-2483.

141.   Miyaura, N., *Journal of Organometallic Chemistry* **2002**, *653* (1-2), 54-57.

142.   Campi, E. M.; Jackson, W. R.; Marcuccio, S. M.; Naeslund, C. G. M., *Journal of the Chemical Society, Chemical Communications* **1994**, (20), 2395.

143.   Song, Z. Z.; Wong, H. N. C., *Journal of Organic Chemistry* **1994**, *59* (1), 33-41.

144.   Moreno-Mañas, M.; Pérez, M.; Pleixats, R., *Journal of Organic Chemistry* **1996**, *61* (7), 2346-2351.

145.   Aramendia, M. A.; Lafont, F.; Moreno-Manas, M.; Pleixats, R.; Roglans, A., *Journal of Organic Chemistry* **1999**, *64* (10), 3592-3594.

146.   Koza, D. J.; Carita, E., *Synthesis* **2002**, (15), 2183-2186.

147.   Yoshida, H.; Yamaryo, Y.; Ohshita, J.; Kunai, A., *Tetrahedron Letters* **2003**, *44* (8), 1541-1544.

148.   Adamo, C.; Amatore, C.; Ciofini, I.; Jutand, A.; Lakmini, H., *Journal of the American Chemical Society* **2006**, *128* (21), 6829-36.

149.   Lakmini, H.; Ciofini, I.; Jutand, A.; Amatore, C.; Adamo, C., *Journal of Physical Chemistry A* **2008**, *112* (50), 12896-903.

150. Vyskočil, Š., Meca, L., Tišlerová, I., Císařová, I., Polášek, M.; Harutyunyan, S. R.; Belokon, Y. N.; Stead, R. M. J.; Farrugia, L.; Lockhart, S. C.; Mitchell, W. L.; Kočovský, P., *Chemistry - A European Journal* **2002**, *8* (20), 4633-4648.

151. Gillis, E. P.; Burke, M. D., *Journal of the American Chemical Society* **2008**, *130* (43), 14084-5.

152. Lazarova, T. I.; Jin, L.; Rynkiewicz, M.; Gorga, J. C.; Bibbins, F.; Meyers, H. V.; Babine, R.; Strickler, J., *Bioorg Med Chem Lett* **2006**, *16* (19), 5022-7.

153. Jagannathan, S.; Forsyth, T. P.; Kettner, C. A., *Journal of Organic Chemistry* **2001**, *66* (19), 6375-80.

154. Allen, L. M.; Roscoe, C. W., *Journal of Pharmceutical Science* **1969**, *58* (3), 368-9.

155. Roth, H. J.; Miller, B., *Archive de Pharmazie (Weinheim)* **1964**, *297*, 513-23.

156. Tyrrell, E.; Brookes, P., *Synthesis* **2003**, (4), 469-483.

157. Hall, D., *Boronic acids : preparation and applications in organic synthesis and medicine*. Wiley-VCH ; Chichester : John Wiley: Weinheim, **2005**; p xxv, 549 p.

158. Kua, J.; Fletcher, M. N.; Iovine, P. M., *Journal of Physical Chemistry A* **2006**, *110* (26), 8158-8166.

159. Tokunaga, Y.; Ueno, H.; Shimomura, Y.; Seo, T., *Heterocycles* **2002**, *57* (5), 787-790.

160. Kuivila, H. G.; Nahabedian, K. V., *Journal of the American Chemical Society* **1961**, *83* (9), 2164-2166.

161. Kuivila, H. G.; Nahabedian, K. V., *Journal of the American Chemical Society* **1961**, *83* (9), 2159-2163.

162. Yan, J.; Springsteen, G.; Deeter, S.; Wang, B., *Tetrahedron* **2004**, *60* (49), 11205-11209.

163. Settepani, J. A.; Stokes, J. B.; Borkovec, A. B., *Journal of Medicinal Chemistry* **1970**, *13* (1), 128-131.

164. Dewar, M. J. S.; Jones, R., *Journal of the American Chemical Society* **1967**, *89* (10), 2408-2410.

Homocoupling of arylboronic acids using a molecular Pd-catalyst in aqueous micellar media

(*kinetic and mechanistic studies*)

Abstract

The micelle-assisted palladium-catalysed aerobic oxidative homocoupling reaction of a series of (substituted) arylboronic acids in aqueous surfactant solutions has been studied. A bisimidazole complex of palladium, *viz.* bis(1-methylimidazole-2-yl)methyl-(methylthiomethyl)-methane palladium chloride [Pd(bimsulfide)Cl$_2$], was found to be a sufficiently stable catalyst to allow kinetic studies. Cetyltrimethylammonium bromide (CTAB) was used as a surfactant and the effect of the surfactant concentration on the reaction rate was found to be in good agreement with the pseudophase model for bimolecular reactions in micellar solutions. A linear relation was observed between the observed rate constant and the catalyst concentration indicating the reaction is first order in catalyst. The effect of arylboronic acid concentration on the reaction rate showed that the reaction is not first-order in the arylboronic acid, with a decrease in the observed rate constant with increasing arylboronic acid concentration. The observed pH-rate profile for the reactions was found to be bell-shaped for all substrates investigated. These bell-shaped pH-rate profiles made us propose several potential mechanisms for the homocoupling reaction, including a) the requirement of acidic and basic forms of the arylboronic acids at two different transmetalation steps in the catalytic cycle, also indicating the presence of a pH-dependent resting step for the catalyst and b) pH-dependent protonation states of both key intermediates on the catalytic cycle and the arylboronic acid so that the bell-shaped pH-rate profile might arise from the combination of the requirement of the acidic form of the catalyst with the basic form of the arylboronic acid in one transmetalation step or *vice versa*. The most likely mechanism involves a palladium-hydroxo complex reacting with the acidic form of the arylboronic acid in the rate-determining step. However, a mechanism involving rate-determining transmetalation involving a palladium-aqua complex reacting with the basic form of the arylboronic acid cannot be excluded.

39

2.1. Introduction

Developing straightforward and more environmentally friendly reactions for aryl–aryl

coupling is a matter of interest, because the bi-aryl motif is present in a large variety of

common organic compounds (*e.g.* pharmaceuticals, herbicides, natural products,

conducting polymers and liquid crystalline materials).[1] The well-known Suzuki-Miyaura

(2010 Nobel prize laureate) cross-coupling reaction[2] (illustrated for arylboronic acids and

aryl halides in Scheme 2.1) allows the synthesis of unsymmetrical bi-aryls in high yields.

The mechanism of the reaction is generally accepted to involve oxidative addition of an

aryl halide to a Pd^0-catalyst followed by a transmetalation step requiring basic conditions.

Upon subsequent reductive elimination, the biaryl product forms and the Pd^0-catalyst is

regenerated.[3]

X= (pseudo)halide
R_1, R_2= H, alkyl, etc.
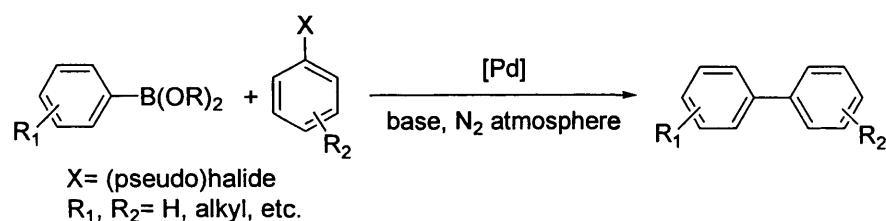
Scheme 2.1

The related palladium-catalysed reductive homocoupling reaction of electrophilic aryl

derivatives Ar'X (X=I, Br, Cl, OTf) in the presence of reducing agents produces

symmetrical biaryls (Scheme 2.2).[4, 5] This reductive coupling has been widely studied and

its mechanism has been elucidated. The key step was found to be the oxidative addition of

the second molecule of the aryl halide to an anionic arylpalladium(0) complex

$ArPd^0(PPh_3)_2^-$, affording a transient pentacoordinated species which undergoes rapid loss

of halide ligand X⁻, followed by reductive elimination to produce the biaryl product and

regenerate the Pd^0 active species.[5, 6]

X = I, Br, Cl, OTf
R_1= H, alkyl, or any other groups
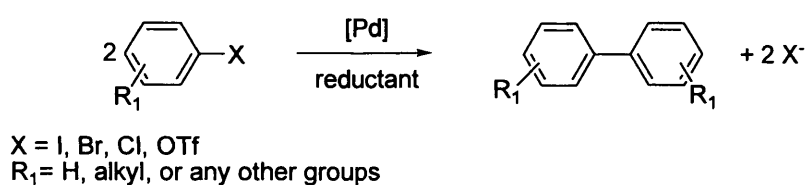
Scheme 2.2

Symmetrical biaryls can similarly be formed via the oxidative homocoupling of

arylboronic acids (Scheme 2.3) which is a known side reaction of the Suzuki cross-

coupling reaction.[2, 7]

R_1= H, alkyl, or any other groups
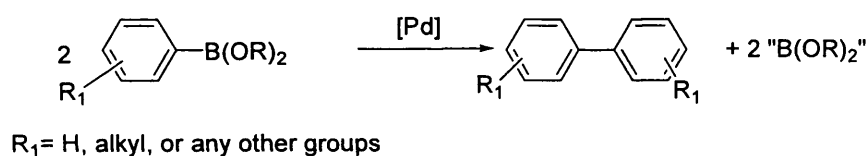
Scheme 2.3

Recently, the oxidative homocoupling reaction of arylboronic acids has been developed

from a side reaction of the Suzuki cross-coupling to a synthetically useful transformation

involving the use of atmospheric dioxygen as an oxidant.[8-17] Typically, these oxidative

homocoupling reactions are carried out in the presence of palladium species carrying

phosphine ligands (Ph_3P) and a base (e.g. NEt_3, TMEDA and Na_2CO_3).[9] More recent

interest in these oxidative dimerisation reactions for the synthesis of symmetric bi-aryls

has focussed on reactions in the absence of either a base[10] or a phosphine ligand,[11-16]

mostly employing polar organic solvents such as DMF and DMSO. Phenols have been

found to be common by-products of the Pd-catalysed homocoupling of arylboronic acids

in the presence of dioxygen.[9, 10, 18]

Despite numerous reports on the development and use of the oxidative homocoupling of a

variety of arylboronic reagents, very little is known about the precise mechanistic details

of the catalysis.[19-21] A first detailed mechanism was proposed by Moreno-Mañas and co-

workers involving the oxidative addition of arylboronic acids to Pd(0) complexes with the

generation of $ArPd^{II}$-$[B(OH)_2](PPh_3)_2$.[8] Almost 10 years after this hypothesis, Adamo *et*

al.[21, 22] reported both kinetic and computational evidence for an alternative mechanism for

the palladium-catalysed homocoupling of $ArB(OH)_2$ in the presence of dioxygen (Scheme

2.4).
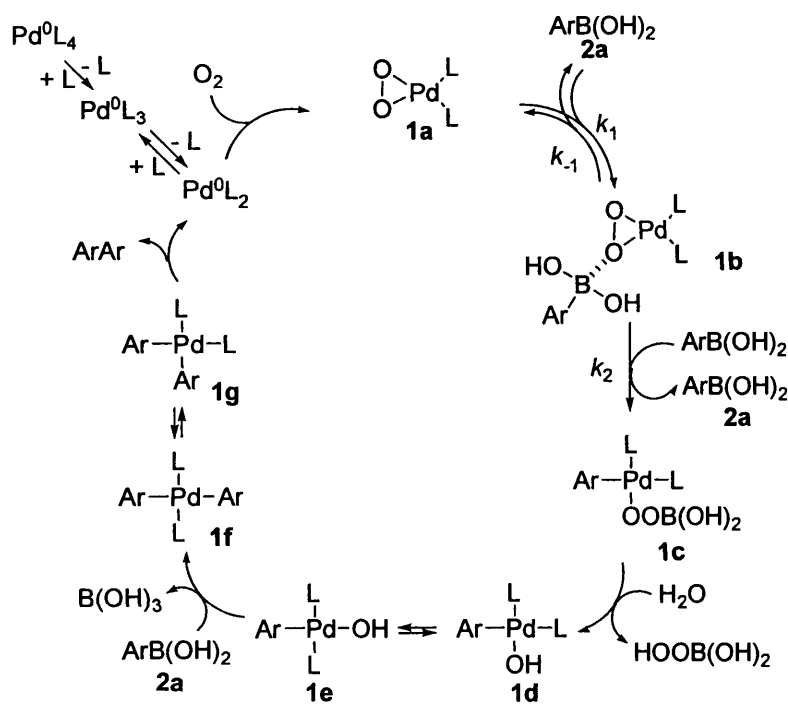
Scheme 2.4 reproduced from ref[20]

Adamo *et al.* showed that a peroxo complex of palladium, *viz.* $(\eta^2\text{-}O_2)Pd(PPh_3)_2$ **1a**, plays a key role in the catalytic homocoupling of arylboronic acids. The authors focussed on this palladium peroxo complex **1a**, which is generated in the reaction of dioxygen with the Pd(0) catalyst. It was found that this peroxo complex is at the origin of the formation of trans-Ar-Pd^{II}(OH)L$_2$ **(1e)** via activation of one of its Pd^{II}-O bonds by a first molecule of arylboronic acid, acting as a Lewis acid catalyst, followed by a transmetalation step involving a second molecule of arylboronic acid. Intermediate **1e** then reacts with a further molecule of arylboronic acid to give trans-ArPdArL$_2$ complex **1f** in a second transmetalation step. The biaryl is formed through the usual reductive elimination. Adamo's kinetic data showed first-order dependence of the reaction rate on the catalyst and second-order dependence on the arylboronic acid. The fact that the reaction is first order in catalyst and second order in the arylboronic acid was interpreted as the step involving the conversion of **1a** to **1c** in Scheme 2.4 being the rate-determining step.

Adamo *et al.* further suggested that H_2O_2 is produced in the Pd-catalysed oxidative homocoupling reaction of phenylboronic acids in the presence of dioxygen as a result of hydrolysis of $HOOB(OH)_2$. H_2O_2 then reacts with a molecule of $ArB(OH)_2$ to form the phenol by-product of the oxidative homocoupling reaction (Scheme 2.5).[21]

$$HOOB(OH)_2 + H_2O \longrightarrow B(OH)_3 + H_2O_2$$

$$ArB(OH)_2 + H_2O_2 \longrightarrow B(OH)_3 + ArOH$$
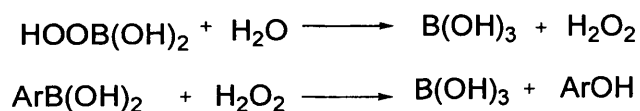
Scheme 2.5

### 2.1.1. Micellar and micelle-assisted catalysis

Unfortunately, many organic compounds as well as organometallic catalysts are insoluble in water. One way to improve the solubility of organic substrates in water is the use of

surfactants that can form micelles.[23] Micelles[24, 25] can enhance to a great extent the solubility of hydrophobic substrates in aqueous media and provide an interesting platform for increasing the rate of a reaction. It has recently been shown that formation of C-C and C-O bonds occurs efficiently in water in the presence of surfactants. For example, Arcadi et al.[26] have demonstrated that a system involving water/surfactant/palladium-catalyst can accomplish the Suzuki-Miyaura (SM) coupling reaction under milder and more environmentally friendly conditions. Other C-C and C-O bond formation reactions were also successfully performed in aqueous micellar solution.[24, 27]

Observed rate effects exerted by micelles are the result of (typically) high local reactant concentrations in combination with local reaction medium effects affecting local rate constants. Scheme 2.6 illustrates micelle-assisted catalysis for a bimolecular reaction involving two reactants (R_A and R_B) also involving the use of oxygen as an oxidant.
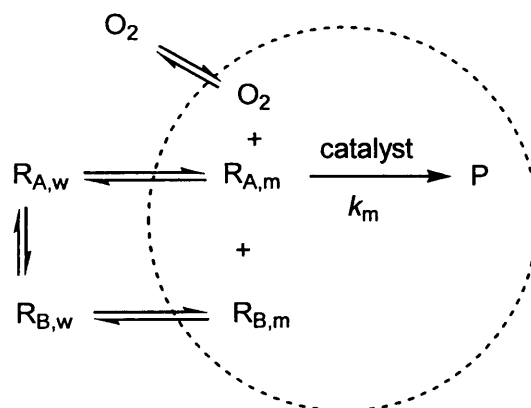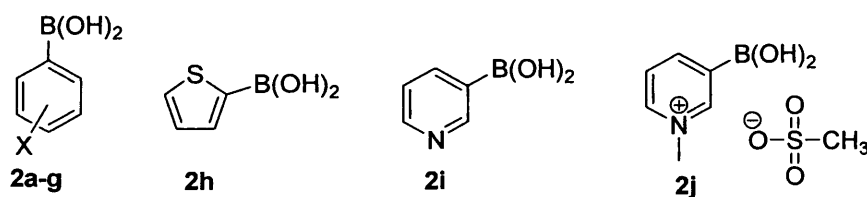

Scheme 2.6

2.2. Aims

Based on the observation that the related Suzuki-Miyaura cross-coupling reaction is compatible with the use of aqueous solvent systems and in light of the advances in

aqueous Pd-catalysed C-C bond-forming reactions in general,[28] we selected the oxidative

coupling reaction of arylboronic acids for detailed kinetic studies using aqueous solutions

as solvent. We further opted for the use of surfactants to avoid heterogeneous systems

consisting of an organic co-solvent in combination with an aqueous solution, facilitating

our kinetic studies.[29]

Here, we report detailed kinetic and mechanistic studies of the aqueous micelle–assisted

catalysis of the oxidative homocoupling reaction of arylboronic acids **2a-j** (Scheme 2.7),

complementing the work of Adamo *et al.*[21] by providing a kinetic description of the

overall processes involved in the aerobic oxidative homocoupling reaction of arylboronic

acids starting with a Pd^{II}-based pre-catalyst.

2a X = H, **2b** X = 4-MeO, **2c** X = 2-MeO, **2d** X = 4-COOH, **2e** X = 4-COCH₃,
2f X = 3,5-difluoro, and **2g** X = 4-NO₂
2h = 2-thiopheneboronic acid, **2i** = 3-pyridineboronic acid,
**2j** = 1-methylpyridinium methyl sulfate-3-boronic acid,

Scheme 2.7

2.3. Results and discussion

2.3.1. Catalyst selection

To allow reproducible kinetics of catalytic reactions, a sufficiently stable (pre) catalyst is

required.[30] For our kinetic studies, we used a Pd^{II} pre-catalyst stabilised by a bidentate

bisimidazole ligand, *viz.* **3** (Scheme 2.8). The selection of this catalyst was based on a

limited screening of Pd-complexes readily available to us, *viz.* Pd⁰(PPh₃)₄, Pd^{II}(OAc)₂,

$Pd^{II}Cl_2(MeCN)_2$, $Pd^0(dba)_2$, Pd-ipr-PEPPSI and $Pd^{II}(bimsulfide)Cl_2$, using catalyst stability in stock solutions and under typical reaction conditions as a sole criterion (Figures 2.1 a and b).

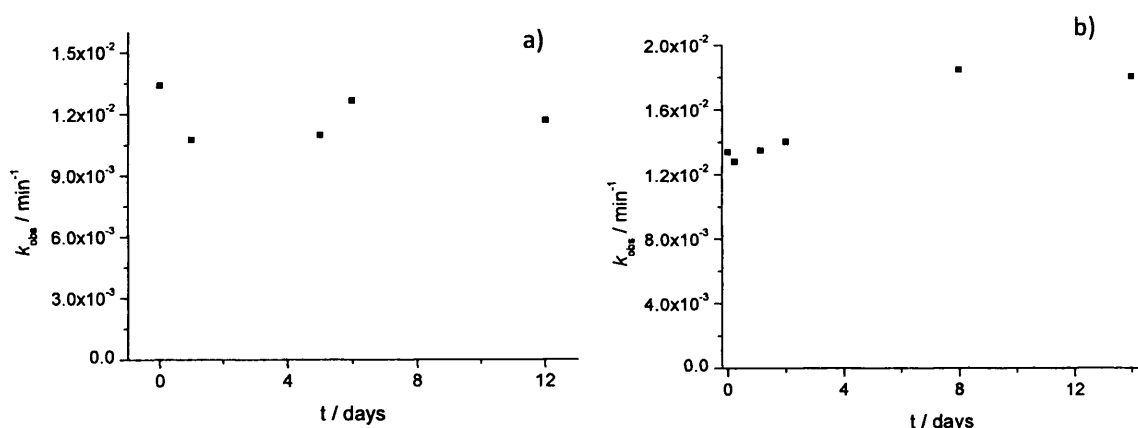**3**   Pd-PEPSI-iPr
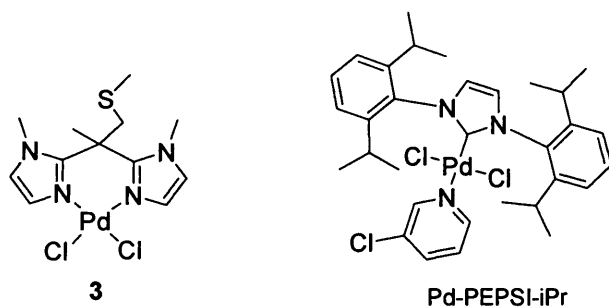
Scheme 2.8

Figure 2.1: k_{obs} for the reaction of 0.1 mM **2a** in 10.0 mM CTAB, 2.0 mM K_2CO_3, 27.0 µM catalyst at 30 °C versus time for which the [Pd(bimsulfide)Cl_2] catalyst was kept prior to kinetic experiments in **a)** acetonitrile stock solution and **b)** under reaction conditions, but in the absence of phenylboronic acid.

Figure 2.1a shows that the observed rate constant (k_{obs}) for the homocoupling reaction of **2a** remains nearly constant over time. Figure 2.1b shows that the catalyst stock solution prepared in CTAB solution gives reproducible kinetics for at least 2 days after which a slight increase in k_{obs} occured. These observations led us to use the catalyst stock solution (in acetonitrile) to allow for reproducible kinetic studies. While Pd^{II}-complex **3** was

selected because it allowed reproducible kinetic studies, it is noted that both Pd^0

complexes led to higher reactivity (*vide infra*).

2.3.2. Non-pseudo-first-order kinetics

The homocoupling reactions of **2a-j** (Scheme 2.9) were followed using UV-Visible

spectroscopy by measuring the absorbance of the reaction mixture at appropriate

wavelengths over time.
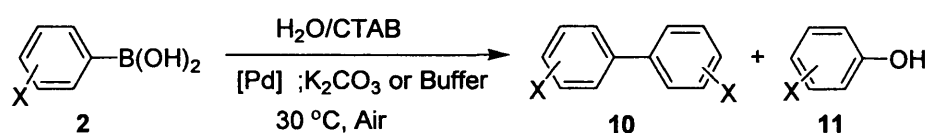
Scheme 2.9

The oxidative homocoupling reaction of phenylboronic acid (used as a model for our

optimisation studies) using complex **3** as a catalyst was followed using UV-Visible

absorption spectroscopy (Figure 2.2).
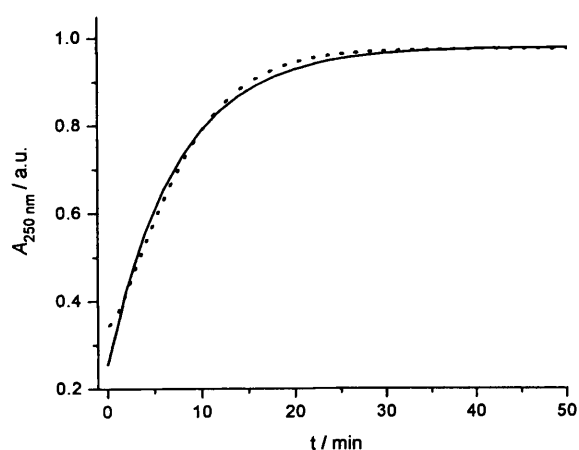
Figure 2.2: Absorbance of the reaction mixture of the homocoupling of 0.1 mM **2a** using 27.0 µM of **3** with time at 250 nm in 10.0 mM CTAB and borate buffer pH 9.2 at 30 °C, experimental data (dotted line), solid line fit to the (pseudo) first-order equation (2.1).

Figure 2.2 shows that the reaction is clearly not (pseudo) first-order. Nevertheless, observed rate constants k_{obs} were determined from plots of absorbance as a function of time, using the first-order rate law (equation 2.1).

$$A_t = A_f + \Delta A \cdot e^{-k_{obs} \cdot t} \qquad\qquad (2.1)$$

Where A_t is the absorbance of the solution at time t, A_f is the final absorbance, ΔA the difference of the absorbance at time zero (A_o) and the final absorbance, and k_{obs} is the observed rate constant for the reaction. Consequently all rate constants are expressed as observed pseudo-first-order rate constants.

The particular pattern of the deviations of the first-order fit from the experimental data suggests that the reaction is subject either to an induction period or zeroth order kinetics at the start. Stronger deviations from the first-order rate law are observed when Pd^{II}-PEPPSI-iPr complex is used as a catalyst (Figure 2.3a) and these are strongly suggestive of an induction period and not zeroth-order behaviour, suggesting that the deviations observed for **3** also correspond to an induction period and not to initial zeroth order behaviour. If, however, a Pd^0-complex ($Pd^0(bda)_2$) is used as a catalyst, under further identical conditions, the observed data follows the first-order rate law well (Figure 2.3b).
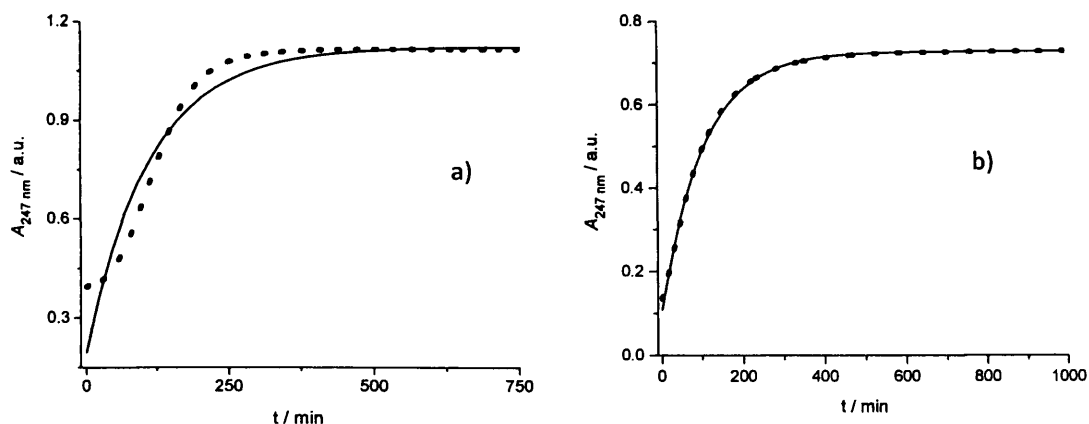
Figure 2.3: Absorbance of the reaction of 0.1 mM **2a** in 10.0 mM CTAB and borate buffer pH 9.2, using a) 27.0 µM Pd^{II}-PEPPSI-ipr catalyst and b) 2.0 µM $Pd^0(dba)_2$ catalyst, at 30 °C versus time. Experimental data (dotted line), solid line fit to the (pseudo) first-order equation (1).

These observations suggest that **3** is a pre-catalyst which is reduced under reaction conditions to form an active Pd^0-species. The idea that a Pd^0 species is the active catalyst is in agreement with observations by Adamo *et al.*[21, 22] The hypothesis that **3** is turned into the active catalyst under reaction conditions was tested by addition of further aliquots of phenylboronic acid to reaction mixtures following experiments (Figures 2.4a-d).
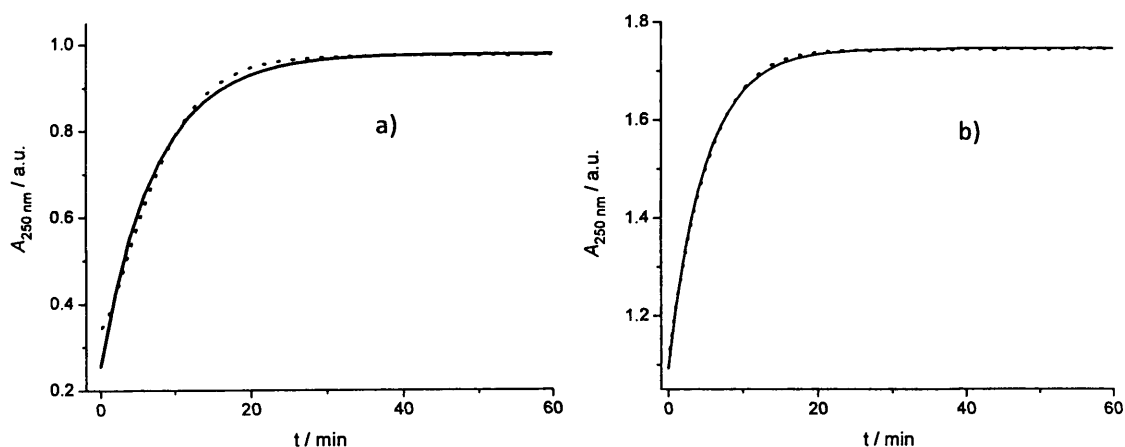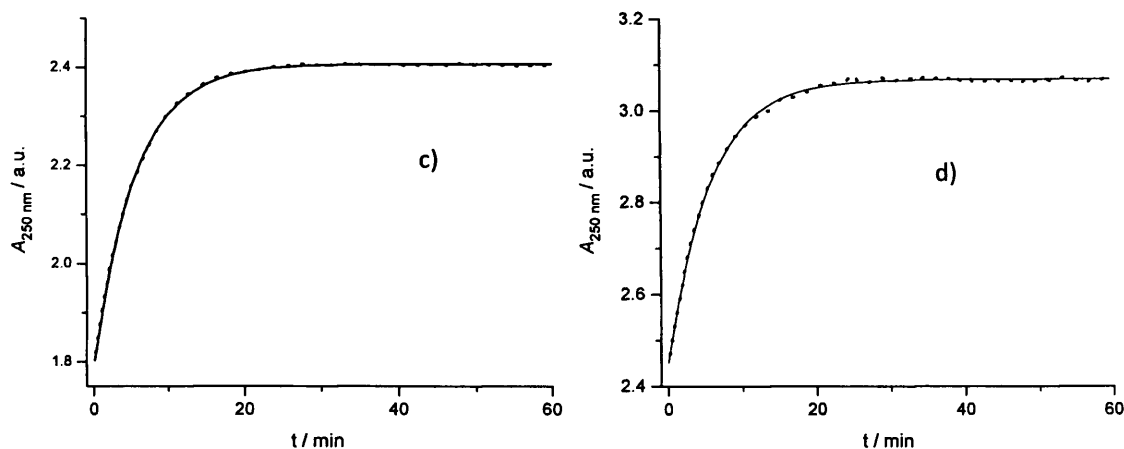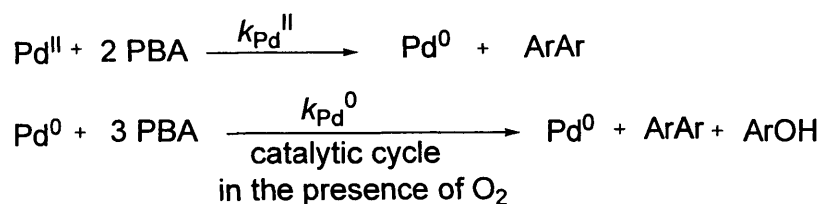
Figure 2.4: Pd^{II}-Pd^0 activation by successive addition of **2a**; a) 0.1 mM, b) +0.1 mM, c) +0.1 mM, and d) +0.1 mM. Reactions were performed using 40.0 µM catalyst, 10.0 mM CTAB and 10.0 mM borate buffer pH 9.2 and at 30 °C. Experimental data (dotted line), solid line fit to the (pseudo) first-order equation (2.1).

Figure 2.4 shows that subsequent additions of **2a** resulted in kinetics following the first-order rate law increasingly well, combined with an increase in k_{obs}.

A mechanism for the reduction of pre-catalyst **3** to form an active Pd^0-complex involves a first homocoupling reaction involving two molecules of phenylboronate or phenylboronic acid (Scheme 2.10).

$$Pd^{II} + 2\ PBA \xrightarrow{\ k_{Pd}^{II}\ } Pd^0 + ArAr$$

$$Pd^0 + 3\ PBA \xrightarrow[\substack{\text{catalytic cycle}\\ \text{in the presence of } O_2}]{\ k_{Pd}^0\ } Pd^0 + ArAr + ArOH$$

Scheme 2.10

The induction period therefore corresponds to a Pd^{II}-mediated homocoupling reaction which also forms a Pd^0-complex. This Pd^0-complex itself is a more active catalyst in the aerobic homocoupling reaction of phenylboronic acids because it can form the particularly

active palladium-peroxo complex postulated by Adamo *et al.*,[21, 22] which itself is formally

a Pd^{II}-species.

Accordingly, the use of oxidants other than molecular oxygen still results in an oxidative

homocoupling reaction of phenylboronic acids, albeit at a lower rate than the aerobic

oxidative homocoupling reaction (*vide infra*).

Preliminary simulation of the system of differential equations corresponding to the

Scheme 2.10 (using MATHCAD) gave us an estimated value of $k_{Pd}^{II} = 6.0 \times 10^2$ M^{-1} s^{-1} and

$k_{Pd}^0 = 36.4 \times 10^2$ M^{-1} s^{-1} for a system mimicking the same conditions as in Figure 2.2.

2.3.3. Product analysis

The composition of the product mixtures of the reaction involving phenylboronic acid

were determined by HPLC and ^1H NMR (*vide infra*) and compared with authentic

samples. It was found that the products (biphenyl and phenol) were formed in a 1:1 ratio

for the reaction of **2a** (also see Table 2.1 for other arylboronic acids) under our optimum

reaction conditions (*vide infra*) (see Figures S6-20 in Appendix 1 for the HPLC

chromatograms and calibration graphs). The fact that the ratio between biphenyl and

phenol is 1:1 for **2a** throughout the reaction of **2a** suggests that the reaction between the

previously proposed peroxide[21] side product and **2a** to produce the phenol is fast.

2.3.4. Effect of phenylboronic acid concentration

In order to further study the order of the reaction in phenylboronic acid, we studied the

effect of phenylboronic acid concentration on the reaction rate under otherwise standard

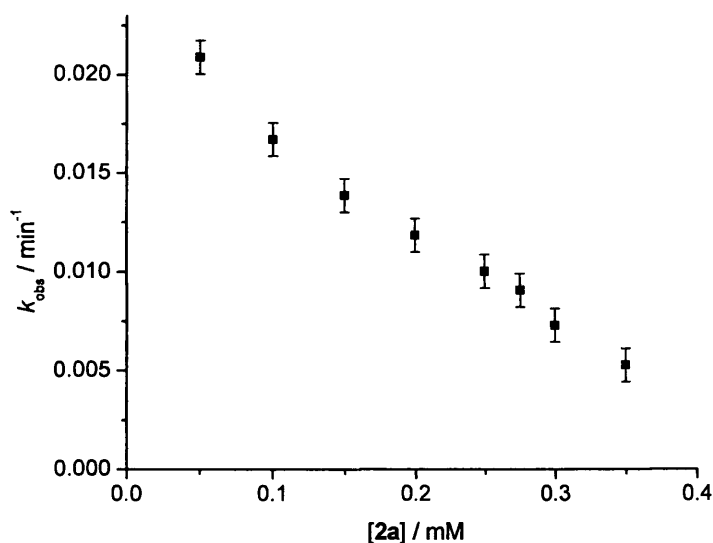conditions (*vide infra*) at 30 °C and pH 9.2 (Figure 2.5).

Figure 2.5: Effect of **2a** concentration on the observed reaction rate constant using 5.0 μM of **3**, 10.0 mM CTAB and borate buffer pH 9.2 at 30 °C. The error margins were determined for one concentration (standard deviation for three repeat measurements), and assumed to be the same for the other data points. This is the case in for error margins for further kinetic experiments as well.

Figure 2.5 shows that the observed pseudo-first-order rate constant decreases with increasing concentration of **2a** (the same trend was observed at pH 7.4 and also after activation of **3**, see Figure S1 in Appendix1). There are several potential explanations for this decrease in the observed rate constant with increasing concentration of phenylboronic acid. *First,* the decrease in rate constant with increasing concentration of phenylboronic acid might be due to a decreasing O_2 concentration during the reaction. However, we have found that stirring does not have any effect on k_{obs} which indicates that O_2 transfer from the atmosphere to the solution is not the rate-limiting step (Figure 2.6).
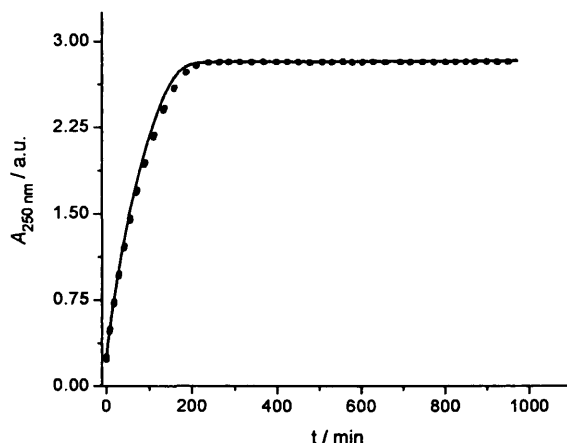
Figure 2.6: Effect of stirring on the observed reaction rate constant for the homocoupling of 0.35 mM **2a** using 10.0 μM of **3**, 10.0 mM CTAB and borate buffer pH 9.2 at 30 °C. With stirring (dotted line), solid line without stirring.

Second, the reaction could be inhibited by either of the products biphenyl or phenol. Experiments involving multiple additions of phenylboronic acid, however, result in constant rate constants suggesting that product inhibition does not occur. Also, we have performed the homocoupling reaction of **2a** under our optimised conditions using solutions containing added biphenyl and phenol (Figure 2.7).
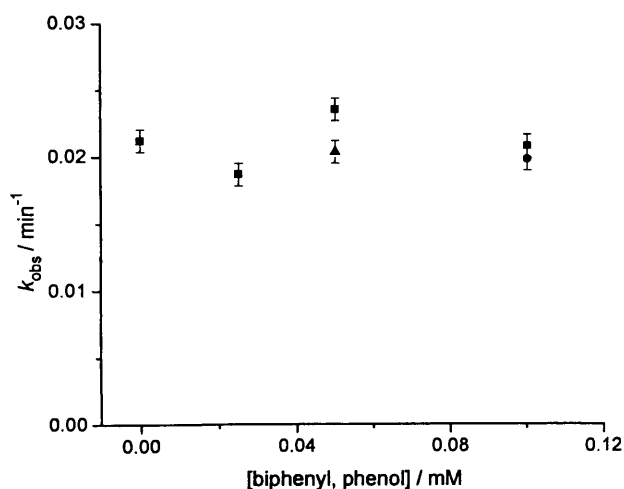

Figure 2.7: Effect of an added mixture of biphenyl and phenol (■), of added biphenyl (▲) and of added phenol (●) on the observed reaction rate constant for the homocoupling of 0.1 mM **2a** using

5.0 μM of **3**, 10.0 mM CTAB and borate buffer pH 9.2 at 30 °C.

Figure 2.7 shows that the pre-addition of biphenyl and phenol mixtures of different concentration does not affect significantly the value of k_{obs} for the aerobic homocoupling reaction of **2a** under our reaction conditions.

Third, phenylboronic acid may dimerise or trimerise,[31] kinetically resulting in inverse dependencies on phenylboronic acid concentration (Scheme 2.11). The dimerisation and trimerisation of phenylboronic acid is most likely to happen in the hydrophobic part (core) of the micelles. However, these dimers and/or trimers hydrolyse easily to the corresponding phenylboronic acids under aqueous conditions.[31, 32] As a result of the highly dynamic structure of the micelles,[33] these dimers and/or trimers will be continuously formed and hydrolysed. The increase of phenylboronic acid concentration increases the possibility of dimer and/or trimer formation which might be one of the causes of decreasing k_{obs} with the increase of phenylboronic acid concentration.
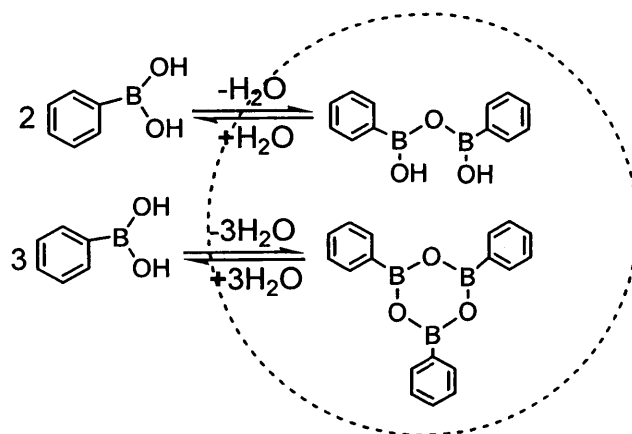
Scheme 2.11

Fourth, the effect of added cetyltrimethylammonium bromide (CTAB) on the reaction varies considerably depending on the phenylboronic acid concentration used (*vide infra*),

suggesting kinetic complexity deriving from phenylboronic acid distribution over the aqueous and micellar pseudophases.

Unfortunately, the origin of the decrease in observed rate constants with increasing phenylboronic acid concentration remains elusive. Nevertheless, hypotheses three and four both stem from equilibrium/distribution effects affecting arylboronic acids, but none of the other reactants. Consequently, in order to avoid difficulties, all further experiments were performed using arylboronic acid concentrations of 100 µM, ensuring virtually constant k_{obs} during experiments.

2.3.5. The homocoupling of boronic acids has a maximum rate near the pK_a of the reactant

Following a preliminary round of optimisation of reaction conditions we studied the effect of base concentration on the reaction as quantified by the observed first-order rate constant using K_2CO_3 as a base because it had previously been found to be a good base for the homocoupling coupling reaction (Figures 2.8 a and b).[6]

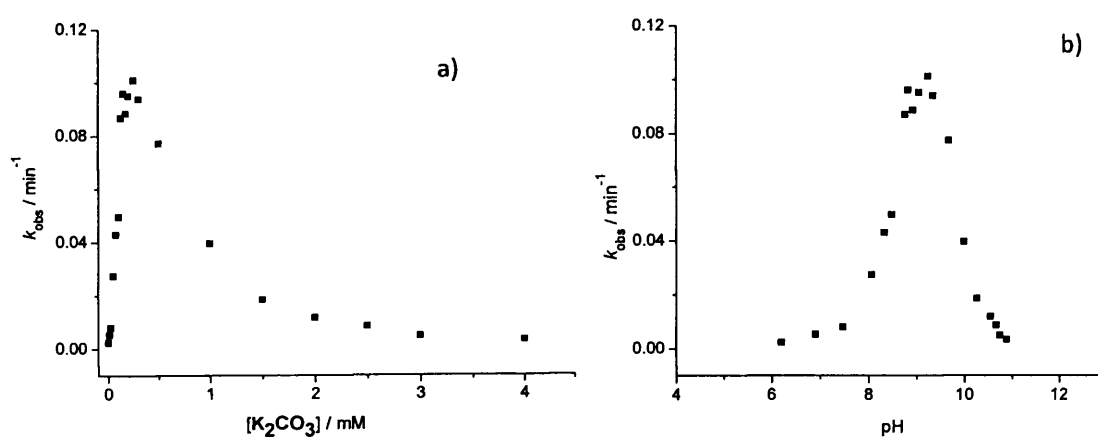**Figure 2.8:** Effect of a) [K_2CO_3] and b) pH on the observed reaction rate constant for the homocoupling of 0.1 mM **2a** using 27.0 µM of **3**, 10.0 mM CTAB at 30 °C.

Figure 2.8 shows a curious dependence on base concentration, which turned out to be the result of an underlying pH-rate profile showing a maximum in k_{obs} in the region covered.

We tested both 2-amino-2-methylpropane-1,3-diol (AMPD) and borate as buffers because both have buffer capacity in the range between 7.2-10. AMDP retarded the homocoupling reaction which we attribute to complex formation with **2a** forming a dative bond (Scheme 2.12). The formation of such a complex was confirmed by a UV-Visible titration and we observed a binding constant of 250.7 mol^{-1} dm^3 for a stoichiometry restricted to a value of 1.0 (see Figure S2 in Appendix 1).
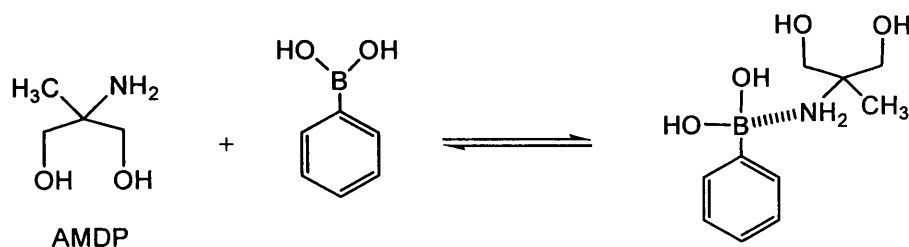
Scheme 2.12

Subsequent reactions were all performed using borate buffer (which has buffer capacity between pH 7.2 and 10) for controlling the pH (*vide infra*). We studied the effect of pH on the reaction using a borate buffer for the reaction of phenylboronic acid (Figure 2.9).
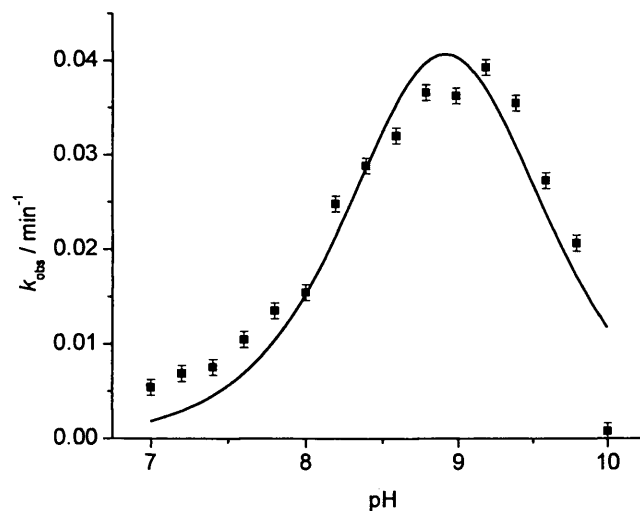
56

Figure 2.9: Effect of pH on k_{obs} for the reaction involving 0.1 mM **2a** (■), solid line is a fit to a Gaussian (eqn. 2.2), using 10 mM CTAB, 10 mM borate buffer and 10 µM of 3 at 30 °C.

The optimum pH for the reaction, pH_{opt}, was estimated by fitting a Gaussian to the kinetic data (equation 2.2).

$$k_{obs} = k' \left(\left(\frac{1}{1+10^{pH-pH_{opt}}} \right) \left(\frac{10^{pH-pH_{opt}}}{1+10^{pH-pH_{opt}}} \right) \right)$$ (2.2)

Where pH_{opt} is the optimum pH of the reaction solution and k' the maximum observed rate constant. It is stressed, however, that this procedure provides an estimate for pH_{opt} and the fit in terms of a Gaussian is not dictated by a pre-conceived mechanism or assumed rate law. The optimum pH for the homocoupling of **2a** was found to be 8.9 which is slightly lower than, but remarkably close to, the pK_a of **2a** of 9.1 as determined under reaction conditions (*vide infra*).

2.3.6. pH optimum for 2a

To investigate whether the observed pH optimum is the result of the entry route into the catalytic cycle (*vide supra*) or whether it is intrinsic to the catalytic cycle, the pH-

dependence of the reaction following catalyst activation was studied (Figure 2.10). The

reactions were performed by addition of different aliquots of 2a at the end of each reaction
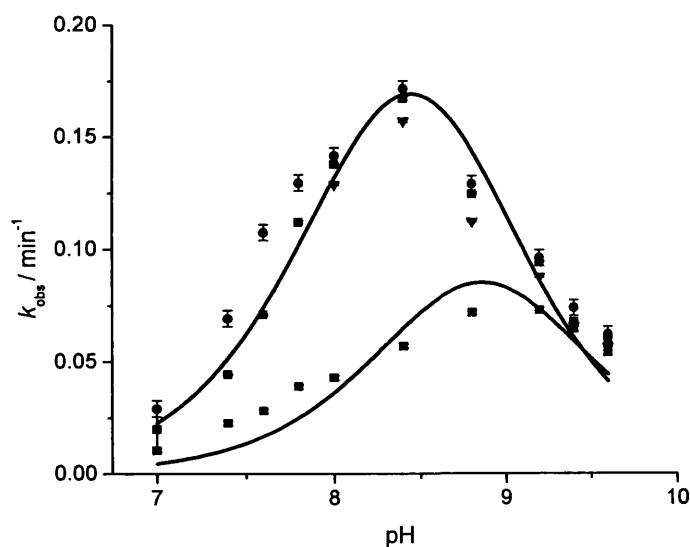
and the kinetics were followed as usual.

Figure 2.10: Pd^{II}-Pd^0 activation and pH effect for the reaction of 0.1 mM **2a** acid using 27.0 µM **3** in 10.0 mM CTAB and borate buffer at 30 °C. Without activation (■), addition of an additional 0.05 mM **2a** (●), addition of a further 0.05 mM **2a** (▲), and addition of third aliquot of 0.05 mM **2a** (▼). solid line is a fit to a Gaussian (eqn. 2.2)

Notwithstanding the shift in optimum pH following catalyst activation (Figure 2.10), the

reaction still shows a rate maximum, *i.e.* the isolated catalytic cycle displays a rate

maximum and the observed pH effect on the aerobic homocoupling reaction of

phenylboronic acid is not (solely) due to the catalyst activation step.

2.3.7. Effect of borate buffer concentration

Under our optimised conditions we studied the effect of borate buffer concentration on the

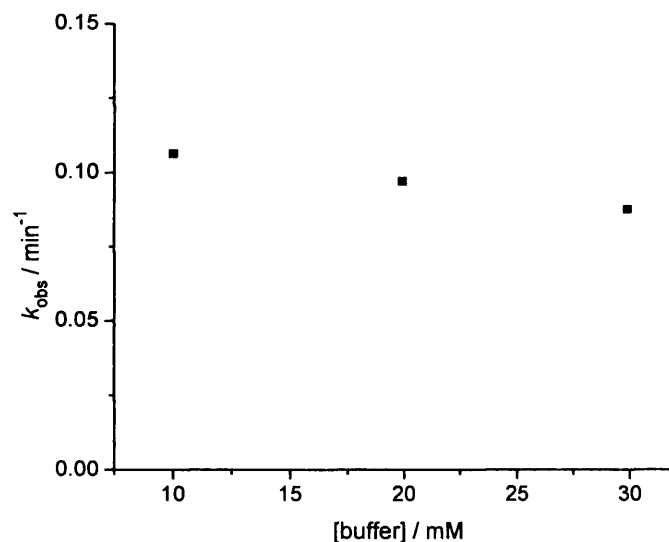observed rate constant for the homocoupling reaction of **2a** (Figure 2.11).

Figure 2.11: Effect of borate buffer concentration on k_{obs} for the reaction of 0.1 mM **2a** using 27.0 μM of **3** in 10.0 mM CTAB and borate buffer pH 9.2 at 30 °C.

Figure 2.11 shows that there is no significant effect of buffer concentration on the observed rate constant. The absence of buffer catalysis is of particular interest because this observation, together with the decrease in k_{obs} with increasing concentration of **2a**, leads us to conclude that the rate-limiting step involving activation of peroxo-Pd-complex **1a** by arylboronic acid **2a** as proposed by Adamo et al.[21] for the reaction in chloroform (Scheme 2.4) is not occurring, or at least not rate limiting, under our reaction conditions.

2.3.8. The observed pH-rate profile is general for arylboronic acids

To check whether the observed maximum in the pH-rate profile for phenylboronic acid is an example of a more generally occurring phenomenon, we similarly studied the effect of pH on the oxidative homocoupling reaction of a series of arylboronic acids of different pK_as. A pH-rate profile showing a clear maximum was found for all arylboronic acids

tested with the exception of **2i** and **2j** (see Figures S5a-h in Appendix 1) and the data are

summarised in Table 2.1.

Table 2.1: Kinetic parameters for the oxidative homocoupling reaction of arylboronic acids[a]

substrate	pK_a		optimum pH[f]				$k_{obs(max)}/10^{-2}$ min^{-1}	biaryl:phenol ratio[d]
	lit[34]	exp[b]	overall process		following catalyst activation			10 : 11
			g	h	g	h		
2b	9.3[c]	9.4±0.1	9.5± 0.1	9.6	8.9± 0.1	9.0	11.5± 0.1	1:1
2c	9.0	9.1±0.1	9.0±0.1	9.2	8.2±0.1	8.4	2.2 ± 0.1	1:1
2a	8.8	9.0±0.1	8.9±0.1	9.2	8.4±0.1	8.4	3.7 ± 0.1	1:1
2d	8.0	8.2±0.1	8.7±0.1	8.4	8.3±0.1	8.2	3.0 ± 0.1	1:1
2e	7.7	7.7±0.1	8.3±0.1	8.2	8.0±0.2	8.0	2.7 ± 0.1	2.3:1
2f	7.4[c]	7.4±0.1	7.8±0.1	7.6	8.0±0.1	7.8	2.7 ± 0.1	2.4:1
2g	7.3[c]		7.9±0.1	7.8	8.0±0.1	7.8	0.85 ± 0.1	9:1
2h	.....	8.1±0.2	8.8				48 ± 1	....
2i	8.1		No reaction at pH 8.6 for at least 24 h					
2j	4.4		No reaction at a wide range of pHs (3.5 – 8.2) for at least 24 h [e]					

a) Typical reaction conditions: 10.0 mM CTAB, 10.0 mM borate buffer at desired pH, 10.0 µM **3**, 100.0 µM **2a-j**, and at 30 °C (for the kinetic traces see Figure S3a-h in Appendix 1)

b) In borate buffer and CTAB at 30 °C, see Figures S4a-g in Appendix 1.

c) deduced from Figure 2 ref[34]

d) The ratios were determined by HPLC for the reaction mixtures after completion at optimum pH for the overall process (see Figures S6-20 in Appendix 1). 100% conversion for all reactions were obtained.

e) Phosphate buffer was used for pH lower than 7.0

f) Fore the pH-rate profiles see Figures S5a-h in Appendix 1 for the studied arylboronic acids.

g) From the fit to a Gaussian, equation 2.2

h) Maximum point in the experimental data (without the fit to a Gaussian, equation 2.2)

Table 2.1 shows that the optimum pH for the overall reaction of the studied arylboronic

acids **2a-2h** is near the corresponding pK_a. However, following catalyst activation the

optimum pH shifts slightly to the acidic side. These observations are discussed in more

details later on in this Chapter. The ratio of the products biphenyl and phenol is 1:1 for the

aerobic homocoupling reactions of **2a-d**, each at optimum overall pH. However

biphenyl:phenol ratios of 2.4:1, 2.3:1 and 9:1 were observed for the aerobic homocoupling

reactions of **2e**, **2f** and **2g**, respectively, each at optimum overall pH. This means that the

phenol formation reaction is slower than the biphenyl formation reaction by more than

two-fold in the cases of **2e** and **2f** and nine-fold for the reaction of **2g**. The product ratio

for the reaction of **2h** was not analysed because the reaction failed to complete. Also, we

were not able to follow the kinetics for the pH effect experiment after activation of the

catalyst for the reaction of **2h** because of precipitate formation at the end of the reaction of

the second aliquot of **2h**. The aerobic homocoupling of 3-pyridine boronic acid **2i** was too

slow to follow, if it proceeded at all. Finally, the aerobic homocoupling of **2j** (which has a

pK_a of 4.4) was not achievable over a wide range of pH which gives important information

about the possible mechanism(s) for the reactions under our conditions (*vide infra*). The

observed maximum pseudo-first-order rate constants ($k_{obs(max)}$) for the overall processes of

the homocoupling reactions of **2a-g** follow the following trend **2h** > **2b** > **2a** > **2d** > **2e** =

2f > **2c** > **2g**. The observed trend indicates that presence of electron-donating groups

enhances the reaction rate (**2b**), while steric effects decrease the reaction rate (**2c**),

electron-withdrawing groups decreases the reaction rate (**2d**, **2e**, **2f** and **2g**). Although

thiopheneboronic acid appears to show the highest reaction rate, the reaction does not

proceed to completion and $k_{obs(max)}$ therefore cannot be compared in a meaningful manner

with the data for other boronic acids.

2.3.9. Solvent kinetic isotope effect (SKIE), product ratio confirmation and kinetics using ^{1}H NMR

The homocoupling reaction of 2a was also studied in D_2O using CTAB and borate buffer at different pH. The kinetics of the reaction were studied using UV-Visible spectroscopy and the pH-rate profile is shown in Figure 2.11.
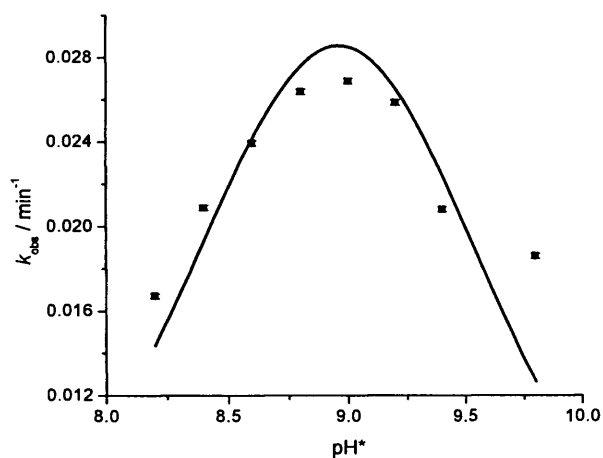

Figure 2.11: pH* effect on k_{obs} for the homocoupling reaction of 2a in D_2O using 10.0 μM 3, 10.0 mM CTAB and borate buffer pH 9.2 at 30 °C. experimental data (■), solid line is a fit to a Gaussian (eqn. 2.2)

Figure 2.11 shows that under our optimised conditions a bell-shaped pH-rate profile was again observed for the aerobic oxidative homocoupling reaction of 2a in D_2O using CTAB and borate buffer. The maximum of the pH*-rate profile in D_2O is at 9.0 ± 0.1 as compared to an optimum pH in H_2O of 8.9 ± 0.1. The maximum observed rate constant decreases from 0.037 to 0.027 min^{-1}. Although the decrease in maximum k_{obs} is significant and is remarkably consistent with the difference in pH_{opt} and pH^*_{opt}, the significance of this maximum itself is critically dependent on further mechanistic interpretation (*vide infra*).

The kinetics of the aerobic homocoupling reaction of **2a** were further studied using ^{1}H

NMR in D_2O at the optimum pH* using **3** as (pre) catalyst and in CTAB and borate buffer

at 37 °C (this temperature was chosen to avoid precipitation in the reaction mixture since

high concentrations of CTAB – with a Krafft temperature of 25 °C - were used). Product

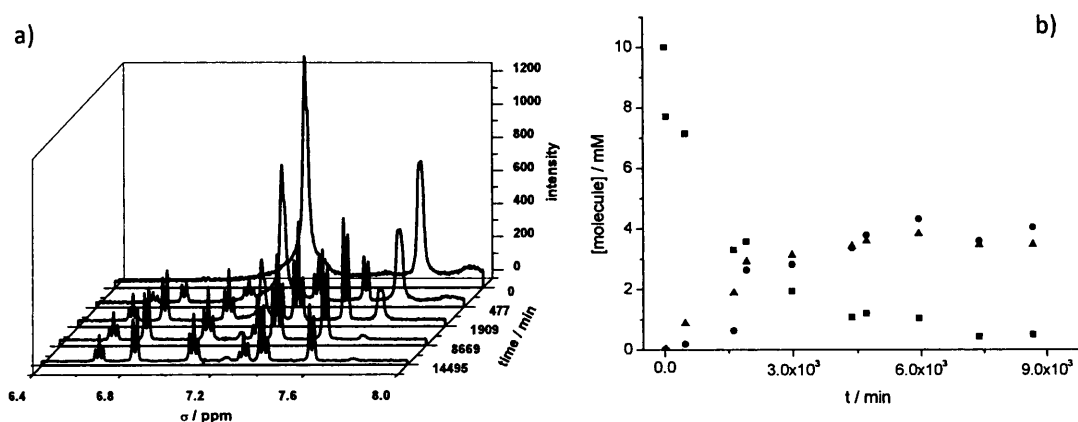formation (biphenyl and phenol) and reactant (**2a**) disappearance were followed (Figures

2.12a and b).

Figure 2.12: Aerobic homocoupling reaction of 10.0 mM **2a** in D_2O, using 10 mM **3** and 50 mM CTAB and borate buffer at pH* 9.0 and 37 °C, a) ^{1}H NMR spectra at different times and b) the calculated concentrations of the biphenyl (▲), phenol (●) and **2a** (■) at different times from the ^{1}H NMR integrals.

Fig 2.12a shows the disappearance of ^{1}H NMR spectral peaks of **2a** and the appearance of

^{1}H NMR spectral peaks of biphenyl and phenol products for the homocoupling reaction of

2a under our reaction conditions. Figure 2.12b shows that phenol formation is lagging

behind biphenyl formation in the beginning of the reaction, which is in agreement with the

conclusion that the Pd^{II} entry route into the catalytic cycle route in Scheme 2.10 only

forms biphenyl (*vide supra*). Following catalyst activation, an approximate 1:1 ratio of

biphenyl and phenol are produced, confirming that in the catalytic cycle the rates of

formation of biphenyl and phenol are similar. This, in turn, suggests that the reaction

between phenylboronic acid and peroxide itself is fast, both compared to alternative

peroxide decomposition pathways and compared to biphenyl formation.

2.3.10. Product ratio confirmation and kinetics using HPLC

Under our optimised conditions product formation and disappearance of the reactants was

also followed using HPLC for the homocoupling reaction of 2a in 10.0 mM CTAB and

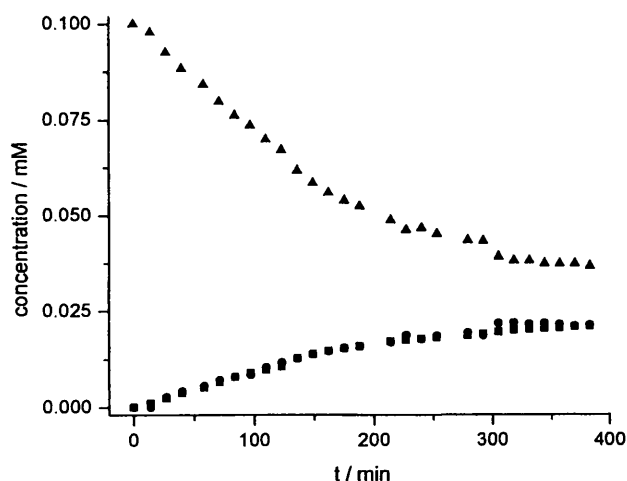borate buffer pH 9.2 using 2.5 μM 3 at 37 °C (Figure 2.13).

Figure 2.13: Concentrations of biphenyl (■), phenol (●) and 2a (▲) as a function of time.

It is clear from Figure 2.13 that the products biphenyl and phenol are formed in a 1:1 ratio.

2.3.11. Effect of the catalyst concentration on the reaction rate

Under our optimised conditions, we studied the effect of the concentration of (pre) catalyst

3 on the observed rate constant for the homocoupling reaction of 2a (Figure 2.14).
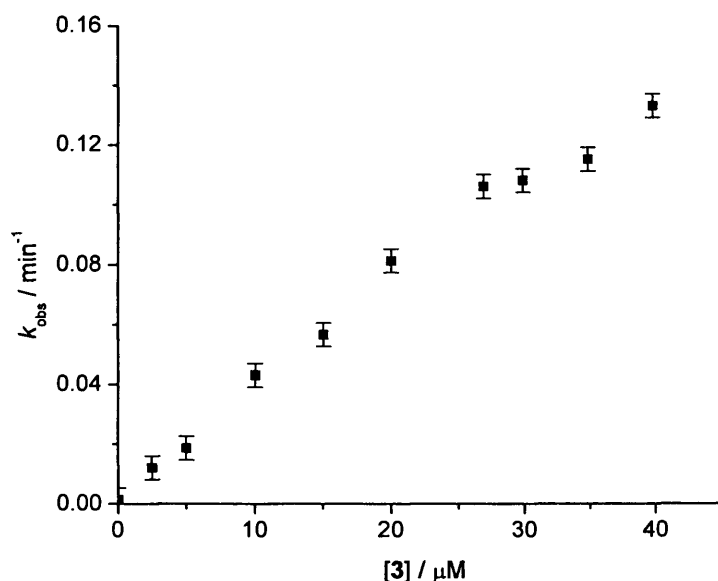
Figure 2.14: Effect of concentration of 3 on k_{obs} for the homocoupling reaction of 2a, in 10 mM CTAB and 10 mM borate buffer pH 9.2 at 30 °C.

Figure 2.14 shows that the reaction is first order in the catalyst, as expected based on the assumption that there is only one catalyst molecule involved in the catalytic cycle. The observation that the reaction is first order in **3** suggests that a monomeric Pd-complex is the active catalyst and that no higher order structures with different catalytic activity are formed at elevated concentrations of **3** (the formation of catalytically less active dimers *etc.* would lead to levelling off of the plot of k_{obs} *vs.* [3] whereas formation of more active dimers etc. would lead to and increase in the slope of k_{obs} *vs.* [3]). Nevertheless, we note that a mechanism involving a dimeric (or higher order) catalyst might also give rise to a first-order dependence on catalyst concentration if the dimeric form of the catalyst is stable with respect to the monomer over the entire range of catalyst concentrations studied.

2.3.12. Effect of surfactant concentration on the reaction rate

The concentration of the added surfactant was found to play a pivotal role on the reaction rate. Taking the homocoupling of phenylboronic acid, we performed the reaction using 100 and 300 µM of phenylboronic acid at different concentrations of CTAB, in 10.0 mM borate buffer pH 9.2 and 10.0 µM of 3 (Figure 2.15).
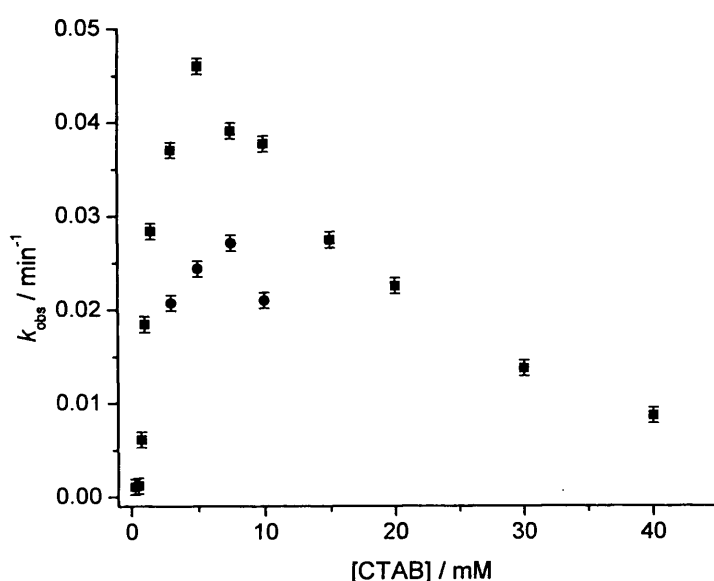

Figure 2.15: Effect of CTAB concentration on the observed rate constant for the reaction of 100 µM 2a (■) and 300 µM 2a (●), using 10 µM 3, at pH 9.2 and 30 °C.

Figure 2.15 shows a rate-enhancing effect of the added surfactant which diminishes at higher surfactant concentrations. This behaviour is typical for second (or higher) order reactions in micellar solutions. Initially an increase in k_{obs} is observed due to the reactants being brought together in the micelles. The subsequent decrease in k_{obs} is the result of dilution of reactant molecules over increasing numbers of micelles with increasing surfactant concentration.[25] Increasing the concentration of 2a leads to a decrease in k_{obs} and shows a maximum at higher CTAB concentration, which suggests more micelles are

needed for full binding at the higher concentration of phenylboronic acid. The decrease in

k_{obs} compared to the case of using 0.1 mM **2a** might be due to the increasing ratio of

dimerisation and/or trimerisation of **2a** in the hydrophobic micellar core (*vide supra*).

These dimers/trimers are assumed to be less reactive towards the aerobic homocoupling

reaction; they have to hydrolyse to the corresponding monomeric boronic acids and can

only then undergo homocoupling.

2.3.13. Knocking out the catalytic cycle

The presence of O_2 in the reaction medium is required for the reaction to occur via the

palladium peroxo species and as such is the soul of the catalytic cycle. The saturation

oxygen concentration in aqueous CTAB solutions at 30 °C and ambient atmospheric

conditions is 0.30 mM.[35] We studied the reaction in the absence of O_2 (by freeze-pump-

thaw degassing the reaction mixture before addition of **2a**), and we found that the reaction

rate decreases significantly in the absence of oxygen (Figure 2.16).
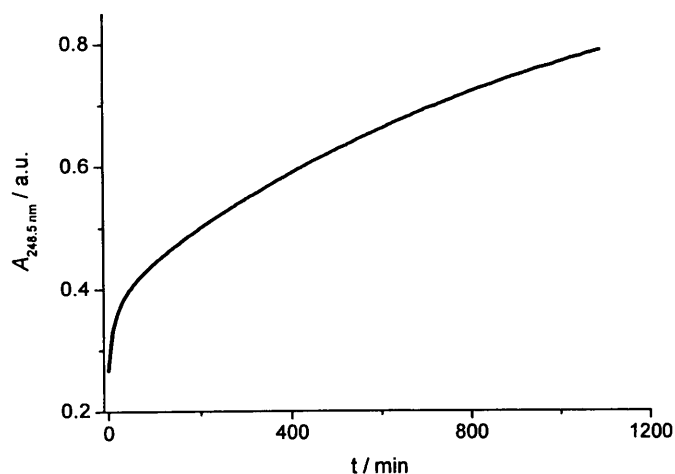
Figure 2.16. Absorbance of the reaction mixture versus time for 0.1 mM **2a**, 27.0μM **3**, in 10.0 mM CTAB and borate buffer pH 9 at 30 °C, in the absence of O_2 (under N_2 atmosphere).

Figure 2.16 shows that in the absence of oxygen, the rate of the reaction is higher during the first stage of the reaction (approximately 30 minutes) than during the second stage. This behaviour is opposite to the induction period observed in the presence of oxygen which indicates that product formation through the Pd^{II} pathway (Scheme 2.10 first step) is now faster than subsequent Pd^0-catalysed oxygen-driven reaction. In fact, the Pd^0-cycle should not occur in the absence of oxygen and the reaction should not go to completion. We attribute the slow reaction during the second stage to oxygen leaking into the cuvette with oxygen transfer now being the rate limiting step.

2.3.14. Homocoupling using $Cu(OAC)_2$ as oxidant

The homocoupling of 2a using 3 as the catalyst, but using an alternative oxidant, was studied by freeze-pump-thaw degassing the mixture of CTAB, borate buffer pH 9.2 and 3 after which $Cu(OAC)_2$ was added together with 2a and the reaction was followed using UV-Visible spectroscopy (Figure 2.17).
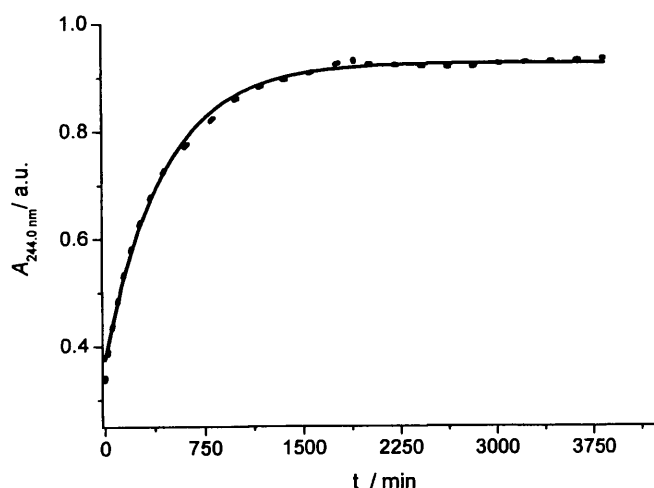
Figure 2.17. Absorbance of the reaction mixture versus time of 0.1 mM 2a, 10.0 μM 3 in 10.0 mM CTAB and borate buffer pH 9.2 at 30 °C, using 0.1 mM $Cu(OAc)_2$ as an oxidant, experimental data (dotted line), solid line fit to the pseudo-first-order rate law (equation 2.1)

Figure 2.17 shows that the homocoupling of **2a** using $Cu(OAc)_2$ under the same optimised conditions as for aerobic conditions proceeds slower. Therefore, we conclude that in the presence of $Cu(OAc)_2$ and the absence of oxygen the homocoupling reaction proceeds mainly via the Pd^{II} pathway and at a lower rate (more than ten-fold slower).

Addition of the oxidant even in the presence of dissolved oxygen (without freeze-pump-thaw degassing the reaction mixture) results in the reaction proceeding more slowly by approximately two-fold under otherwise identical reaction conditions. The decrease in k_{obs} upon addition of extra oxidant is attributed to competition between the Pd(0)-peroxo cycle and the Pd(II) cycle; as soon as the Pd(0) catalyst is regenerated during reductive elimination, it can react either with dioxygen (leading to quick catalytic turnover) or it can be oxidised by $Cu(OAc)_2$ (leading to slower turnover, at least at pH 9.2).

2.3.15. pK_a of 3 and formation of an aqua palladium complex

Palladium(II) complexes can ex-change weakly coordinated ligands with water molecules when they are placed in hydrous or aqueous media (See Chapter 1). As a result, they form aqua complexes which are more soluble in water and undergo an acid/base equilibrium. Based on the literature (discussed in Chapter 1),[36-43] the formation of a Pd-aqua-complex from **3** is possible (Scheme 2.13) although we do not have direct evidence to confirm its formation.
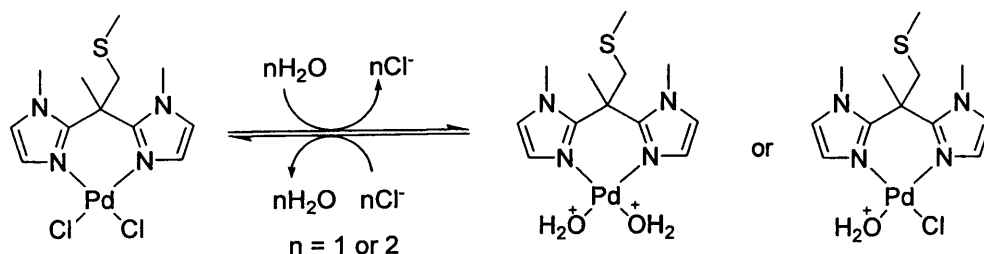
Scheme 2.13

However, we have measured the extinction coefficient of **3** (or its derivatives) using UV-
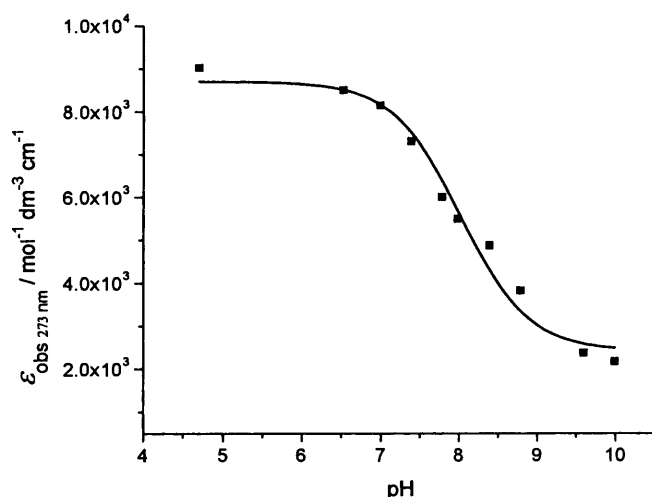
Visible spectroscopy as a function of pH (Figure 2.18).

Figure 2.18: Extinction coefficient (ε) at 273 nm versus pH for 27.0 µM **3** in 10.0 mM CTAB and 10.0 mM borate buffer at 30 °C, (■) experimental data and (solid line) fit in terms of sigmoidal equation 2.3.

Figure 2.18 shows a sigmoidal dependence of ε with pH, suggesting that **3** has a pK_a of 8.0

± 0.1 (calculating by fitting sigmoidal equation 2.3 to the data) in aqueous solution of

borate buffer and CTAB.

$$\varepsilon_{obs} = \left(\frac{1}{1 + 10^{pH-pK_a}} \right) \times \varepsilon_a + \left(\frac{10^{pH-pK_a}}{1 + 10^{pH-pK_a}} \right) \times \varepsilon_b \qquad (2.3)$$

Where variables are defined as before, ε_{obs}, ε_a and ε_b are the observed, acidic and basic

extinction coefficient of complex **3**, respectively.

The calculated pK_a from Figure 2.18 might be for protonation and deprotonation of the

formed aqua complex from **3** (Scheme 2.14). Protonation on the bisimidazole supporting

ligand of complex **3** is unlikely; although imidazole and imidazole-H$^+$ have pK_as of 14.58

and 7.1, respectively,[44, 45] one of the nitrogen atoms (unmethylated nitrogen) is already

engaged in a coordination bond with the Pd atom and protonation of the other nitrogen

atom (the pyrrole-like methylated nitrogen) is thermodynamically unfavourable because it

leads to the loss of the aromaticity in the imidazole ring (protonated methylimidazole has

a very low pK_a of around -4). This indicates that under our conditions (pH 5-10) the

methylated nitrogens of 3 remain deprotonated.
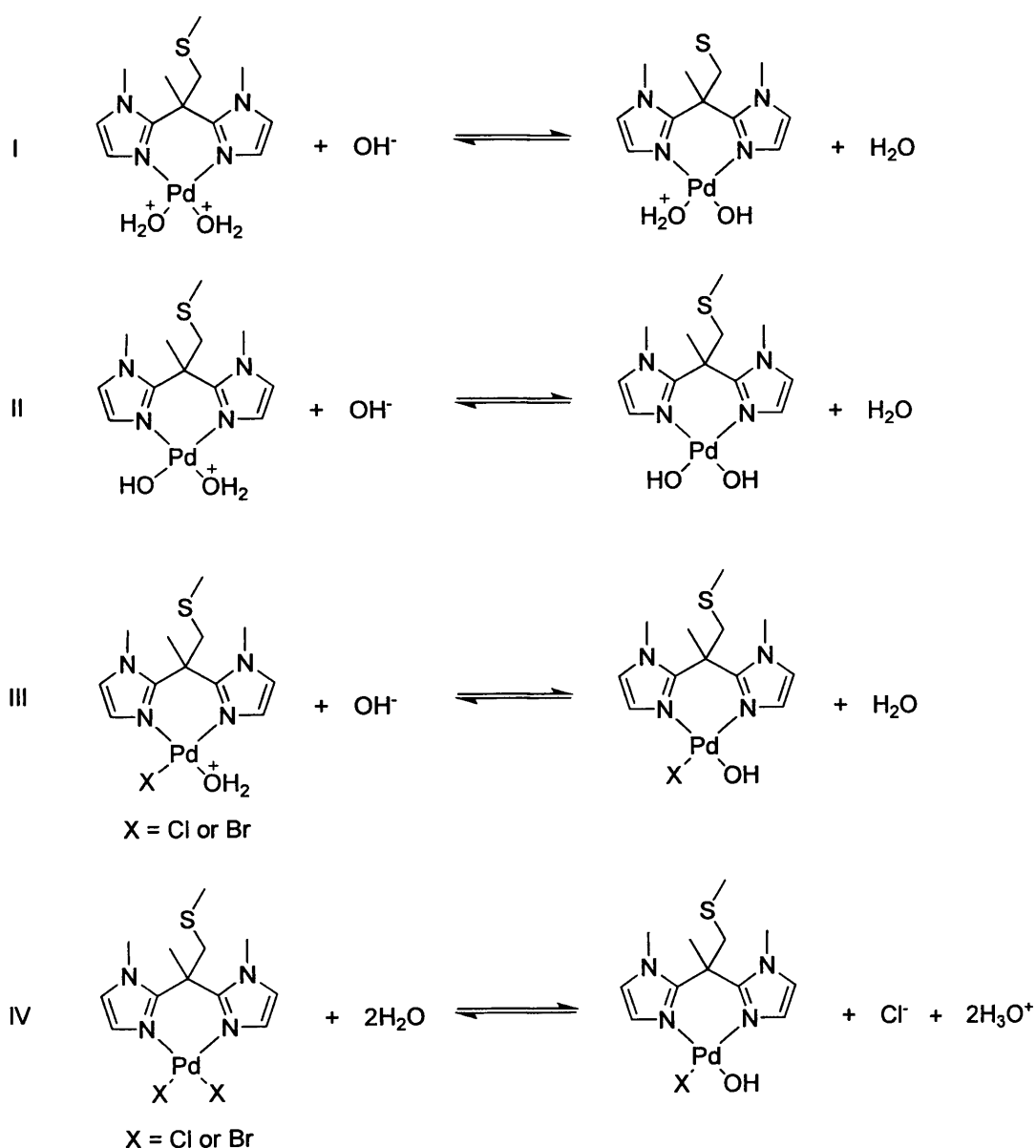
**Scheme 2.14.** Possible acid base equilibria of the aqua-complex of 3

Considering that the pK_a of palladium aqua complexes carrying a single positive charge is typically in the range between 7 and 8 (See Chapter 1), the most likely (de)protonation events corresponding to the observed pK_a of 8 are reactions II and III in Scheme 2.14. Although reaction IV cannot be ruled out, it would be rather a coincidence if this equilibrium were to give rise to an apparent pK_a so similar to typical values for palladium-aqua complexes.

We believe that the acid/base equilibrium for the catalyst together with the pH-dependent form of 2a are the cause for the bell-shaped pH-rate profile observation (*vide infra*).

2.4. Possible mechanisms of the oxidative homocoupling reaction of arylboronic acids

2.4.1. Catalyst activation.

Our kinetic data clearly shows that the aerobic oxidative coupling reaction of arylboronic acids involves an induction period. During the induction period, Pd^{II} species 3 (or one of its derivatives[i]) is reduced to (formal) Pd^0 species 4 in a first turnover which couples two molecules of arylboronate 2 (Scheme 2.15).

$$2\ ArB(OH)_3^- \quad 2\ X^-$$
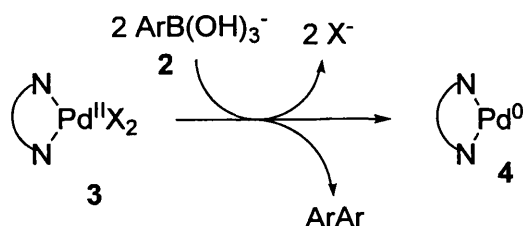
$$X^- = Cl^-,\ Br^-,\ ^-OH,\ H_2O\ or\ combinations\ of\ these$$

Scheme 2.15

---

[i] The Cl ligands of complex 3 might undergo exchange with the Br counter ion of CTAB, with OH⁻, or it might be replaced by H_2O.

The proposed requirement for the boronate rather than the boronic acid form of 2 stems

from the slightly shifting optimum pH after activation of the catalyst (the catalytic cycle

only) to the acidic side (see Table 2.1). This behaviour is less pronounced for arylboronic

acids with electron- withdrawing group substituents.

2.4.2. Involvement of molecular oxygen

Oxidative addition of molecular oxygen (dissolved in the reaction medium) to the formed

Pd^0-complex forms peroxo-Pd^{II}-complex 5 and starts the catalytic cycle (Scheme 2.16).

The peroxo-Pd^{II}-complex is the key intermediate in the catalytic cycle of aerobic oxidative

homocoupling reactions of arylboronic acids as it was proposed by Adamo et al.[21] The

peroxo complex could hydrolyse in the presence of water to form hydroxy-hydroperoxo-

Pd^{II} complex 6 which has a pH-dependent protonation state (Scheme 2.16).
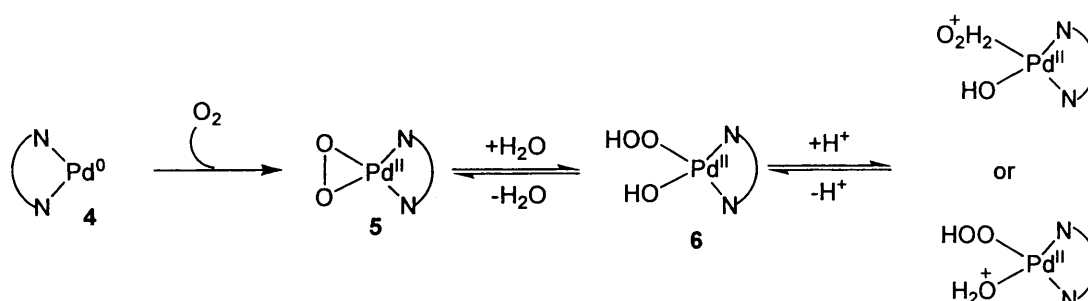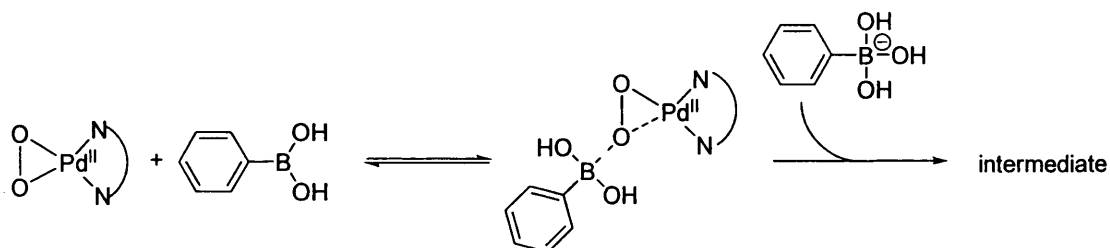

Scheme 2.16

2.4.3. Bell-shaped pH-rate profile

The key observation of the bell-shaped pH-rate profile for the reaction under our

conditions made us conclude that one of the reactants or intermediates has to be present in

its acidic form and one (not necessarily different) reactant or intermediate has to be

present in its basic form. Therefore, together with literature information, four different mechanisms are possible.

2.4.3.1. Acidic and basic forms of arylboronic acid are required in the same step

First, the bell-shaped pH-rate profile could be the result of requiring arylboronic acid and arylboronate anion in a pre-equilibrium followed by a rate-determining step, as exemplified using a suitably modified version of the mechanism proposed by Adamo *et al.*[21] (Scheme 2.17).

Scheme 2.17

This possibility gives rise to rate equation 2.4.

$$\frac{d[\text{intermediate}]}{dt} = k_{obs} \cdot [\text{Pd catalyst}] \cdot [\text{ArBA}_a] \cdot [\text{ArBA}_b] \qquad (2.4)$$

Where [Pd catalyst], [ArBA$_a$], [ArBA$_b$] and [intermediate] are the concentrations of Pd-catalyst, acidic form of arylboronic acid, basic form of arylboronic acid and intermediate respectively, k_{obs} is the observed rate constant for the reaction, and t is time.

Equation 2.4 predicts second-order dependence of the reaction rate on ArBA concentration and our experimental data do not show any second-order behaviour in ArBA (Figure 2.5). Also, the observed optimum pH (for the catalytic cycle only) is different from the pK_a for

the reaction of arylboronic acids whereas a mechanism such as that in Scheme 2.17 would

be accompanied by an exact match between optimum pH and pK_a. The observations

together make this mechanism unlikely for the reaction.

2.4.3.2. Acidic and basic forms of arylboronic acid are required in different steps in the catalytic cycle

Second, the bell-shaped pH-rate profile could suggest that both acidic and basic forms of

the arylboronic acid are needed, but in different reaction steps of the catalytic cycle. A

difference in the pK_a and optimum pH in such a mechanism is not unexpected. Based on

this proposition one can suggest that the maximum in the pH-rate profile for the aerobic

oxidative homocoupling reaction of arylboronic acids is the result of the boronic acid

being required in its acidic form in the first transmetalation whereas it is required in its

basic form in the second transmetalation (this suggestion is mainly based on Adamo's

proposed mechanism[21] and ignores the acid/base equilibria of the catalyst). The difference

between the two transmetalation events could stem from the direct involvement of oxygen.

The kinetic consequences of the difference between the two transmetalation steps are

illustrated using a simplified kinetic scheme (Scheme 2.18).

$$\text{ArB(OH)}_2 \text{ and O}_2$$
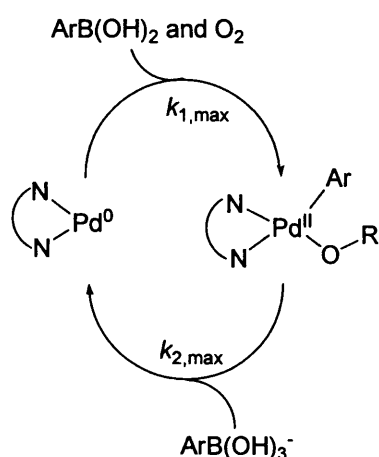
Scheme 2.18

Kinetic equation (2.5) is derived for Scheme 2.18 using steady state approximation and shows the observed dependence of k_{obs} on the pH.

$$k_{obs} = \frac{k_{1,max} k_{2,max}}{k_{1,max}(1 + 10^{pK_a - pH}) + k_{2,max}(1 + 10^{pH - pK_a})}[Pd_{tot}]$$

(2.5)

Where variables are as defined before, $k_{1,max}$ and $k_{2,max}$ are the second-order rate constants for the two reaction steps in Scheme 2.18, respectively, pK_a is the acid dissociation constant for corresponding arylboronic acids, and $[Pd_{tot}]$ is the total concentration of the Pd catalyst (for the full derivation of equation 2.5, see section A.1.8 in Appendix 1).

In terms of Scheme 2.18, the rate-determining step for the catalytic cycle at low pH (excess arylboronic acid) is the step involving the arylboronate, whereas at high pH (excess boronate), the step involving the boronic acid is rate determining. As a corollary, the resting state of the catalytic cycle is pH dependent, viz. the Pd^0 species is the resting state at high pH whereas the Pd^{II} species is the resting state at low pH (Figure 2.19a).
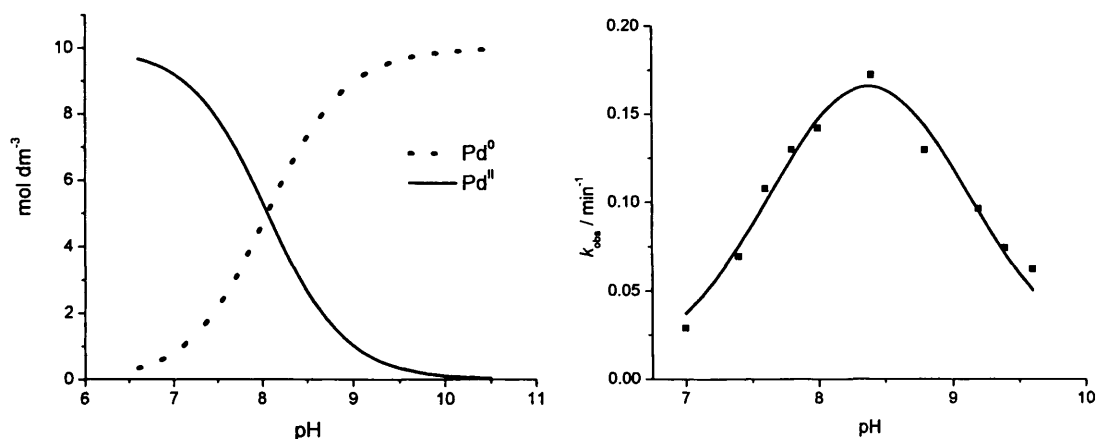
Figure 2.19. a) Concentration of Pd^0 and Pd^{II} intermediates as a function of pH, b) k_{obs} of the reaction after 2nd addition of 0.05 mM **2a** with 10.0 µM **3**, as a function of pH at 30 °C, experimental data (■) and fit to equation 2.4 (solid line).

Figure 2.19b shows the concentration of the two resting states as a function of pH which gives a maximum at a pH around 8.4 for the aerobic homocoupling of **2a** from analysis of our experimental data in terms of equation 2.5. The fit further provides $k_{1,max}$ and $k_{2,max}$ values.

Similarly, one can analyse the rate as a function of pH for the different arylboronic acids (Figure S21a-g in Appendix 1). Consequently, $k_{1,max}$ and $k_{2,max}$ can be found from fitting equation 2.5 to the bell-shaped pH-rate profiles for different substituted arylboronic acids. Using the values for $k_{1,max}$ and $k_{2,max}$, a Hammett plot can be constructed showing the substituent effect on the aryl ring of the boronic acids on the intrinsic rate constants $k_{1,max}$ and $k_{2,max}$ for two transmetalation steps (Figure 2.20).
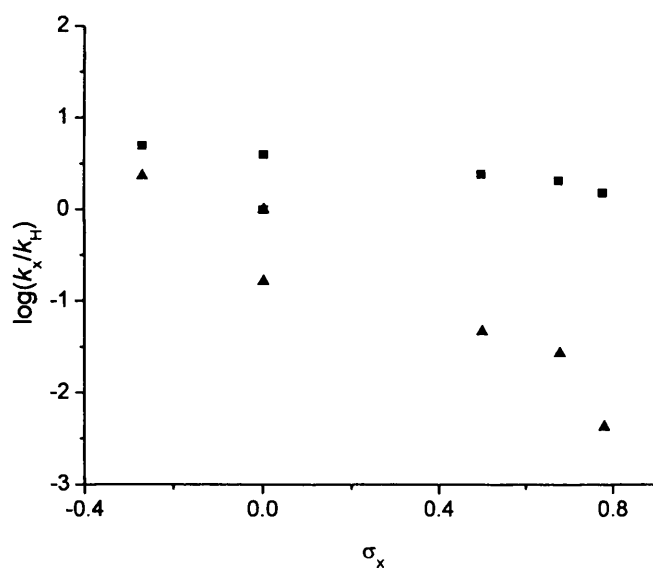
Figure 2.20. $\log(k_x/k_H)$ as a function of substituent constant σ_X for different arylboronic acids (**2a**, **2b**, **2d**, **2e**, **2f** and **2g**), where k_x, $k_H = k_{1,max}$ (■) and k_x, $k_H = k_{2,max}$ (▲).

Figure 2.20 shows that the $k_{1,max}$ is unaffected by the substituents on the aryl ring of **2**, whereas $k_{2,max}$ is strongly dependent on the type of the substituents on the aryl ring of **2**. The negative slope (ρ value) in the Hammett plot indicates a disappearance of a negative charge or a development of a positive charge in the transition state of the reaction (second transmetalation). Adamo *et al.*[21] have shown that the substituent effects on the overall conversion of **1a** into **1c** (Scheme 2.4) in $CHCl_3$ and DMF follows the order $k_{obs(CN)}>k_{obs(H)}>k_{obs(OMe)}$. It was further argued that the observed substituent effects on the conversion of **1a** to **1c** can be separated into a substituent effect on the equilibrium between **1a** and **1b** and a substituent effect on the rate constant for the conversion of **1b** into **1c**. As the conversion of **1b** into **1c** involves a transmetalation, Adamo *et al.* assumed $k_{CN}<k_H<k_{OMe}$ because electron-donating substituents render the arylboronic acid m ore nucleophilic. The corresponding equilibrium constants for formation of **1b** then follow the order $K_{CN}>>K_H>>K_{OMe}$, which again is reasonable considering the analogous trend in

acidity[34] of substituted boronic acids. In our case, the overall transmetalation involving the arylboronic acid probably also includes both formation of the dative bond between the boronic acid and the palladium peroxo complex and nucleophilic attack on the palladium centre. The observed lack of variation of $k_{1,max}$ with σ is therefore not unreasonable.

The transmetalation corresponding to $k_{2,max}$ by the arylboronate can be assumed to involve a direct transmetalation, $i.e.$ a direct nucleophilic attack on the palladium centre. Analogous to the argument by Adamo $et\ al.$, the reactivity of the different arylboronates in this step are expected to follow the order $k_{CN} < k_H < k_{OMe}$ [NOTE: this assumes that substituent effects on the nucleophile are larger than substituent effects on the Ar-Pd species]. This expectation is born out in practice: for the step corresponding to $k_{2,max}$, ρ is strongly negative. In this mechanism, the overall pH dependence of the reaction is the result of the addition of the first molecule of arylboronic acid in its acidic form to the Pd-complex with the addition of the second molecule of arylboronic acid in its basic form. Although Adamo's proposal seems to fit well with our proposed kinetic Scheme (Scheme 2.18), our kinetic data in D_2O shows a slight shift in optimum pH* for the reaction of 2a towards basic region, accompanied by a decrease in k_{obs} at optimum pH. For the above mentioned mechanism to be valid, using D_2O as the solvent should not affect the value of k_{obs} compared to the reaction in H_2O under the same conditions. In the absence of proton transfer in the rate-determining step, a solvent kinetic isotope effect should appear as a shift of the whole peak of pH-rate profile (reflecting only the different pK_a in D_2O). For this reason the abovementioned mechanism is also unlikely to be correct for the reaction under our conditions.

2.4.3.3. A specific combination of protonation states of the catalyst (intermediates) and arylboronic acids are required in the rate-limiting step.

The bell-shaped pH-rate profile may also be the result of a combination of (de)protonation

equilibria for catalyst (or, better, intermediates on the catalytic cycle) and arylboronic

acids. Such a mechanism takes into account that the (pre) catalyst **3** has a pK_a of 8.0 in

aqueous CTAB solution (*vide supra*). Several of the possible intermediates within the

catalytic cycle are likely to have properties similar to those of **3** and are therefore likely to

be involved in acid/base equilibria. For example, peroxo Pd-complex **5**, which hydrolyses

easily in the presence of water,[46] forms intermediate **6a** which is likely to be in

equilibrium with **6b** (Scheme 2.19, *Cf.* Scheme 2.16). Similarly, the protonation state of

intermediate **8** is likely to be pH dependent in a similar manner as **3** (Scheme 2.19, *Cf.*
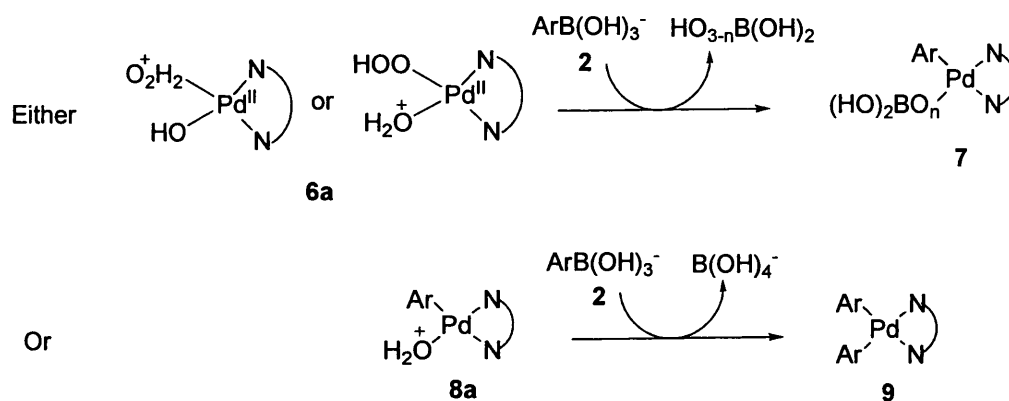
Scheme 2.14).
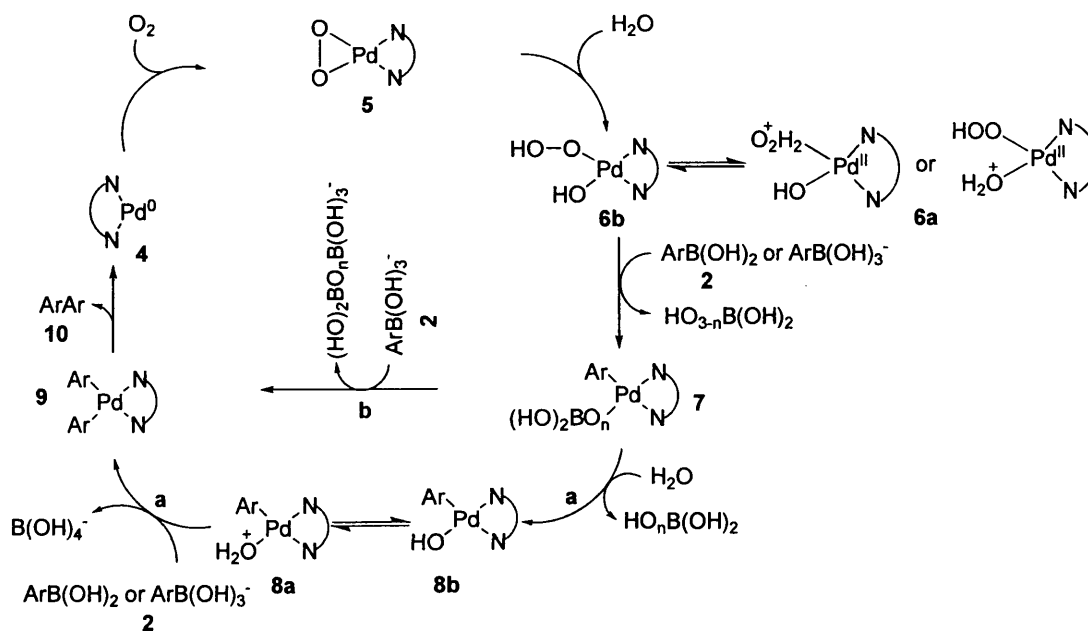
Scheme 2.19

For these possible mechanism(s) the pK_as of intermediates **6** and **8** are not known but we expect them to be close to the pK_a of the aqua-derivative of complex **3** (Figure 2.18) which is around 8. Accordingly, a third and a fourth possible mechanism can be proposed.

2.4.3.3.1. The basic form of the arylboronic acid is required together with the acidic form of a catalyst (intermediate) in the rate-limiting step.

Third, the bell-shaped pH-rate profile could be the result of the rate-limiting step involving the acidic (aqua) form of an intermediate on the catalytic cycle such as **6a** or **8a** and the basic form of PBA (Scheme 2.20).

Scheme 2.20

For a rate-determining step according to scheme 2.20, the rate equation would be one of the following equations.

$$\frac{d[7]}{dt} = k_{obs}[6a][2]_b \tag{2.6a}$$

$$\frac{d[9]}{dt} = k_{obs}[8a][2]_b \tag{2.6b}$$

Where the variables are as defined before, [7], [6a], [9], [8a] and $[2]_b$ are the molar concentrations of **7**, **6a**, **9**, **8a**, and the basic form of **2**, respectively.

From equations 2.6a and b it is clear that the reaction is first-order in **2** and the catalyst

(active species **6a** or **8a**). Although our kinetic data do not show first-order dependence in

2, we attributed that to the complexity in the micellar medium (*vide supra*). Equations 2.6a

and b are in agreement with our bell-shaped pH-rate profiles for the reaction if the pH

dependence of [**6a**] or [**8a**] and [**2**]$_b$ is explicitly incorporated. In this mechanism, the

observed bell-shaped pH-rate profile is the result of the coincidental similarity in the pK_a

of the boronic acids used and the palladium complex. Using an arylboronic acid which has

a pK_a far below the assumed pK_a of the catalytic intermediates could therefore provide

further confirmation of this mechanism because a wide plateau in the pH-rate profile is

expected if this mechanism is true. For this reason we have tested N-methylpyridinum-2-

boronic acid **2j** which has a pK_a of 4.4 and we observed no reaction over a wide range of

pH. This observation appears to suggest that this mechanism is unlikely for the reaction

under our conditions. Care has to be taken, however, with this interpretation of the

observed lack of reactivity of **2j** (*vide infra*).

2.4.3.3.2. The acidic form of the arylboronic acids is required together with the basic form of a catalytic intermediate in the rate-limiting step.

Fourth, the bell-shaped pH rate profile could be the result of the rate-limiting step

involving the basic (hydroxo) form of catalytic intermediate **6b** or **8b** and the acidic form

of **2** (Scheme 2.21).
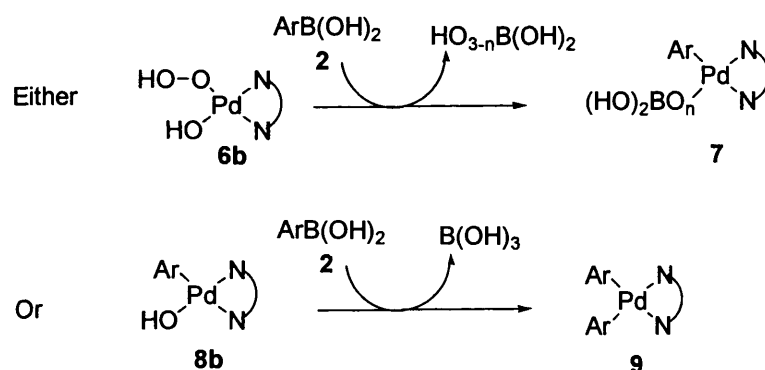
Scheme 2.21

For reaction according to Scheme 2.21, the rate equation would be one of the following equations.

$$\frac{d[7]}{dt} = k_{obs}[6b][2]_a \tag{2.7a}$$

$$\frac{d[9]}{dt} = k_{obs}[8b][2]_a \tag{2.7b}$$

Where the variables are as defined before, [7], [6b], [9], [8b] and $[2]_a$ are the molar concentrations of 7, 6b, 9, 8b, and the acidic form of 2, respectively.

The same arguments discussed in the previous section regarding equations 2.6a and b and our kinetic data are applicable for equations 2.7a and b as well. Equations 2.7a and b reproduce our pH-rate profile displaying an optimum pH, supporting the idea that the basic form of an intermediate on the catalytic cycle is required in combination with the acidic form of the arylboronic acids for the rate-limiting step (one of the transmetalation steps). This possibility appears to be further supported by the fact that no reaction was observed (over a wide range of pH) using 2j (which has a pK_a of 4.4 far below the assumed pK_a of the catalytic intermediates). For this mechanism, the low pK_a of the boronic acid means that the sigmoidal curves for both the required catalyst intermediate(s)

and the acidic form of **2j** do not overlap at any pH to allow the reaction to occur (Figure
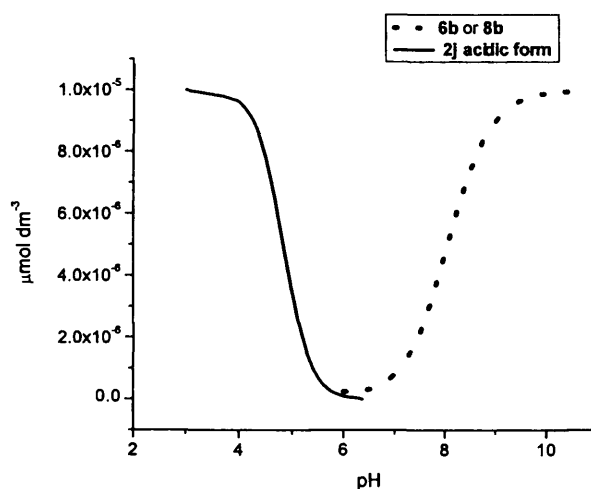
2.21).

Figure 2.21. Hypothetical data for the concentration of Pd^{II} intermediate(s) **6b** or **8b** (dotted line) and the acidic form of **2j** (solid line) as a function of pH.

From Figure 2.21 we conclude that the homocoupling reaction is expected to be very slow

if the pK_a of the boronic acid is far below the pK_a of the catalyst (or catalytic

intermediates) for a mechanism involving the hydroxo-form of the palladium catalyst and

an arylboronic acid.

2.4.3.3.3. Kinetic models for reaction according to Schemes 2.20 and 2. 21.

Our kinetic data can be analysed using the following equations based on Schemes 2.20 and

2.21, respectively.

$$k_{obs} = \frac{k_a [Pd]_{tot}}{[(1+10^{pK_{a(PBA)}-pH})(1+10^{pH-pK_{a(Pd)}})]}$$ (2.8a)

$$k_{obs} = \frac{k_b [Pd]_{tot}}{[(1+10^{pK_{a(Pd)}-pH})(1+10^{pH-pK_{a(PBA)}})]}$$ (2.8b)

Where the variables are as defined before, $pK_{a(PBA)}$, $pK_{a(Pd)}$ are the acidity constants for

PBA and the Pd catalyst (intermediate), respectively, k_a and k_b are the intrinsic second-

order rate constants for the mechanisms in Schemes 2.20 and 2.21, respectively.

Equations 2.8a and b are used to analyse our experimental data displaying the bell-shaped

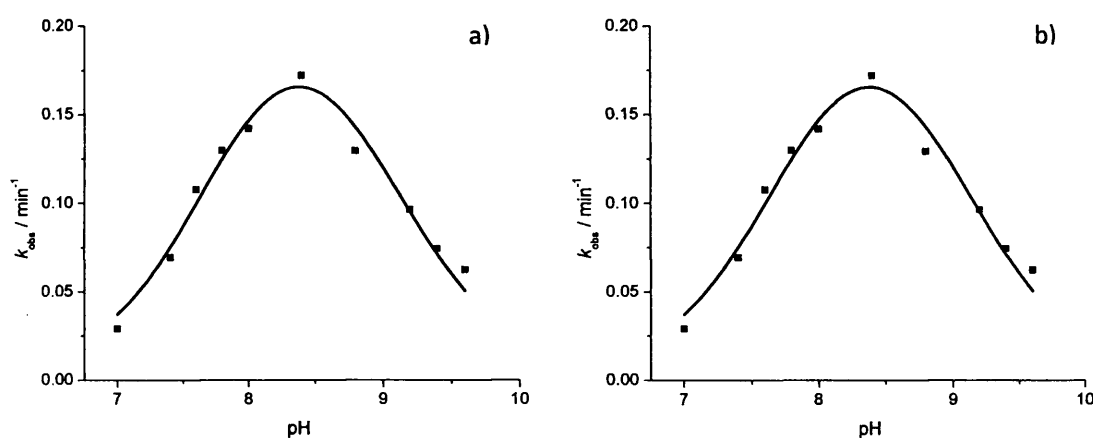pH-rate profile after addition of the second aliquot of PBA (*i.e.* for the catalytic cycle only

- Figures 2.22a and b)

Figure 2.22. k_{obs} for the homocoupling reaction of after the 2nd addition of 0.05 mM **2a** with 10.0 μM **3** as a catalyst as a function of pH at 30 °C, experimental data (■) and solid line a) fit to equation 2.8a and b) fit to equation 2.8b

By fitting equations 2.8a and 2.8b to the experimental data in Figures 2.22a and b (at fixed

$pK_{a(PBA)}$ and $[Pd]_{tot}$) the values of k_a and k_b can be determined for the homocoupling

reaction of **2a** under our reaction conditions. A value for $pK_{a(Pd)}$ can be determined from

the fit as well. Similarly one can find the values for k_a, k_b and $pK_{a(Pd)}$ for other substituted

arylboronic acids (see Figures S22a-g and S23a-g in Appendix 1). The fits (for both

mechanisms) for the studied arylboronic acids give values of $pK_{a(Pd)}$ of around 8 and

different values of k_a and k_b. The value for $pK_{a(Pd)}$ is remarkably close to the anticipated

value. Using the values of k_a, k_b, a Hammett plot can be constructed showing the

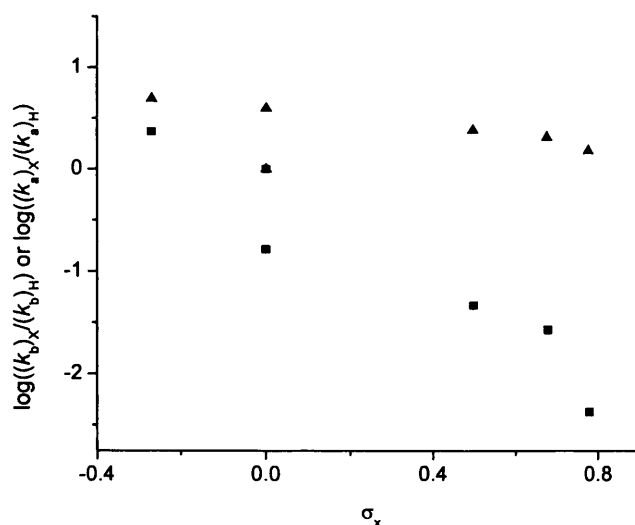substituent effects on the reaction rate constants (Figure 2.23).

Figure 2.20. $\log((k_b)_X/(k_b)_H)$ (▲) or $\log((k_a)_X/(k_a)_H)$ (■) as a function of substituent constant σ_X for different arylboronic acids (**2a, 2b, 2d, 2e, 2f** and **2g**), where k_a and k_b are the intrinsic second order rate constants for the reactions in Scheme 2.20 and 2.21, respectively.

Figure 2.20 shows the substituent effects on the intrinsic rate constants k_a and k_b for the homocoupling reaction of substituted arylboronic acids under our conditions for the two possible reaction mechanisms (*i.e.* according to equations 2.8a and b). The slope (which gives the ρ value) in the case of an acidic Pd intermediate reacting with basic PBA (Scheme 2.20) is more negative than the ρ value if one assumes reaction involving a basic Pd intermediate and acidic PBA (Scheme 2.21). The negative ρ in both cases indicates the acceleration of the rate of the reaction with the introduction of electron-donating groups. This is in fact in agreement with the increase in maximum k_{obs} for the reaction under our conditions (see Table 2.1) but the effect is more pronounced for the system assuming the rate-determining step to involve acidic catalyst, *i.e.* an aqua complex, and basic PBA.

The fact that no reaction was observed for **2j** under our reaction conditions needs to be reconsidered in light of the Hammett plots (Figure 2.20). Our initial interpretation that the lack of reactivity of **2j** indicated that arylboronic acids in their basic forms do not react

with the acidic Pd complex is unwarranted. Since **2j** has a high σ value (estimated to be

1.6 on the basis of the pK_a of **2j** of 4.4), its intrinsic reactivity as quantified by k_a is

predicted to be very low *i.e.* $\log((k_b)_X/(k_b)_H)$ or $\log((k_a)_X/(k_a)_H)$ will be very small

compared to other boronic acids. This provides an alternative explanation for the observed

lack of reactivity of **2j**, *viz.* that the intrinsic reactivity of **2j** is too low. The lack of

reactivity of **2j** therefore does not necessarily provide information on the required

protonation states of the boronic acids and the intermediates on the catalytic cycle.

We note that Adamo's[21] suggestion of the decrease of the intrinsinc rate constant of the

transmetalation step with the presence of electron-withdrawing groups is in agreement

with our observations.

Finally, both the mechanism in Scheme 2.20 and the mechanism in Scheme 2.21 can, in

principle, account for the observed solvent kinetic isotope effect. If the pK_a-shift upon

going from H_2O to D_2O is different for the palladium complex and the arylboronic acid,

the optimum pH will change, but the maximum k_{obs} will change as well. The solvent

kinetic isotope effect may in fact allow us to distinguish between these two mechanisms,

see Chapter 5).

In summary, our kinetic data does not currently allow us to distinguish between the

mechanisms in Scheme 2.20 and 2.21.

Mechanism 2.21 is known to work in DMF and chloroform (in a Suzuki coupling).[47] The

mechanism explains the bell-shaped pH-rate profile, the observed SKIE and the

observation that **2j** does not react. Similarly, it is tempting to see this mechanism as fitting

with the observation that trifluoroborate does not react (see Chapter 5). The involvement

of the basic form of Pd complexes *i.e.* $(L)_nPd-OH$ (L = PPh$_3$) with the acidic form of

boronic acid in the transmetalation step for Suzuki cross-coupling reaction was also

proposed by Amatore et al.[47] who showed that the boronate ion retards the transmetalation

even when $(L)_nPd\text{-}X$ (X= I, Cl or Br) intermediate was used in DMF solvent. They have

observed a bell-shaped profile for the effect of OH^- concentration on the reaction rate of

the transmetalation step. The authors have attributed the increase in the rate to the

formation of $(L)_nPd\text{-}OH$ intermediate from $(L)_nPd\text{-}X$, whereas the decrease in the rate was

due to the formation of unreactive arylboronate $ArB(OH)_3^-$ species. However, Mechanism

2.20 cannot be excluded based on the kinetic data. It may even be that Mechanism 2.20

only contributes to reactivity in aqueous solutions where the formation of the required

charged species is facilitated by the high solvent polarity. Mechanism 2.20 would also be

in agreement with the suggestion of Ogo et al. [48] who claim that boronate reacts with Pd-

aqua complex in water. We note, however, that Ogo's conclusion is critically dependent

on the assumption that tetraphenylborate reacts as an analogue of arylboronates.

Overall, we currently favour the mechanism in Scheme 2.21 and we therefore propose a

catalytic cycle for the aerobic homocoupling reaction of arylboronic acids under our

conditions in which one of the transmetalation steps is the rate-limiting step (Scheme

2.21).
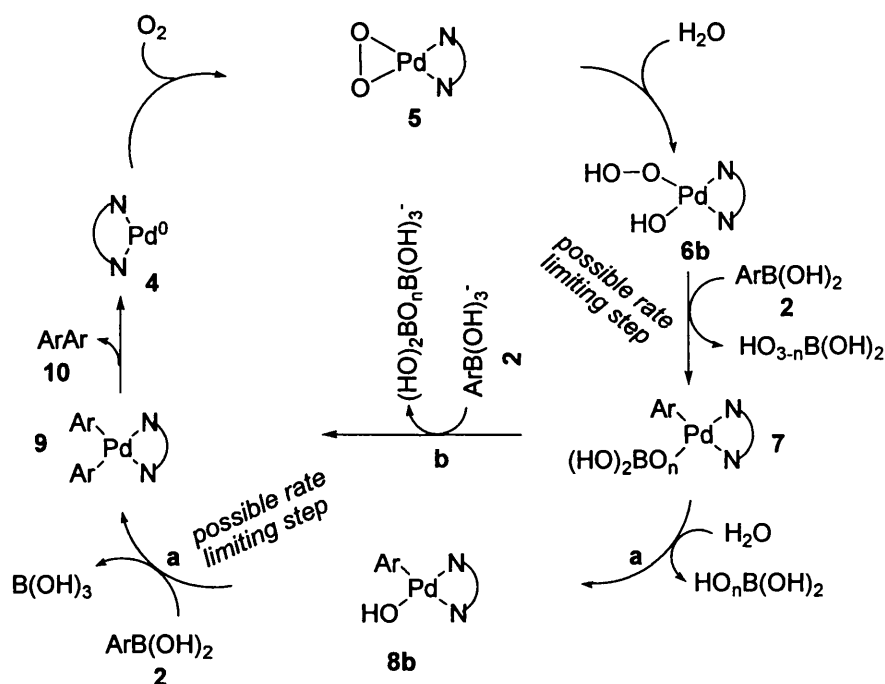
Scheme 2.22

In Scheme 2.22 intermediates **6b** and **8b** are in their basic (hydroxo) forms which favour interaction with the acidic forms of the arylboronic acids. Therefore, the bell-shaped pH-rate profile is the result of one of the transmetalation steps in Scheme 2.22 being the rate-limiting step. Coincidentally, the reason why the arylboronic acids interact with the palladium complex (Pd-OH) even in the presence of an abundance of water molecules in the aqueous reaction mixture is related to the pK_a of palladium-aqua complex of around 8, suggesting that Pd-OH is considerably more nucleophilic than water which has pK_a around 14.

2.5. Conclusions

[Pd(bimsulfide)Cl$_2$] is a good and stable (pre) catalyst for kinetic studies of the aerobic oxidative homocoupling reaction of arylboronic acids under aqueous conditions. The reaction rate increases using micelles but the effect diminishes at higher surfactant concentrations because of dilution of the reactants over more micelles. The catalysis involves an induction period during which two molecules of 2 (possibly in the basic form) are coupled to form the biaryl product and reduce Pd^{II} to Pd^0 (providing entry to the catalytic cycle). Running the reaction in the absence of air (and thus in the absence of O$_2$) reduces the reaction rate to a large extent which confirms the key role of O$_2$ as an oxidant for the catalyst to form a peroxo-Pd complex 5 which is consistent with the literature. Using Cu(OAC)$_2$ as an oxidant instead of O$_2$ (air) reduced the reaction rate which again confirms the importance of O$_2$ in the reaction. We observed a surprising effect of phenylboronic acid concentration on the reaction rate that we believe is mostly due to dimerisation and/or trimerisation of 2a in the micellar hydrophobic core (although we do not have any evidence to confirm that). The observed rate constant for the reaction, k_{obs}, increases linearly with the catalyst concentration indicating that the reaction is first-order in the catalyst. Presence of electron-donating groups increases the reaction rate, and steric factors (in the case of 2-MeOPBA) decrease the reaction rate. We observed bell-shaped pH-rate profiles for the aerobic homocoupling reactions of different arylboronic acids using 3 under our reaction conditions. The bell-shaped pH-rate profiles made us explore four possible mechanisms for the reactions. The most promising mechanism involves one of the transmetalation reactions as the rate-limiting step of the reaction involving the basic form of one of the intermediate palladium complexes on the catalytic cycle reacting with the acidic form of the arylboronic acid. However, we cannot rule out a mechanism

involving a transmetalation step involving the acidic form of a catalytic Pd-based

intermediate with the basic form of the arylboronic acid.

2.6. Experimental

2.6.1. Equipment

JASCO V630 and V650 UV-Visible spectrophotometers were used to monitor reactions

by either time resolved absorption (spectra) or parallel kinetic measurements. Both

machines were equipped with a Peltier thermostated cell holder to control the temperature.

A HANNA pH211 microprocessor pH meter equipped with a VWR 662-1759 glass

electrode was used for determining the pH of solutions. ^{1}H NMR spectra were recorded in

D_2O on a Bruker spectrometer (400 MHz). HPLC analysis was carried out using an

Agilent1200 instrument with a ZORBAY (Eclipse XDB-C18 4.6X150 mm, 5 μm)

column. Water was purified using an ELGA option-R 7BP. Mass spectra were recorded

using Waters Micromass LCT Premier Mass Spectrometer.

2.6.2. Chemicals

All chemicals were commercially available (Acros, Alfa Aesar, Aldrich, Fisher Scientific,

ICT, and Maybridge) and used as purchased without further purification, apart from

bis(imidazol-2-yl)methylmethane palladium chloride [Pd(bimsulfide)Cl_2] which was

prepared in the group of Prof. Cavell at Cardiff university with an estimated purity of 98-

99% (unpublished results), and 1-methylpyridinium-2-boronic acid which was prepared

according to literature procedures,[49] ^{1}H-NMR (D_2O) δ 2.68 (s, 3, SO_2CH_3), 4.25 (s, 3, $^+$N-

CH_3), 7.9 (t, 6.9 Hz, 1, Py-H), 8.6 (dd, 6.1 Hz, 7.8 Hz, 1, Py-H), 8.8 (s, 1, Py-H); ^{13}C

NMR (D_2O) δ 38.57, 48.07, 127.35, 145.54, 148.83, 149.71; mass spectrum, m/e 138.07

(M^+). Acetonitrile and deionised water were used as solvents for the preparation of stock

solutions. A 1:1 mixture of acetonitrile and deionised water was used as a solvent for the

preparation of all arylboronic acid and phenol stock solutions apart from 1-methyl-

pyridinium-2-boronic acid (which was prepared in deionised water alone). Acetonitrile

was used to prepare Pd-catalyst and precatalyst and biaryl (authentic standards) stock

solutions. Deionised water was the solvent for all other stock solutions.

2.6.3. Typical kinetic experiments

2.6.3.1. Kinetic measurement using UV-Visible spectroscopy

2.6.3.1.1. Time resolved absorption peak measurements

Reactions were carried out in 1.00 cm pathlength stoppered quartz cuvettes (Hellma)

holding approximately 1.00 cm^3 of headspace (*i.e.* under aerobic conditions), at 30 °C.

Typical concentrations were 100 μM for arylboronic acids and a required amount of the

catalyst. Product formation (biaryl and phenol) was followed through changes in UV-

Visible absorbance with time at a selected wavelength where maximum changes in

absorbance occurred, which has been selected through UV-Visible time resolved

absorption spectra measurement for the reaction of each arylboronic acid (250.0 nm for

2a, 269.0 nm for 2b, 242.5 nm for 2c, 280.0 nm for 2d, 302.0 nm for 2e, 247.5 nm for 2f,

324.0nm for 2g, and 305.0 nm for 2h.).

Typically in a 1.0 cm pathlength cuvette and to a total volume of 2.5 mL, the required

reagents (CTAB, K_2CO_3 or borate buffer, and catalyst) were mixed by pipetting the

desired amount from the concentrated stock solutions. The cuvette was allowed to

thermally equilibrate for about 5-10 minutes. Subsequently, the required amount of arylboronic acid was added to the reaction mixture from a concentrated stock solution. The kinetics were monitored by measuring the time resolved absorption peak. Reversing the order of addition of arylboronic acids and the catalyst did not affect the kinetic measurements. Whereas the reactions are clearly not (pseudo) first-order, observed rate constants k_{obs} were determined from plots of absorbance as a function of time, using the pseudo first-order rate law (equation 2.1). Consequently all rate constants are expressed as observed pseudo-first-order rate constants.

2.6.3.1.2. Parallel kinetic measurements

Parallel kinetic measurements at fixed wavelength were performed using a 6-cuvette cell changer using a JASCO V-650 UV-Visible spectrometer at constant temperature following the abovementioned procedure. Effects of the base concentration, pH, buffer concentration, CTAB concentration, catalyst concentration, and arylboronic acids concentration were all studied by UV-Visible parallel kinetic measurements.

2.6.3.1.3. Kinetics using ^{1}H NMR

An aqueous (D_2O) solution containing 50 mM CTAB, 50 mM borate buffer (pH 9.0), 10 mM phenylboronic acid and 10 μM Pd(bimsulfide)Cl_2 were mixed in a small capped container and kept at 37 °C (water bath). ^{1}H NMR spectra were recorded by taking aliquots of the reaction mixture into NMR tubes at different time points. The appearance of products (biphenyl and phenol) and disappearance of reactant (phenylboronic acid) were followed with time by following the increase/decrease of the integration of the

related ^{1}H-NMR peaks. ^{1}H-NMR (D$_2$O) δ 7.72 (d, 7.72 Hz, 2, PBA), 7.56 (d, 7.76 Hz, 4,

PhPh), 7.37 (t, 7.5 Hz, 4, PhPh), 7.28 (t, 7.31 Hz, 2, PhPh), 7.21 (m, 3, PBA), 7.07 (t, 7.78

Hz, 2, PhOH), 6.79 (d, 8.08 Hz, 2, PhOH), 6.65 (t, 7.29 Hz, 1, PhOH),

2.6.3.1.4. Kinetics using HPLC

In a small capped container, an aqueous solution containing 10 mM CTAB, 10 mM borate

buffer (pH 9.2), 0.1 mM phenylboronic acid were mixed at 35 °C (the temperature was

controlled by flowing a constant stream of warm air into the auto-sampler compartment of

the HPLC instrument and temperature was monitored by a thermometer). The required

amount of Pd(bimsulfide)Cl$_2$ was added and the reaction kinetics were followed by

recording HPLC chromatograms as a function of time. The appearance of products

(biphenyl and phenol) and the disappearance of reactant (arylboronic acids) were

monitored over time, through measuring the area under the peak for each substance

2.6.4. pK_a measurements

The UV-Visible spectra of arylboronic acids or Pd(bimsulfide)Cl$_2$ were recorded in CTAB

and borate buffer at different pH using a JASCO UV-Visible V-650 spectrometer. The

absorbances at a fixed wavelength were plotted against pH and the pK_a was determined

through data analysis in terms of a sigmoidal curve.

2.6.5. Product analysis and calibration graphs by HPLC

Product distributions in the coupling reactions of the arylboronic acids were analysed

using HPLC using the following HPLC method. 1) solvent gradient of 95% water and 5%

acetonitrile (for 4-COOHPBA the solvent gradient was 65% water, 30% trifluoroacetate

(0.02% concentration) and 5% acetonitrile) with a gradient time table 5.0 minutes 100%

(50% for 4-COOHPBA) acetonitrile and 9.0 minutes 100% (80% for 4-COOHPBA)

acetonitrile, 2) solvents flow rate was 1.0 mL / min, 3) column temperature was 40 °C, 4)

the spectra detection wavelength was 254 nm with a band width of 50 nm for PBA and 2-

MeOPBA, 254 ± 70 nm for 4-AcOPBA and 4-MeOPBA, 270 ± 50 nm for 4-COOˉPBA,

284 ± 70 nm for 4-NO$_2$PBA, 5) 60 µL of the reaction mixture was injected and 6) 1.0

minute of post time and 10 minutes of stop time were allowed. To quantify the amount of

the products in the reaction mixtures, calibration graphs in the concentration range from

0.025 mM to 0.2 mM were generated using commercially available standards (see Figure

S6-20 in Appendix 1).

Acknowledgements
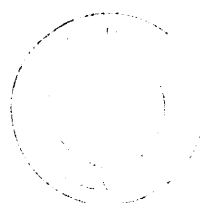
References

1.   Stanforth, S. P., *Tetrahedron* **1998**, *54* (3-4), 263-303.

2.   Miyaura, N.; Suzuki, A., *Chemical Reviews* **1995**, *95* (7), 2457-2483.

3.   Suzuki, A., *Journal of Organometallic Chemistry* **1999**, *576* (1-2), 147-168.

4.   Hassan, J.; Sevignon, M.; Gozzi, C.; Schulz, E.; Lemaire, M., *Chemical Reviews* **2002**, *102* (5), 1359-1469.

5.   Jutand, A.; Mosleh, A., *Journal of Organic Chemistry* **1997**, *62* (2), 261-274.

6.   Amatore, C.; Carre, E.; Jutand, A.; Tanaka, H.; Ren, Q. H.; Torii, S., *Chemistry-a European Journal* **1996**, *2* (8), 957-966.

7.   Butters, M.; Harvey, J. N.; Jover, J.; Lennox, A. J.; Lloyd-Jones, G. C.; Murray, P. M., *Angewandte Chemie - International Edition* **2010**, *49* (30), 5156-5160.

8.   Moreno-Mañas, M.; Perez, M.; Pleixats, R., *Journal of Organic Chemistry* **1996**, *61* (7), 2346-2351.

9.   Wong, M. S.; Zhang, X. L., *Tetrahedron Letters* **2001**, *42* (24), 4087-4089.

10.   Yoshida, H.; Yamaryo, Y.; Ohshita, J.; Kunai, A., *Tetrahedron Letters* **2003**, *44* (8), 1541-1544.

11.   Parrish, J. P.; Jung, Y. C.; Floyd, R. J.; Jung, K. W., *Tetrahedron Letters* **2002**, *43* (44), 7899-7902.

12.   Cravotto, G.; Palmisano, G.; Tollari, S.; Nano, G. M.; Penoni, A., *Ultrasonics Sonochemistry* **2005**, *12* (1-2), 91-94.

13.   Klingensmith, L. M.; Leadbeater, N. E., *Tetrahedron Letters* **2003**, *44* (4), 765-768.

14.   Demir, A. S.; Reis, O.; Emrullahoglu, M., *Journal of Organic Chemistry* **2003**, *68* (26), 10130-10134.

15.   Du, X. L.; Suguro, M.; Hirabayashi, K.; Mori, A.; Nishikata, T.; Hagiwara, N.; Kawata, K.; Okeda, T.; Wang, H. F.; Fugami, K.; Kosugi, M., *Organic Letters* **2001**, *3* (21), 3313-3316.

16.   Zhou, C. X.; Larock, R. C., *Journal of Organic Chemistry* **2006**, *71* (8), 3184-3191.

17.   Zhou, L.; Xu, Q. X.; Jiang, H. F., *Chinese Chemical Letters* **2007**, *18*, 1043-1046.

18.   Aramendia, M. A.; Lafont, F.; Moreno-Manas, M.; Pleixats, R.; Roglans, A., *Journal of Organic Chemistry* **1999**, *64* (10), 3592-3594.

19.   Wilke, G.; Schott, H.; Heimbach, P., *Angewandte Chemie-International Edition* **1967**, *6* (1), 92-93.

20.   Amatore, C.; Aziz, S.; Jutand, A.; Meyer, G.; Cocolios, P., *New Journal of Chemistry* **1995**, *19* (10), 1047-1059.

21. Adamo, C.; Amatore, C.; Ciofini, I.; Jutand, A.; Lakmini, H., *Journal of the American Chemical Society* **2006**, *128* (21), 6829-6836.

22. Lakmini, H.; Ciofini, I.; Jutand, A.; Amatore, C.; Adamo, C., *Journal of Physical Chemistry A* **2008**, *112* (50), 12896-12903.

23. Rabeyrin, C.; Sinou, D., *Journal of Molecular Catalysis a-Chemical* **2004**, *215* (1-2), 89-93.

24. Dwars, T.; Paetzold, E.; Oehme, G., *Angewandte Chemie-International Edition* **2005**, *44* (44), 7174-7199.

25. Buurma, N. J., *Advances in Physical Organic Chemistry* **2009**, *43*, 1-37.

26. Arcadi, A.; Cerichelli, G.; Chiarini, M.; Correa, M.; Zorzan, D., *European Journal of Organic Chemistry* **2003**, (20), 4080-4086.

27. Cerichelli, G.; Cerritelli, S.; Chiarini, M.; De Maria, P.; Fontana, A., *Chemistry-a European Journal* **2002**, *8* (22), 5204-5210.

28. Shaughnessy, K. H.; DeVasher, R. B., *Current Organic Chemistry* **2005**, *9* (7), 585-604.

29. Miyaura, N., *Journal of Organometallic Chemistry* **2002**, *653* (1-2), 54-57.

30. Kedia, S. B.; Mitchell, M. B., *Organic Process Research & Development* **2009**, *13* (3), 420-428.

31. Kua, J.; Fletcher, M. N.; Iovine, P. M., *Journal of Physical Chemistry A* **2006**, *110* (26), 8158-8166.

32. Tokunaga, Y.; Ueno, H.; Shimomura, Y.; Seo, T., *Heterocycles* **2002**, *57* (5), 787-790.

33. Khan, M. N., *Micellar catalysis*. Taylor & Francis: Boca Raton, **2006**; pp 482.

34. Yan, J.; Springsteen, G.; Deeter, S.; Wang, B. H., *Tetrahedron* **2004**, *60* (49), 11205-11209.

35. Prapaitrakul, W.; King, A. D., *Journal of Colloid and Interface Science* **1985**, *106* (1), 186-193.

36. Vicente, J.; Arcas, A., *Coordination Chemistry Reviews* **2005**, *249* (11-12), 1135-1154.

37. Wimmer, S.; Castan, P.; Wimmer, F. L.; Johnson, N. P., *Inorganica Chimica Acta* **1988**, *142* (1), 13-15.

38. Ogo, S.; Takebe, Y.; Uehara, K.; Yamazaki, T.; Nakai, H.; Watanabe, Y.; Fukuzumi, S., *Organometallics* **2006**, *25* (2), 331-338.

39. Hohmann, H.; Hellquist, B.; Vaneldik, R., *Inorganica Chimica Acta* **1991**, *188* (1), 25-32.

40. Hohmann, H.; Van Eldik, R., *Inorganica Chimica Acta* **1990**, *174* (1), 87-92.

41. Berger, J.; Kotowski, M.; Van Eldik, R.; Frey, U.; Helm, L.; Merbach, A. E., *Inorganic Chemistry* **1989**, *28* (19), 3759-3765.

42.   Wimmer, F. L.; Wimmer, S.; Afcharian, A.; Castan, P.; Fabre, P. L., *Journal of Chemical Research - Part S* **1999,** (3), 194-195.

43.   Jaganyi, D.; Tiba, F.; Munro, O. Q.; Petrovic, B.; Bugarcic, Z. D., *Dalton Transaction* **2006,** (24), 2943-9.

44.   Albert, A., *Heterocyclic chemistry : an introduction.* 2nd ed. ed.; Athlone Press: London, 1968; pp 559.

45.   Gilson, R.; Durrant, M. C., *Dalton Trans* **2009,** (46), 10223-30.

46.   Sheldon, R. A.; Kochi, J. K., Metal-catalyzed oxidations of organic compounds : mechanistic principles and synthetic methodology including biochemical processes. Academic Press: New York ; London, 1981; pp 71-119.

47.   Amatore, C.; Jutand, A.; Le Duc, G., *Chemistry* **2011,** *17* (8), 2492-503.

48.   Nakai, H.; Ogo, S.; Watanabe, Y., *Organometallics* **2002,** *21* (8), 1674-1678.

49.   Mohler, L. K.; Czarnik, A. W., *Journal of the American Chemical Society* **1993,** *115* (7), 2998-2999.

Chapter 3

Homocoupling or phenylboronic acid using Pd-CTAB

nanoparticles

Abstract

We have synthesised monodisperse Pd-CTAB nanoparticles (NPs) with an average size of

3.0 ± 0.1 nm. Pd-CTAB NPs are good catalysts for the aerobic oxidative homocoupling

reaction of phenylboronic acid (PBA) in aqueous micellar media, giving good pseudo-

first-order kinetics and also reducing phenol by-product formation compared to the use of

a molecular Pd catalyst. A bell-shaped pH-rate profile was observed using Pd-CTAB NPs,

which is in line with our previous observation using molecular Pd-catalysts. The reaction

was first-order in Pd-CTAB NPs. The effect of phenylboronic acid concentration on the

observed reaction rate constant was observed to show mixed second-order kinetics (at low

PBA concentration) and first-order kinetics (at high PBA concentration). The combined

observations provide some insights into the possible mechanism(s) of the reaction under

our conditions, with strong similarities to the possible mechanisms for catalysis by

molecular complexes. The key conclusion is that the activity of catalytic centres is

modulated through (de)protonation and is thus pH dependent.

3.1. Introduction

3.1.1. Palladium nanoparticles (Pd NPs)

Metal nanoparticles (NPs) have been known for more than two millennia and transition-metal NPs have been used since the 1970s in catalysis.[1-3] However, since the last decade, catalysis using metal NPs has gained dramatic interest and offered promising solutions for carrying out reactions efficiently under "greener conditions", *i.e.* mild and environmentally benign conditions.[4] NP catalysis is described as a frontier between homogeneous and heterogeneous catalysis and often referred to as "semi-heterogeneous catalysis".[5] Usually NP catalysts are prepared from a metal salt, a reducing agent, and a stabiliser. Possible nanoparticle stabilisers include dendrimers, specific ligands, ionic liquids, surfactants, proteins, membranes, carbon nanotubes, polymers and a variety of oxides.[6-8]

Because of the popularity of Pd chemistry, the synthesis of Pd NPs is increasing, using a variety of Pd precursors and stabilisers. For example, Gittins and Caruso[9] have used Na_2PdCl_4 and (4-dimethylamino)pyridine to synthesise stable Pd NPs. They have shown that (4-dimethylamino)pyridine acts both as a phase transfer agent and as a stabiliser of Pd NPs. Polymers have been regularly used as stabilising agents for Pd NPs, with the most commonly used polymer being poly-(N-vinyl-2-pyrollidone) (PVP). However, many other polymers have been used to stabilise Pd NPs including, polyurea,[10] polysilane,[11] polyacrylonitrile or/and poly-(acrylic acid),[12] polysiloxane,[13] oligosuccharides,[14] poly-(ethylene glycol).[15] Dendrimers have also proven to be good stabilisers for Pd NPs.[16, 17] Furthermore, surfactants and micelles have been commonly used as Pd NPs stabilisers for Pd NPs. For instance, Yang *et al.*[18] have used sodium dodecylsulfate (SDS) as a stabiliser for Pd NPs. Tan *et al.*[19] have synthesised monodisperse water soluble Pd-CTAB NPs by light decomposition of $Pd(PPh_3)_4$ in aqueous CTAB solution without need for a reducing

agent. Using UV–Visible spectroscopy, high resolution transmission electron microscope, energy dispersive X-ray analysis and powder X-ray diffraction methods to confirm the size and morphology of the formed NPs, they have found that face-centred-cubic (fcc) Pd-CTAB NPs of different sizes (2.5, 5 and 10 nm) were formed by simply tuning the concentration of CTAB-micelles. In other work, Fan and coworkers[20] demonstrated for the first time that nearly monodisperse single-crystalline palladium (Pd) nanocubes and nanodendrites could be prepared in aqueous solution at room temperature. The authors utilised the equilibrium between the dissolution and precipitation of the Pd-CTAB complexes in the synthesis of the NPs. Moreover, they have found that addition of foreign halide ions (Cl⁻ and Br⁻) can be used to tune the morphology of the obtained Pd nanocrystals. Furthermore, the formation of the single-crystalline pure Pd structures with fcc crystal lattice was confirmed by selected area electron diffraction (SAED) and X-ray diffraction (XRD) techniques. Recently, Lee *et al.*[21] demonstrated the effect of changing the injection sequence of CTAB and the reducing agent on the morphology of formed Pd-CTAB NPs from $K_2 PdCl_4$ in aqueous media.

Furthermore, bimetallic core-shell Au-Pd NPs stabilised by polymers were developed by Toshima's group.[22-24] For example, core-shell Au-Pd NPs stabilised by PVP have shown enhanced catalytic activity compared to the corresponding single metallic Pd NPs stabilised by PVP.[25] The synthesis and catalytic activity of bimetallic Pd NPs will be discussed in more detail in Chapter 4.

3.1.2. Pd-nanopartile-catalysed Suzuki cross-coupling and oxidative homocoupling of arylboronic acids

Because of the reputation of Pd as one of the most efficient and frequently used metals in catalysis, and especially in C-C bond formation (*e.g.* the Suzuki reaction), there has been

immense interest in the use of Pd NPs in catalysis.[4, 5, 26] Various Pd NPs have been used to

catalyse Suzuki-Miyaura reactions. For instance, Han and coworkers[27, 28] have used

ligandless Pd NPs generated *in situ* in polyethylene glycol (PEG-400) for Suzuki cross-

coupling reactions under mild conditions. They have shown that arylboronic acids

promote the formation of the NPs by acting as a reducing agent for the Pd^{II} salt. The

authors also observed that the *in situ* generated NPs were more efficient than pre-prepared

NPs for the reactions under the same conditions. Desmarets *et al.*[29] have synthesised Pd

NPs of *ca.* 25 nm particle size by reducing $PdCl_2$ and stabilising the NPs using N,N'-bis(4-

methoxyphenyl)-(1,1'-binaphthyl)-4,4'-diamine (naphthidine) in dioxane. The formed NPs

have shown good catalytic efficiency towards a Suzuki reaction using dioxane as a solvent

at 80 °C. Moreover, Diallo *et al.*[30] have used Pd NPs stabilised by dendrimers for a

Suzuki reaction using a H_2O/EtOH mixture as solvent. Gallon *et al.*[31] have developed Pd

NPs supported on polyaniline nanofibers as good catalysts for Suzuki reactions in water.

Unfortunately, most of the abovementioned procedures involve the use of expensive

ligands or supports for the NPs, the use of organic solvents, or the reaction rate was low.

Nevertheless, Saha *et al.*[32] have developed a fast, simple, and environmentally friendly

one-pot Suzuki reaction protocol using Na_2PdCl_4, SDS surfactant, K_3PO_4 and water as a

solvent. The reactions were conducted under aerobic ligand-free conditions. They have

shown that the catalysis occurred through *in situ* generated Pd^0 NPs stabilised by SDS and

K_3PO_4. The average size of the produced NPs was measured using TEM by taking an

extract of the reaction mixture at the end of the reaction, and it was found to be in the

range of 6-8 nm. The authors demonstrated easy recovery and reusability of up to three

runs of the catalyst. Prastaro *et al.*[33] ha ve prepared water-soluble spherical palladium

nanoparticles stabilised within the cage of a DNA-binding protein from starved cells of a

thermophilic bacterium "*Thermosynechoccus elongatus*" (Te-Dps) (Pd NP/Te-Dps). The average size of these NPs was 3.5 ± 0.5 nm from TEM images; they also observed that part of the Pd metal was on the surface of the protein. Prastaro *et al.* demonstrated that these NPs can be used as catalysts for the Suzuki-Miyaura cross-coupling reaction under aerobic phosphine-free conditions in aqueous media at 100 °C. In other work, Sawoo *et al.*[15] have developed a cheap and readily available method for the synthesis of spherical Pd nanoparticles with an average size of 7-10 nm by a novel reduction of Pd^{II} using a Fischer carbene complex and utilising poly ethylene glycol (PEG) as stabiliser and water as a solvent. They have found that PEG wraps around the nanoparticles to provide stabilisation and prevents agglomeration of the Pd metal. The size of the formed nanoparticles was controlled by tuning the Pd:PEG ratio. The authors have demonstrated that the formed water-soluble Pd-PEG NPs provide an efficient catalytic system for Suzuki, Sonogashira, and Stille reactions using water as the only solvent. The reactions were performed under mild conditions without any necessity for excluding air from the reaction mixture (*i.e.* no inert atmosphere is required).

In addition, as discussed in Chapter 2, different homogeneous[34-38] and heterogeneous[39, 40] palladium catalysts have been used to catalyse oxidative homocoupling reactions of arylboronic acids. However, to the best of our knowledge, there are few reports on the homocoupling reaction of arylboronic acid using Pd NPs. For example, Willis *et al.*[41] have synthesised Pd^{II} NPs of 15 nm average size, supported on CeO_2, TiO_2, SiO_2 and ZrO_2 surfaces. The synthesis was carried out by deposition-precipitation of $Pd^{II}(NO_3)_2$ on the surface of CeO_2, TiO_2, SiO_2 and ZrO_2. These (solid) NPs showed reasonable (heterogeneous) catalytic reactivity towards homocoupling reaction of phenylboronic acids in toluene at 60 °C under anhydrous conditions. The selectivity towards biphenyl

formation was 75% with the production of benzene and phenol by-products. The authors

have suggested that individual Pd atoms leaching out from the solid NPs were the cause of

the catalysis. Prastaro *et al.*[42] have used the abovementioned system consisting of

palladium nanoparticles (Pd^0 NPs) stabilised primarily within a protein cavity as a

(homogeneous) catalyst for the synthesis of symmetrical biaryls from arylboronic acids

and also from potassium aryltrifluoroborate in water under aerobic and phosphine-free

conditions.

Furthermore, Au NPs have been used as a catalyst to perform aerobic oxidative

homocoupling of arylboronic acids.[41, 43, 44] Our attempts at catalysis using Au-based

systems (Au NPs and Au-Pd core-shell NPs supported by a polymeric shell) are described

in Chapter 4.

3.1.3. Possible mechanisms of Pd-nanoparticle-catalysed C-C coupling reactions (Suzuki reaction and oxidative coupling of arylboronic acids)

Despite the fact that Pd NPs have been used to a great extent in the Suzuki coupling

reaction and in one instance even in the oxidative homocoupling of arylboronic acids,

there are no detailed mechanistic studies explaining the exact catalytic role of the Pd NPs.

However, some efforts have been made to describe the catalytic role of the Pd NPs and

these efforts are briefly reviewed here.

For the Heck reaction involving Pd-nanoparticles a mechanism has been proposed

involving Pd atom escape (leaching) from the Pd NPs and recombination after catalysis.[4,

45] This mechanism(s) could also apply to catalysis of the Suzuki-Miyaura reaction. [4, 30] For

instance, studies by Biffis' group[46] and by Liu and Hu[47] attribute the catalytic activity of

microgel- and polymer-encapsulated Pd NPs, respectively, in the Suzuki reaction to

leaching Pd^0 species. There are two hypotheses explaining the leaching of Pd atoms or

ions from the surface of the Pd NPs. The first hypothesis was formulated suggesting that

the leaching occurs after the oxidative addition of the aryl halide to the Pd^0 NPs in which

case the X-Pd^{II}-Ar complex escapes from the surface of the NPs and leaches out into the

solution. At the end of the catalytic cycle the reduced Pd^0 atoms will be redeposited on the

surface of the NPs (Scheme 3.1).[4]
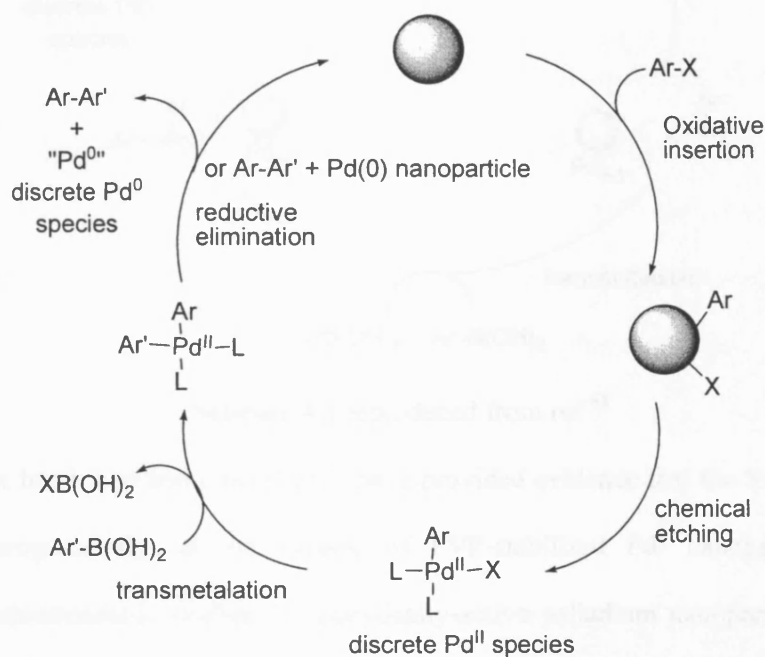
Scheme 3.1 reproduced from ref[4]

The second hypothesis suggests that Pd atom leaching occurs without involvement of the

aryl halide (Scheme 3.2). For example, Arai and coworkers' studies[45, 48] of Heck reactions

using Pd-NPs show that the reduced Pd species are more easily leached out into the

solvent compared with the oxidised species.[48]

However, Gaikwad *et al.* have suggested that both Pd^0 atom and Pd^{II} ion leaching is likely

to occur simultaneously and both types of leaching together are responsible for the

catalysis in the Suzuki reaction.[49]

106
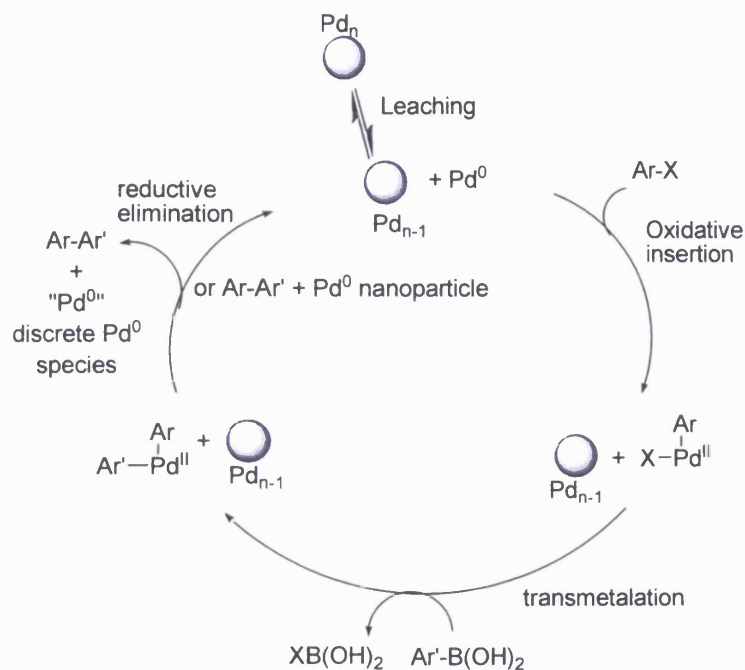
Scheme 3.2 reproduced from ref[48]

On the other hand, Lee and coworkers[50] have provided evidence that the Suzuki coupling occurs heterogeneously, at the surface of PVP-stabilized Pd^0 nanoparticles. X-ray absorption spectroscopic studies of catalytically-active palladium nanoparticles during a Suzuki-Miyaura cross-coupling reaction revealed that the nanoparticles were stable under the reaction conditions, and that cross-coupling involved the direct participation of surface palladium defect sites in the catalytic cycle (Scheme 3.3). Selective chemical and structural poisons provided further evidence for a heterogeneous active site.
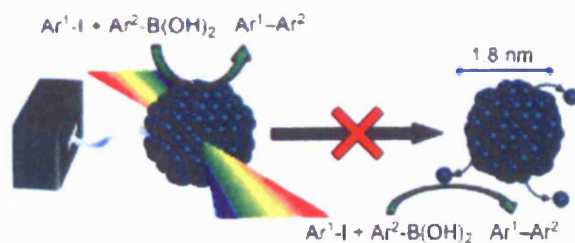
Scheme 3.3 taken from ref[50]

To the best of our knowledge, there is no report explaining the mechanism of homocoupling of arylboronic acids using Pd NPs. However, Prastaro et al.[51] have hinted (without details) that the reaction proceeds through a Pd-peroxo complex under aerobic conditions based on the proposal by Adamo et al.[38, 52] for molecular Pd catalyst.

3.1.4. Aims

We aim to synthesise a stable catalytically-active system consisting o f water-soluble monodisperse spherical Pd-CTAB NPs. UV-Visible spectroscopy and transmission electron microscopy (TEM) will be used for the characterisation of the prepared NPs. We use these NPs as catalysts for kinetic and mechanistic studies of micelle-assisted aerobic oxidative homocoupling reactions of phenylboronic acid in aqueous media.

3.2. Results and discussion

3.2.1. Synthesis of Pd-CTAB nanoparticles

Pd nanoparticles are of interest for our oxidative coupling reaction of arylboronic acids on the basis of their successful use in the Suzuki coupling reaction. We took a simple approach[19, 20] to synthesise nearly monodisperse spherical Pd-CTAB nanoparticles in water at 30 °C using $PdCl_2$ as a source of Pd and $NaBH_4$ as a reducing agent (Scheme 3.4)

$$PdCl_2 + 2HCl \longrightarrow H_2PdCl_4$$

$$H_2PdCl_4 + CTAB \xrightarrow[\text{stirring, 30 °C}]{NaBH_4} Pd^0\text{-CTAB NPs}$$
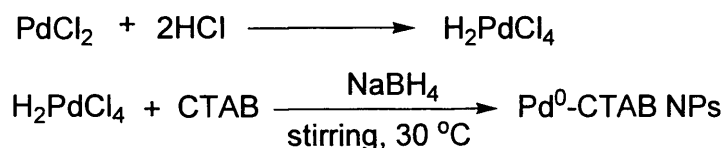
Scheme 3.4

The formed Pd-CTAB NPs were characterised using transmission electron microscopy (TEM) and UV-Visible spectroscopy (Figures 3.1a and b).
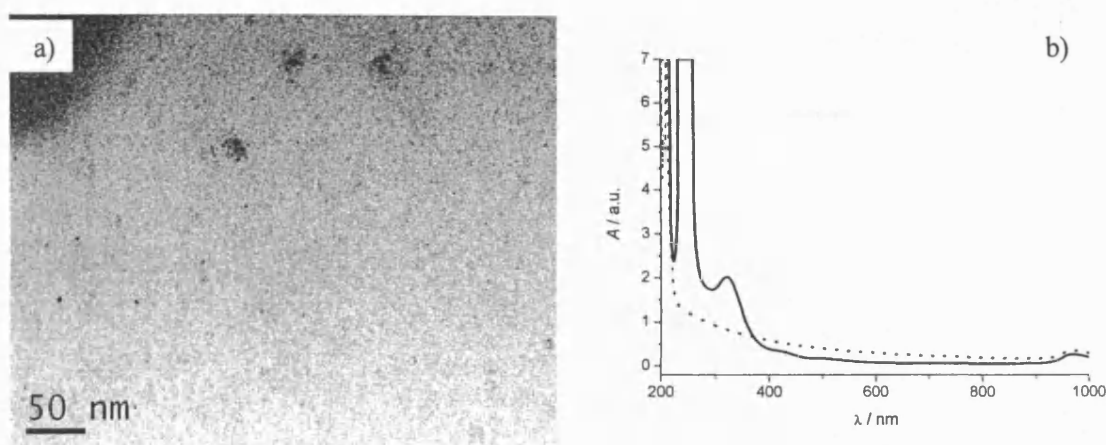
Figure 3.1: a) TEM image for Pd-CTAB nanoparticles, b) UV-Visible spectra of 0.25 mM H_2PdCl_4 in 8.0 mM CTAB (solid line) and 0.25 mM (Pd-content) Pd-CTAB NPs (dotted line).

Figure 3.1a (TEM image) shows monodisperse spherical Pd-CTAB NPs (black dots) with an average size of 3.0 ± 0.1 nm. Figure 3.1b shows the disappearance of the UV-Visible peaks at 223.5 and 307.0 nm for H_2PdCl_4 which is an indication of the reduction of Pd^{II} to Pd^0 (the height of the peak at 223.5 nm is an artefact).

3.2.2. Kinetics of the homocoupling reaction of PBA using Pd-CTAB nanoparticles

Using UV-Visible spectroscopy, we have followed the kinetics of the reaction of 0.1 mM PBA in the presence of 8.0 mM CTAB, 10.0 mM borate buffer and *ca.* 0.1 mM (in terms of Pd content) Pd-CTAB NPs (the concentration of CTAB is 8.0 mM in the Pd-CTAB NP preparation) (Scheme 3.5) (Figure 3.2).
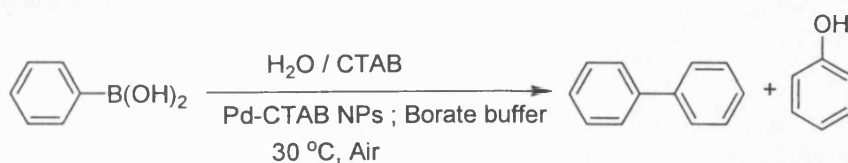
Scheme 3.5
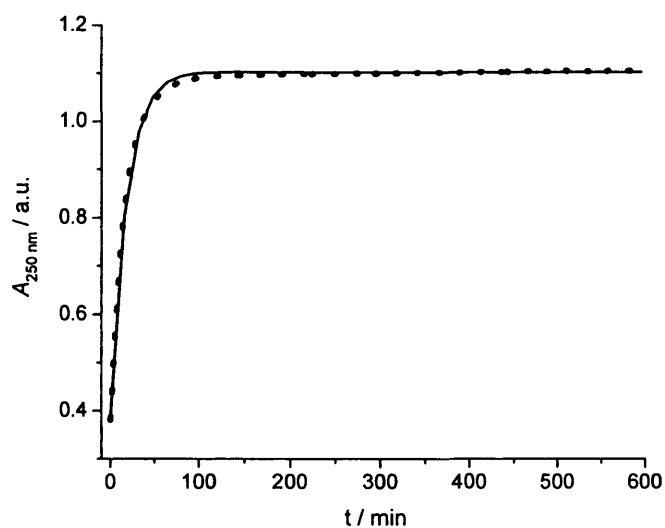
Figure 3.2: The absorbance of the reaction mixture of *ca*. 0.115 mM Pd-content in Pd-CTAB NPs in 8.0 mM CTAB, 10.0 mM borate buffer pH 8.8, and 0.1 mM Pd-CTAB NPs as catalyst at 30 °C versus time (dotted line), solid line fit to the (pseudo) first order equation (equation 2.1 in Chapter 2).

Figure 3.2 shows that the homocoupling reaction of phenyl boronic acid using Pd-CTAB

NPs follows the pseudo first-order rate law.

The product ratio for the reaction was found to be 3:1 biphenyl:phenol by HPLC (see

Figure S2.1 in Appendix 2), which corresponds to a reduction of the production of phenol

by 3 times compared to using molecular Pd catalyst 3 (Chapter 2) under similar conditions.

The Pd-CTAB NPs stability was tested and it was found that they stay stable over at least

one week without changing their catalytic activity towards the oxidative homocoupling of

PBA (Figure 3.3).
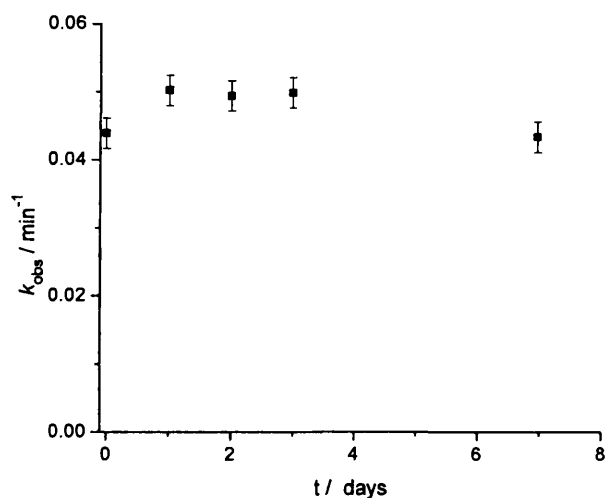
Figure 3.3: Pd-CTAB NPs catalyst activity represented by k_{obs} versus NP storage time for the reaction of 0.1 mM of PBA using 0.1 mM Pd-content in Pd-CTAB NPs in 8.0 mM CTAB and 10. mM borate buffer pH 8.8 at 30 °C.

Figure 3.3 shows the stability of the catalyst over a period of 7 days.

3.2.2.1. Effect of pH on k_{obs} of the homocoupling reaction using Pd-CTAB NPs

We have studied the effect of pH on k_{obs} for the homocoupling reaction of phenylboronic acid using borate buffer (Figure 3.4).
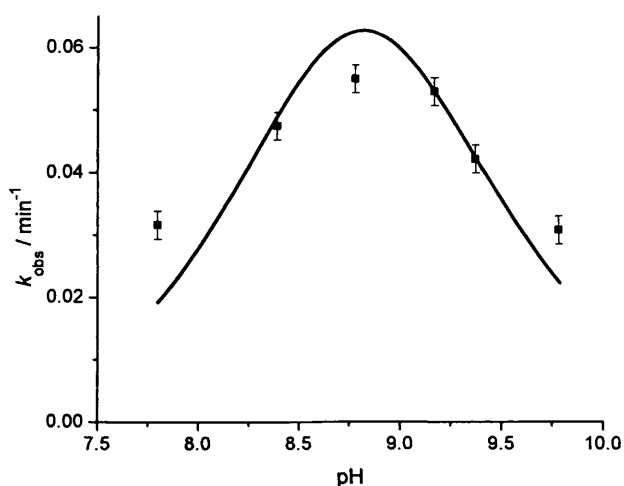
Figure 3.4: Effect of pH on k_{obs} for the reaction of 0.1 mM PBA, in 8.0 mM CTAB and 10.0 mM borate buffer using 0.115 mM Pd-content in Pd-CTAB NPs at 30 °C, (■) experimental data, solid line fit to Gaussian (eqn. 2.2).

Figure 3.4 shows a bell-shaped pH-rate profile for the homocoupling reaction of PBA using Pd-CTAB NPs, with a maximum in k_{obs} at pH close to the pK_a of PBA. This finding is in line with our previous results using a molecular Pd catalyst (see Chapter 2), which suggests different possibilities regarding the mechanism(s) of the reaction (vide infra).

3.2.2.2. Effect of PBA concentration on k_{obs}

We have studied the effect of [PBA] on k_{obs} for the reaction using 10 mM borate buffer and 0.1 mM Pd-CTAB NPs at pH 8.8 and 30 °C (Figure 3.5)
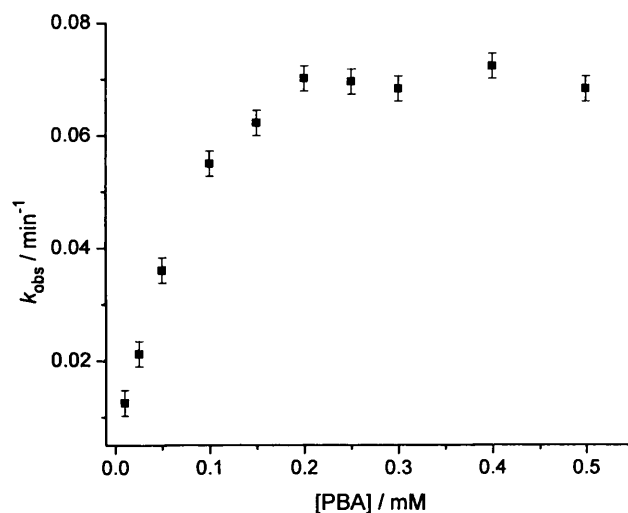
Figure 3.5: Effect of PBA concentration on k_{obs} for the aerobic oxidative homocoupling reaction of 0.1 mM PBA using 0.115 mM Pd-content in Pd-CTAB NPs in 8.0 mM CTAB and 10 mM borate buffer pH 8.8 at 30 °C.

Figure 3.5 shows that the reaction follows second-order kinetics when the PBA concentration is less than 0.2 mM but follows first-order kinetics at higher PBA concentrations. However, the reactions give reasonably good fits to pseudo-first-order kinetic equation 2.1 at all PBA concentrations (see Figures S2.2a-j in Appendix 2). This suggests that deviation from pseudo-first-order kinetics is not obvious from the kinetic fits. However, the mixed second- and first-order behaviour is in agreement with a kinetic

scheme involving a pre-equilibrium in which a first molecule of PBA binds to the surface

of the NP (or leaches a Pd atom) followed by a rate-determining step involving a second

molecule of PBA (Scheme 3.6).
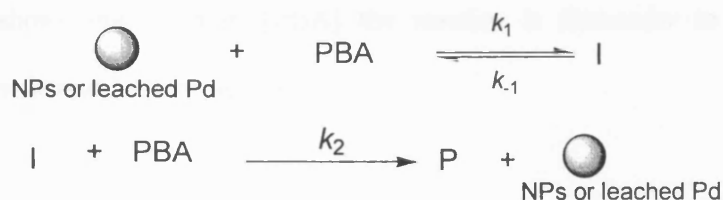
Scheme 3.6

Solving the kinetic equations of Scheme 3.6 using the steady state approximation results in

rate equation 3.1.

$$\frac{d[p]}{dt} = \frac{k_1 k_2 [PBA]^2}{k_{-1} + k_2 [PBA]}$$ (3.1)

Where k_1, k_{-1} and k_2 are intrinsic rate constants as defined in Scheme 3.6, [P] is product

concentration, and [PBA] is the phenylboronic acid concentration. For the full derivation

of equation 3.1 see section A2.3 in Appendix 2. At low PBA concentration k_2[PBA] in the

denominator is much less than k_{-1} and therefore the term k_2[PBA] is negligible and

equation 3.1 simplifies to equation 3.2.

$$\frac{d[p]}{dt} = \frac{k_1 k_2 [PBA]^2}{k_{-1}}$$

$$\text{then } \frac{d[p]}{dt} = k_{obs}[PBA]^2 \qquad \text{where, } \frac{k_1 k_2}{k_{-1}} = k_{obs}$$ (3.2)

Equation 3.2 shows that at low [PBA] the reaction is second-order in PBA.

However, at high PBA concentration k_{-1} in the denominator is much smaller than k_2[PBA],

therefore k_{-1} is negligible and equation 3.1 simplifies to equation 3.3.

$$\frac{d[p]}{dt} = \frac{k_1 k_2 [PBA]^2}{k_2 [PBA]} \qquad \text{where} \qquad \frac{k_1 k_2}{k_2} = k_{obs}$$

then $\dfrac{d[p]}{dt} = k_{obs}[PBA]$ (3.3)

Equation 3.3 shows that at high [PBA] the reaction is first-order in PBA for the mechanism summarised in Scheme 3.6.

3.2.2.3. Effect of Pd-CTAB NP concentration on k_{obs} for the homocoupling reaction of PBA

We have studied the effect of [Pd-CTAB NPs] on k_{obs} for the reaction of PBA using 10 mM borate buffer at pH 8.8 at 30 °C (Figure 3.6).
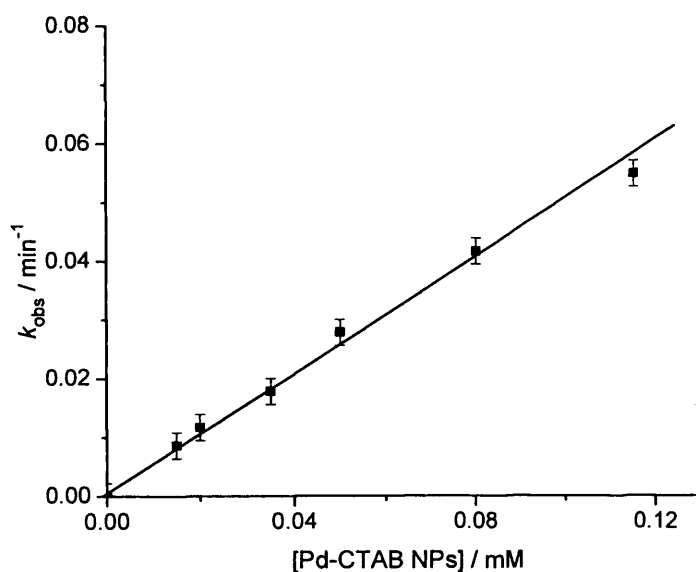
Figure 3.6: Effect of Pd-content in Pd-CTAB NPs concentration on k_{obs} of the aerobic oxidative homocoupling reaction of 0.1 mM PBA using 8.0 mM CTAB and 10.0 mM borate buffer pH 8.8 at 30 °C.

Figure 3.6 shows that the reaction is first-order in Pd-CTAB nanoparticles. This indicates the involvement of one catalyst active species (*vide supra*) in the rate-limiting step of the reaction.

3.2.2.4. Effect of borate buffer concentration on k_{obs} of the reaction

We have studied the effect of borate buffer concentration on k_{obs} for the reaction of 0.1

mM PBA using 10 mM borate buffer at pH 8.8 and at 30 °C (Figure 3.7).
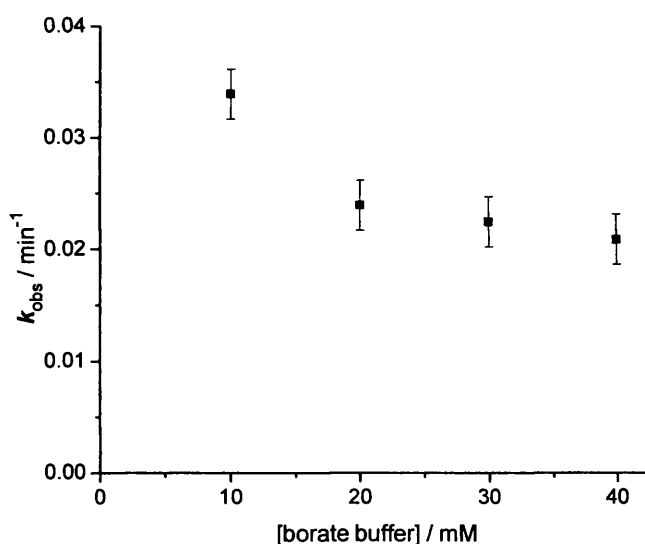
Figure 3.7. Effect of borate buffer concentration on the k_{obs} of the reaction of 0.1 mM PBA using 0.07 mM Pd-content in Pd-CTAB NPs, 8.0 mM CTAB at pH 8.8 and 30 °C.

Figure 3.7 shows that k_{obs} for the homocoupling reaction of PBA using Pd-CTAB NPs

decreases slightly with increasing borate buffer concentration. This behaviour, again,

mimics the behaviour of our molecular catalyst (Chapter 2). Clearly, buffer catalysis does

not occur and the slight decrease might be the result of small changes in ionic strength

(which was not held constant).

3.2.2.5. Possible mechanism(s) for the reaction

Based on our kinetic data and in line with the proposed mechanisms for the Suzuki-

Miyaura cross-coupling reaction using Pd NPs (*vide supra*), catalysis might occur at the

surface of the NPs or after leaching of Pd atom and/or ions. The possible pathways for

catalysis are: a) on the surface of the NPs in general, b) at so-called defect sites of the NP

surface, c) on leached Pd atom/ions, d) on Pd-atoms and/or ions which were removed from

the NP after the oxidative addition step (addition of molecular O_2) and/or e) Pd-atoms

and/or ions removed from the NP surface through the first transmetalation step.

In all possible catalysis pathways, and in agreement with our findings in Chapter 2 and in

Adamo's work[38], a peroxo-Pd^{II} intermediate is likely to be formed through an oxidative

addition step by (dissolved) molecular oxygen to Pd^0-CTAB NPs either on the surface of

the NPs or through reaction with a leached Pd^0 atom. The peroxo-Pd^{II}-complex likely

undergoes hydrolysis in the presence of water to form a OH-Pd^{II}-OOH complex which is

likely to be involved in acid/base equilibria as observed in Chapter 2 and therefore lead to

pH-dependent behaviour in aqueous media. The bell-shaped pH-rate profile makes us

suggest the same possible scenarios regarding the mechanisms(s) of the transmetalation

steps as discussed in Chapter 2. Consequently, reductive elimination forms the product

biphenyl.

As we have mentioned in Chapter 2 the by-product phenol forms as a result of the reaction

of peroxide (which is assumed to be formed within the catalytic cycle) with phenylboronic

acid. The formation of less phenol by-product compared to the same reaction under the

same conditions using the molecular Pd catalyst in Chapter 2 might be due to less

hydrogen peroxide formation within the catalytic cycle. The change in the kinetic-order

from 2nd to 1st order suggests the presence of a pre-equilibrium reaction involving PBA

before the rate-limiting step(s) of the reaction (Scheme 3.6). The first transmetalation

involves an equilibrium reaction between a molecule of PBA with a molecule of the

catalyst to form an intermediate. This intermediate then reacts with another molecule of

PBA to form another intermediate which then leads to the formation of the products by

reductive elimination.

116

The bell-shaped pH-rate profile is a result of either the acidic form of boronic acid needed in one step and the basic form in the other, or the catalyst is pH dependent and possibly has a pK_a slightly lower than the pK_a of PBA which leads to the contribution of acidic form of PBA and the basic form of the catalyst in the rate determining step. No Pd-black was observable at the end of the reaction which suggests that the reaction proceeds on the surface of NPs or the leached Pd atoms were redeposited on the NP surface, which then leads to the formation of bigger NPs (Ostwald ripening). However, we do not have any evidence confirming Ostwald ripening to occur during/after the catalysis. The Br counter ion of surfactant could possibly bind to the Pd atoms after being oxidised to Pd^{II} (either on the surface or after leaching) this might be partly responsible for the bell-shaped pH-rate profile behaviour.

Finally, the observation that the Suzuki-Miyaura cross-coupling reaction has been successfully catalysed by Pd NPs[50] suggests that if the reaction occurs on the surface of the nanoparticles, the reaction is restricted to individual Pd atoms or ions. If aryl groups were free to move across the NP surface, more homocoupling products (of both aryl halide and aryl boronic acid) would have been expected.

3.3. Conclusion

We have followed a simple approach to synthesise monodisperse Pd-CTAB nanoparticles of size 3.0 ± 0.1 nm. These Pd-CTAB NPs were found to be a good catalyst system for the aerobic oxidative homocoupling reaction of PBA, giving good pseudo-first-order kinetics and also reducing the ratio of the phenol by-product formation compared to the use of the molecular Pd catalyst discussed in Chapter 2. The observed effect of phenylboronic acid concentration on the reaction rate using Pd-CTAB NPs indicates mixed second-order (at low concentration) and first-order (at high concentration) kinetics. This behaviour suggests

the existence of a pre-equilibrium binding event involving a first molecule of PBA before the rate-determining step of the reaction, which involves a second molecule of PBA. The reaction was first-order in Pd-CTAB NPs suggesting involvement of one NP or leached Pd atom/ion in the rate-limiting step of the reaction.

Based on our kinetic data and in light of published proposals for the mechanism of the Suzuki cross-coupling reaction catalysed using Pd NPs we have no evidence to confirm that the catalysis occurs on the surface of Pd-CTAB NPs or via leached Pd-atoms/ions from the surface of the NPs. In both cases (based on our previous findings and Adamo's work[38]) a peroxo-Pd^{II} intermediate likely forms by an oxidative addition step by (dissolved) molecular oxygen. This peroxo complex undergoes hydrolysis in the presence of water to form a (OH)-Pd-(OOH) complex, the protonation state of which is pH dependent. This behaviour, together with the pH-rate profile, suggests that both arylboronic acids are involved in the rate determining step in a way that either the acidic form of PBA is needed in the pre-equilibrium step and the basic form in the step following it or *vice versa*. Another possibility is that the active species of the catalyst (OH)-Pd^{II}-(OOH) has a pK_a close to that of PBA which then favours the reaction to occur between the acidic form of PBA and the basic form of the catalyst or *vice versa*.

3.4. Experimental

3.4.1. Equipment

JASCO V630 and V650 UV-Visible spectrophotometers were used to monitor reactions by either time resolved absorption (spectra) or parallel kinetic measurements. Both machines were equipped with a Peltier thermostated cell holder to control the temperature. Reactions were carried out in 1.0 cm path length stoppered quartz cuvettes (Hellma) holding approximately 1.0 cm^3 of headspace (*i.e.* under aerobic conditions), at 30 °C. A

HANNA pH211 microprocessor pH meter equipped with a VWR 662-1759 glass

electrode was used for determining the pH of solutions. HPLC analysis was carried out

using an Agilent1200 instrument with a ZORBAY (Eclipse XDB-C18 4.6X150 mm, 5 μm)

column. Water was purified using an ELGA option-R 7BP and a Milli-Q system

(Millipore) water purifier. Transmission electron microscopy (TEM) was performed using

a JEOL JEM 1010 microscope operating at an acceleration voltage of 100 kV.

3.4.2. Chemicals

All chemicals were commercially available (Acros, Alfa Aesar, Aldrich and Fisher

Scientific) and used as purchased without further purifications. Acetonitrile and deionised

water were used as solvents for the preparation of stock solutions, 1:1

acetonitrile:deionised water mixture was used as a solvent for the preparation of

arylboronic acids and phenol stock solutions. Acetonitrile was used to prepare the

biphenyl (authentic standard) stock solution. Deionised water was the solvent for all other

stock solutions.

3.4.3. Synthesis of Pd-CTAB nanoparticales

Monodisperse spherical Pd-CTAB nanoparticles with an average size of 3.0±0.1 nm

(determined by TEM) were prepared by the addition of 2.0 mL of 100 mM of a freshly

prepared aqueous solution of $NaBH_4$ to a 48 mL aqueous solution containing 0.25 mM

H_2PdCl_4 (10 mM stock solution prepared by completely dissolving 44.5 mg of $PdCl_2$ in 5

mL of 100 mM HCl and 19 mL of deionised water) and 8.0 mM CTAB under magnetic

stirring at 30 °C. The mixture was allowed to stir for 1.0 h and the colour of the

homogeneous solution gradually changed from orange to dark brown which was

interpreted together with UV-Visible spectra as an indication for the reduction of Pd^{II} to Pd^0.

3.4.4. Typical kinetic experiments

3.4.4.1. Kinetic measurement using UV-Visible spectroscopy

3.4.4.1.1. Time resolved absorption peak measurements

Reactions were carried out in 1.00 cm pathlength stoppered quartz cuvettes (Hellma) holding approximately 1 cm^3 of headspace (*i.e.* under aerobic conditions), at 30 °C. Typical concentrations were 100 µM for arylboronic acids and a specified amount of the catalyst. Product formation (biaryl and phenol) was followed through changes in UV-Visible absorbance with time at 250 nm because this is where maximum changes in absorbance occur. The procedure was as follows: The reaction reagents (CTAB, borate buffer, and catalyst) were mixed in a 1.0 cm pathlength cuvette by pipetting the desired amount from the concentrated stock solutions. The cuvette was allowed to thermally equilibrate for about 5-10 minutes. Subsequently, the required amount of arylboronic acid was added to the reaction mixture from a concentrated stock solution to give a total volume of 2.5 mL. The reaction was monitored by measuring the time-resolved absorption peak. Reversing the order of the addition of arylboronic acid and the catalyst did not have any effect on the kinetic measurements. The observed rate constants k_{obs} were determined from plots of absorbance as a function of time, using the pseudo-first-order rate law (equation 2.1 Chapter 2) for analysis. Consequently all rate constants were expressed as observed pseudo-first-order rate constants.

3.4.4.1.2. Parallel kinetic measurements

Parallel kinetic measurements at fixed wavelength were performed using UV-Visible spectroscopy (JASCO V-650 spectrometer) using a six-cuvette cell changer at constant

temperature following the abovementioned procedure. Effects of pH, buffer concentration, catalyst concentration, and PBA concentration, were all studied by UV-Vis parallel kinetic measurements.

3.4.4.2. Product analysis and calibration graphs by HPLC

The same HPLC method as described in Chapter 2 was used to quantify the amount of the products (biphenyl and phenol) in the reaction mixture, using the same calibration.

Acknowledgements

References

1. Anton, D. R.; Crabtree, R. H., *Organometallics* **1983**, *2* (7), 855-859.

2. Toshima, N.; Yonezawa, T., *New Journal of Chemistry* **1998**, *22* (11), 1179-1201.

3. Widegren, J. A.; Finke, R. G., *Journal of Molecular Catalysis a-Chemical* **2003**, *198* (1-2), 317-341.

4. Astruc, D., *Inorganic Chemistry* **2007**, *46* (6), 1884-1894.

5. Astruc, D.; Lu, F.; Aranzaes, J. R., *Angewandte Chemie - International Edition* **2005**, *44* (48), 7852-7872.

6. Bonnemann, H.; Brijoux, W.; Joussen, T., *Angewandte Chemie - International Edition in English* **1990**, *29* (3), 273-275.

7. Bonnemann, H.; Brijoux, W.; Brinkmann, R.; Dinjus, E.; Fretzen, R.; Joußen, T.; Korall, B., *Journal of Molecular Catalysis* **1992**, *74* (1-3), 323-333.

8. Ozkar, S.; Finke, R. G., *Journal of the American Chemical Society* **2002**, *124* (20), 5796-5810.

9. Gittins, D. I.; Caruso, F., *Angewandte Chemie - International Edition in English* **2001**, *40* (16), 3001-3004.

10. Ley, S. V.; Mitchell, C.; Pears, D.; Ramarao, C.; Yu, J. Q.; Zhou, W., *Organic Letters* **2003**, *5* (24), 4665-8.

11. Kidambi, S.; Dai, J.; Li, J.; Bruening, M. L., *Journal of the American Chemical Society* **2004**, *126* (9), 2658-9.

12. Demir, M. M.; Gulgun, M. A.; Menceloglu, Y. Z.; Erman, B.; Abramchuk, S. S.; Makhaeva, E. E.; Khokhlov, A. R.; Matveeva, V. G.; Sulman, M. G., *Macromolecules* **2004**, *37* (5), 1787-1792.

13. Chauhan, B. P. S.; Rathore, J. S.; Bandoo, T., *Journal of the American Chemical Society* **2004**, *126* (27), 8493-8500.

14. Sanji, T.; Ogawa, Y.; Nakatsuka, Y.; Tanaka, M.; Sakurai, H., *Chemistry Letters* **2003**, *32* (10), 980-981.

15. Sawoo, S.; Srimani, D.; Dutta, P.; Lahiri, R.; Sarkar, A., *Tetrahedron* **2009**, *65* (22), 4367-4374.

16. Ornelas, C.; Boisselier, E.; Martinez, V.; Pianet, I.; Ruiz Aranzaes, J.; Astruc, D., *Chemical Communications (Cambridge)* **2007**, (47), 5093-5.

17. Ornelas, C.; Salmon, L.; Aranzaes, J. R.; Astruc, D., *Chemical Communications (Cambridge)* **2007**, (46), 4946-8.

18. Yang, C. C.; Wan, C. C.; Wang, Y. Y., *Journal of Colloid and Interface Science* **2004**, *279* (2), 433-439.

19.   Tan, H.; Zhan, T.; Fan, W. Y., *Chemical Physics Letters* **2006**, *428* (4-6), 352-355.

20.   Fan, F. R.; Adel, A.; Sur, U. K.; Chen, J. B.; Xie, Z. X.; Li, J. F.; Bin, R.; Tian, Z. Q., *Crystal Growth and Design* **2009**, *9* (5), 2335-2340.

21.   Wook Lee, Y.; Kim, M.; Woo Han, S., *Chemical Communications* **2010**, *46* (9), 1535-1537.

22.   Shiraishi, Y.; Hirakawa, K.; Yamaguchi, J. I.; Toshima, N., *Studies in Surface Science and Catalysis*, **2001**, 132 , 371-374.

23.   He, J.; Ichinose, I.; Kunitake, T.; Nakao, A.; Shiraishi, Y.; Toshima, N., *Journal of the American Chemical Society* **2003**, *125* (36), 11034-40.

24.   Matsumoto, H.; Mitsuhara, K.; Visikovskiy, A.; Akita, T.; Toshima, N.; Kido, Y., *Nuclear Instruments and Methods in Physics Research, Section B: Beam Interactions with Materials and Atoms* **2010**, *268* (13), 2281-2284.

25.   Sablong, R.; Schlotterbeck, U.; Vogt, D.; Mecking, S., *Advanced Synthesis and Catalysis* **2003**, *345* (3), 333-336.

26.   Lu, F.; Ruiz, J.; Astruc, D., *Tetrahedron Letters* **2004**, *45* (51), 9443-9445.

27.   Han, W.; Liu, C.; Jin, Z., *Advanced Synthesis and Catalysis* **2008**, *350* (3), 501-508.

28.   Han, W.; Liu, C.; Jin, Z. L., *Organic Letters* **2007**, *9* (20), 4005-4007.

       29.   Desmarets, C.; Omar-Amrani, R.; Walcarius, A.; Lambert, J.; Champagne, B.; Fort, Y.; Schneider, R., *Tetrahedron* **2008**, *64* (2), 372-381.

30.   Diallo, A. K.; Ornelas, C.; Salmon, L.; Aranzaes, J. R.; Astruc, D., *Angewandte Chemie-International Edition* **2007**, *46* (45), 8644-8648.

31.   Gallon, B. J.; Kojima, R. W.; Kaner, R. B.; Diaconescu, P. L., *Angewandte Chemie-International Edition* **2007**, *46* (38), 7251-7254.

32.   Saha, D.; Chattopadhyay, K.; Ranu, B. C., *Tetrahedron Letters* **2009**, *50* (9), 1003-1006.

33.   Prastaro, A.; Ceci, P.; Chiancone, E.; Boffi, A.; Cirilli, R.; Colone, M.; Fabrizi, G.; Stringaro, A.; Cacchi, S., *Green Chemistry* **2009**, *11* (12), 1929-1932.

34.   Smith, K. A.; Campi, E. M.; Jackson, W. R.; Marcuccio, S.; Naeslund, C. G. M.; Deacon, G. B., *Synlett* **1997**, (1), 131-&.

35.   Aramendia, M. A.; Lafont, F.; Moreno-Manas, M.; Pleixats, R.; Roglans, A., *Journal of Organic Chemistry* **1999**, *64* (10), 3592-3594.

36.   Yamaguchi, S.; Ohno, S.; Tamao, K., *Synlett* **1997**, (10), 1199-&.

37.   Wong, M. S.; Zhang, X. L., *Tetrahedron Letters* **2001**, *42* (24), 4087-4089.

38.   Adamo, C.; Amatore, C.; Ciofini, I.; Jutand, A.; Lakmini, H., *Journal of the American Chemical Society* **2006**, *128* (21), 6829-6836.

39. Chen, J. S.; Krogh-Jespersen, K.; Khinast, J. G., *Journal of Molecular Catalysis a-Chemical* **2008**, *285* (1-2), 14-19.

40. Cravotto, G.; Palmisano, G.; Tollari, S.; Nano, G. M.; Penoni, A., *Ultrasonics Sonochemistry* **2005**, *12* (1-2 SPEC. ISS.), 91-94.

41. Willis, N. G.; Guzman, J., *Applied Catalysis A: General* **2008**, *339* (1), 68-75.

42. Prastaro, A.; Ceci, P.; Chiancone, E.; Boffi, A.; Fabrizi, G.; Cacchi, S., *Tetrahedron Letters* **2010**, *51* (18), 2550-2552.

43. Tsunoyama, H.; Sakurai, H.; Ichikuni, N.; Negishi, Y.; Tsukuda, T., *Langmuir* **2004**, *20* (26), 11293-6.

44. Gonzalez-Arellano, C.; Corma, A.; Iglesias, M.; Sanchez, F., *Chemical Communications (Cambridge)* **2005**, (15), 1990-2.

45. Zhao, F.; Bhanage, B. M.; Shirai, M.; Arai, M., *Chemistry - A European Journal* **2000**, *6* (5), 843-848.

46. Biffis, A.; Zecca, M.; Basato, M., *Journal of Molecular Catalysis a-Chemical* **2001**, *173* (1-2), 249-274.

47. Liu, Y. B.; Khemtong, C.; Hu, J., *Chemical Communications* **2004**, (4), 398-399.

48. Zhao, F.; Shirai, M.; Ikushima, Y.; Arai, M., *Journal of Molecular Catalysis A: Chemical* **2002**, *180* (1-2), 211-219.

49. Gaikwad, A. V.; Holuigue, A.; Thathagar, M. B.; Ten Elshof, J. E.; Rothenberg, G., *Chemistry - A European Journal* **2007**, *13* (24), 6908-6913.

50. Ellis, Peter J.; Fairlamb, Ian J. S.; Hackett, Simon F. J.; Wilson, K.; Lee, Adam F., *Angewandte Chemie International Edition* **2010**, *49* (10), 1820-1824.

51. Prastaro, A.; Ceci, P.; Chiancone, E.; Boffi, A.; Fabrizi, G.; Cacchi, S., *Tetrahedron Letters* *51* (18), 2550-2552.

52. Lakmini, H.; Ciofini, I.; Jutand, A.; Amatore, C.; Adamo, C., *Journal of Physical Chemistry A* **2008**, *112* (50), 12896-12903.

Chapter 4

Homocoupling of phenylboronic acid using Au@Pd@pNIPAM nanoparticles and Pd-pNIPAM nanocomposites

Abstract

We have synthesised monodisperse bimetallic core-shell gold-palladium nanoparticles encapsulated in poly(N-isopropylacrylamide) shells (Au@Pd@pNIPAM NPs) of different Au-core/Pd-shell sizes and morphologies (spherical with a Au core of 64nm and Pd shells of 4.0, 10.9, 10.8 nm and with a Au core of 104 nm with a Pd shell of 9.9 nm; as well as rod-shaped Au cores of 48x23 nm carrying rocket-shaped Pd shells). Positive and negative Pd-pNIPAM nanocomposites were also successfully synthesised. The nanoparticles and nanocomposites were characterised using UV-Vis spectroscopy, transmission electron microscopy (TEM) and dynamic light scattering (DLS) techniques. The transition temperatures (T_c) separating the swollen and collapsed states of the pNIPAM shells were found to be 308, 305 and 306 K for Au@Pd@pNIPAM NPs, positively and negatively charged Pd-pNPAM nanocomposites, respectively. The synthesised NPs and nanocomposites were tested as catalysts for the aerobic oxidative homocoupling reaction of phenylboronic acid (PBA) in aqueous micellar solution. The reaction follows pseudo-first-order kinetics and displays a bell-shaped pH-rate profile. First-order reaction kinetics in the NPs and nanocomposites were observed. The reactions were first order in PBA using Au@Pd@pNIPAM NPs, but mixed second and first-order kinetics in PBA was observed using negatively charged Pd-pNIPAM nanocomposites. The effect of temperature on k_{obs} of the homocoupling of PBA is distinctly non-Eyring-like. The increase in k_{obs} below T_c is followed by a sudden decrease upon increasing the temperature above the T_c. Further increase of temperature results in an increase in k_{obs} again.

4.1. Introduction

Metal nanoparticles and nanocomposites have gained considerable attentions, due to their application in many fields, such as catalysis,[1, 2] photonics, electronics, optics, biomedicine,[3] and biosensing.[4] Catalysis using colloidal nanoparticles (NPs) of transition metals has been widely used in many types of chemical transformations, including C-C bond-forming reactions, and in particular the Suzuki-Miyaura and Heck reactions.[5] The applications of NPs in catalysis have been motivated by the improvements in efficiency and selectivity of NP-catalysed reactions and also by the ease of recovery and recyclability of the catalysts.[6, 7] Improvements in catalytic efficiency are typically achieved by particle size optimisation and surface modification of the nanoparticles. In line with these developments, the synthesis and characterisation of nanoparticles has dramatically advanced during the last two decades.[7, 8] In general, nanoparticles can be synthesised with different morphologies and sizes, simply by changing synthesis conditions and tuning the structure of the stabilising agents.[9, 10]

Gold nanoparticles (Au NPs) have been around for millennia, although for much of this time they have been predominantly used in the work of artists and craftsmen due to their magnificent interactions with light to produce vivid visible colour. Nowadays, Au NPs are also popular amongst scientists to work with, due to their facile synthesis, long-term stability, and because they are condutive to surface-molecule (ligand) modifications.[11] In particular, Au NPs are perfect for the formation of core-shell architectures, in which a layer of inorganic or organic material surrounds metal NPs. The introduction of shell around metal NPs has been investigated in terms of improving the stability and the surface chemistry of the core nanoparticles, but also to access new physical properties that were not accessible from the nanomaterial alone.[12]

4.1.1. Synthesis of Au NPs

Variety of synthetic protocols has been used to synthesise Au NPs with different sizes and morphologies. For example, spherical Au NPs of a wide size range can be prepared in aqueous solutions of the cationic surfactant cetyltrimethylammonium bromide (CTAB), through a seeded growth method where HAuCl₄ is catalytically reduced by a mild reducing agent such as ascorbic acid, on preformed Au seeds.[13, 14] Reducing capabilities similar to ascorbic acid have been reported for other organic acids such as salicylic acid,[15] which has the ability to reduce Au(III)-CTAB complexes to Au(I)-CTAB. However, reduction to Au(0) can only take place on catalytic metallic gold surfaces. Recently, Yavuz et al.[16] have shown the reducing capability of the vinyl group toward HAuCl₄, in the presence of water, so that Au(0) NPs could be formed.

Encapsulating NPs within stimuli-responsive polymeric shells gives them additional merits, because such shells offer possibilities for external switching and manipulation.[17] A common example of responsive material poly(N-isopropylacrylamide)   (pNIPAM), which is a thermoresponsive polymer that undergoes a phase transition from a hydrophilic, water-swollen, state to a hydrophobic collapsed, state when heated above its lower critical solution temperature (LCST), which is about 32-34 °C in water.[18] The addition of cross-linkers and co-monomers affects the swelling/shrinking ratio of the microgels and also the responsiveness towards different stimuli such as light,[19] pH,[20, 21] ionic strength[22, 23] or temperature.[24]

Contreras-Cáceres et al.[25, 26] have recently reported the growth of thermosensitive pNIPAM microgels on the surface of gold nanoparticles. The synthesis was carried out using several steps, including the formation of a first thin polystyrene layer, followed by pNIPAM

polymerisation after the required purification. Although gold nanoparticle growth could be achieved within the microgel shell, this synthesis was restricted to spherical nanoparticle seeds, whereas for example nanorods (which display a much more interesting optical response) could not be properly incorporated. Simplification of the coating process and making it more widely general was therefore needed. Thus, the same group in another recent paper[27] have published a novel procedure where butenoic acid is used both as a reducing agent and an a provider of vinyl functionality for the synthesis of Au NP in aqueous surfactant solutions, in the presence of preformed Au seeds. Providing the particles with vinyl functionality was required for direct pNIPAM polymerisation on the NP surface, while avoiding complicated surface functionalisation steps. Butenoic acid has the ability to adsorb on Au NP surfaces (both spheres and rods) and replace CTAB molecules. This procedure has facilitated the smooth and homogeneous polymerisation of pNIPAM on the metal core. Also, the authors have shown that the improved stability of the nanocomposites and the porosity of the pNIPAM shell allows the subsequent reduction of metal atoms on the metal core, which was exploited for the overgrowth of pNIPAM-encapsulated Au spheres and rods with both Au and Ag under mild conditions.

Bimetallic Au-Pd NPs of different structures, such as core-shell,[28] inverted core-shell,[28] and alloy[29] of different sizes and morphologies have been synthesised and intensively investigated. [28, 30] Because of their interesting catalytic activity, bimetallic Au-Pd NPs have been used as catalysts for many reactions e.g. acetylene hydrogenation,[31] direct hydrogen peroxide synthesis from H_2 and O_2,[32] synthesis of vinyl acetate,[24] hydrodechlorination of trichloroethane[33] and oxidation of alcohols to aldehydes.[34]

Au-Pd core-shell NPs of different sizes and morphologies have been synthesised using successive[35, 36] and simultaneous[28, 37, 38] reduction methods using different stabilising agents. The physical and chemical properties of the bimetallic core-shell NPs depend on whether the core and the shell elements are chemically separated or intimately alloyed.[39]

4.1.2. Au nanoparticles as catalysts

Au NPs have been used as catalysts in many organic transformations,[40, 41]due to their remarkable catalytic activities. For instance, Yan Lu *et al.*[42] have prepared spherical polyelectrolyte brushes (SPB), which are polystyrene cores surrounded by a dense surface layer of polyelectrolyte. The SPBs were used as carriers to incorporate metal NPs (such as Pd, Ag and Au). This catalytic system worked robustly, efficiently and in a "green" fashion in the hydrogenation of butyraldehyde in aqueous media at ambient temperature.[43, 44] However, SPB are "passive carriers", *i.e.* they are not sensitive to external stimuli.

Carregal-Romero *et al.*[45] have used Au@pNIPAM NPs as a catalyst in the electron-transfer reaction between hexacyanoferrate(III) and borohydride ions. The authors have demonstrated that the diffusion of reactants to the catalytic Au-cores was controlled by the thermosensitive pNIPAM network which acts as a "nanogate" that can be opened or closed to a certain extent. Interestingly, they have studied the effect of the crosslinker on the thermal response, the polymeric density of the shell and the extent of the volume change, of the Au@pNIPAM system and found that both temperature and composition of the shell affect the catalytic activity of the encapsulated gold nanoparticles. Finally, the authors have provided a mathematical model to reproduce the key features of the temperature-controlled catalysis, to

confirm the effect of the variation in diffusion rate through the shell of the NPs on the actual

observed reaction rate.

Tsunoyama et al.[46] have prepared and characterised Au NPs of less than 2 nm particle size

stabilised by poly(N-vinyl-2-pyrrolidone) (Au:PVP NPs) by simple reduction of $AuCl_4^-$ with

$NaBH_4$ in the presence of PVP. The catalytic activities of these NPs have been tested towards

the aerobic oxidative homocoupling reaction of phenylboronic acid (PBA) in water and in the

presence of base. They found that biphenyl and phenol were formed as major and minor

products of the reaction. The authors have proposed a catalytic cycle for the reaction (Scheme

4.1). Initially, dissolved O_2 molecules oxidatively add to the Au NP surface in a superoxo-like

form. Two subsequent transmetalation steps involving the basic form of PBA to the partially

oxidised Au NPs form phenyl-adsorbed Au NPs and boron peroxide. Finally, this

intermediate reductively eliminates to form biphenyl and regenerate Au(0) NPs. The phenol

byproduct is assumed to be formed from the reaction of PBA with hydrogen peroxide arising

from the reaction of peroxyboron and water.
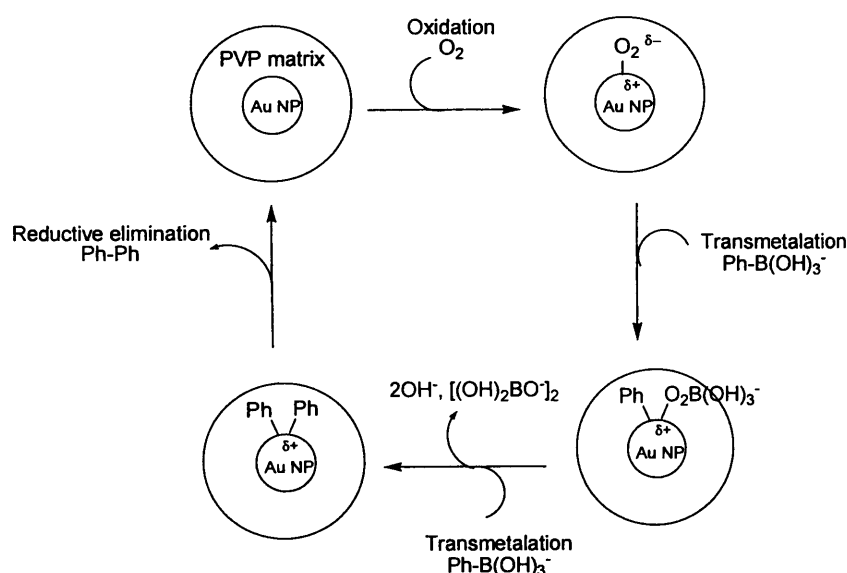
Scheme 4.1 reproduced from ref[46]

Gonzalez-Arellano et al.[47] have demonstrated a widely applicable approach for the homocoupling of arylboronic acids using a series of homogeneous and heterogenised Au(III)-Schiff base-complexes as selective and general catalysts using xylene as a solvent and K_2CO_3 as a base. They proposed a tentative mechanism for the reaction in which they assume that the oxidative addition does not occur on the gold complex, but the reaction follows two transmetalation steps of phenylboronate without changing the oxidation state of the Au(III) complex. Subsequently, the biphenyl product was formed in the usual reductive elimination step. Recently, Chaicharoenwimolkul and coworkers[48] have synthesised Au NPs (ca. 3 nm size, from TEM) stabilised by ligands containing ferrocene moieties. The authors observed that these Au NPs were not very efficient catalysts for the aerobic oxidative homocoupling of phenylboronic acids but instead were highly active towards demetalation of ferrocenylboronic acids.

Willis et al.[49] have deposited Au and Pd NPs with an average diameter of 10 and 15 nm, respectively, on different metal oxide surfaces, viz. CeO_2, TiO_2, ZrO_2, and SiO_2. A solution of $HAuCl_4$ or $Pd(NO_3)_2$ was simply deposited–precipitated on the metal oxide surface. They have used these NPs as heterogeneous catalysts for the oxidative homocoupling reaction of arylboronic acids under anhydrous conditions. They observed that, under the same reaction conditions, the supported Pd^{II} catalysts are less active than the supported Au^{III} catalysts. Also, the Pd catalysts show a selectivity of about 75% towards biphenyl with formation of benzene and phenol as byproducts. However, when supported Au is used for the reaction, a selectivity of 100% towards biphenyl is obtained in all cases except when SiO_2 is used as support. They have suggested that leaching of Pd is the source of catalysis when using supported Pd NPs

since the selectivity and reactivity was increased with increasing temperature. No leaching

was observed using supported Au NPs. Finally, the authors have observed that the activity of

the supported Au catalysts increases as the size of the crystallite support particles decreases

and as the initial surface coverage of OH groups in the supports increases.

As mentioned before Au and Pd NPs have been used separately as catalysts for both Suzuki

coupling reactions and oxidative homocoupling of arylboronic acids (vide supra and also see

Chapter 3). However, to the best of our knowledge, only one report, has been published using

Au-Pd NPs as a catalyst for the Suzuki reaction,[50] and no reports, so far, have been published

for the oxidative homocoupling reaction of arylboronic acids using Au-Pd NPs as catalyst.

4.1.3. Aims

Due to the stability and remarkable features of thermoresponsive Au@pNIPAM NPs and the

widespread applications of Pd catalysis, we aim to synthesise bimetallic core-shell Au-Pd NPs

encapsulated in pNIPAM shells (Au@Pd@pNIPAM NPs), with different sizes and

morphologies. Also, we are interested in the synthesis of positively (+ve) and negatively (-ve)

charged Pd-pNIPAM nanocomposites. The synthesised NPs and nanocomposites were tested

as catalysts for the aerobic oxidative homocoupling reaction of PBA in aqueous micellar

solution. Finally, the temperature effect of the nanoparticles and nanocomposites was studied.

4.2. Results and discussions

4.2.1. Synthesis of core-shell Au@Pd@pNIPAM NPs

We have followed the method developed by Contreras-Cáceres et al.[27] to synthesise spherical

Au@pNIPAM NPs using a seeded growth protocol of preformed Au-CTAB seeds. The Au-

CTAB seeds of ca. 15 nm size were prepared by citrate reduction of $HAuCl_4$. The overgrowth of the Au-CTAB seeds to ca. 64 nm was carried out via butenoic acid reduction of $HAuCl_4$ in CTAB solution. An excess of butenoic acid is used to allow its adsorption on the surface of the formed Au-NPs through their carboxylic groups. This strategy provides the NPs with a vinyl group, which is used to encapsulate the NPs with pNIPAM shell. The encapsulation process of these NPs with pNIPAM was achieved by removal of excess CTAB, and addition of the NIPAM monomer, N,N`-methylenebisacrylamide (BIS) as a crosslinker and 2,2`-azobis(2-methylpropionamidine) dihydrochloride (AAPH) as a cationic initiator under N_2 atmosphere. The UV-Vis NIR spectrum for the resulting Au-sphere(64 nm)@pNIPAM NPs is shown in Figure 4.1a and a representative TEM image is shown in Figure 4.1b. The average Au-core size measured from TEM was 64.0± 4.0 nm.
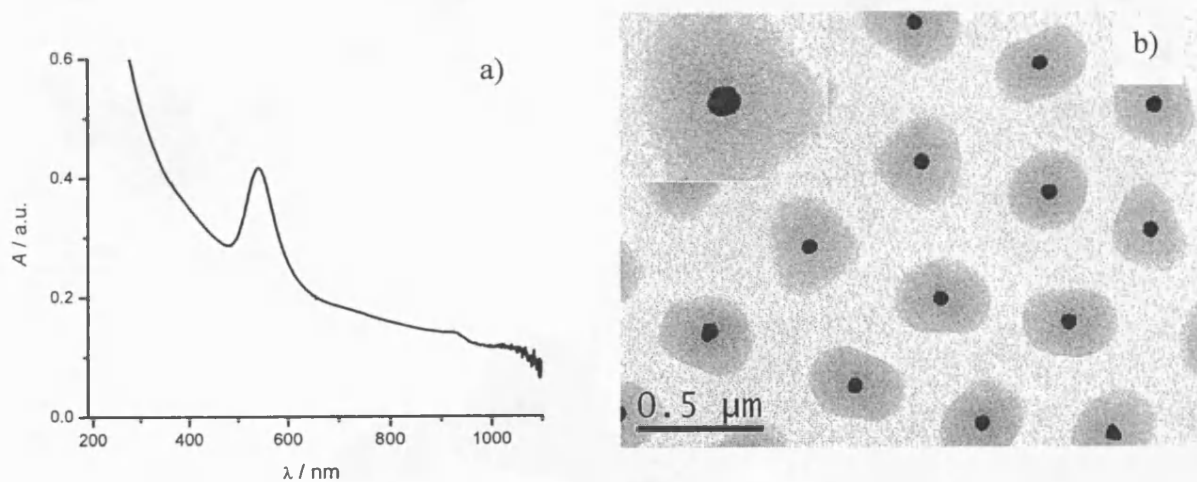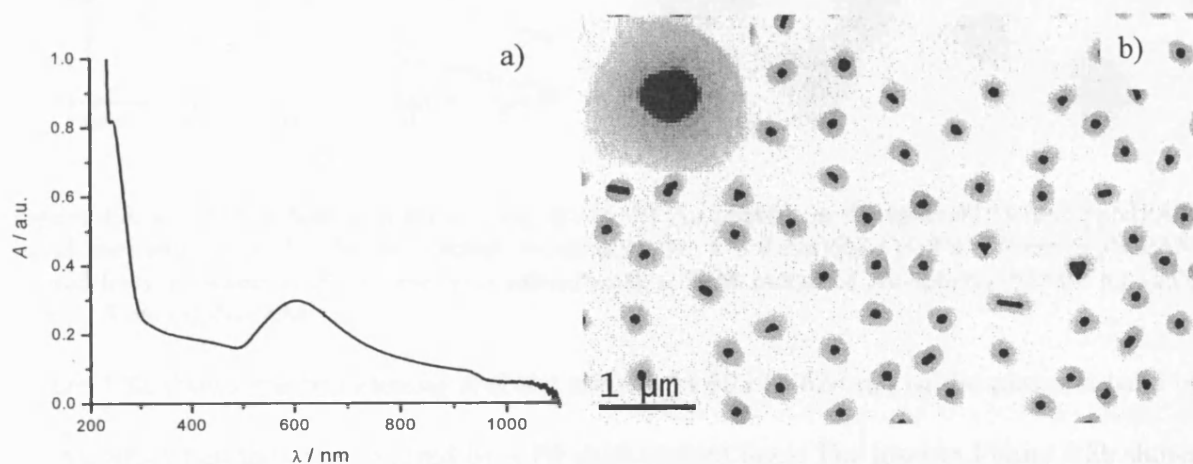

Figure 4.1. a) UV-Vis-NIR spectrum of 0.09 mM Au content in Au-sphere(64 nm)@pNIPAM in water at 25 °C and b) representative TEM image of Au-sphere(64 nm)@pNIPAM.

Figure 4.1a shows the significant plasmon band of Au-sphere(64 nm)@pNIPAM at 541 nm. The corresponding TEM images in Figure 4.1b show the encapsulation of the spherical Au core in the middle of the spherical pNIPAM shell.

Coating of the Au-core with Pd was carried out in CTAB using different concentrations of Na_2PdCl_4 as the source of palladium and ascorbic acid (AA) as the reducing agent. The CTAB concentration has a significant effect on the coating morphology of Pd on the Au surface (Figures 4.2a-e).
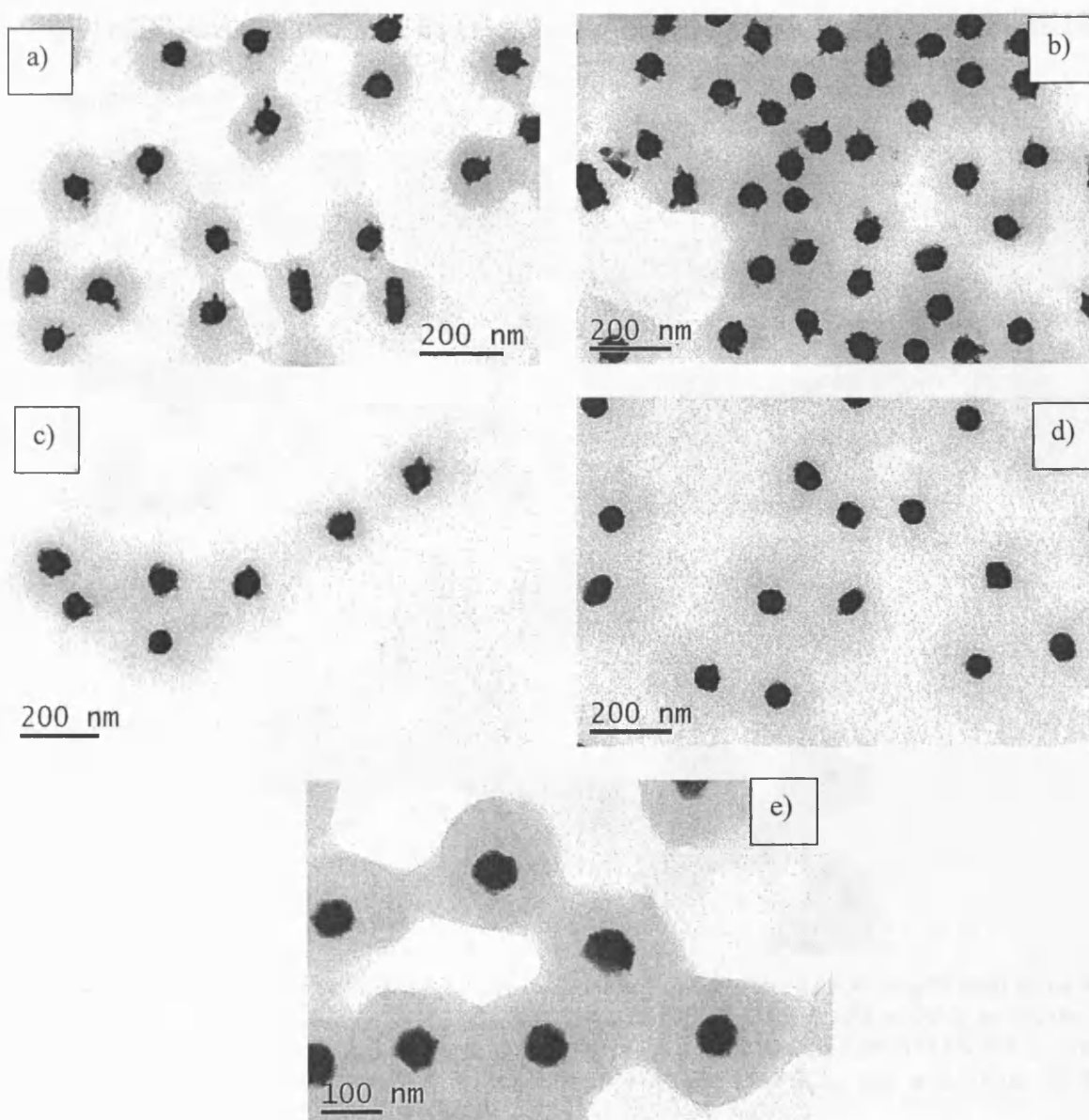
Figure 4.2. Representative TEM image of Au-sphere(64 nm)@Pd@pNIPAM synthesised using 0.09 mM (Au) in Au-sphere(64 nm)@pNIPAM NPs, 0.04 mM Na_2PdCl_4 and 2.0 mM ascorbic acid in: a) 15 mM CTAB, b) 50 mM CTAB, c) 100 mM CTAB, d) 200 mM CTAB and c) 300 mM CTAB.

Figure 4.2 shows that symmetrical coating of Pd on the Au core can be achieved when the

CTAB concentration is around 300 mM.

Additionally, the effect of Na_2PdCl_4 concentration on the thickness of the Pd coating was

studied, and it was found that increasing $[Na_2PdCl_4]$ from 0.04 mM to 0.08 mM increases the

Pd shell thickness up to two fold, however further increase of $[Na_2PdCl_4]$ does not affect the

coating thickness (Figure 4.3).
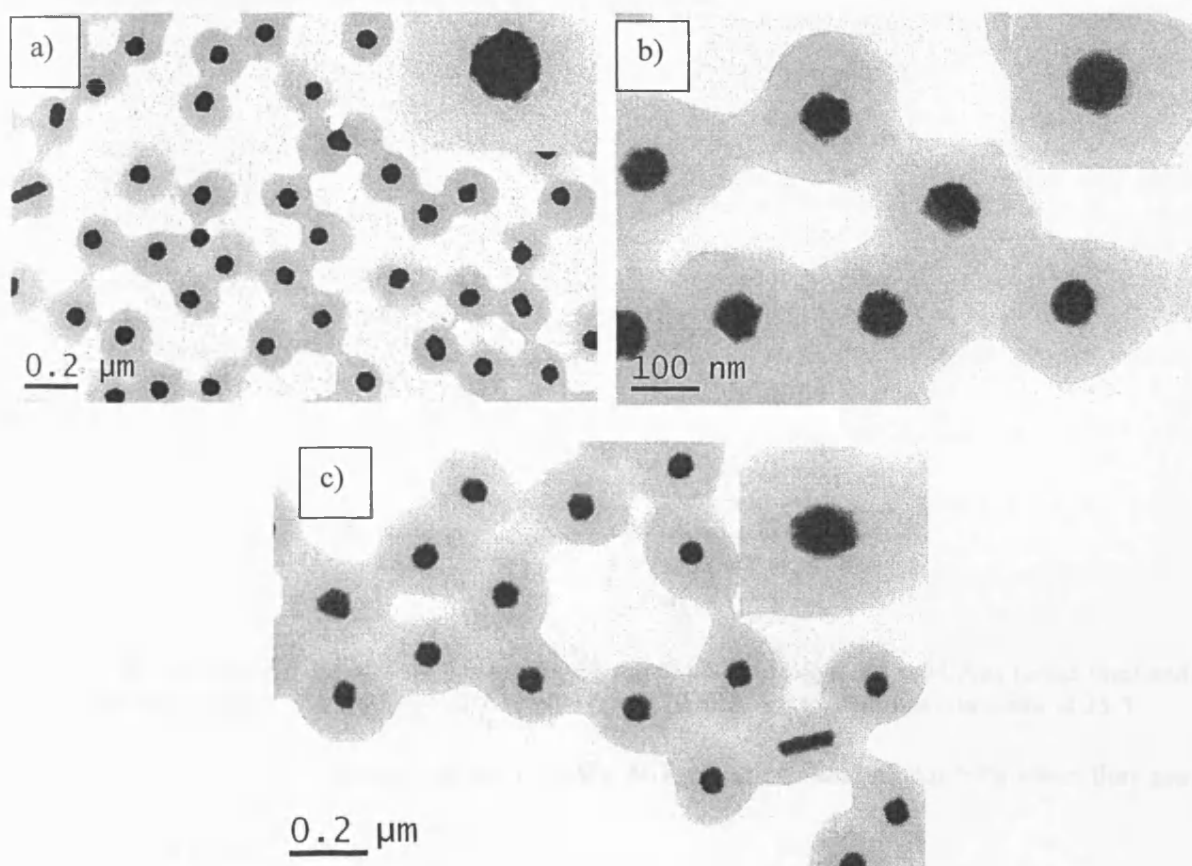
Figure 4.3. Representative TEM image of Au_sphere(64 nm)@Pd@pNIPAM, synthesised using 0.09 mM (Au) in Au-sphere(64 nm)@pNIPAM NPs, 300 mM CTAB and 2.0 mM ascorbic acid using: a) 0.04 mM Na_2PdCl_4, with a resulting Pd shell thickness of 4.0 ± 1.0 nm, b) 0.08 mM Na_2PdCl_4, with a resulting Pd shell thickness of 10.9 ± 2.0 nm and c) 0.16 mM Na_2PdCl_4, with a resulting Pd shell thickness of 10.8 ± 2.0 nm.

The insets in Figures **4.3a-c** show the typical intensity contrast between the Au core and the

Pd shell (due to the electron scattering differences between both metals), clearly revealing the

uniform coating for both geometries. The average core size and shell thickness from TEM

images were measured using image tool software and were a Au-sphere of 64 ± 4 nm, with Pd

shell thicknesses of 4.0 ± 1.0 nm, 10.9 ± 2.0 nm and 10.8 ± 2.0 nm resulting from the use of

0.04 , 0.08 and 0.16 mM of Na_2PdCl_4, respectively.

The UV-Vis NIR spectra of the formed Au-sphere(64 nm)@Pd(10.9 nm)@pNIPAM NPs

compared to Au@pNIPAM NPs is shown in Figure 4.4.
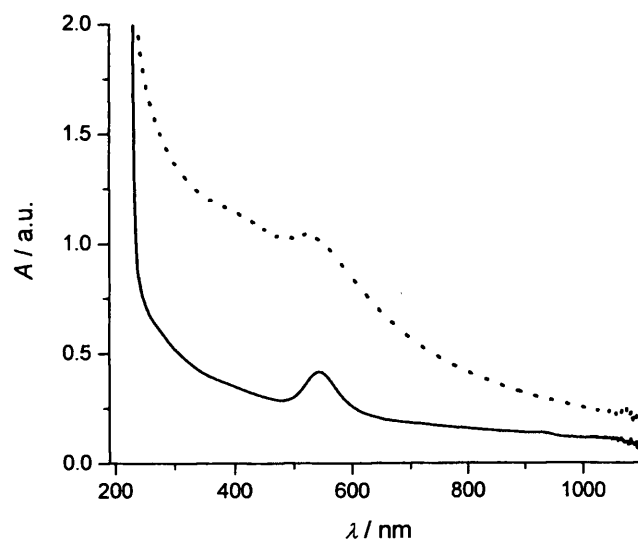
Figure 4.4. UV-Vis-NIR spectra of Au-sphere(64 nm)@pNIPAM (ca. 0.5 mM Au) (solid line) and Au-sphere(64 nm)@Pd(10.9 nm)@pNIPAM NPs (ca. 0.79 mM Au) (dotted line), in water at 25 °C.

Figure 4.4 shows the broadening of the UV-Vis NIR plasmon band of Au NPs when they are

covered by a Pd shell.

The thermoresponsive properties of the Au-sphere(64 nm)@Pd(10.9 nm)@pNIPAM NPs core-

shell systems were initially characterised by photon-correlation spectroscopy (PCS) both in

water and CTAB (Figures 4.5a&b, respectively).

137
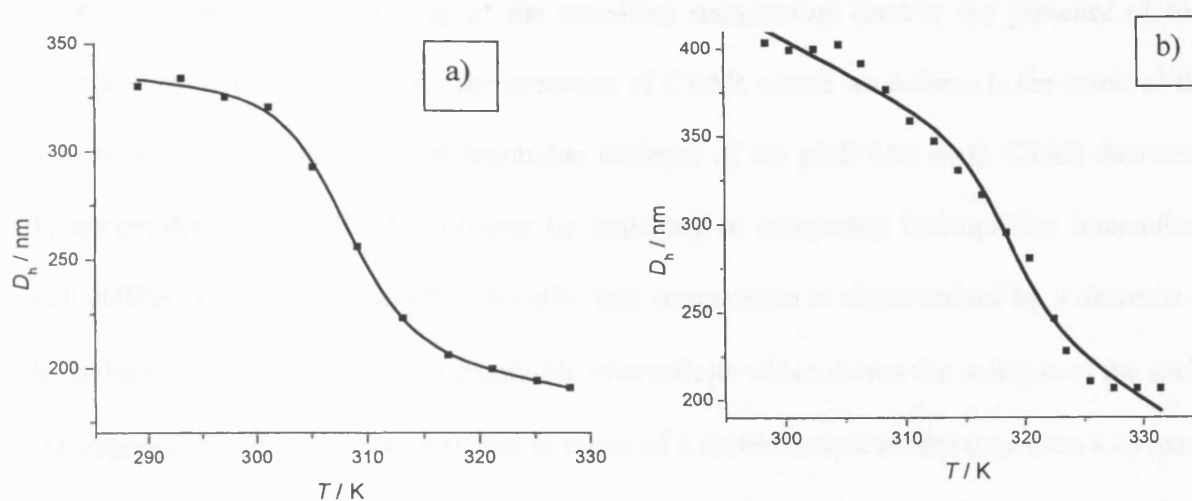
Figure 4.5. Temperature dependence of the hydrodynamic diameter (D_h) for Au-sphere(64 nm)@Pd (10.9 nm)@pNIPAM NPs in; a) deionised water and b) 10 mM aqueous CTAB. (■) experimental data, (solid line) fit to eq 4.2 (*vide infra*).

Figure 4.5a&b display the variation of the hydrodynamic diameter (D_h) of Au-sphere(64 nm)@Pd(10.9 nm)@pNIPAM NPs in water when the temperature was varied between 16 and 60 °C (289-333 K). Well-defined volume phase-transition temperatures (T_c) around 308 ± 1 K and 318 ± 4 K were determined (from the value of $\Delta H/\Delta S$ obtained by fitting to eq 4.2 (*vide infra*)) in water and 10 mM CTAB respectively. At high temperatures, the pNIPAM shell is completely collapsed, whereas at low temperatures the microgel is swollen (Scheme 4.2).
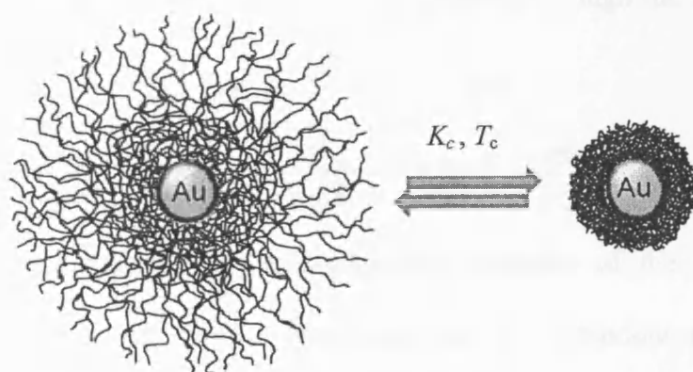
Scheme 4.2 taken from ref [45]

138

Figure 4.5b shows a broadening of the transition temperature (and/or the presence of two successive transitions) caused by the presence of CTAB which we believe is the result of the decreased cooperativity of the hydrophobic collapse of the pNIPAM shell. CTAB decreases the cooperativity of pNIPAM collapse by engaging in competing hydrophobic interactions with pNIPAM chains. Thermodynamically, this competition is characterised by a decrease in the enthalpy change ΔH of the hydrophobic interactions which drives the collapse of the shell. The experimental data can be analysed in terms of a mathematical model (equation 4.2) based on the assumption that the behaviour under study correlates linearly with temperature above and below the LCST or "collapse temperature" (T_c). The T_c itself is given by the temperature dependence of the equilibrium constant for the process underlying the collapse.

$$K_c = \exp(-(\Delta H_c - T \cdot \Delta S_c)/(R \cdot T)) \tag{4.1}$$

Where K_c is the equilibrium constant for the collapse-swelling process, ΔH_c and ΔS_c are the enthalpy and entropy of the process, T is the absolute temperature and R is the gas constant.

At T_c, K_c equals 1. As a result, T_c is given by the ratio $\Delta H_c /\Delta S_c$. The full behaviour as a function of temperature then becomes a weighted average over the low and high temperature behaviours ("low" and "high" with respect to T_c) as given through the equilibrium constant (equation 4.2).

$$\text{signal} = \frac{1}{1 + K_c} \cdot \text{low\_}T\text{\_behaviour} + \frac{K_c}{1 + K_c} \cdot \text{high\_}T\text{\_behaviour} \tag{4.2}$$

Where "signal" is, for example the hydrodynamic diameter of the NPs (D_h); both the behaviour at low temperatures (low_T_behaviour) and the behaviour at high temperatures (high_T_ behaviour) can themselves be temperature dependent (equations 4.3a and 4.3b).

low_T_behaviour = low offset + low slope * T (4.3a)

(This gives linear behaviour below T_c)

high_T_behaviour = high offset + high slope * T (4.3b)

(This gives linear behaviour above T_c)

The thermoresponsive zeta potential of the Au-shpere(64nm)@Pd(10.9 nm)@pNIPAM NPs in water was also measured using PCS when the temperature was varied between 16 to 60 °C (Figure 4.6).
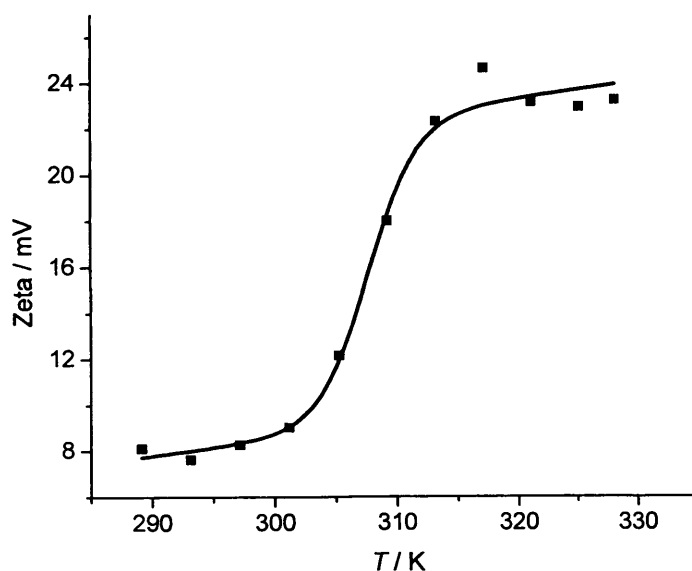
Figure 4.6. Temperature dependence of the zeta potential for Au-sphere(64 nm)@Pd(10.9 nm)@pNIPAM NPs in deionised water, (■) experimental data and (solid line) fit to eq 4.2.

Figure 4.6 shows a transition temperature of around 35 °C (308 K) between the collapsed and swollen states of the NPs, Also it is obvious from the values of the zeta potential that the pNIPAM shells are positively charged. Analysis of the experimental data in terms of eq. 4.1 gives the T_c similar to that of DLS.

Synthesis of Au-sphere (104 nm)@pNIPAM NPs

Further growth of the Au core in Au-sphere(64 nm)pNIPAM NPs was achieved using the method developed by Rodríguez-Fernández *et al.*[14] in which $HAuCl_4$ is added to the Au-sphere(64 nm)@pNIPAM NPs in CTAB solution and ascorbic acid (AA) is used as the reducing agent. The UV-Vis NIR spectrum of the formed Au-sphere(104 nm) is shown in Figure 4.7a and a representative TEM image is shown in Figure 4.7b.

Figure 4.7. a) UV-Vis-NIR spectrum of 0.5 mM Au content in Au-sphere(104 nm)@pNIPAM in water at 25 °C. and b) representative TEM image of Au-sphere(104±8.0 nm)@pNIPAM.

The UV-Vis spectrum in Figure 4.7a shows the plasmon band of Au-sphere(104 nm)@pNIPAM NPs at 603 nm which is clearly red shifted compared to the plasmon band for Au-sphere(64 nm)@pNIPAM which was centred at 540 nm. The measured average core size from TEM images was 104 ± 8.0 nm (measured using image tool software).

Au-sphere(104 nm)@Pd@pNIPAM NPs

Coating of Au-sphere(104 nm)@ pNIPAM NPs with a Pd shell was carried out using the same approach which was used for Au-sphere(64 nm)@pNIPAM (*vide supra*) using 0.08 mM

Na$_2$PdCl$_4$. A representative TEM image and the UV-Vis spectrum (compared to the spectrum

without Pd shell) for the produced NPs are shown in Figures 4.8a and b, respectively.
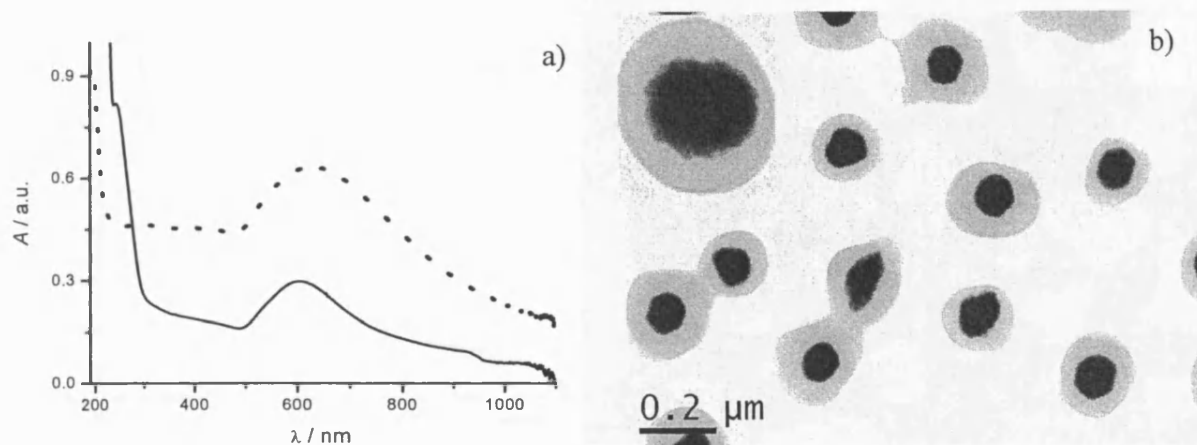
Figure 4.8. a) UV-Vis-NIR spectrum of *ca.* 0.09 mM Au content in Au-sphere(104 nm)@pNIPAM (solid line) and *ca.* 0.26 mM Au content Au-sphere(104 ± 8.0 nm)@Pd (9.9 ± 1.9 nm)@pNIPAM (dotted line), in water at 25 °C and b) a representative TEM image of Au-sphere(104±8.0 nm)@Pd (9.9 ± 1.9 nm)@pNIPAM.

Figure 4.8a shows the broadening and red shift from 603 to 626 nm of the plasmon band of

the Au NPs when they are covered by a Pd shell (dotted line). The inset in Figure 4.8b shows

the typical intensity contrast between the Au core and the Pd shell (due to the electron

scattering differences between both metals), clearly revealing the uniform coating. The

average core size and shell thickness from TEM was measured using image tool software to

be a Au-sphere of 104 ± 8 nm with a Pd-shell of a thickness of 9.9 ± 1.9 nm.

Au-rod@Pd@pNIPAM NPs

Au-rod@pNIPAM NPs were synthesised using Contreras-Cáceres *et al.*[27] protocol. Initially

Au rod colloids are synthesised using the seed mediated synthesis reported by Guyot-Sionnest

et al.[51] The encapsulation process by pNIPAM is carried out using the abovementioned

method for Au-sphere(64 nm)@pNIPAM NPs. The UV-Vis spectrum of the formed NPs is

shown in Figure 4.9a and a representative TEM image is shown in Figure 4.9b.
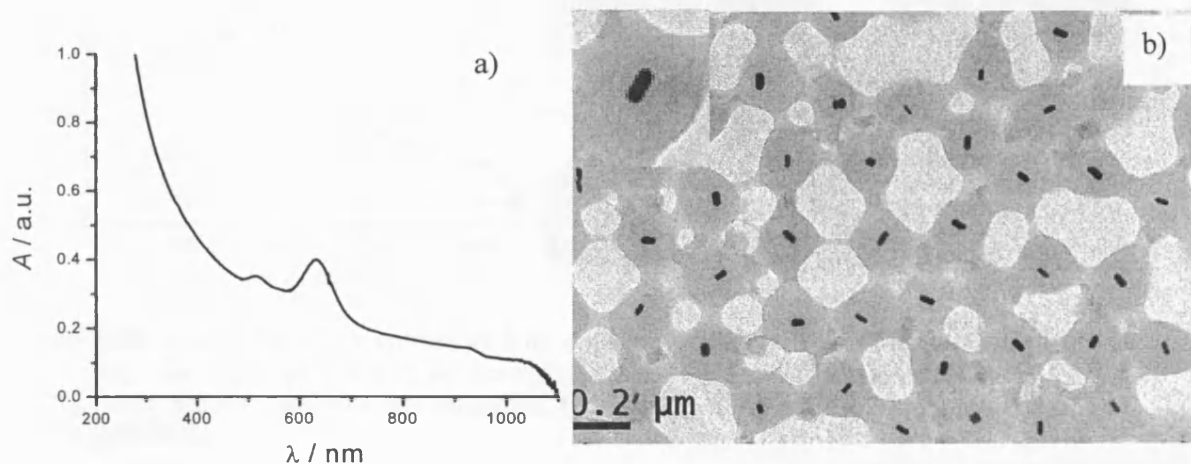
Figure 4.9. a) UV-Vis-NIR spectrum of 0.04 mM Au content in Au-rod(48x24nm)@pNIPAM in water at 25 °C. and b)representative TEM image of Au-rod@pNIPAM.

The UV-Vis spectrum in Figure 4.9a shows the plasmon band of Au-rod(48x24

nm)@pNIPAM NPs at 632 nm which has clearly red shifted compared to plasmon bands for

Au-sphere(64 and 104 nm)@pNIPAM which were 540 and 603 nm, respectively. The

measured average core sizes from the TEM image were a length of 48 ± 5 nm and a width of

24 ± 3.0 nm (measured using image tool software).

Coating of these Au-rod(48 x 24 nm)@ pNIPAM NPs with a Pd shell was carried out using

the same approach which was used for Au-sphere(64 nm)@pNIPAM (*vide supra*) using 0.32

mM Na$_2$PdCl$_4$. A representative TEM image and the UV-Vis spectrum (compared to the

spectum for the Au nanorods without Pd shell) for the produced NP are shown in Figures

4.10a and b, respectively.
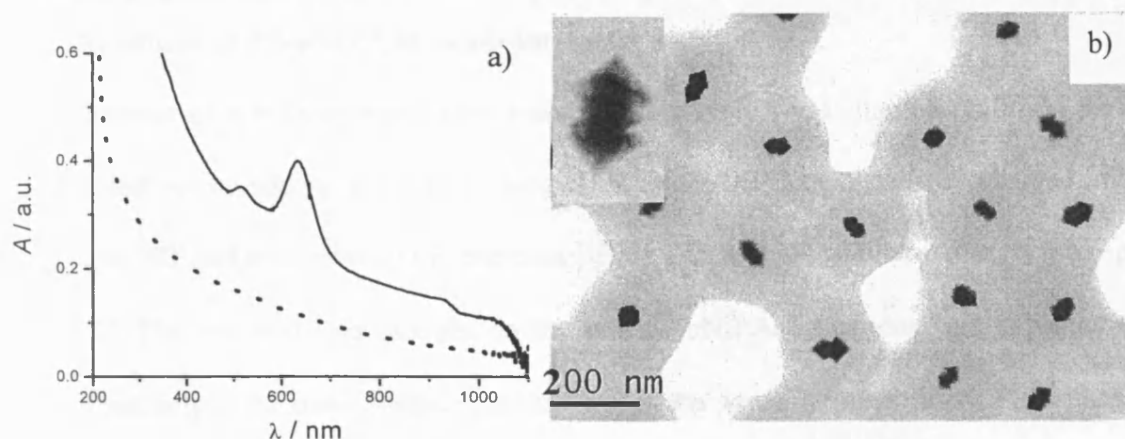
Figure 4.10. a) UV-Vis-NIR spectrum of 0.04 mM Au content in Au-rod(48x24nm)@pNIPAM (solid line), and 0.08 Au content in Au-rod(48x24nm)@Pd(rocket shape)@pNIPAM (dotted line), in water at 25 °C, and b) a representative TEM image of Au-rod(48x24nm nm)@Pd (rocket shape)@pNIPAM.

Figure 4.10a shows the remarkable disappearance of the UV-Vis NIR plasmon band of Au-rod NPs (solid line) when they are covered by the Pd shell (dotted line). Figure 4.10b shows a representative TEM image of the formed Au-rod(48x24nm nm)@Pd (rocket shape)@pNIPAM NPs. The inset in Figures 4.10b shows the typical intensity contrast between the Au core and the Pd shell (due to the electron scattering differences between both metals), clearly revealing the rocket-shaped coating of the Pd on the Au nanorod core. We were not able to measure the shell thickness from TEM using image tool software, because of the non-uniformity of the geometry of the Pd-shell.

It is important to mention that the palladium content is unknown in all types of the synthesised Au@Pd@pNIPAM NPs. The values of Au content are approximately known, however, from the spectra of the starting Au seeds.

4.2.2. Synthesis of Pd-pNIPAM nanocomposites

The synthesis of spherical positively (+ve) and negatively (-ve) charged pNIPAM particles

was carried out by adding positively charged initiator AAPH or negatively charged initiator

$K_2S_2O_8$ to NIPAM monomer in the presence of 5% BIS as a crosslinker under N_2 atmosphere

at 70 °C. The +ve and −ve charges on the porous pNIPAM "spheres" are expected to be

present not only at the outer surface but also within the pores. Representative TEM images of

+ve and -ve pNIPAM nanogels are shown in Figure 4.11.
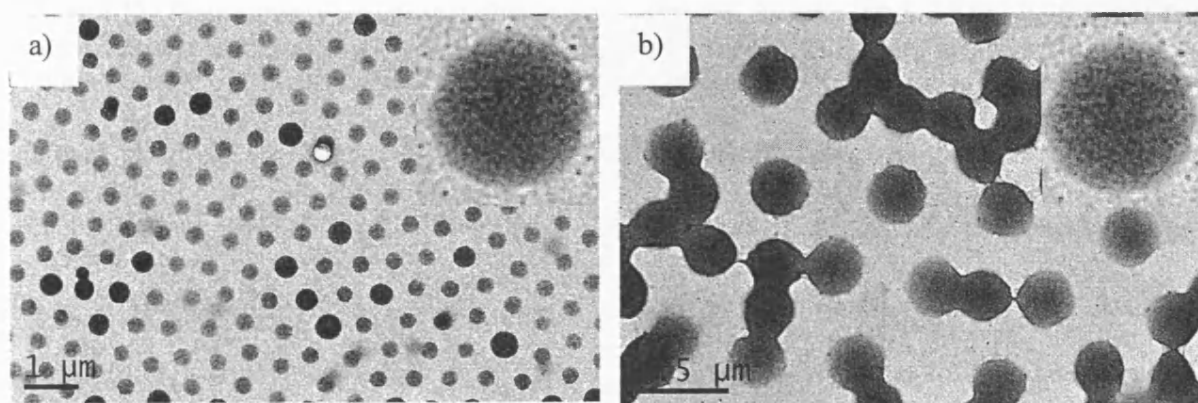
Figure 4.11. Representative TEM image of pNIPAM a) negatively charged and b) positively charged.

Figures 4.11a and b show the formation of monodiperse spherical negatively and positively

charged pNIPAM nanogels, respectively.

The thermoresponsive properties of the pNIPAM systems (+ve and −ve) were characterised by

photon-correlation spectroscopy (PCS) in water (Figures 4.12a&b, respectively).

145
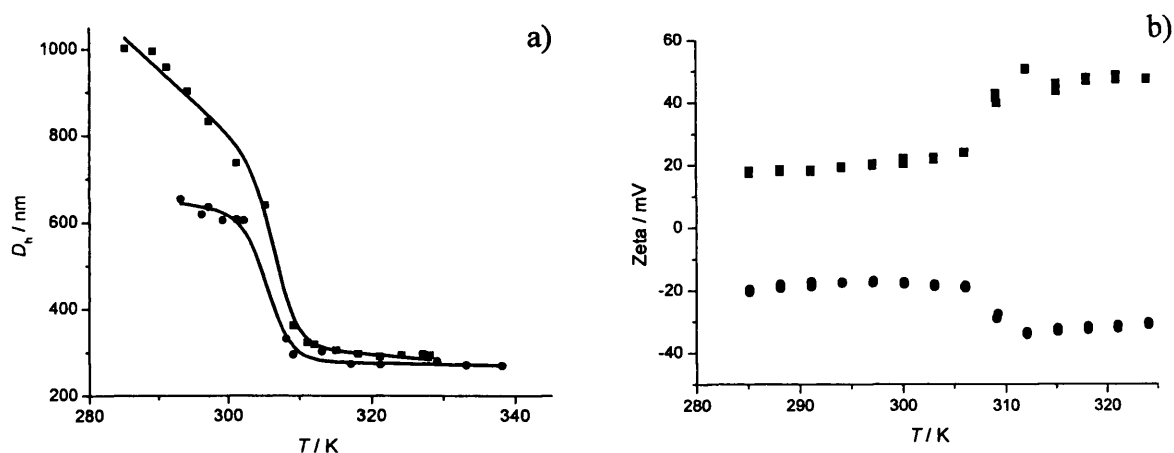
Figure 4.12. Temperature dependence of the a) hydrodynamic diameter (D_h) and b) zeta potential for Pd-pNIPAM nanocomposite (■) positive and (●) negative, in water. Solid lines in (a) are fits to eq 4.2. Figure 4.12a show the variation of D_h with temperature for both positively and negatively

charged pNIPAM particles. Well-defined volume phase-transition temperature (T_c) around

305 ± 1 K and 306 ± 1 K were determined (from the values of $\Delta H_c/\Delta S_c$ obtained by fitting

the experimental data to eq. 4.2) for +ve and –ve pNIPAM, respectively. At high

temperatures, the pNIPAM shell is completely collapsed, whereas at low temperatures the

microgel is swollen. The transition temperature together with the positive and negative charge

of the microgel is confirmed by the zeta potential values in Figure 4.12b.

Pd-pNIPAM nanocomposites

Introduction of Pd^0 to the synthesised spherical pNIPAM (+ve or –ve) was carried out by

reducing Na_2PdCl_4 in a stirred aqueous solution of the pNIPAM nanogels using $NaBH_4$ as a

reducing agent at room temperature. The formation of Pd-pNIPAM (+ve and –ve)

nanocomposites (after washing,) was confirmed by TEM images shown in Figures 4.13a and

b, respectively.

146
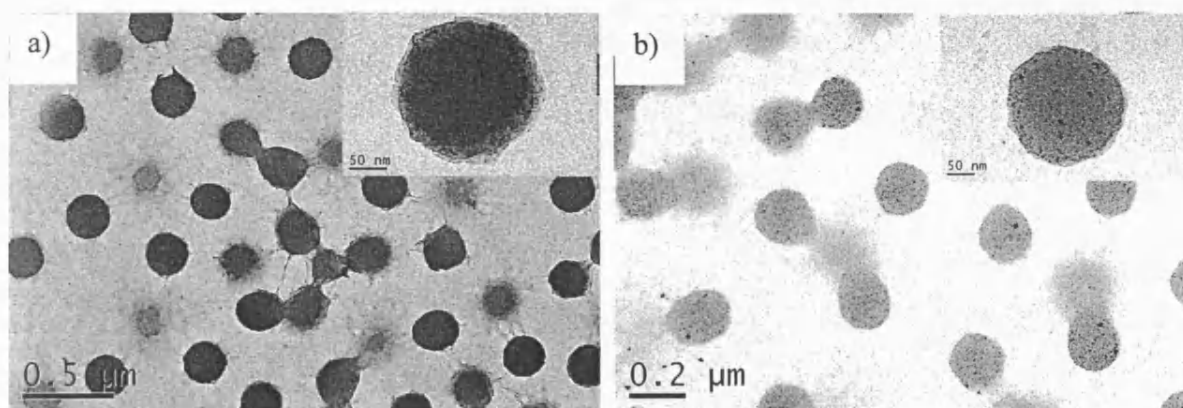
Figure 4.13. Representative TEM images of Pd-pNIPAM a) negatively charged and b) positively charged.

The insets in Figure 4.13a and b clearly show the Pd^0 distributed evenly (small black dots) within the pNIPAM particle, confirming the formation of the Pd-pNIPAM (-ve and +ve) nanocomposites.

4.2.3. Kinetic studies of the aerobic oxidative homocoupling reaction of PBA

The oxidative homocoupling reaction of phenylboronic acid using Au-sphere(64 nm)@Pd (10.9 nm)@pNIPAM NPs (used as a model for our optimisation studies) as a catalyst (Scheme 4.3) was followed using UV-Visible absorption spectroscopy. Product formation (biaryl and phenol) was followed through changes in absorbance with time at 250 nm where the maximum change in absorbance occurred for reaction of PBA (Figure 4.14).
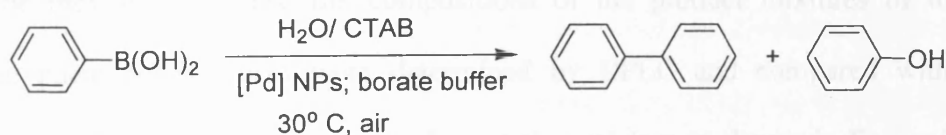
Scheme 4.3
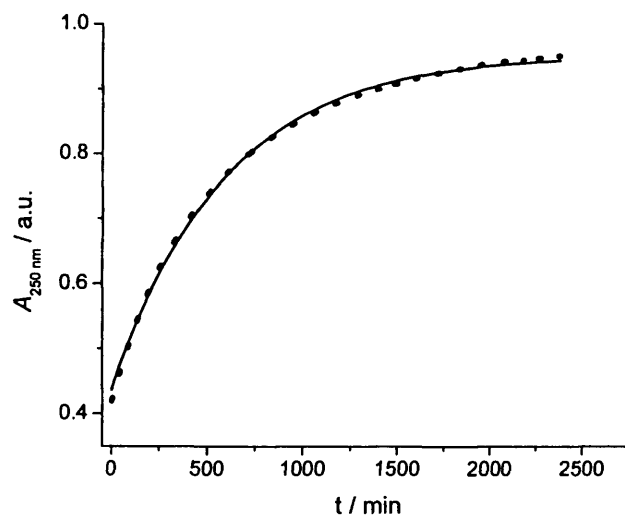
Figure 4.14. Absorbance of the reaction mixture of the homocoupling of 0.1 mM PBA using Au-sphere(64 nm)@Pd (10.9 nm)@pNIPAM (60.8 µM Au) with time at 250 nm in 10.0 mM CTAB and borate buffer pH 8.8 at 30 °C , experimental data (dotted line), solid line fit to a (pseudo) first-order rate equation (2.1).

Figure 4.14 shows that the homocoupling reaction of phenyl boronic acid using Au-sphere(64 nm)@Pd (10.9 nm)@pNIPAM follows first-order rate law reasonably well. Consequently all rate constants are expressed as observed pseudo-first-order rate constants. Although the Au concentration is approximately known, the concentration of Pd^0 in the catalyst stock solution is not precisely known, and hence subsequent kinetic experiments were performed using the same catalyst stock solution.

4.2.3.1. Product analysis

As in the previous Chapters, the compositions of the product mixtures of the reaction involving phenylboronic acid were determined by HPLC and compared with authentic samples. The HPLC chromatogram for the reaction mixture is shown in Figure S3.1 in the Appendix 3. Biphenyl and phenol were formed in a 1.3:1 ratio for the reaction of PBA (under our optimum reaction conditions) (*vide infra*). This observation suggests that the reaction

between the previously proposed peroxide[52] side product and phenylboronic acid to produce

the phenol is faster than alternative peroxide decomposition routes (see Chapter 2).

4.2.3.2. Effect of PBA concentration

In order to study the order of the reaction in phenylboronic acid, we determined the effect of

phenylboronic acid concentration on the observed first-order rate constant (k_{obs}) under

otherwise standard conditions (*vide infra*) at 30 °C and pH 8.2 (Figure 4.15).
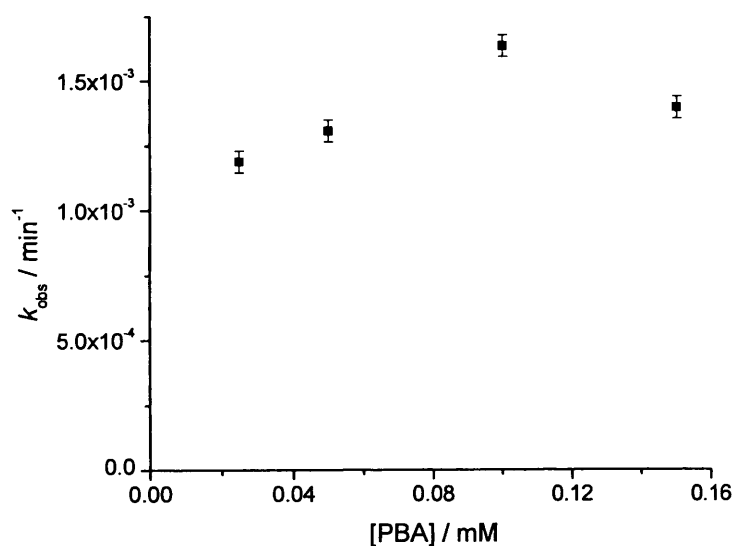
Figure 4.15. Effect of PBA concentration on the observed reaction rate constant using 60.8 μM Au in Au-sphere(64 nm)@Pd (10.9 nm)@pNIPAM, 10.0 mM CTAB and borate buffer pH 8.2 at 30 °C. For the kinetic traces at each concentration see Figure S3.5a-d in Appendix 3.

Figure 4.15 shows little variation in the observed rate constants, indicating that the reaction

follows first-order kinetics in PBA in the concentration range of 0.025-0.15 mM was

observed. This behaviour is surprisingly different from that when using Pd-CTAB NPs

(Chapter 3) and Pd-NIPAM nanocomposites (*vide infra*) where mixed second- and first-order

kinetics was observed. However, the current dataset does not exclude the possibility of

second- order kinetics in PBA at lower concentrations (less than 0.025 mM).

4.2.3.3. Effect of pH on the reaction rate

We studied the effect of pH on the reaction of phenylboronic acid using a borate buffer
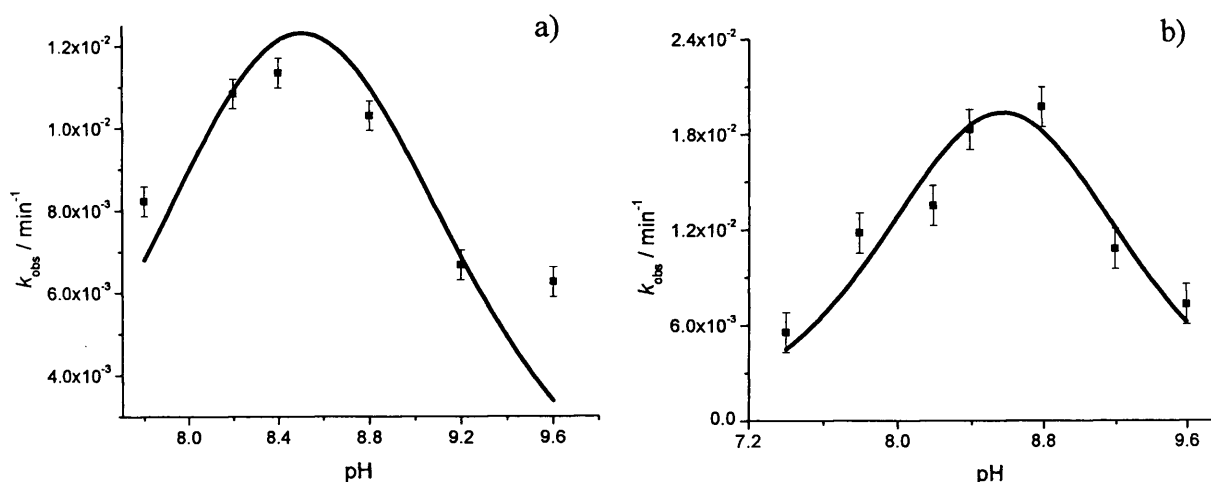
(Figure 4.16).
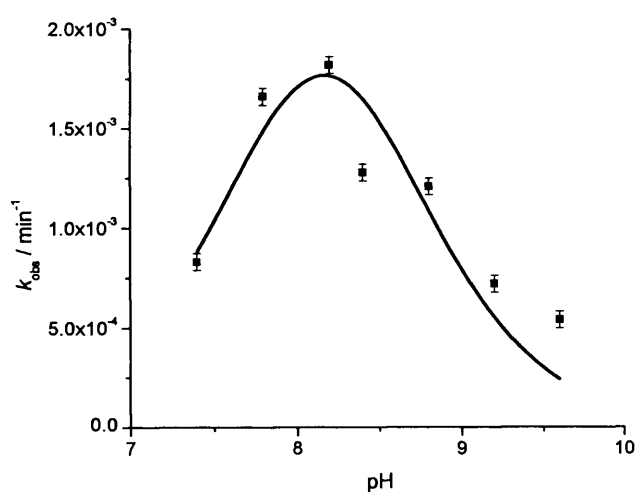
Figure 4.16. Effect of pH on k_{obs} for the reaction involving 0.1 mM PBA (■), solid line is a fit to a Gaussian (eq. 2.2, see Chapter 2). Using 10 mM CTAB, 10 mM borate buffer and using Au-sphere(64 nm)@Pd (10.9 nm)@pNIPAM (182.4 μM Au) at 30 °C. For the kinetic traces at each pH see Figure S3.4a-g in Appendix 3. Error margins were determined for one repeating experiments and assumed to be the same for the other data points.

Figure 4.16 shows that the optimum pH for the homocoupling of PBA is around 8.2 ± 0.1

which is roughly 1 pK_a unit lower than the pK_a of PBA of 9.1 as determined under reaction

conditions (see Chapter 2). As discussed in Chapters 2 and 3, the observation of a pH

maximum suggests two possible scenarios. The first scenario involves a requirement for the

acidic and basic forms of PBA in two different steps within the catalytic cycle. The second

scenario involves the formation of a Pd-aqua/hydroxo complex (either on the surface of the

NPs or involving catalytically active leached Pd-atoms/ions) which is pH dependent and either the acidic form of the catalyst and basic form of PBA is required in the rate-limiting step or *vice versa*.

4.2.3.4. Effect of the catalyst concentration on the reaction rate

Under our optimised conditions, we studied the effect of the concentration of Au-sphere(64 nm)@Pd(10.9 nm)@pNIPAM NPs on the observed rate constant for the homocoupling reaction of PBA (Figure 4.17).
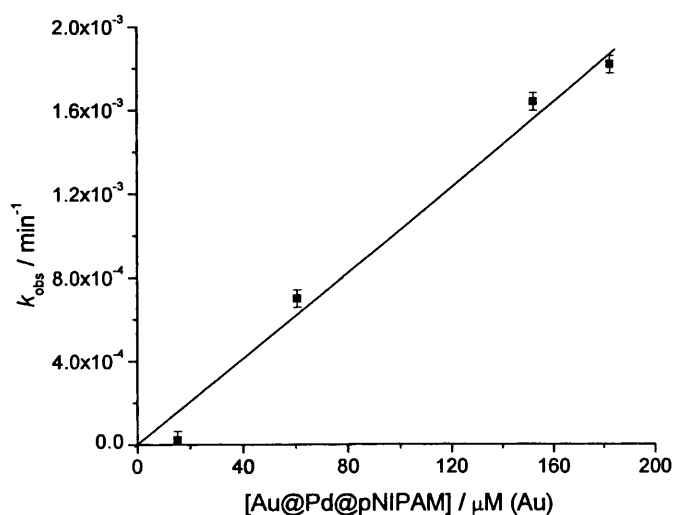
Figure 4.17. Effect of Au-sphere(64 nm)@Pd (10.9 nm)@pNIPAM concentration on k_{obs} for the homocoupling reaction of PBA, in 10 mM CTAB and borate buffer pH 8.2 at 30 °C (For the kinetic traces at each concentration see Figures S3.6a-d in Appendix 3).

Figure 4.17 shows that the reaction is first-order in the catalyst.

4.2.3.5. Effect of temperature on k_{obs}

The thermoresponsive and porosity properties of the microgel shell dictate the diffusion of the reactant to the core surface of the NPs and/or reactivity at the surface of the metal core of the particle. Accordingly, changing the temperature might have an effect on the k_{obs} which differs

from conventional Arrhenius (or Erying) equations. In particular, when the temperature is

high the shrunken microgel shell is anticipated to lower the rate of diffusion of the reactant to

the core NPs which leads to a decrease in k_{obs} if diffusion is at least partially rate limiting.

Alternatively, the reaction medium offered by the collapsed pNIPAM shell is different from

the reaction medium offered by the hydrophilic swollen shell. The change in the local reaction

medium could affect the rate constant on the surface of the metal NP core either way, i.e.

accelerate or retard reaction. Again the overall effect of the change in reaction medium on k_{obs}

depends on the extent to which the chemical reaction is rate determining. We have studied the

effect of temperature on the observed rate constant of the aerobic homocoupling reaction of

PBA in the presence of Au-sphere(64 nm)@Pd(10.9 nm)@pNIPAM NPs (Figure 4.18a).
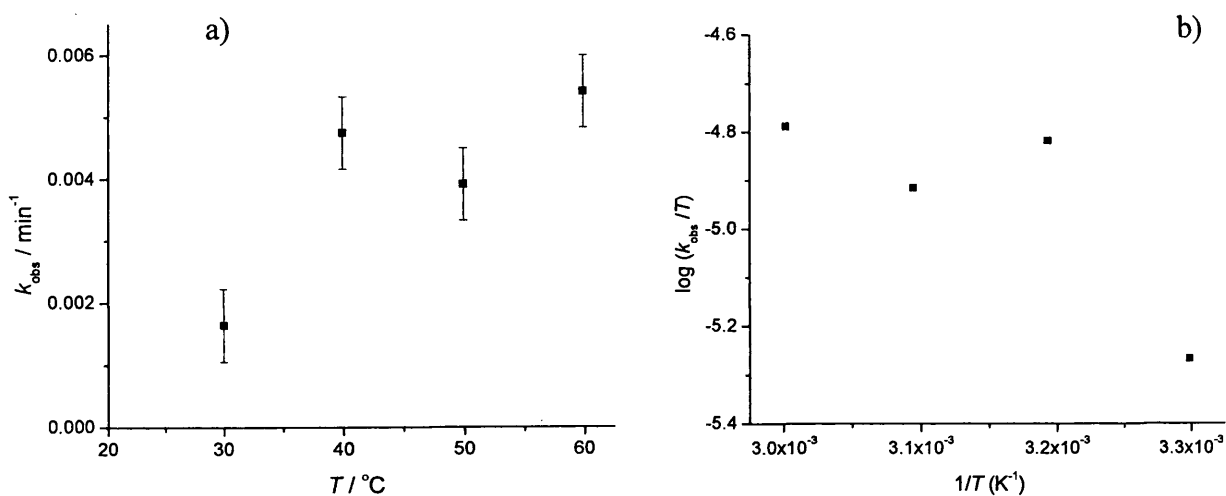
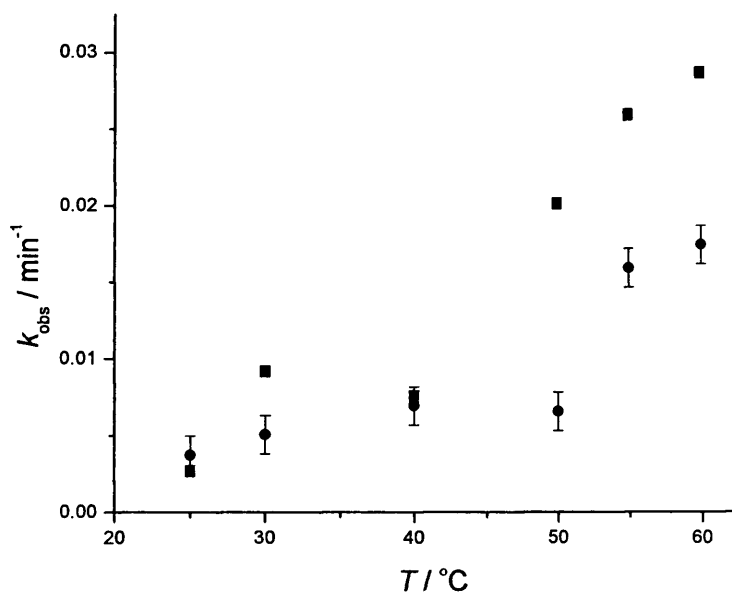**Figure 4.18.** a) Effect of temperature on k_{obs} for the homocoupling reaction of PBA, in 10 mM CTAB and borate buffer pH 8.2, using Au-sphere(64 nm)@Pd (10.9 nm)@pNIPAM NPs (152 μM Au) as catalyst. For the kinetic traces at each pH see Figure S3.7a-e in Appendix 3. b) Eyring plot for the experimental data in (a).

Figure 4.18 shows an increase in k_{obs} b y incre asing the temperature from 30 to 40 °C,

increasing the temperature to 50 °C leads to decrease of k_{obs}, and further increase of

temperature to 60 °C increases k_{obs} again. Although the decrease in k_{obs} is not outside error

margins, we note that it occurs near T_c, as expected if the state of the pNIPAM shell effects

the reaction kinetics. Our experimental data of Figure 4.18a do not appear to follow Arrhenius

(or Eyring) behaviour (Figure 4.18b). The drop in k_{obs} comes after 40 °C which is slightly

above T_c of the NPs in CTAB. Figure 4.18a allows us to qualitatively describe the effect of

the collapsed and swollen state of the pNIPAM shell on the k_{obs}. The increases in k_{obs} below

and above T_c correspond to "normal" Arrhenius (Eyring) behaviour. Unfortunately, the

number of data points and the error margins do not allow us to draw a definitive conclusion

about the source (diffusion control or reaction medium effect) of the temperature effect on

k_{obs}.

4.2.4. Kinetic studies of the aerobic oxidative homocoupling reaction of PBA using Au-sphere(104 nm)@Pd(9.9 nm)@pNIPAM NPS

The kinetics of the aerobic homocoupling reaction of PBA in buffered aqueous micellar

solution was studied using Au-sphere(104 nm)@Pd(9.9 nm)@pNIPAM NPs and Au-rod(48x23

nm)@Pd(rocket)@pNIPAM using UV-Vis spectroscopy under the same conditions as

mentioned before (Figures 4.20 a and b).
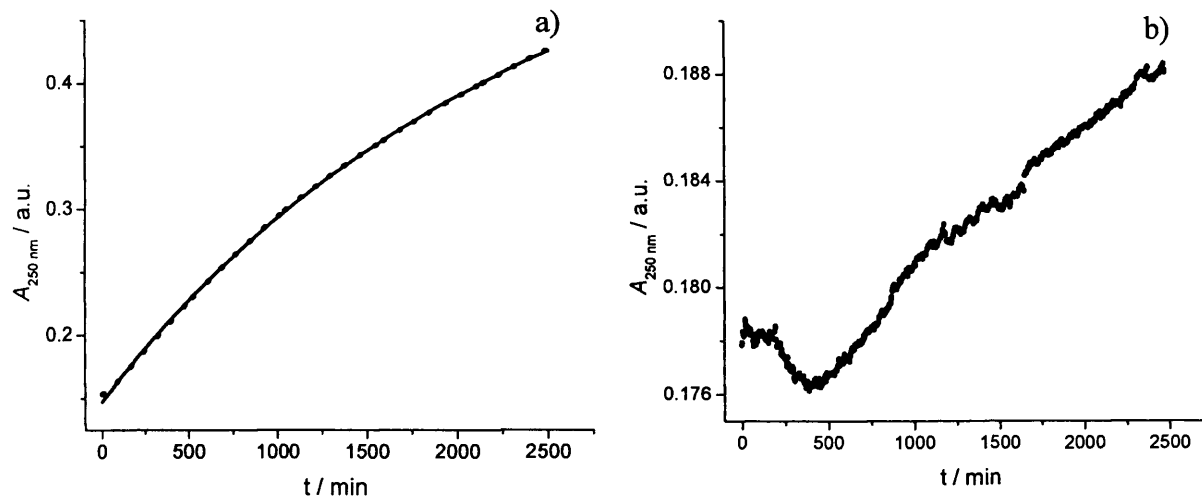
Figure 4.19. Absorbance of the reaction mixture of the homocoupling of 0.1 PBA with time at 250 nm in 10.0 mM CTAB and borate buffer pH 8.2 at 25 °C , a) using 104 μM Au(content) Au-sphere(104 nm) @Pd(9.9 nm)@pNIPAM NPs and b) 120 μM Au-rod(48x23 nm)@Pd-rocket@pNIPAM, experimental data (dotted line), solid line fit to the (pseudo) first order equation (2.1).

Figures 4.19a and b show that the aerobic homocoupling reactions using Au-sphere(104 nm)@Pd(9.9 nm)@pNIPAM NPs and Au-rod(48x23 nm)@Pd- rocket@pNIPAM as catalysts are slow compared to the reaction catalysed by Au-sphere(64 nm)@Pd(10.9 nm)@pNIPAM. We believe that the size of the nanoparticles plays a pivotal role in slowing down the reaction rate, with the bigger particles leading to a lower reaction rate.

4.2.5. Kinetic studies of the aerobic oxidative homocoupling reaction of PBA using Pd-pNIPAM (+ve and –ve) nanocomposites as catalysts

Using the Pd-pNIPAM nanocomposites (+ve or –ve) as catalysts, we have followed the kinetics of the aerobic oxidative homocoupling reaction of PBA in aqueous micellar solution using UV-Vis spectroscopy. As before product formation (biaryl and phenol) was followed through changes in absorbance with time at a selected wavelength where maximum changes in absorbance occur for the reaction of PBA (Figures 14.20a and b).

154

a)

b)

t / min

t / min
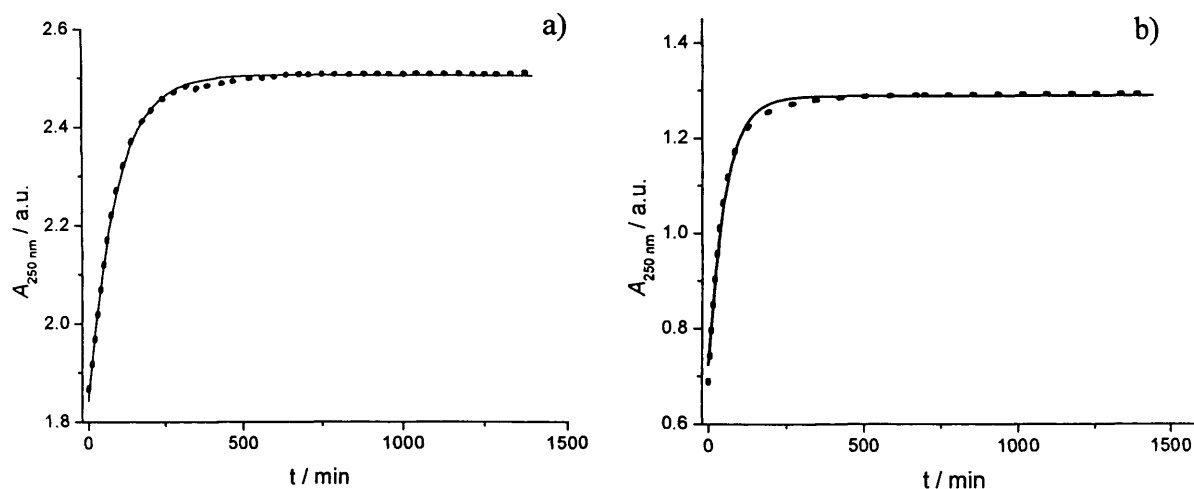
Figure 4.20. Absorbance of the reaction mixture of the homocoupling of 0.1 PBA with time at 250 nm in 10.0 mM CTAB and borate buffer at 30 °C, a) using 200 µL Pd-pNIPAM (+ve) pH 8.4 and b) 200 µL Pd-pNIPAM (-ve) pH 8.8, experimental data (dotted line), solid line fit to the (pseudo) first order equation (4.1).

Figures 4.20a&b show reasonable pseudo-first-order fits and the values of k_{obs} of 0.0113 and 0.01972 min^{-1} are reasonably comparable for the reactions using +ve and -ve Pd-pNIPAM nanocomposites as catalysts, respectively (each of them at the optimum pH *vide infra*). However, the concentration of Pd^0 in each solution is not precisely known and subsequent experiments were performed using the same catalyst stock solutions.

4.2.5.1. Product analysis

As before, the composition of the product mixtures of the reaction involving phenylboronic acid were determined by HPLC and compared with authentic samples. The HPLC chromatograms are shown in Figures S3.2 and S3.3 in Appendix 3. It was found that the products (biphenyl and phenol) were formed in a 1.3:1 and 1.2:1 ratio for the reaction of PBA using Pd-pNIPAM +ve and -ve, respectively, under the respective optimum reaction conditions (*vide infra*). As before, this observation suggests that the reaction between the

previously proposed peroxide[52] side product and phenylboronic acid to produce the phenol is

faster than peroxide decomposition (see Chapter 2)..

4.2.5.2. Effect of pH on the reaction rate

We studied the effect of pH on the reaction of phenylboronic acid using a borate buffer
(Figure 4.21).

Figure 4.21. Effect of pH on k_{obs} for the reaction involving 0.1 mM PBA (■), using 10 mM CTAB, 10
mM borate buffer and using 200 μL Pd –pNIPAM a) +ve and b) –ve, at 30 °C. Solid lines are fits to
Gaussians (eq. 2.2) (For the kinetic traces at each pH see Figures S3.8a-f and S3.9a-g in Appendix 3).

Figures 4.21a&b show that the optimum pH for the homocoupling of PBA were found are 8.5

and 8.6 using +ve and –ve Pd-pNIPAM nanocomposites as catalysts, respectively. As before,

the fact that the reactions show bell-shaped pH-rate profiles suggests the same possible

scenarios regarding the rate limiting step and the reaction mechanism as explained for the

reaction using Au@Pd@pNIPAM NPs as catalyst (*vide supra*).

4.2.5.3. Effect of PBA concentration

In order to determine the order of the reaction in phenylboronic acid, we studied the effect of

phenylboronic acid concentration on the observed first-order reaction rate constant under

otherwise standard conditions (*vide supra*) at 30 °C and pH 8.8 (Figure 4.22).
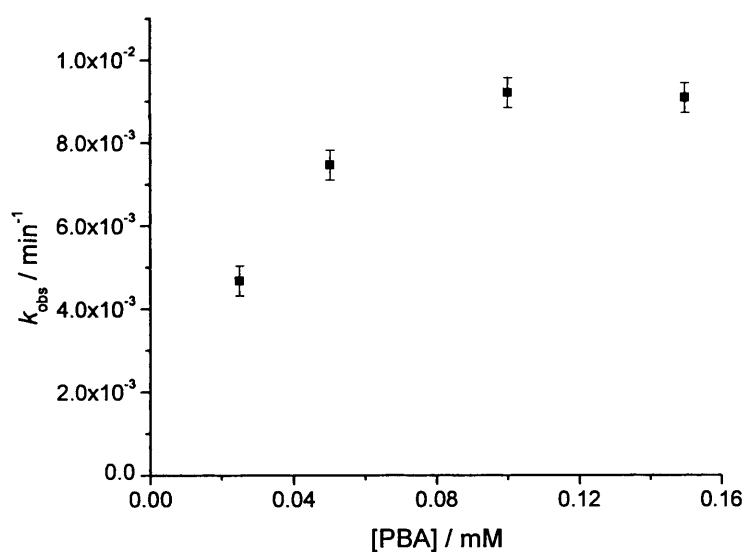
Figure 4.22. Effect of PBA concentration on the observed reaction rate constant using 100 µL Pd-pNIPAM (-ve), 10.0 mM CTAB and borate buffer pH 8.8 at 30 °C. (For the kinetic traces at each PBA concentration see Figures S3.10a-d in Appendix 3).

Figure 4.22 shows that the reaction follows mixed second- and first-order kinetics in PBA

which mimics our results when using Pd-CTAB NPs and makes us suggest again that the

reaction follows a mechanism in which one PBA molecule reacts with the catalyst in a pre-

equilibrium step before the rate-limiting step which involves the reaction of a second

molecule of PBA with the product (intermediate) of the pre-equilibrium step (see Chapter 3).

This together with the pH-rate profile provides vital information about the possible

mechanism(s) of the reaction under our conditions (*vide infra*).

4.2.5.4. Effect of Pd-pNIPAM (-ve) concentration on the reaction rate

Under our optimised conditions, we studied the effect of Pd-pNIPAM (-ve) NP concentration

on the observed rate constant for the homocoupling reaction of PBA (Figure 4.23).
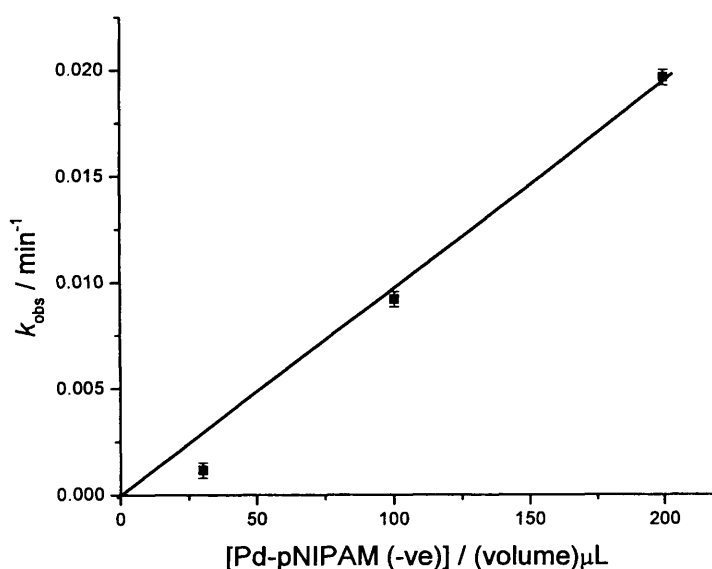
Figure 4.23. Effect of Pd-pNIPAM(-ve) concentration represented in volume (μL) on k_{obs} for the homocoupling reaction of PBA, in 10 mM CTAB and borate buffer pH 8.8 at 30 °C. For the kinetic traces at each PBA concentration see Figures S3.11a-c in Appendix 3.

Figure 4.23 shows that the reaction is first-order in the catalyst, which suggest that the rate

limiting step involves only one catalyst (here one nanoparticle or leached Pd atom/ion) in the

catalytic cycle.

4.2.5.5. Effect of temperature on k_{obs}

We have investigated the effect of temperature on k_{obs} for the homocoupling of PBA under

our optimum reaction conditions using both the negatively and positively charged Pd-

pNIPAM nanocomposites as the catalyst (Figure 4.24).

Figure 4.24. Effect of temperature on the k_{obs} for the homocoupling reaction of PBA, in 10 mM CTAB and borate buffer pH (8.8(-ve) and 8.4(+ve)), using 100 μL Pd-pNIPAM -ve (■) and +ve (●) as catalyst. For the kinetic traces at each temperature see Figures S3.12a-n in Appendix 3.

Figure 4.24 shows an increase in k_{obs} below T_c for the homocoupling reaction of PBA using

Pd-pNIPAM (-ve or +ve) as catalyst; for fully swollen pNIPAM the reaction follows

Arrhenius (or Eyring) behaviour. k_{obs} decreases upon increasing the temperature from 30 °C to

40 °C, i.e. through T_c, when the pNIPAM shell collapses. Further increase of temperature

leads to an increase in k_{obs} again and k_{obs} (at least qualitatively) follows Arrhenius (or Eyring)

behaviour again. As for the Au@Pd@pNIPAM NPs, full analysis of the data is required to

illucidate whether diffusion control or local reaction medium effects underpin the observed

deviations from Eyring behaviour.

4.2.6. Mechanism of the reaction

As discussed in Chapter 3 the homocoupling reaction could be catalysed either by palladium atoms/ions at the surface of the NPs or by Pd atoms/ions leached to the bulk reaction medium. The same steps as in the catalytic cycle proposed in Chapter 3 are applicable for the aerobic oxidative homocoupling reaction of PBA using both Au@Pd@pNIPAM NPs and the Pd-pNIPAM nanocomposites as catalysts. The catalytic cycle starts with the oxidative addition of O_2 to a Pd^0 atom on the NPs (or to a leached Pd^0 atom) to form a peroxo-Pd^{II} complex. The formed peroxo-Pd^{II} complex is likely to undergo hydrolysis in water to form a hydroxy-hydroperoxo-Pd^{II} intermediate, the protonation state of which is likely to be pH dependent. A first transmetalation step involves a molecule of PBA (in its acidic form, as discussed in Chapter 2) reacting with the hydroxyl-hydroperoxo-Pd^{II} intermediate (I) in a pre-equilibrium reaction forming an intermediate (II). This intermediate (II) reacts with another molecule of PBA (in its acidic form, see Chapter 2) in a second transmetalation step to form intermediate (III). Subsequent reductive elimination of intermediate (III) will lead to the formation of the biphenyl product and regenerates Pd^0 which then will start another cycle. Our temperature dependence of k_{obs} shows that the reaction is affected by the state of the pNIPAM shells of the studied NPs and nanocomposites. More detailed analysis is required to identify whether the observed decreases in k_{obs} (compared to what is expected from extrapolation of the data below T_c in terms of the Eyring equation) results from either a decrease in diffusion to the NP surface or a change in local reaction medium resulting from pNIPAM shell collapse.

4.3. Conclusions

The synthesis of bimetallic Au-Pd core-shell NPs encapsulated in a pNIPAM shell *viz.* Au@Pd@pNIPAM has been carried out using a straightforward synthetic approach. Different Au-Pd core-shell sizes were achievable by controlling the experimental conditions. Spherical Au-Pd, (64 ± 4 nm)-(4.0± 1 nm), (64 ± 4 nm)-(10.9± 2 nm), (64 ± 4 nm)-(10.8± 2 nm), (104 ± 8 nm)-(9.9±1.9 nm), and rod Au cores (48x24 nm) carrying a rocket-shaped Pd shell were synthesised. Pd-pNIPAM nanocomposites with negative and positive surface charges were also synthesised. TEM and DLS were used to characterise the formed NPs. All NPs and nanocomposites show a LCST (or "collapse temperature" T_c) of around 35 °C. These NPs and nananocomposites were used as catalysts in kinetic and mechanistic studies of the oxidative homocoupling reactions of phenylboronic acid. First, spherical Au (64 nm)@Pd (10.9 nm)@pNIPAM was used as a model for the kinetic studies and optimisation of reaction conditions for all Au@Pd@pNIPAM NPs. Product analysis showed the formation of biphenyl and phenol in the ratio of 1.3:1 under optimum conditions. The reaction showed reasonably good pseudo-first-order kinetics. The reaction was first order in PBA within the range of 0.025-0.15 mM PBA and first-order in the catalyst. A bell-shaped pH rate profile was observed for the reaction with a maximum around pH 8.2. This observation is in line with our previous findings using molecular Pd-catalyst **3** and Pd-CTAB NPs but with the maximum pH shifting slightly towards more acidic conditions. Second, the Pd-pNIPAM (+ve or −ve) nanocomposites were used as catalysts for kinetic and mechanistic studies of the aerobic oxidative homocoupling of PBA in aqueous micellar medium. The reactions showed good pseudo-first-order kinetics. A bell-shaped pH-rate profile was observed with pH optima of 8.4 and 8.8 using Pd-pNIPAM +ve and −ve, respectively. Product analysis showed the formation

of biphenyl and phenol in ratios of 1.3:1 and 1.2:1 using +ve and –ve Pd-pNIPAM, respectively, at optimum conditions. The reaction was first order in the catalyst Pd-pNIPAM (–ve), and mixed second and first-order kinetics in PBA was observed. Regarding the mechanism of the reaction using both Au@Pd@pNIPAM and Pd-pNIPAM catalytic systems the same arguments as those in Chapters 2 and 3 are applicable here. Catalysis occurs either through surface catalysis or leaching out of Pd atoms (or ions) to the reaction medium. Surface (or leached) Pd^0 atom(s) undergo an oxidative addition reaction by dissolved O_2 molecule to form a peroxo-Pd^{II} complex. This complex is likely to undergo hydrolysis under our aqueous conditions to form a hydroxyl-hydroperoxo-Pd^{II} intermediate the protonation state of which is likely to be pH dependent. Our kinetic results showed first-order dependency of the reaction rate in the catalyst which suggests the involvement of one catalyst nanoparticle or molecule in the rate-limiting step. Also, mixed second- and first-order kinetics in PBA was observed, suggesting, a mechanism involving a pre-equilibrium reaction in which a molecule of PBA attached to the NP surface before a rate-determining step involving a second molecule of PBA (this result is similar to our results in Chapter 3). The bell-shaped pH-rate profile is in line with our findings in Chapters 2 and 3 which suggest the involvement of the acidic form of PBA and the basic form of the catalyst in the rate-limiting step of the reaction (transmetalation step). Finally, the effect of temperature on k_{obs} of the homocoupling reaction using both catalytic systems showed non-Eyring-like behaviour. This was interpreted as the dependence k_{obs} on the state (swollen/collapse) of the pNIPAM shell. An increase of k_{obs} below T_c was observed followed by a sudden decrease upon increasing the temperature. Further increase of temperature led to an increase of k_{obs} again. The sudden decrease of k_{obs} with increasing the temperature resulted from either decrease of a diffusion rate of the

reactants to the NP surface or a change of local reaction medium resulting from the collapse

of pNIPAM shell.

4.4. Experimental

4.4.1. Equipment

UV-Vis-NIR spectra were recorded using a Cary 5000 UV-Vis-NIR spectrophotometer.

Transmission electron microscopy (TEM) was performed using a JEOL JEM 1010

microscope operating at an acceleration voltage of 100 kV. Photon Correlation Spectroscopy

(PCS) was carried out on a Zetasizer Nano S (Malvern Instruments, Malvern UK) using a

detection angle of 173°.

The kinetic studies were carried out using JASCO V630 and V650 UV-Vis

spectrophotometers, monitoring reactions by either time resolved absorption (spectra) or

parallel kinetic measurements. Both machines were equipped with a Peltier-thermostated 6-

cell holder to control the temperature. Reactions were carried out in 1.0 cm path length

stoppered quartz cuvettes (Hellma) holding approximately 1.0 cm^3 of headspace (*i.e.* under

aerobic conditions), at 30 °C (unless otherwise mentioned). A HANNA pH211

microprocessor pH meter equipped with a VWR 662-1759 glass electrode was used for

determining the pH of solutions. HPLC analyses were carried out using an Agilent1200

instrument with a ZORBAY (Eclipse XDB-C18 4.6X150 mm, 5 μm) column. Water was

purified using an ELGA option-R 7BP or a Milli-Q system (Millipore) water purifier.

4.4.2. Chemicals

All chemicals were commercially available (Acros, Alfa Aesar, Aldrich, Fisher Scientific, ICT, and Maybridge) and used as purchased without further purification. Acetonitrile and deionised water were used as solvents for the preparation of stock solutions.

4.4.3. Synthesis of Au@Pd@pNIPAM nanoparticles

Au-sphere(64nm)@pNIPAM nanoparticles. The synthesis was carried out following the method developed by Contreras-Cáceres *et al.*[27] Au seeds (64 nm) were prepared through a seeded growth method. Briefly, 35 mL of ca. 15 nm Au nanoparticles (previously prepared by citrate reduction) was added to 15 mL of 0.03 M CTAB aqueous solution. 4.5 mL of this seed solution was added to a growth solution prepared by adding 800 μL of butenoic acid under gentle stirring to 50 mL of an aqueous solution containing 1.0 mM $HAuCl_4$ and 15 mM CTAB at 70 °C. After 10 min, excess butenoic acid and CTAB were removed by centrifugation at 4500 rpm for 30 min. After redispersing the pellet in 50 mL of 4.0 mM CTAB, the dispersion was centrifuged at 4500 rpm for 40 min and the precipitate redispersed in 10 mL of water. Subsequently this Au colloidal dispersion was heated at 70 °C under N_2 flow and then 0.1698 g NIPAM and 0.0234 g BIS were added under magnetic stirring. After 15 min, the nitrogen flow was removed and the polymerization was initiated with the addition of AAPH (100 μL 0.1 M). After 2 h at 70 °C, the white mixture was allowed to cool down to room temperature under stirring. Finally, it was diluted with water (50 mL), centrifuged (30 min at 4500 rpm) and redispersed in water (5 times). The Au core size measured using TEM was 64 ± 4.0 nm.

Au-sphere(104nm)@pNIPAM. The growth of the Au core was carried out following the method developed by Rodriguez-Fernández *et al.*[14] as follows; 180 μL of AA 100 mM was added to 10 mL of an aqueous solution containing Au-sphere(64nm)@pNIPAM (0.25 mM), CTAB (100 mM) and HAuCl₄ (0.9 mM), under magnetic stirring at room temperature. After 30 min the growth process was finished. The Au core size measured using TEM was 104.0 ± 8.0 nm.

Au-rod@pNIPAM. The synthesis of Au-rod@pNIPAM NPs was carried out as described above for Au-sphere(64nm)@Au@pNIPAM, but by using 0.8 mM HAuCl₄ and 160 μL of 0.1 M AA. The final average Au core size determined using TEM was (48.1 ± 5.1) nm length × (24.0 ± 3.0) nm width.

Au-sphere(64nm)@Pd@pNIPAM. To a 0.3 M aqueous solution of CTAB, *ca.* 0.09 mM Au-sphere(64nm)@Pd@pNIPAM was added at 27 °C in a water bath. The solution was mixed and (0.04, 0.08, or 0.16) mM Na₂PdCl₄ was added. After mixing, 2.0 mM of ascorbic acid was added and the mixture was left overnight in a capped container at 27 °C in a water bath. The excess of ascorbic acid and CTAB was removed by centrifugation at 4500 rpm for 30 min., redispersing in 10 mL of water and centrifugation (30 min at 4500 rpm) (this procedure was repeated 3 times). The UV-Vis spectra of aqueous solutions were then recorded. TEM images were taken for the synthesised NPs. The average Au-core/Pd-shell measured from TEM were: a) Au-core size 64.0 ± 4.0 nm and Pd-shell of 4.0 ± 1.0 nm (when 0.04 mM Na₂PdCl₄ was used), b) Au-core size 64.0 ± 4.0 nm and Pd-shell size 10.9 ± 2.0 nm, (when 0.08 mM Na₂PdCl₄ was used) and c) Au-core size 64.0 ± 4.0 nm and Pd-shell size 10.8 ± 2.0 nm, (when 0.16 mM Na₂PdCl₄ was used).

Au-sphere(104nm)@Pd@pNIPAM. The same procedure as for Au-sphere (64nm)@Pd@pNIPAM was used for the coating of Au-spheres(105nm) with Pd. The Au-core and the Pd-shell sizes as measured from TEM were Au 104.0 ± 8.0 nm and Pd-shell of 8.0 ± 2.0 nm (when 0.08 mM Na_2PdCl_4 was used)

Au-nanorod@Pd@pNIPAM. The same procedure as for Au-sphere(64nm)@Pd@pNIPAM was used for the palladium coating of Au-nanorods with a core size of (48.1 ± 5.1) nm length $\times$ (24.0 ± 3.0) nm width, using 0.04 mM of Au-nanorod@pNIPAM and 0.32 mM Na_2PdCl_4. A rocket-like Pd-shell was observed in the corresponding TEM image. Because of the non-uniformity of the Pd-shell shape the shell thickness was not determined.

4.4.4. Synthesis of Pd^0-pNIPAM nanocomposite

pNIPAM (positively or negatively charged). 0.0078 g of crosslinker BIS was added to 0.1132 g of NIPAM in 10 mL deionised water under a flow of N_2 and at 70 °C. After 15 min, the nitrogen flow was removed and polymerization was initiated with the addition of $K_2S_2O_8$ or AAPH (100 μL 0.1 M) to obtain (-ve) and (+ve) pNIPAM, respectively. After 2 h at 70 °C, the white mixture was allowed to cool down to room temperature under stirring. Finally, it was diluted with water (50 mL), centrifuged (60 min at 8000 rpm) and redispersed in 10 mL of water (3 times). pNIPAM (+ve and –ve) particle sizes (for a dry sample) measured using TEM were 299.28 ± 16.47 nm and 294.78 ± 23.61 nm respectively.

Pd^0-pNIPAM. 1.0 mL of a pNIPAM (-ve or +ve) solution in deionised water was added to 4.0 mL of deionised water and then mixed with 0.25 mM (final concentration) of Na_2PdCl_4 under magnetic stirring and at 25 °C, followed by addition of 300 μL of 10.0 mM $NaBH_4$.

After about one hour the solution was diluted with water (50 mL), centrifuged (60 min at 8000 rpm) and redispersed in 10 mL of water. This process was repeated three times. Finally, the Pd^0-pNIPAM (+ve and –ve) nanocomposites were characterized using TEM.

4.4.5. Typical kinetic experiments

4.4.5.1. Kinetic measurement using UV-Visible spectroscopy

4.4.5.1.1. Time resolved absorption peak measurements

Reactions were carried out in 1.00 cm pathlength stoppered quartz cuvettes (Hellma) holding approximately 1.00 cm^3 of headspace (*i.e.* under aerobic conditions), at 30 °C. Typical concentrations were 100 µM for phenylboronic acid and a specified amount of the catalyst. Product formation (biaryl and phenol) was followed through changes in UV-Vis absorbance with time at 250nm.

The procedure was as follows: in a 1.00 cm pathlength cuvette and to a total volume of 2.5 mL, CTAB, borate buffer, and catalyst were mixed by pipetting the required volumes from concentrated stock solutions. The cuvette was allowed to thermally equilibrate for about 5-10 minutes. Subsequently, the required amount of arylboronic acid was added to the reaction mixture from a concentrated aqueous stock solution. The kinetics were monitored by measuring the time-resolved absorption peak. Reversing the order of the addition of phenylboronic acid and the catalyst did not have any effect on the kinetic measurements. The observed rate constants, k_{obs}, for the reactions were determined from plots of absorbance as a function of time, using the pseudo first-order rate law (equation 2.1 see chapter 2).

4.4.5.1.2. Parallel kinetic measurements

Parallel kinetic measurements at fixed wavelength were performed using UV-Vis spectroscopy (using a JASCO V-650 spectrometer equipped with a 6-position thermostated cuvette holder) at constant temperature following the abovementioned procedure. Effects of pH, catalyst concentration, phenylboronic acid concentration and temperature were all studied by UV-Vis parallel kinetic measurements.

Acknowledgements

References

1.   Lim, B.; Jiang, M.; Camargo, P. H.; Cho, E. C.; Tao, J.; Lu, X.; Zhu, Y.; Xia, Y., *Science* **2009**, *324* (5932), 1302-5.

2.   Schrinner, M.; Ballauff, M.; Talmon, Y.; Kauffmann, Y.; Thun, J.; Moller, M.; Breu, J., *Science* **2009**, *323* (5914), 617-20.

3.   Huang, X.; Jain, P. K.; El-Sayed, I. H.; El-Sayed, M. A., *Nanomedicine (London)* **2007**, *2* (5), 681-93.

4.   Scodeller, P.; Flexer, V.; Szamocki, R.; Calvo, E. J.; Tognalli, N.; Troiani, H.; Fainstein, A., *Journal of American Chemical Society* **2008**, *130* (38), 12690-7.

5.   Moreno-Manas, M.; Pleixats, R., *Accounts of Chemical Research* **2003**, *36* (8), 638-43.

6.   Astruc, D.; Lu, F.; Aranzaes, J. R., *Angewandte Chemie, International Edition in English* **2005**, *44* (48), 7852-72.

7.   Daniel, M. C.; Astruc, D., *Chemical Reviews* **2004**, *104* (1), 293-346.

8.   Burda, C.; Chen, X.; Narayanan, R.; El-Sayed, M. A., *Chemical Communications* **2005**, *105* (4), 1025-102.

9.   Gual, A.; Axet, M. R.; Philippot, K.; Chaudret, B.; Denicourt-Nowicki, A.; Roucoux, A.; Castillon, S.; Claver, C., *Chemical Communications (Cambridge)* **2008**, (24), 2759-61.

10.   Guin, D.; Baruwati, B.; Manorama, S. V., *Organic Letters* **2007**, *9* (7), 1419-21.

11.   Jennings, T.; Strouse, G., *Adv Exp Med Biol* **2007**, *620*, 34-47.

12.   Guerrero-Martinez, A.; Perez-Juste, J.; Liz-Marzan, L. M., *Advanced Materials* **2010**, *22* (11).

13.   Jana, N. R.; Gearheart, L.; Murphy, C. J., *Langmuir* **2001**, *17* (22), 6782-6786.

14.   Rodriguez-Fernandez, J.; Perez-Juste, J.; Garcia de Abajo, F. J.; Liz-Marzan, L. M., *Langmuir* **2006**, *22* (16), 7007-10.

15.   Okamoto, S.; Hachisu, S., *Journal of Colloid and Interface Science* **1977**, *62* (1), 172-181.

16.   Yavuz, M. S.; Li, W.; Xia, Y., *Chemistry - A European Journal* **2009**, *15* (47), 13181-13187.

17.   Kang, Y.; Erickson, K. J.; Taton, T. A., *Journal of American Chemical Society* **2005**, *127* (40), 13800-1.

18.   Pelton, R., *Adances.in Colloid and Interface Science.* **2000**, *85* (1), 1-33.

19.   Gorelikov, I.; Field, L. M.; Kumacheva, E., *Journal of American Chemical Society* **2004**, *126* (49), 15938-9.

20.   Das, M.; Mardyani, S.; Chan, W. C. W.; Kumacheva, E., *Advanced Materials* **2006**, *18* (1), 80-83.

21.   Karg, M.; Lu, Y.; Carbo-Argibay, E.; Pastoriza-Santos, I.; Perez-Juste, J.; Liz-Marzan, L. M.; Hellweg, T., *Langmuir* **2009**, *25* (5), 3163-7.

22.   Daly, E.; Saunders, B. R., *Physical Chemistry Chemical Physics* **2000**, *2* (14), 3187-3193.

23.   Lopez-Leon, T.; Ortega-Vinuesa, J. L.; Bastos-Gonzalez, D.; Elaissari, A., *Journal of Physical. Chemistry B* **2006**, *110* (10), 4629-36.

24.   Berndt, I.; Pedersen, J. S.; Richtering, W., *Angewandte Chemie, International Edition* **2006**, *45* (11), 1737-41.

25.   Contreras-Caceres, R.; Pacifico, J.; Pastoriza-Santos, I.; Perez-Juste, J.; Fernandez-Barbero, A.; Liz-Marzan, L. M., *Advanced Functional Materials* **2009**, *19* (19), 3070-3076.

26.   Contreras-Caceres, R.; Sanchez-Iglesias, A.; Karg, M.; Pastoriza-Santos, I.; Perez-Juste, J.; Pacifico, J.; Hellweg, T.; Fernandez-Barbero, A.; Liz-Marzan, L. M., *Advanced Materials* **2008**, *20* (9), 1666-1670.

27.   Contreras-Caceres, R.; Pastoriza-Santos, I.; Alvarez-Puebla, R. A.; Perez-Juste, J.; Fernandez-Barbero, A.; Liz-Marzan, L. M., *Chemistry* **2010**, *16* (31), 9462-7.

28.   Gopalan, A.; Ragupathy, D.; Kim, H. T.; Manesh, K. M.; Lee, K. P., *Spectrochimica Acta - Part A: Molecular and Biomolecular Spectroscopy* **2009**, *74* (3), 678-684.

29.   Liu, F.; Wechsler, D.; Zhang, P., *Chemical Physics Letters* **2008**, *461* (4-6), 254-259.

30.   Lee, A. F.; Baddeley, C. J.; Hardacre, C.; Ormerod, R. M.; Lambert, R. M.; Schmid, G.; West, H., *Journal of physical chemistry* **1995**, *99* (16), 6096-6102.

31.   Choudhary, T. V.; Sivadinarayana, C.; Datye, A. K.; Kumar, D.; Goodman, D. W., *Catalysis Letters* **2003**, *86* (1-3), 1-8.

32.   Edwards, J. K.; Solsona, B.; Landon, P.; Carley, A. F.; Herzing, A.; Watanabe, M.; Kiely, C. J.; Hutchings, G. J., *Journal of Materials Chemistry* **2005**, *15* (43), 4595-4600.

33.   Nutt, M. O.; Hughes, J. B.; Michael, S. W., *Environmental Science and Technology.* **2005**, *39* (5), 1346-53.

34.   Enache, D. I.; Edwards, J. K.; Landon, P.; Solsona-Espriu, B.; Carley, A. F.; Herzing, A. A.; Watanabe, M.; Kiely, C. J.; Knight, D. W.; Hutchings, G. J., *Science* **2006**, *311* (5759), 362-5.

35.   Harada, M.; Asakura, K.; Toshima, N., *Journal of physical chemistry* **1993**, *97* (19), 5103-5114.

36.   Ferrer, D.; Torres-Castro, A.; Gao, X.; Sepulveda-Guzman, S.; Ortiz-Mendez, U.; Jose-Yacaman, M., *Nano Lett.* **2007**, *7* (6), 1701-5.

37.   Kan, C.; Cai, W.; Li, C.; Zhang, L.; Hofmeister, H., *Journal of Physics D: Applied Physics* **2003**, *36* (13), 1609-1614.

38.   Kim, Y. G.; Garcia-Martinez, J. C.; Crooks, R. M., *Langmuir* **2005**, *21* (12), 5485-91.

39.   Liu, H. B.; Pal, U.; Medina, A.; Maldonado, C.; Ascencio, J. A., *Physical Review B - Condensed Matter and Materials Physics* **2005**, *71* (7), 1-6.

40.   Corma, A.; Gonzalez-Arellano, C.; Iglesias, M.; Sanchez, F., *Angewandte Chemie, International Edition* **2007**, *46* (41), 7820-2.

41.   Carrettin, S.; Guzman, J.; Corma, A., *Angewandte Chemie, International Edition* **2005**, *44* (15), 2242-5.

42.   Ballauff, M., *Progress in Polymer Science (Oxford)* **2007**, *32* (10), 1135-1151.

43.   Mei, Y.; Sharma, G.; Lu, Y.; Ballauff, M.; Drechsler, M.; Irrgang, T.; Kempe, R., *Langmuir* **2005**, *21* (26), 12229-12234.

44.   Anastas, P. T.; Kirchhoff, M. M., *Accounts of Chemical Research* **2002**, *35* (9), 686-694.

45.   Carregal-Romero, S.; Buurma, N. J.; Pérez-Juste, J.; Liz-Marzan, L. M.; Hervas, P., *Chemistry of Materials* **2010**, *22* (10), 3051-3059.

46.   Tsunoyama, H.; Sakurai, H.; Ichikuni, N.; Negishi, Y.; Tsukuda, T., *Langmuir* **2004**, *20* (26), 11293-6.

47.   Gonzalez-Arellano, C.; Corma, A.; Iglesias, M.; Sanchez, F., *Chemical Communications (Cambridge)* **2005**, (15), 1990-2.

48.   Chaicharoenwimolkul, L.; Munmai, A.; Chairam, S.; Tewasekson, U.; Sapudom, S.; Lakliang, Y.; Somsook, E., *Tetrahedron Letters* **2008**, *49* (51), 7299-7302.

49.   Willis, N. G.; Guzman, J., *Applied Catalysis A: General* **2008**, *339* (1), 68-75.

50.   Zheng, Z.; Li, H.; Liu, T.; Cao, R., *Journal of Catalysis* **2010**, *270* (2), 268-274.

51.   Liu, M.; Guyot-Sionnest, P., *Journal of Physical Chemistry B* **2005**, *109* (47), 22192-22200.

52.   Adamo, C.; Amatore, C.; Ciofini, I.; Jutand, A.; Lakmini, H., *Journal of the American Chemical Society* **2006**, *128* (21), 6829-6836.

Epilogue

Exploring the possibility of aerobic oxidative cross-coupling

reactions of arylboronic acids and their derivatives

Outlook and challenges for the future mechanistic studies of

aqueous (cross) coupling reactions

Abstract

One of the possible interpretations of the observed bell-shaped pH-rate profile for the homocoupling reaction in Chapter 2 suggested that the aerobic oxidative cross-coupling reaction of two different arylboronic acids and derivatives of significantly different pK_as might be feasible. Here, we present some preliminary results of exploratory studies of the micelle-assisted palladium-catalysed aerobic oxidative cross-coupling reaction of a series of (substituted) arylboronic acids and derivatives in aqueous surfactant solutions. A bisimidazole complex of palladium, *viz*. [Pd(bimsulfide)Cl$_2$] (**3**), was used as a catalyst based on our findings for the aerobic homocoupling (see Chapter 2). Cetyltrimethylammonium bromide (CTAB) was used as a surfactant. In addition, general conclusions, an outlook and future challenges and suggestions about the work presented in this thesis finish the Chapter.

5.1. Introduction

One of the possible explanations for the maximum in the pH-rate profile for the aerobic

oxidative homocoupling reaction of arylboronic acids involves the boronic acid being

required in its acidic form in the first transmetalation step whereas it is required in its basic

form in the second transmetalation step (Chapter 2). The kinetic consequences of the

difference between the two transmetalation steps were illustrated using a simplified kinetic

scheme (Scheme 5.1).
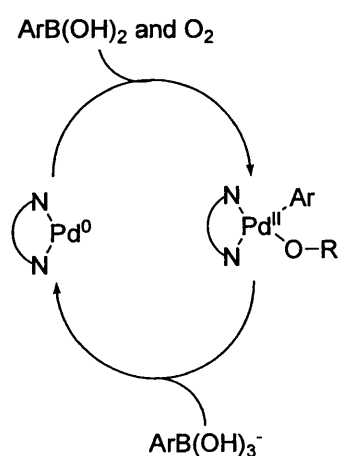
Scheme 5.1

A rate equation based on the mechanism in Scheme 5.1 reproduces the trend in optimum

pH relative to pK_a for the different arylboronic acids, but the mechanism failed to account

for the observed solvent kinetic isotope effect. Although the Curtin-Hammett principle

does not allow us to do so, it is extremely tempting to interpret Scheme 5.1 as suggesting

the possibility of oxidatively cross-coupling arylboronic acids of sufficiently different pK_a

through careful control of the pH. We decided to explore this reaction, further stimulated

by the fact that purely statistical reaction at equal reactant concentrations would already

lead to 50% yield of the cross-coupled product. In addition, we explored the

homocoupling reactions of compounds related to arylboronic acids such as
phenyltrifluoroborate, which has been suggested as an alternative for phenylboronate.

The hypothesis that arylboronic acids are required in both their acidic and basic forms
suggests that the reaction might be turned into an oxidative cross-coupling reaction of
boronic acids, with the Curtin-Hammett caveat mentioned above. In such a cross-coupling
reaction, two different boronic acids with sufficiently different pK_a act at different stages
of the process if one selects a pH at which one arylboronic acid is present mainly in its
acidic form and the other arylboronic acid is present mainly in its basic form (Scheme 5.2).
Phenol as a by-product should mainly result from the acidic arylboronic acid, according to
our proposed mechanism (see Chapter 2).
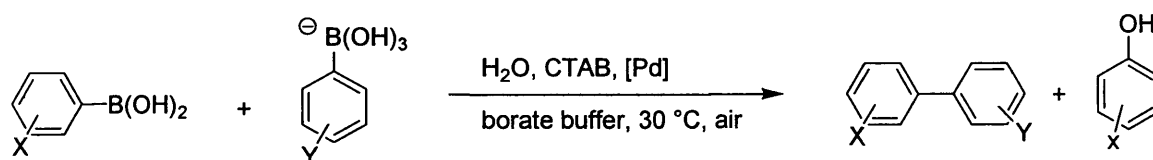
Scheme 5.2

The studied arylboronic acids and derivatives and their corresponding biphenyl and phenol
products are listed in Scheme 5.3.
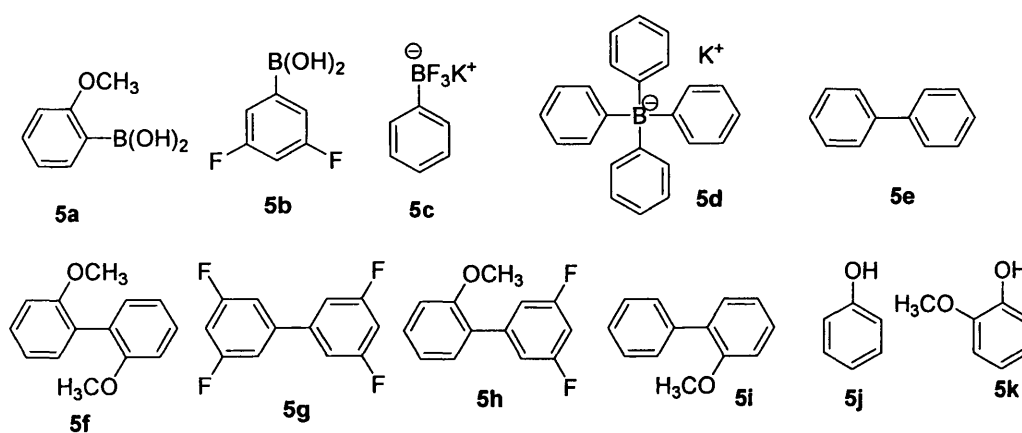
Scheme 5.3

5.2. Homocoupling reactions of potassium phenyltrifluoroborate and potassium tetraphenylborate

Aerobic homocoupling eactions of phenyltrifluoroborate and potassium tetraphenylborate (5c and 5d) have been studied under our optimum conditions at pH 9.2 and 8.4, respectively, using 3 as a (pre) catalyst (Figures 5.1 a and b).
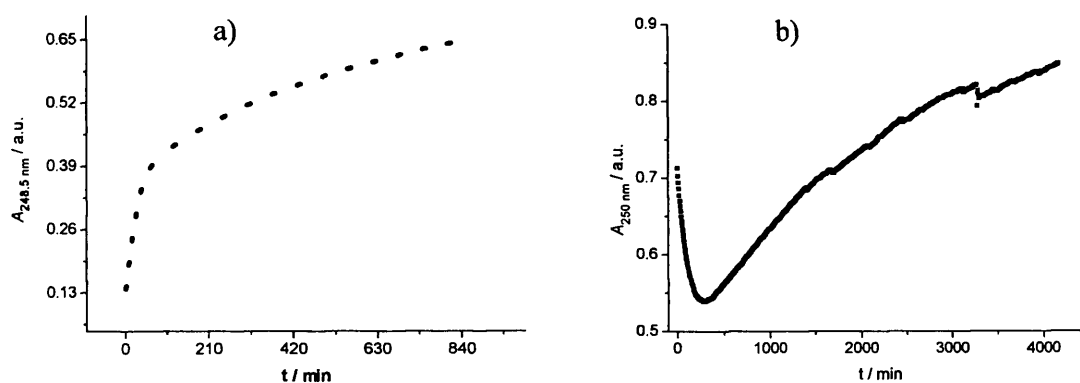
Figure 5.1. Absorbance versus time for the homocoupling reaction of a) 0.1 mM **5c** and b) 0.025 mM **5d**, using 10.0 and 20.0 μM of **3**, respectively, 10.0 mM CTAB and borate buffer at pH 9.2 and 8.4, respectively, and at 30 °C.

Figure 5.1a shows that the homocoupling (from the absorbance, the steepness of first part of the graph) of **5c** proceeds fast at the beginning of the reaction (first 2 hours), suggesting that the reaction proceeds mainly through the Pd^{II} pathway (the first step in Scheme 2.10, Chapter 2) since there is no acidic form of the boronic acid in the reaction. However, **5c** can hydrolyse and form phenylboronic acid in aqueous media (Scheme 5.4).[1,2] As a result, the reaction continues through the catalytic cycle but at a lower rate than observed for phenylboronic acid (**2a**, Chapter 2).
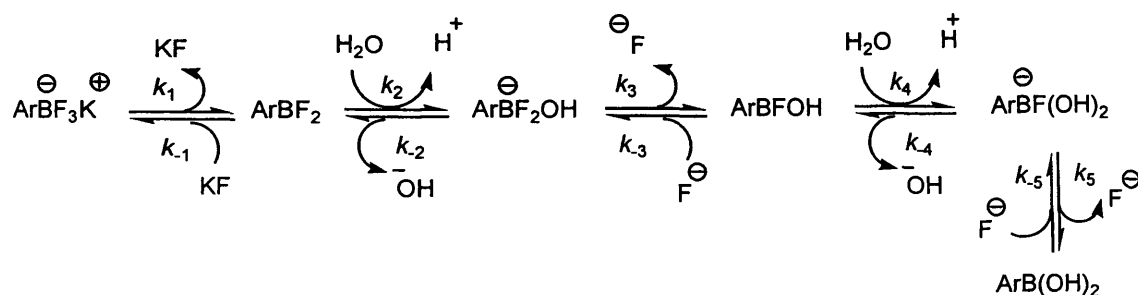
Scheme 5.4 taken from ref[2]

Homocoupling of **5d** is possible but it appears to require a long induction period (Figure 5.1b) which might be due to a stepwise decomposition[3, 4] of **5d** to form phenylboronic acid. In the presence of O_2 phenol is formed during the decomposition of tetraphenylboronate according to the literature.[4]

5.3. Cross-coupling of arylboronic acids and derivatives

We studied the oxidative cross-coupling reaction of 2-methoxyphenylboronic acid with 3,5-difluorophenylboronate using complex **3** as a (pre)catalyst (Scheme 5. 5) b y UV-visible absorption spectroscopy at different pH (Figure 5.2).
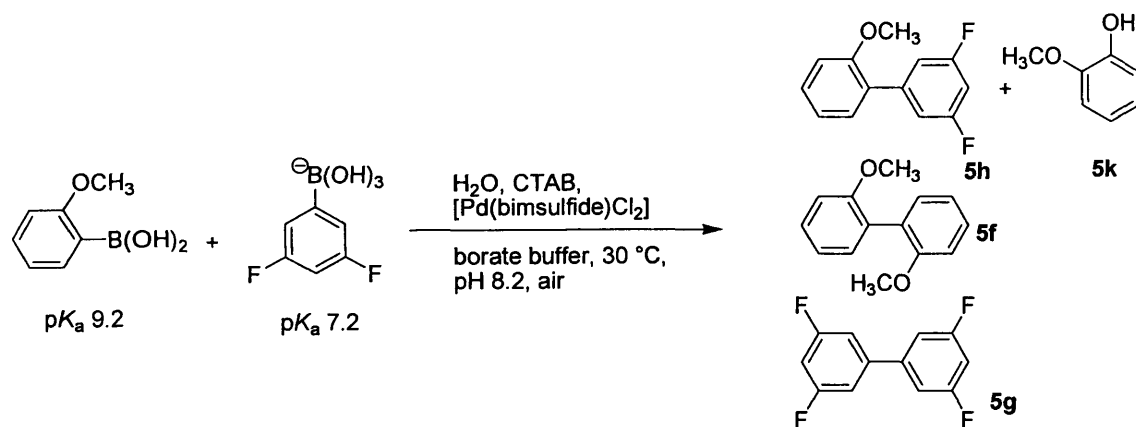
Scheme 5.5
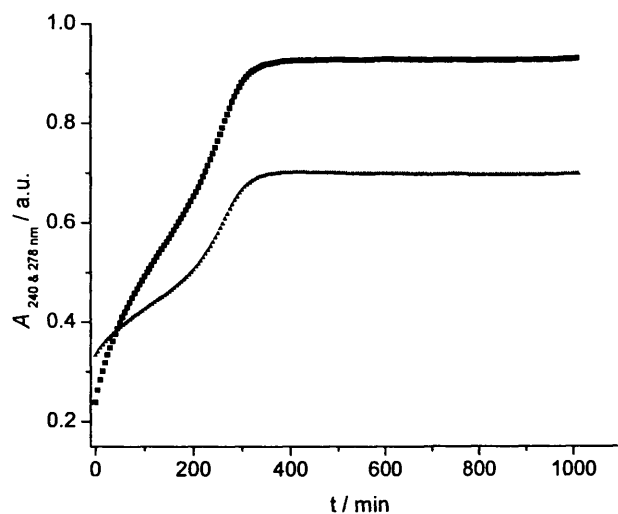
Figure 5.2: Absorbance at 240 nm (■) and 270 nm(▲) for the reaction of 0.1 mM **5a** with 0.1 mM **5b** using 27.0 μM cat and 10 mM CTAB in 10 mM buffer, with time at 30 °C and pH 8.2.

Figure 5.2 shows that the reaction follows complex kinetics and that the rate of the reaction is not fast. The product ratio was determined using HPLC (Figure 5.3).
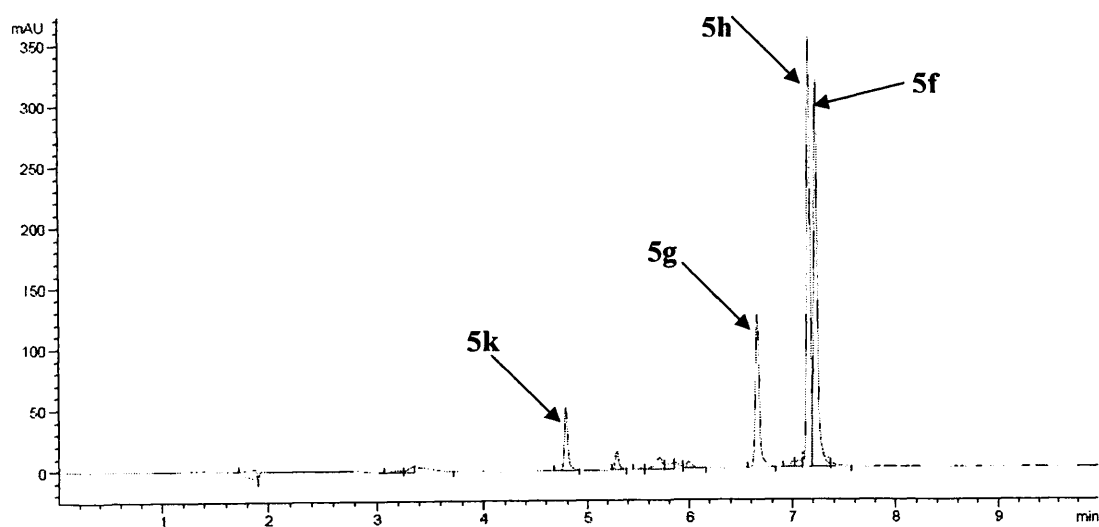
Figure 5.3. HPLC chromatograms and product analyses for the reaction of 0.1 mM **5a** with 0.1 mM **5b** in 10 mM CTAB and buffer using 10 μM of **3** as catalyst at 30 °C and pH 8.2.

Figure 5.3 shows that the reaction was not selective towards the cross-coupling product **5h**.

The lack of selectivity might be due to the selection of the reaction pH (in addition to

alternative explanations), which made us consider the use of alternative arylboronate

reagents. Therefore, we studied the possible oxidative cross-coupling reaction of

phenylboronic acid with potassium phenyltrifluoroborate using complex **3** as a catalyst

(Scheme 5.6) by UV-visible absorption spectroscopy at different pHs (Figure 5.4). We

expected the products of the reaction to be mainly the cross-coupled biphenyl **5i** and

phenol **5k** as the main by-product (Scheme 5.6).

Scheme 5.6
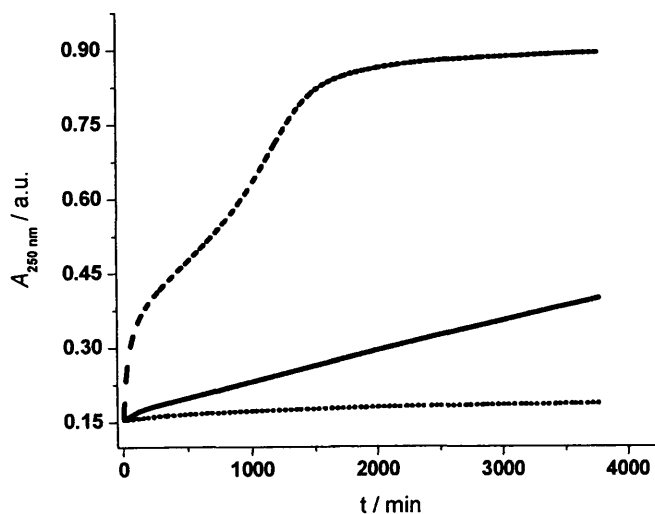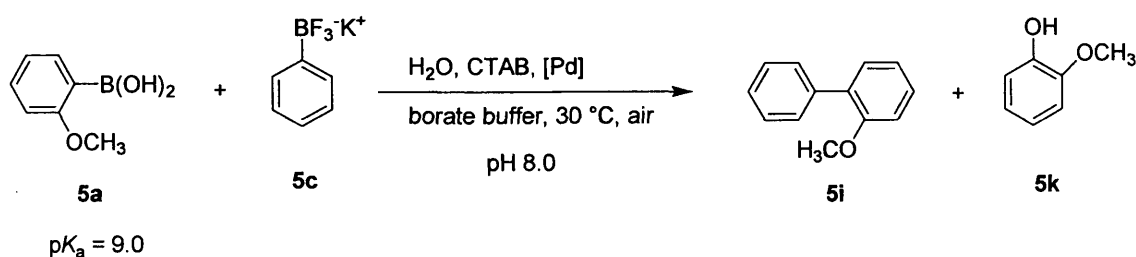
Figure 5.4: Absorbance of the reaction of 0.1 mM **5a** with 0.1 mM **5c** using 27.0 μM cat and 10 mM CTAB in 10 mM buffer, with time, at: pH 4 (dotted line), pH 7 (solid line), and pH 8 (dashed line), at 30 °C

Figure 5.4 shows that the reaction follows complex kinetics and that the reaction is slow

and clearly pH dependent. The reaction is particularly slow at low pH. This was not

anticipated if the trifluouroborate reacts with the acidic form of the arylboronic acid.

Our HPLC results for the reaction mixture showed five different products, two for the

homocoupling reactions of **5a** and **5c**, one for the cross-coupling of **5a** with **5c** and two

phenols resulting from **5a** and **5c** (Scheme 5.7 and Figure 5.5)
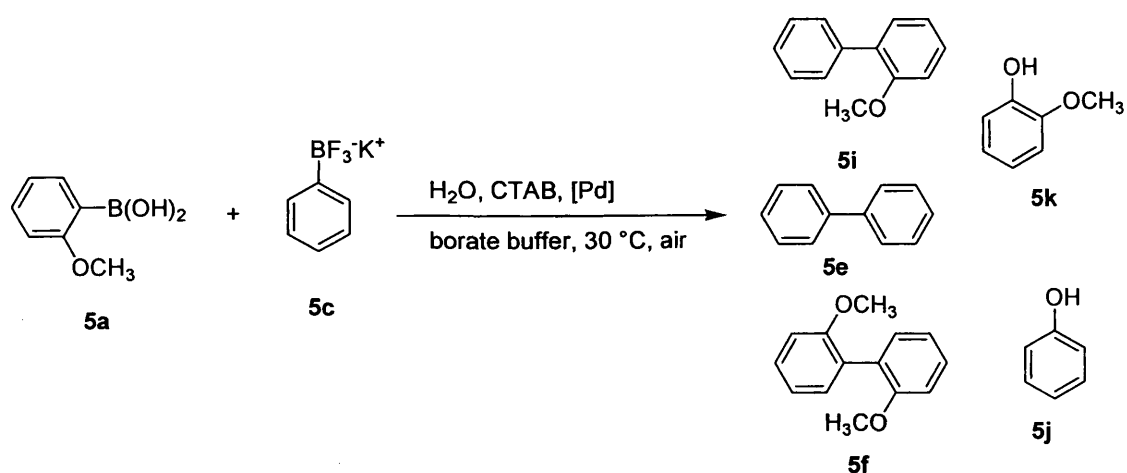
Scheme 5.7
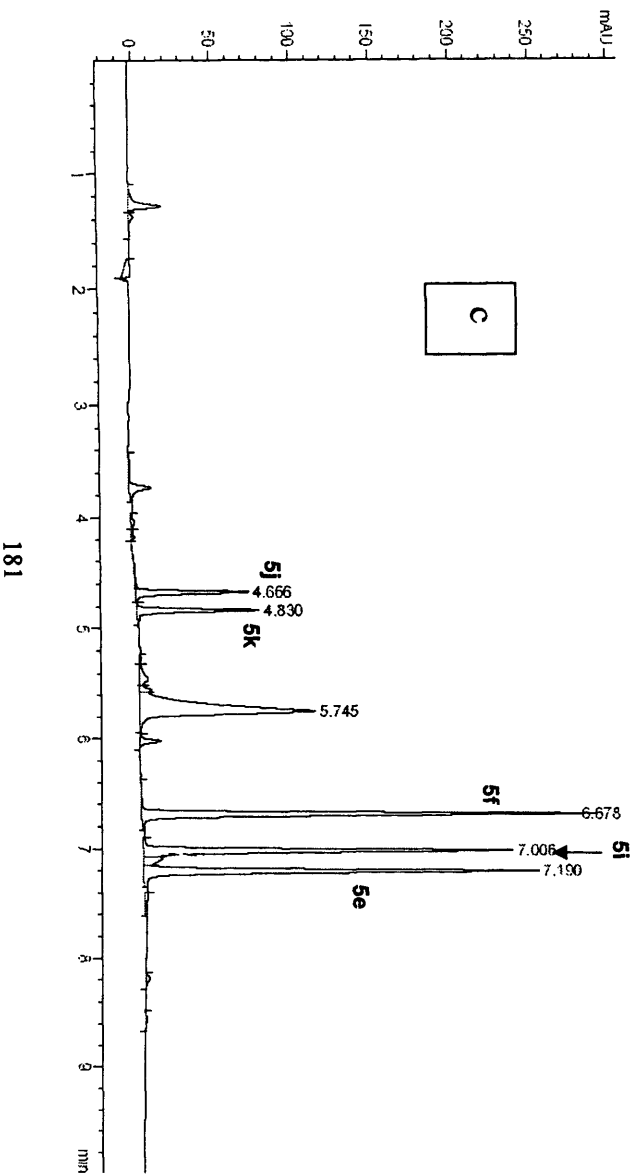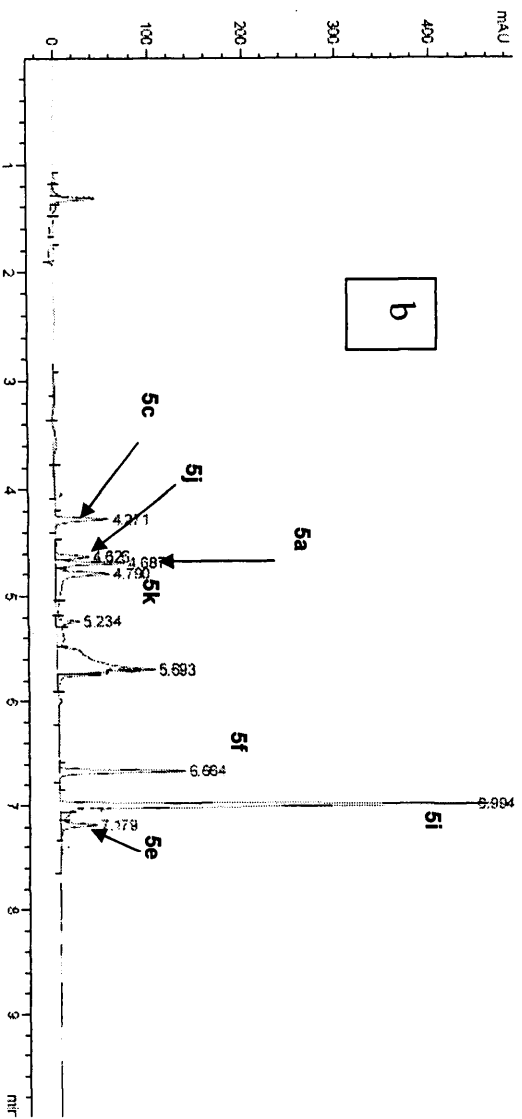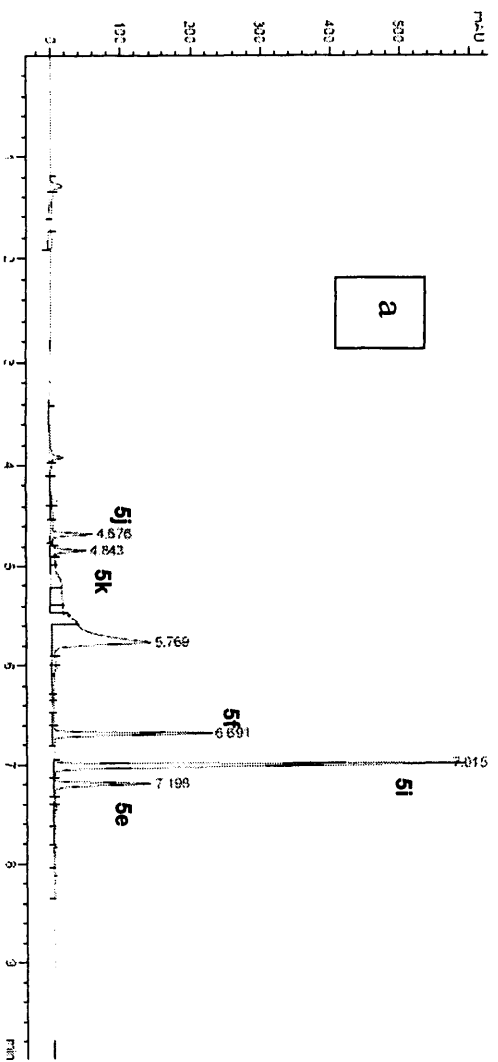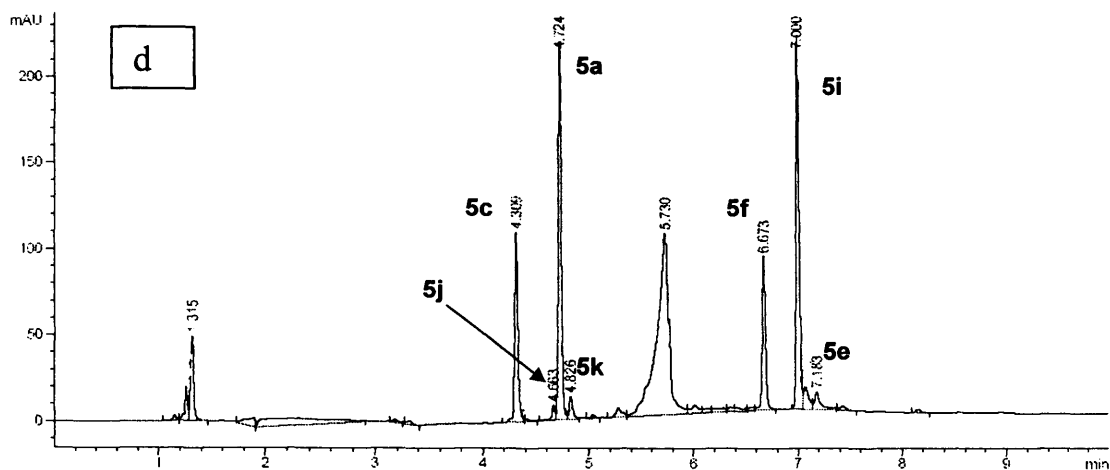
Figure 5.5. HPLC chromatograms and product analyses for the reaction of 0.1 mM **5a** with 0.1 mM **5c** in 10 mM CTAB and buffer using 10 μM of **3** as catalyst at 30 °C at pH 7.0 (a), pH 5.6 (b), pH 8.0 (c), and pH 4.0 (d).

The HPLC chromatograms (Figure 5.5) were analysed to provide the product ratios in the

various solutions (Table 5.1).

Table 5.1. Products ratio of the aerobic micelle-assisted Pd catalysed oxidative cross-coupling

reaction of **5a** with **5c** at different pHs.

pH	Product ratio					Reaction time / days	conversion
	5i	**5e**	**5f**	**5j**	**5k**		
4	2	unknown*	1	unknown*	unknown*	7	incomplete
5.6	5	1	2	unknown*	unknown*	1	incomplete
7	4	1	2	1	2	1	complete
8	2	1	1.5	1	4	3	complete

*Unknown because the base line of the HPLC chromatogram is not flat at that region (see Figure 5.5), two or more compounds have very similar retention times.

Table 5.1 suggests that the selectivity of the reaction towards the cross-coupling product is

indeed affected by the pH. In addition, Table 5.1 shows that the time required for the

reaction to complete is strongly dependent on pH as well, in line with the data in Figure

5.4. Our results show that pH 5.6 gives the best product ratios and selectivity towards the

cross-coupling reaction of 5a and 5c.

According to our proposed mechanism and the work of Adamo et al.,[5] phenol should only

form from the acidic form of the boronic acid. HPLC clearly shows the formation of

phenol from 5a and 5c. The homocoupling product of 5c is also present more than

anticipated since the Pd^{II} activation step should have been the only way for the formation

of biphenyl from 5c. According to the literature[2, 6], 5c can hydrolyse in basic medium to

form boronic acid (see Scheme 5.4), so we attribute the formation of phenol and biphenyl

from 5c to the hydrolysis of 5c. A mechanism requiring hydrolysis of 5c also explains the

slow reaction at low pH; the hydrolysis of 5c is rate limiting at low pH and only becomes

fast enough to support the coupling around neutral pH. The observed selectivity of the

reaction for the cross-coupled product is probably the result of the slow generation of the

acidic form of 5c (which is in this case is phenyl boronic acid) keeping its concentration

low at all times. This would suppress formation of 5e (which was used for normalisation

of the data in Table 5.1), making the selectivity for other products look better.

5.4. General conclusions, remarks and outlook

The kinetics of the aerobic oxidative homocoupling reaction of a set of arylboronic acids

were studied under ambient conditions in aqueous micellar solutions using different

palladium (pre) catalysts to catalyse the reaction. In Chapter 2 of the present thesis,

$Pd(bimsulfide)Cl_2$ was found to be a stable (pre) catalyst for our kinetic studies of the

aerobic oxidative homocoupling reactions. The reactions followed first-order kinetics in

the catalyst. The effect of arylboronic acid concentration on the observed rate constant was

found to follow inverse kinetic order and we attributed this behaviour to the complexity

within the micellar medium. It would be interesting to study this inverse kinetic order in

more detail. For example, running the reaction under homogeneous conditions but in the

absence of surfactants should eliminate micellar complexity. Using a water soluble

boronic acid, *e.g.* 4-carboxyboronic acid, would be good for this purpose. Work in this

area is in progress in our laboratory.

The effect of surfactant concentration was observed to be in agreement with common

bimolecular reactions in which the observed rate constant approaches a maximum with

increasing surfactant concentrations then decreases with further increase of surfactant

concentration due to dilution of the reactants over more micelles. The reactions were

slower in the absence of air (oxygen) indicating the important role of O_2 as an oxidant for

the Pd^0 species presumably through formation of a peroxo-Pd^{II}-complex (which is in

agreement with literature). The reactions were pH-dependent and we have observed a bell-

shaped pH-rate profile for the reaction of all studied arylboronic acids. Our experimental

data suggests different possible mechanisms for the reaction under our conditions. The

common steps in the mechanisms are: first, the reaction of two molecules of

phenylboronic acid (possibly in the basic form) with Pd(bimsulfide)Cl_2 pre-catalyst to

form the biphenyl product and the Pd^0 species (entry to the catalytic cycle). Second, a

dissolved O_2 molecule in the aqueous micellar solution oxidises the Pd^0 species and forms

a peroxo-Pd^{II}-complex (the start of the catalytic cycle). The bell-shaped pH-rate profile

suggests different possible mechanisms for the consequent transmetalation steps of the

reaction (rate limiting step(s)). The most likely mechanism is that the basic form of the

catalyst is involved in the rate-limiting step together with the acidic form of the

arylboronic acid. The key points in the possible mechanisms of the rate limiting step are

summarised in Scheme 5.8.

A)   Pd-OH   +   Ar—B⟨OH / OH ⟩ ──────► Pd-Ar

B)   Pd-$\overset{\oplus}{O}H_2$ +   Ar—$\overset{\ominus}{\underset{OH}{B}}$-OH ──────► Pd-Ar

C)   Pd-Br   ⇌   Pd-OH
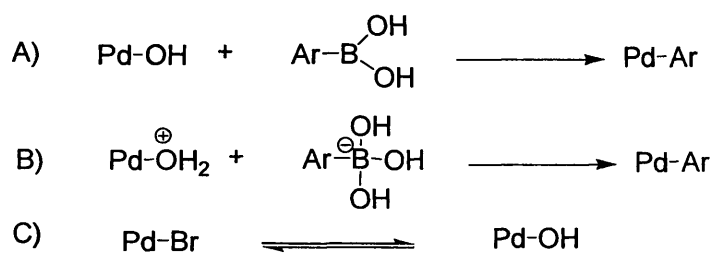
Scheme 5.8

Mechanisms A and B could be distinguished on the basis of the experiments involving H_2O and D_2O on the basis of solvent isotope effects. Mechanism C could be eliminated by using non-ionic surfactant which eliminates the counter anions. Also, the fact that Pd-OH_2^+ does not react with Ar-BF$_3^-$ (as suggested by our kinetic data for the cross-coupling at low pH) is in favour of mechanism A and not of mechanism B. On the other hand, the suggestion that Pd-OH_2^+ does not react with (Ph)$_4$-B$^-$ (See ref [7]) is in favour of mechanism B.

In the third Chapter, Pd-CTAB NPs were used to catalyse the aerobic homocoupling reaction of phenylboronic acid. The reaction was slower compared to when the molecular Pd (pre) catalyst **3** was used as catalyst. The reaction was first-order in the catalyst and mixed second- and first-order in PBA. A bell-shaped pH-rate profile was again found for the reaction under our conditions. A possible mechanism for the rate-limiting step of the reaction based on our kinetic results (and employing the preferred mechanism from Chapter 2) includes a pre-equilibrium step involving the basic form of the catalyst and the acidic form of PBA to form an intermediate which then reacts with another molecule of PBA to form a biaryl intermediate which reductively eliminates to form the biphenyl and reproduces the Pd^0 catalyst. We do not have evidence to confirm whether the reaction occurs on the surface of the NPs or through leached Pd atoms and/or ions. One way of

beginning to test this would be to carry out the reaction on a large scale and place the nanoparticles within dialysis tubing. When the dialysis tubing is removed, the reaction should stop immediately if the reaction happens on the NP surface. However, if the reaction continues for some time, leached atoms have escaped from the dialysis tubing and are catalytically active.

The fourth Chapter involved the synthesis of bimetallic core-shell Au-Pd NPs encapsulated in pNIPAM shells (Au@Pd@pNIPAM) of different sizes and morphologies. Pd-pNIPAM (-ve and +ve) were also synthesised. The kinetics of the aerobic homocoupling reaction of phenylboronic acid was followed using both catalytic systems. The reactions were slower compared to those using 3 and Pd-CTAB NPs under otherwise similar conditions. A bell-shaped pH-rate profile was again observed. The reaction was first-order in the catalyst and mixed second- and first-order in PBA. Our kinetic results suggest the same mechanism as in Chapter 3. Furthermore, our preliminary data indicated that the presence of the thermoresponsive pNIPAM shell results in non-Erying-like behaviour. The experimental data of the temperature effect on the reaction rate constant could be further analysed by restricting the values of ΔH and ΔS to the values determined from the temperature dependence of the particle size (D_h), see Chapter 4.

Finally, our findings could have important implications for other Pd (or metal)-catalysed reactions (*e.g.* Heck, Sonogashira, Stille, etc.), at least in aqueous solutions but possibly in organic solvents as well.

References

1.   Yuen, A. K. L.; Hutton, C. A., *Tetrahedron Letters* **2005**, *46* (46), 7899-7903.

2.   Ting, R.; Harwig, C. W.; Lo, J.; Li, Y.; Adam, M. J.; Ruth, T. J.; Perrin, D. M., *Journal of Organic Chemistry* **2008**, *73* (12), 4662-4670.

3.   Cooper, J. N.; Powell, R. E., *Journal of the American Chemical Society* **1963**, *85* (11), 1590-1592.

4.   Crawford, C. L.; Barnes, M. J.; Peterson, R. A.; Wilmarth, W. R.; Hyder, M. L., *Journal of Organometallic Chemistry* **1999**, *581* (1-2), 194-206.

5.   Adamo, C.; Amatore, C.; Ciofini, I.; Jutand, A.; Lakmini, H., *Journal of the American Chemical Society* **2006**, *128* (21), 6829-6836.

6.   Butters, M.; Harvey, J. N.; Jover, J.; Lennox, A. J.; Lloyd-Jones, G. C.; Murray, P. M., *Angewandte Chemie - International Edition* 2010 *49* (30), 5156-5160.

7.   Nakai, H.; Ogo, S.; Watanabe, Y., *Organometallics* **2002**, *21* (8), 1674-1678.

Appendix 1

This Appendix is for Chapter 2

Homocoupling of arylboronic acids using molecular Pd- catalyst

in aqueous micellar medium (kinetic and mechanistic studies)

A1.1. Effect of **2a** concentration on the k_{obs} at pH 7.4
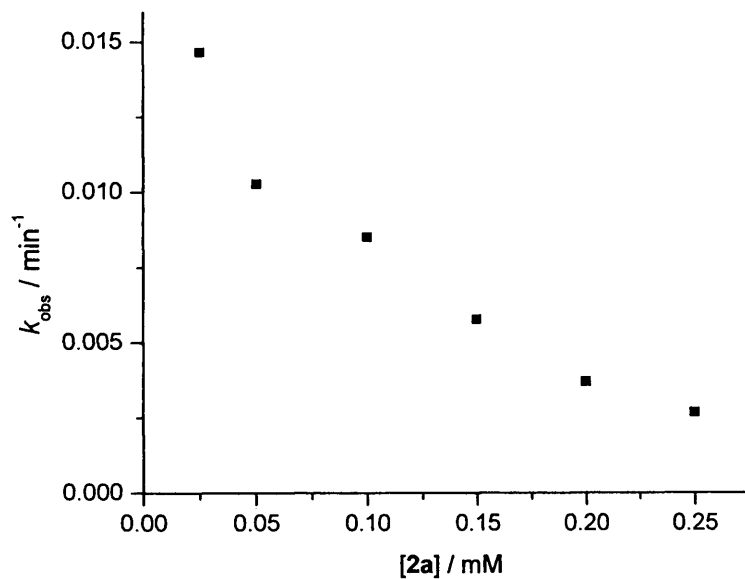
Figure S1: Effect of **2a** concentration on the observed reaction rate constant using 5.0 µM of **3**, 10.0 mM CTAB and borate buffer pH 7.4 at 30 °C.

A1.2. Titration of **2a** with AMDP in CTAB
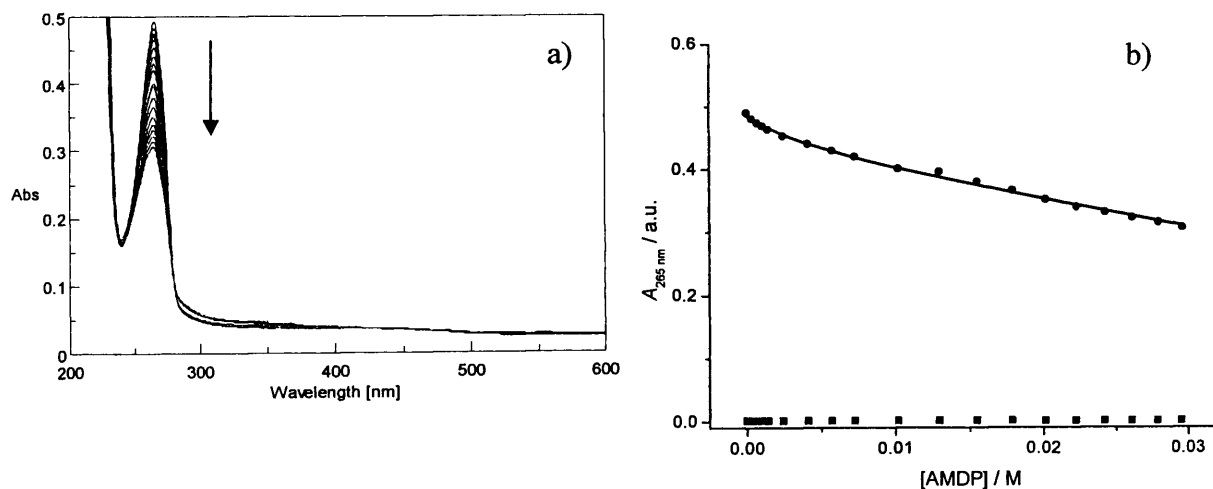
Figure S2: Titration spectra (a) and absorbance at 265 nm versus AMDP concentration (b) for the addition of AMDP to 1.0 mM **2a** in 10 mM CTAB at pH 8.8 and 30 °C.

A1.3. Kinetic traces of the homocoupling reaction of 2a-h
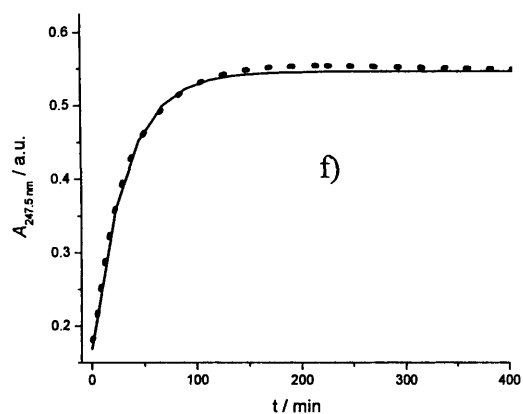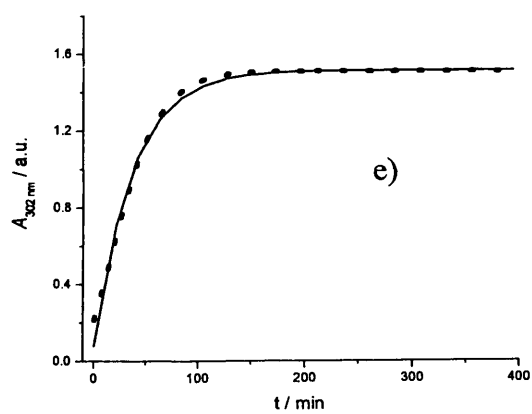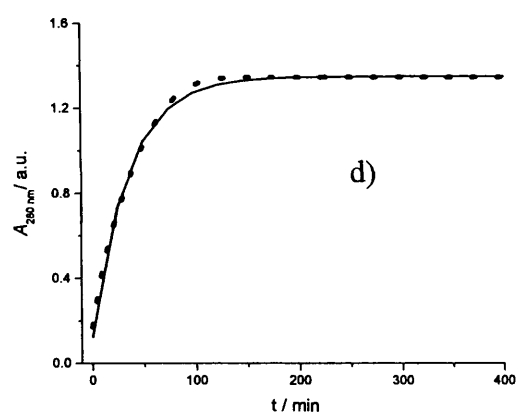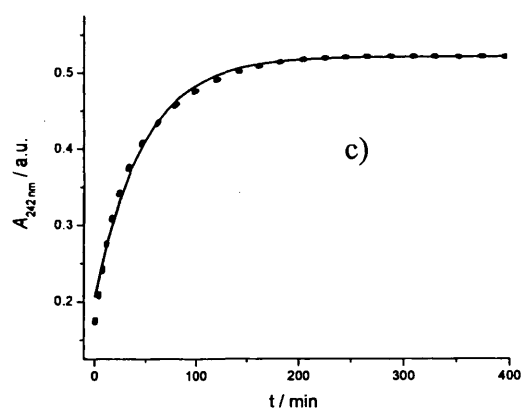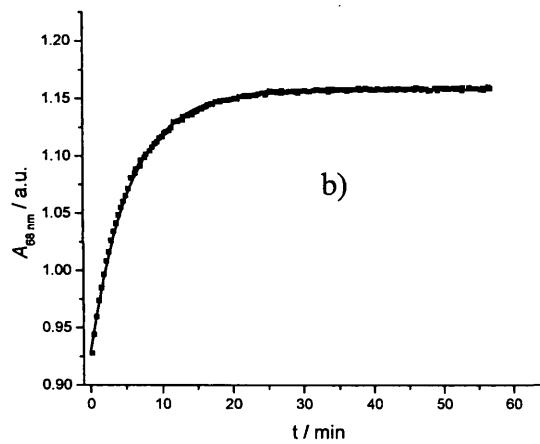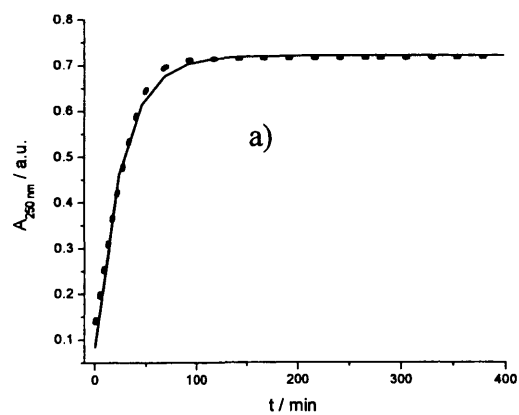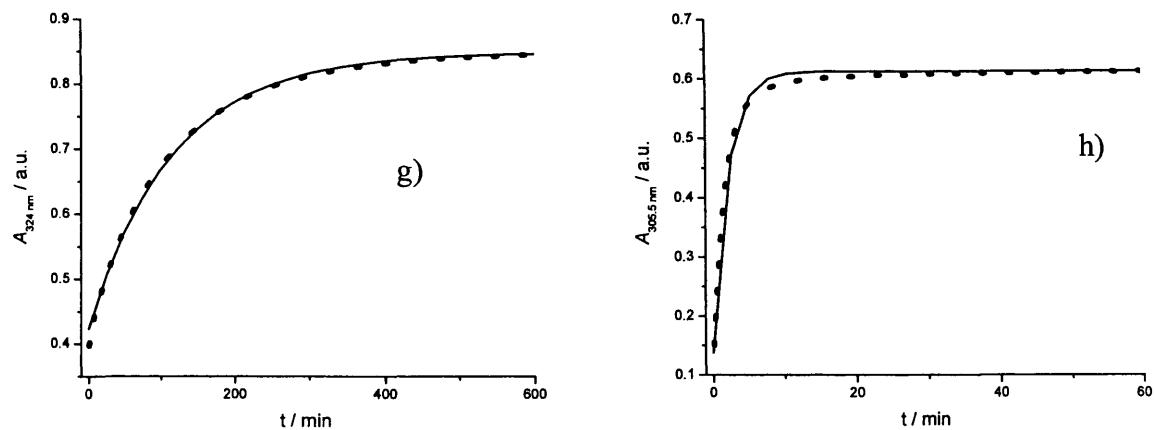
Figure S3a-h: Absorbance of the reaction mixture of homocoupling of 0.1mM **2a-h** using 10.0 μM of **3** with time 1 max in 10.0 mM CTAB and borate buffer pH optimum at 30 °C, experimental data (dotted line) and solid line fit to the (pseudo) first order equation (2.1).

A1.4. pK_a of measurements of **2a-h** in CTAB and borate buffer
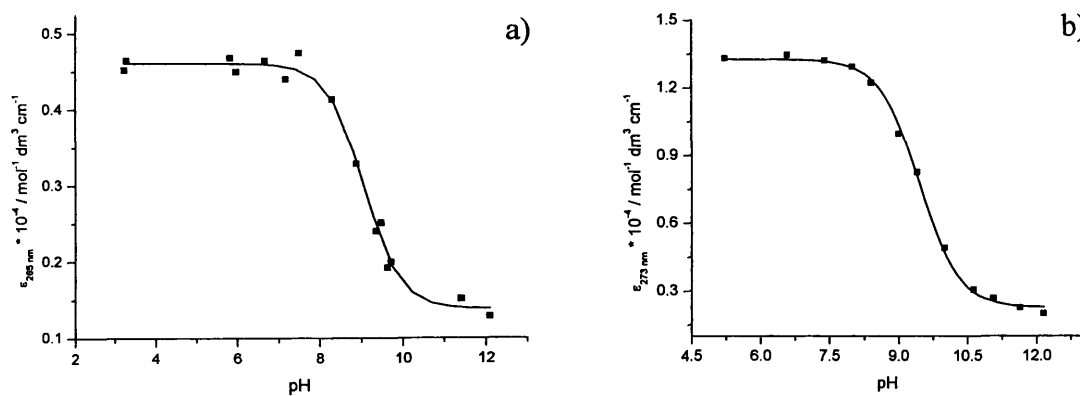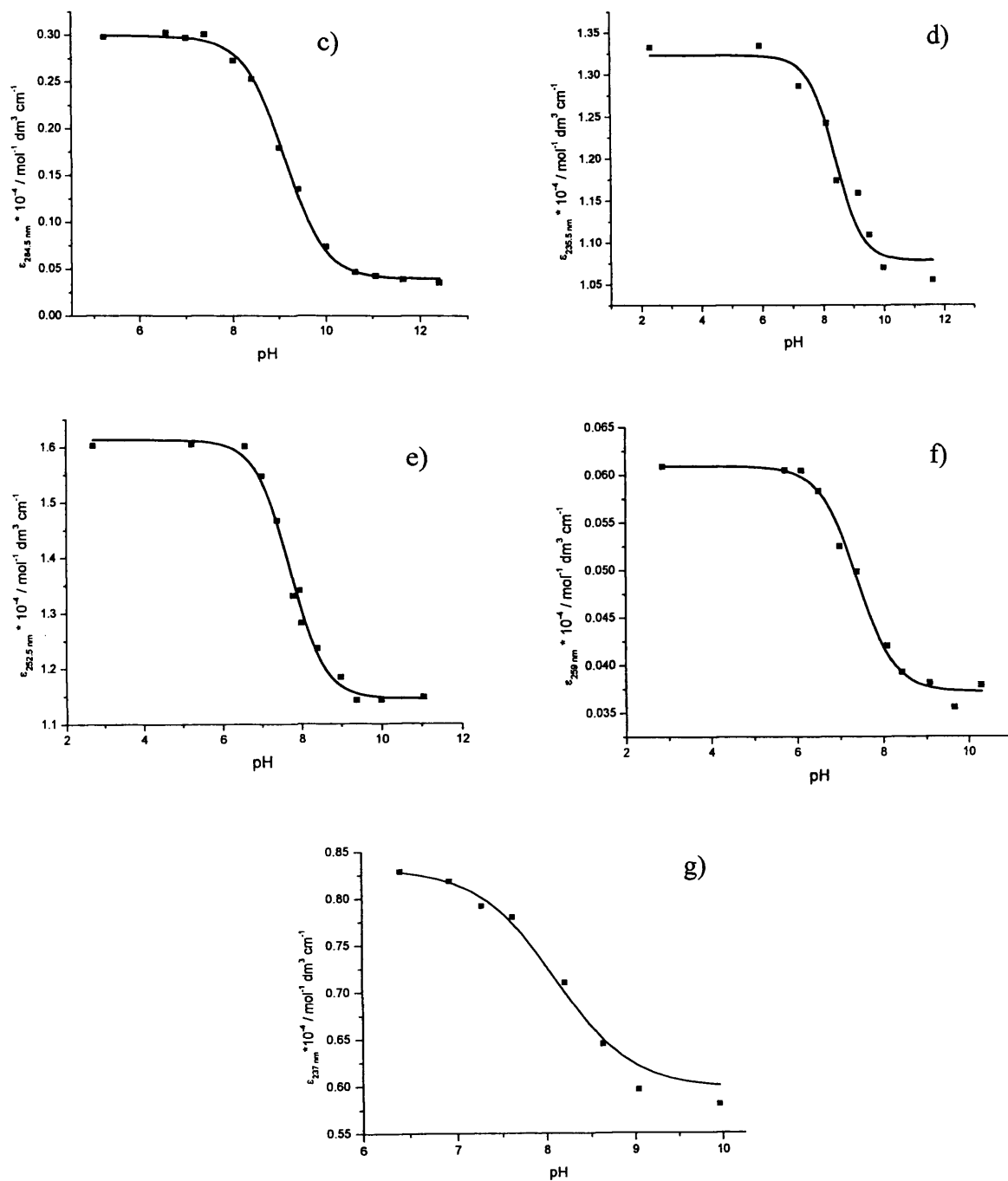
Figure S4a-h.. Effect of pH on extibction coefficient of 0.1 mM a) **2a**, b) **2b**, c) **2c**, d)**2d**, e) **2e**, f) **2f**, and g) **2h**, in 10.0 mM CTAB and 10.0 mM borate buffer at 30 °C (■), solid line fit to (equation 2.3).

A1.5. pH-k_{obs} of the reaction relation of **2a-h**

a)

b)

c)

d1)

d2)
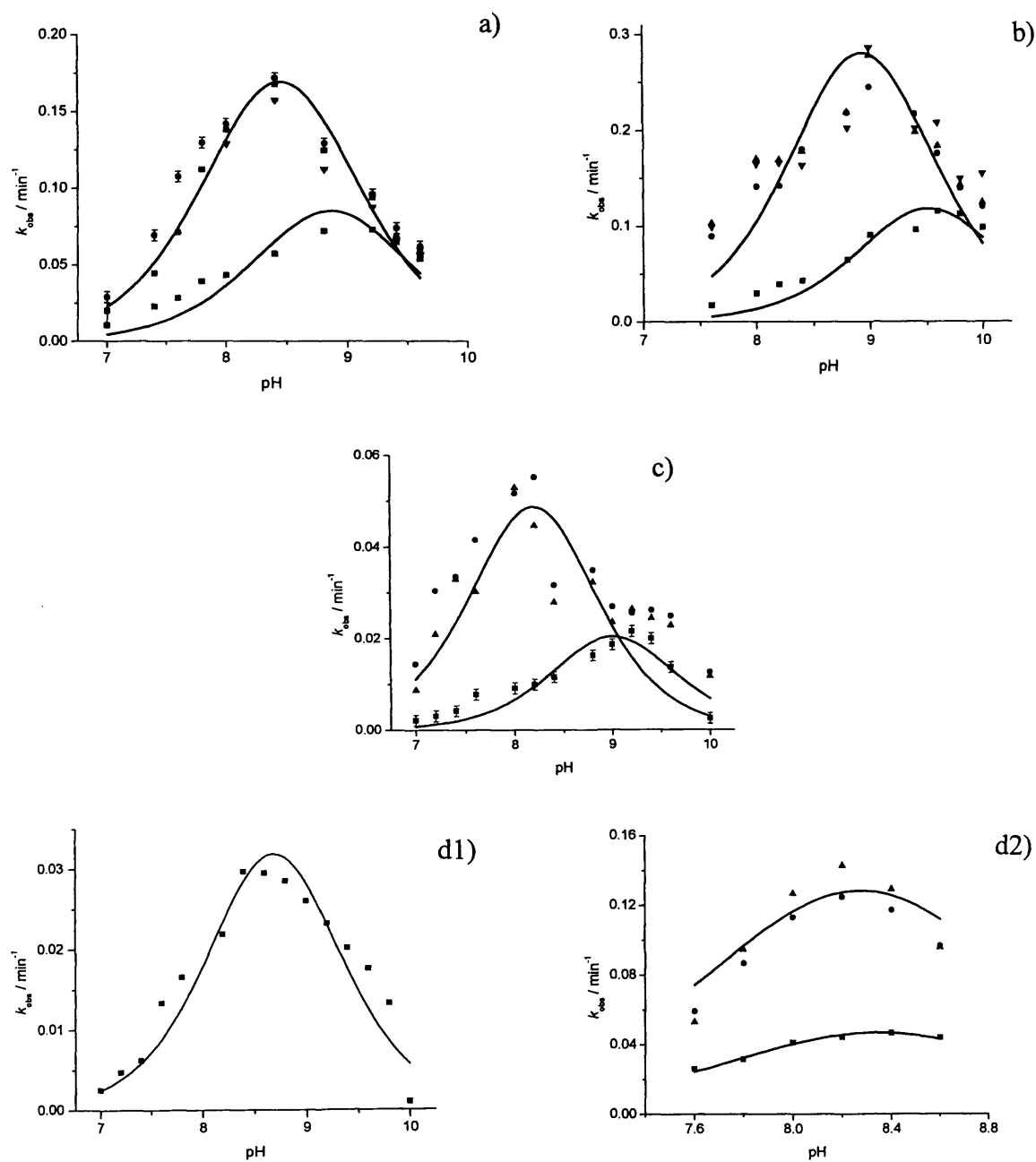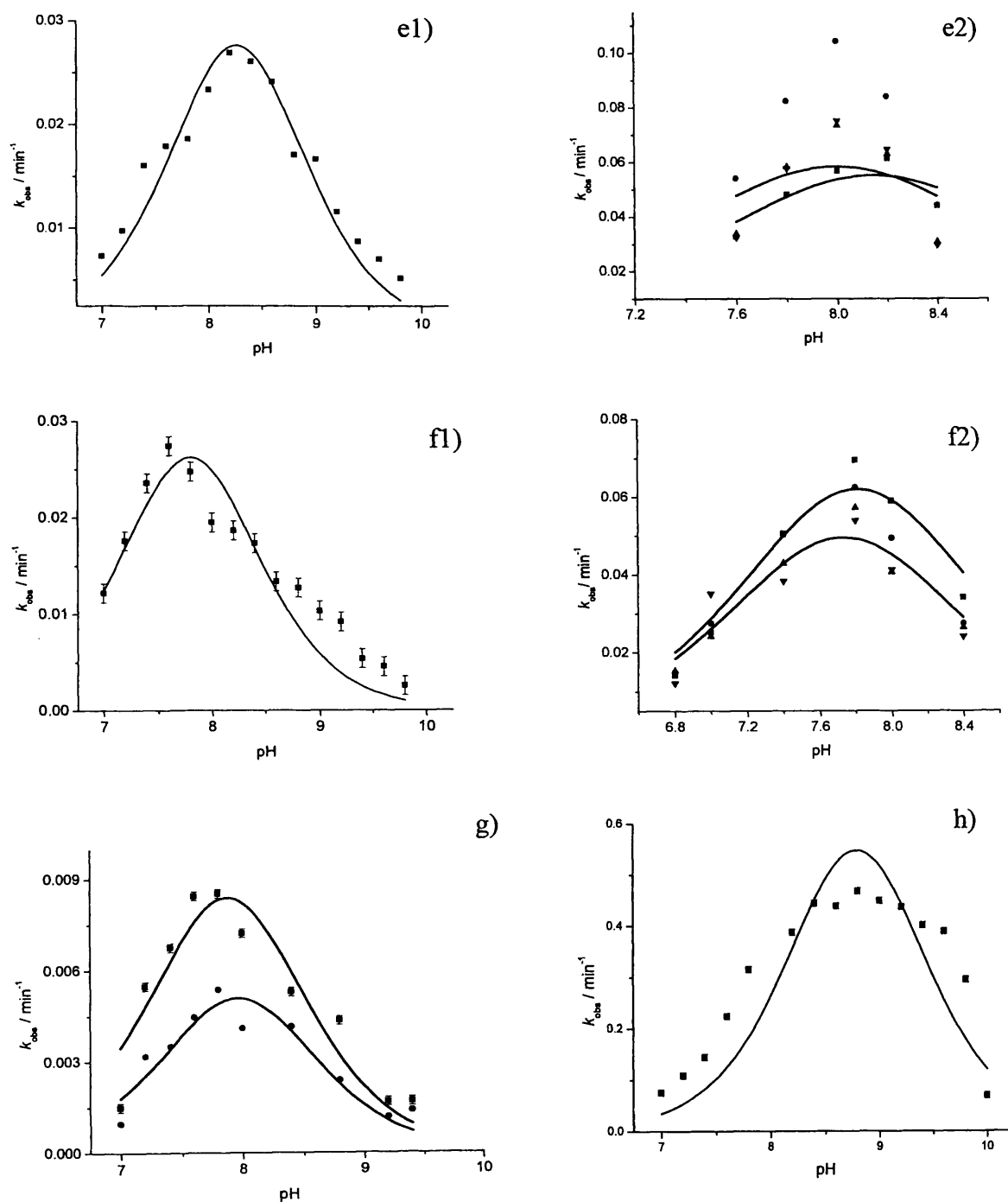
Figure S5a-h: Effect of pH on k_{obs} for the reaction involving 0.1 mM **2a-h** (■), addition of an additional 0.05 mM **2a-h** (●), addition of a further 0.05 mM **2a-h** (▲), and addition of third aliqout of 0.05 mM **2a-h** (▼), using 10 mM CTAB, 10 mM borate buffer and (a) 27 μM of **3** (b) 10 μM of **3** (c) 10 μM of **3**, (d1) 10 μM of **3**, (d2) 15 μM of **3**, (e1) 10 μM of **3**, (e2) 27 μM of **3** (f1) 10 μM of **3**, (f1) 27 μM of **3**, and (g) 10 μM of **3**, and (h) 10 μM of **3**all at 30 °C, solid line is a fit to a Gaussian (eqn. 2.2).

Note: for **2e** the Gausian fit (eq. 2.2) to the experimental data after activation is not good.

We were able to perform only one set of pH-rate profile after activation for the reaction of **2g**

due to precipitate formation upon further addition of **2g**. Also, the fact that the 2nd addition

pH-rate-profile for the reaction of **2g** is less than 1st addition is possibly due to the solubility

limit of the products **10g** and **11g**

A1.6. HPLC chromatogram and calibration graph for the products (phenol **10a-h** and biaryl

11a-h) of the reaction of **2a-h**.
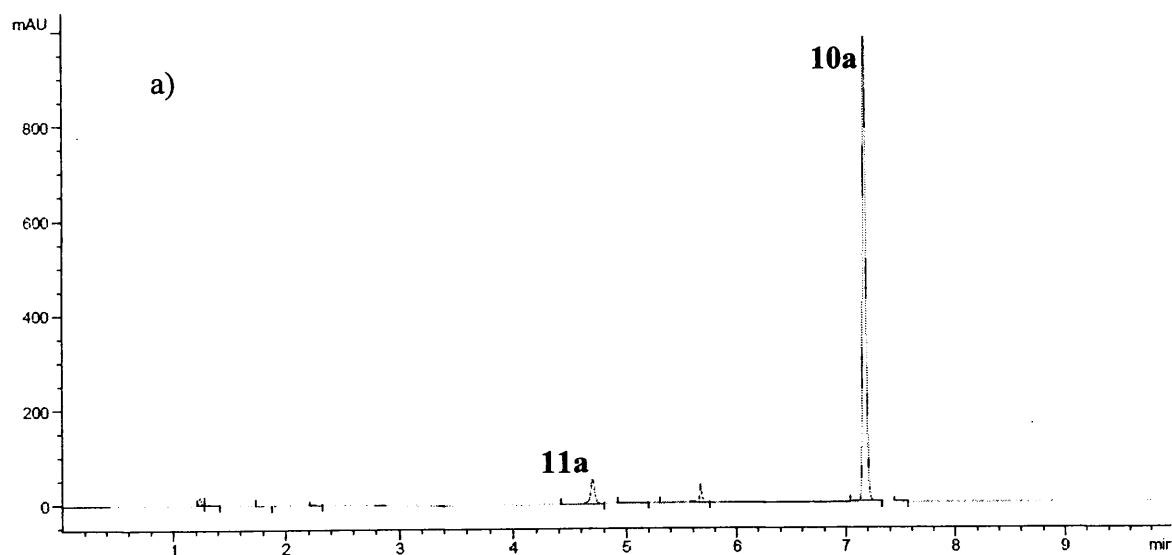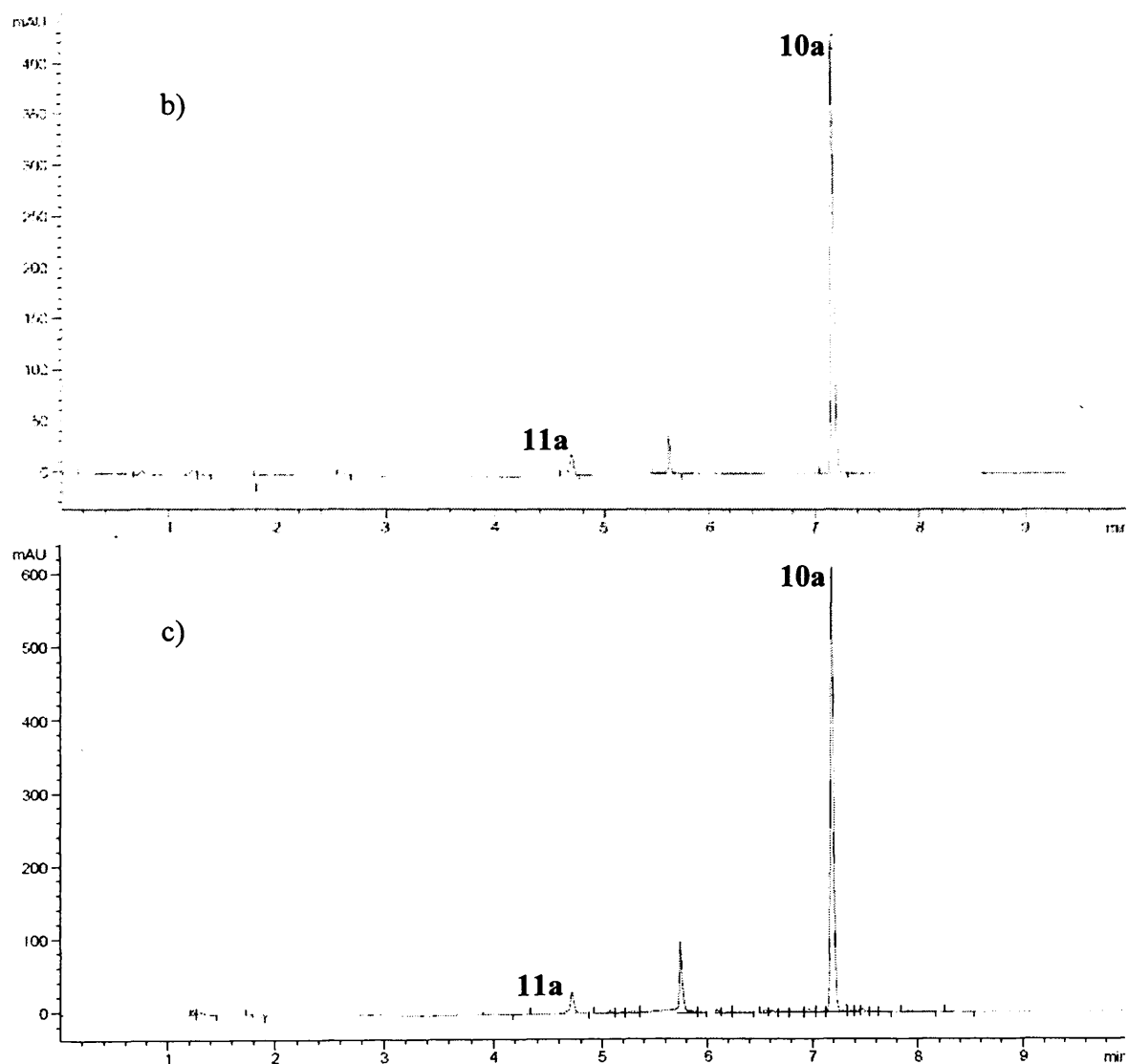
Figure S6. HPLC chromatograms for a) 0.05 mM, b) 0.1 mM of authentic phenol (**11a**) and biphenyl (**10a**) in 10 mM CTAB and borate buffer pH 9.2, and c) reaction mixture of 0.1 mM **2a** in 10 mM CTAB and borate buffer buffer using 10 μM of **3** as catalyst at 30 °C at pH 9.2.
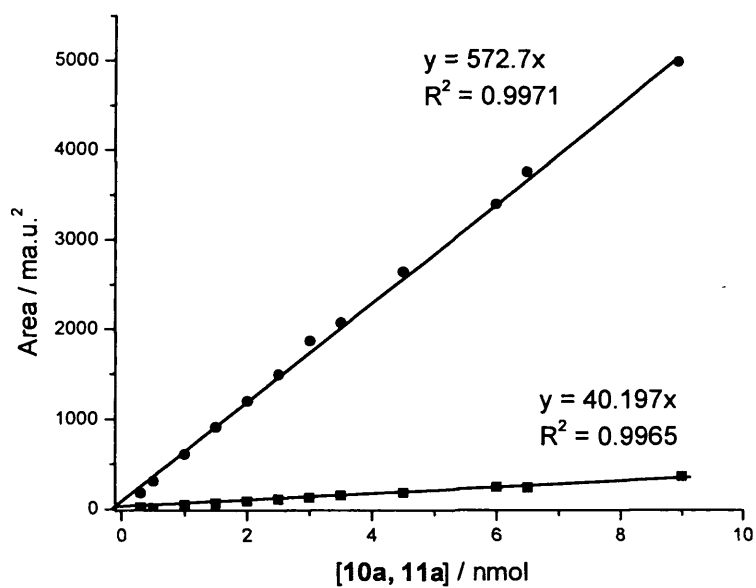
Figure S7. Calibration graph of **10a** (•) and **11a** (■) in CTAB and borate buffer pH 9.2, based on the related area under the peak of the related HPLC chromatogram.
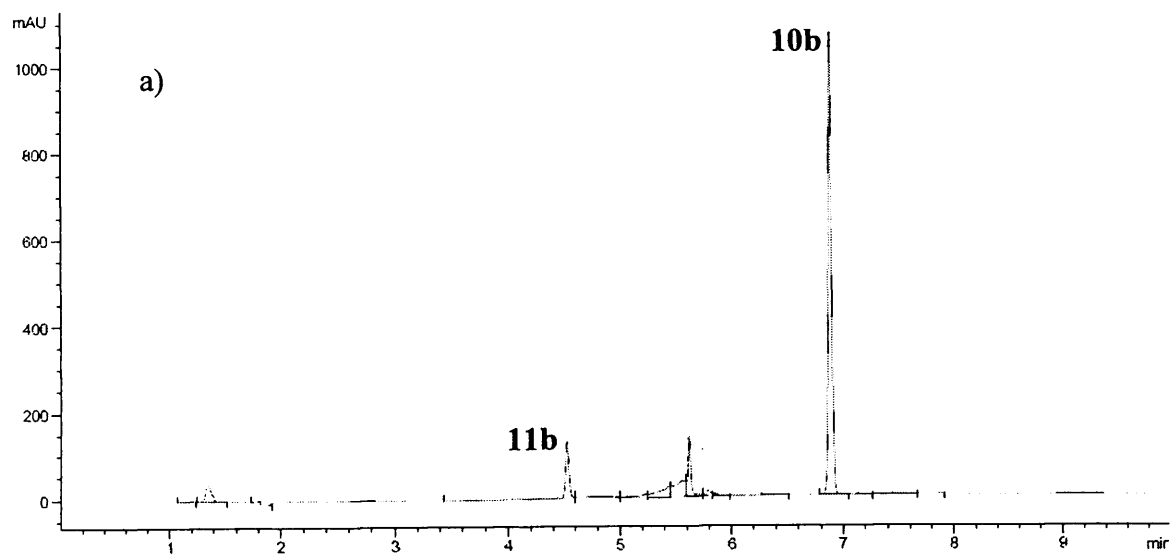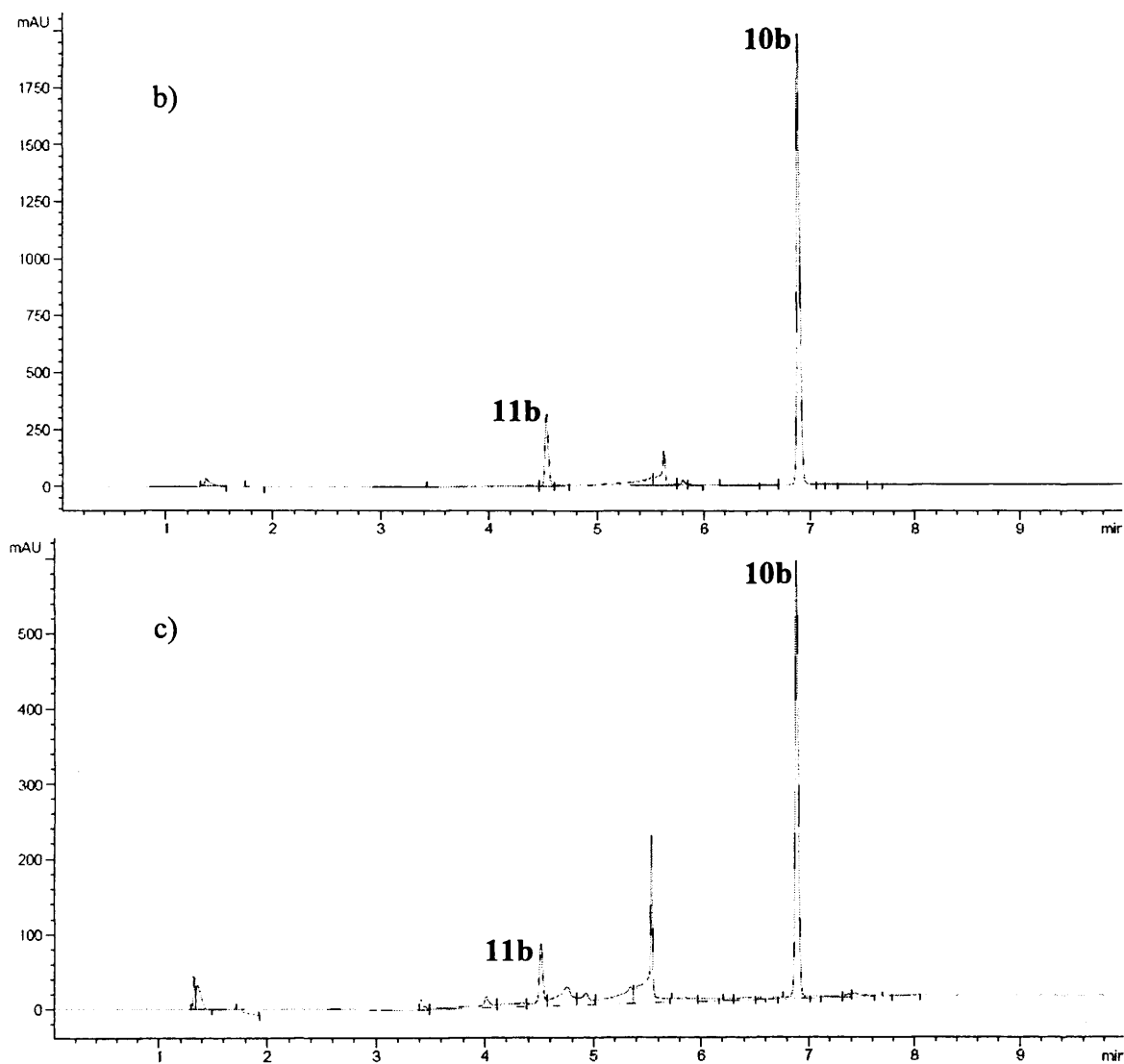
Figure S8. HPLC chromatograms for a) 0.05 mM, b) 0.1 mM of authentic 4-methoxyphenol (**11b**) and 4,4'-dimethoxybiphenyl (**10b**) in 10 mM CTAB and borate buffer pH 9.6, and c) reaction mixture of 0.1 mM **2b** in 10 mM CTAB and borate buffer buffer using 10 μM of **3** as catalyst at 30 °C at pH 9.6.
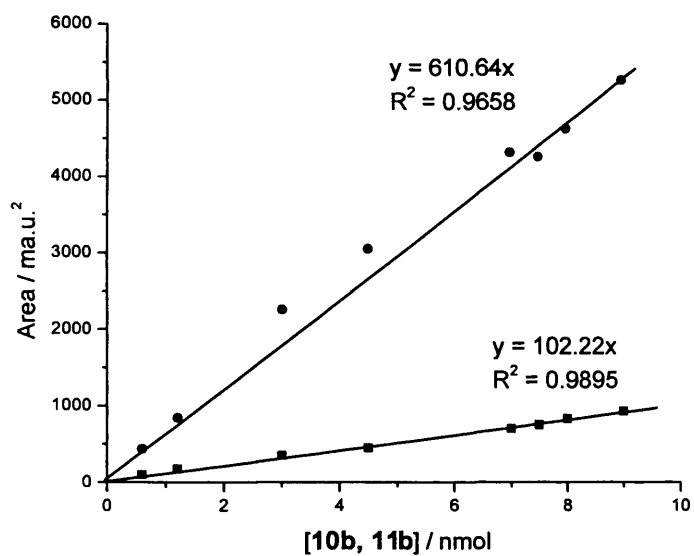
Figure S9. Calibration graph of **10b** (•) and **11b** (■) in CTAB and borate buffer pH 9.6, based on the related area under the peak of the related HPLC chromatogram
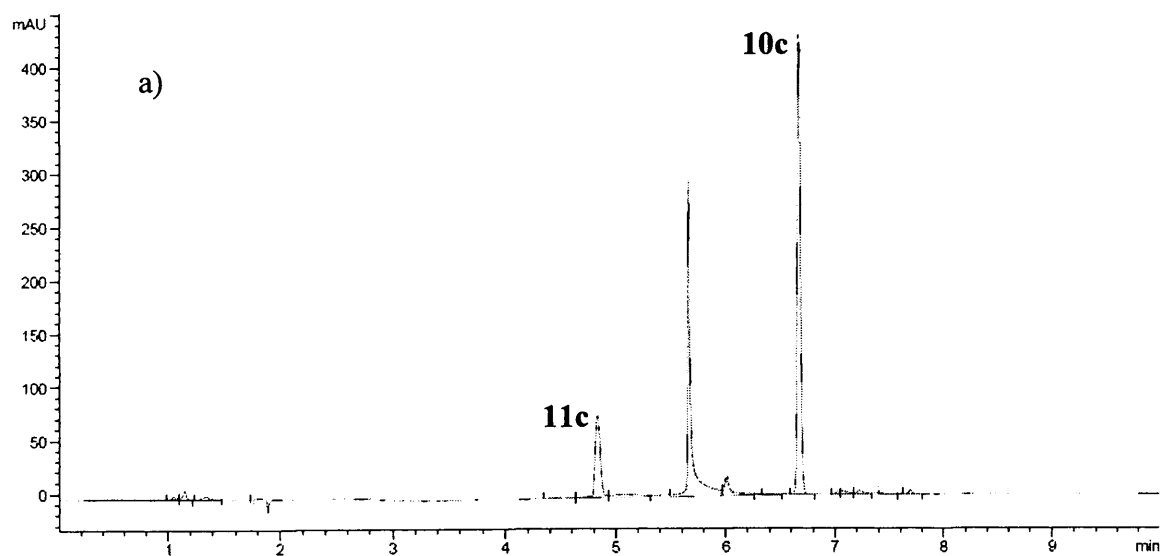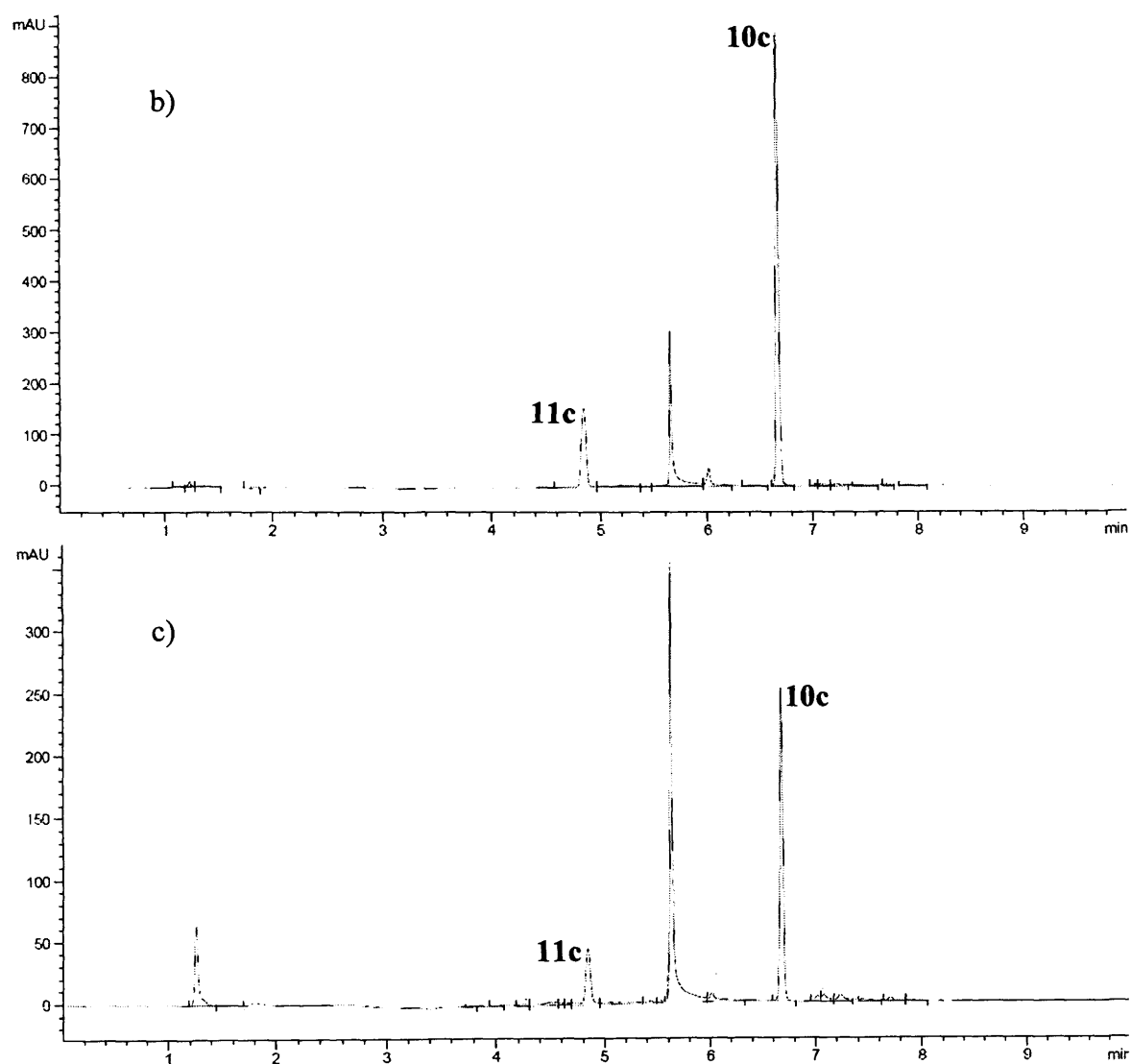
Figure S10. HPLC chromatograms for a) 0.05 mM, b) 0.1 mM of authentic 2-methoxyphenol (**11c**) and 2,2'-dimethoxybiphenyl (**10c**) in 10 mM CTAB and borate buffer pH 9.2, and c) reaction mixture of 0.1 mM **2c** in 10 mM CTAB and borate buffer buffer using 10 μM of **3** as catalyst at 30 °C at pH 9.2.
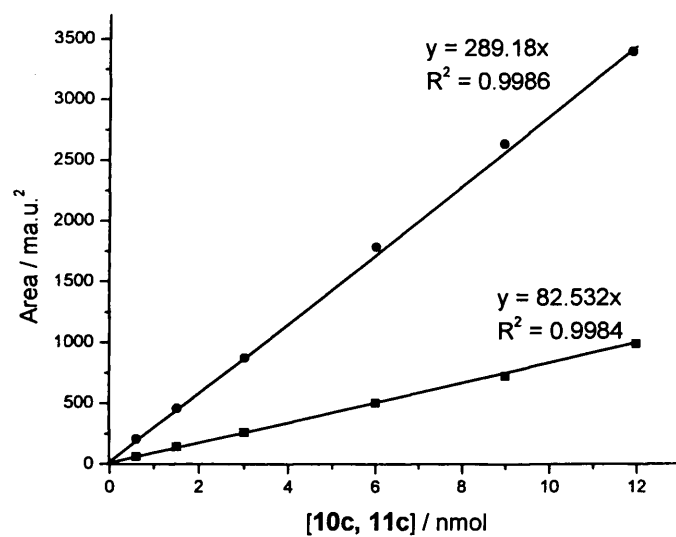
Figure S11. Calibration graph of **10c** (•) and **11c** (■) in CTAB and borate buffer pH 9.2, based on the related area under the peak of the related HPLC chromatogram
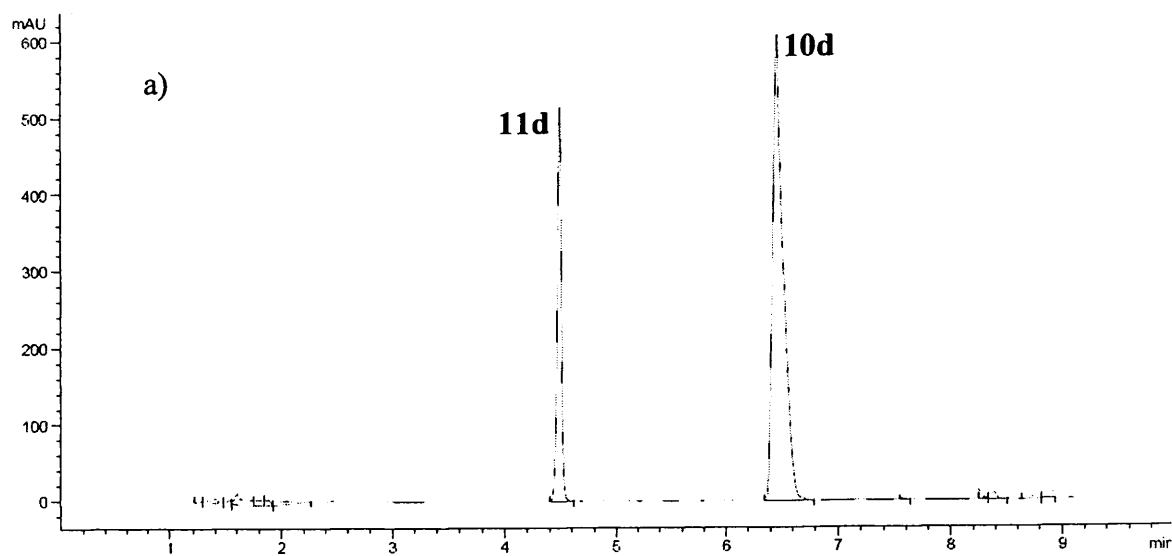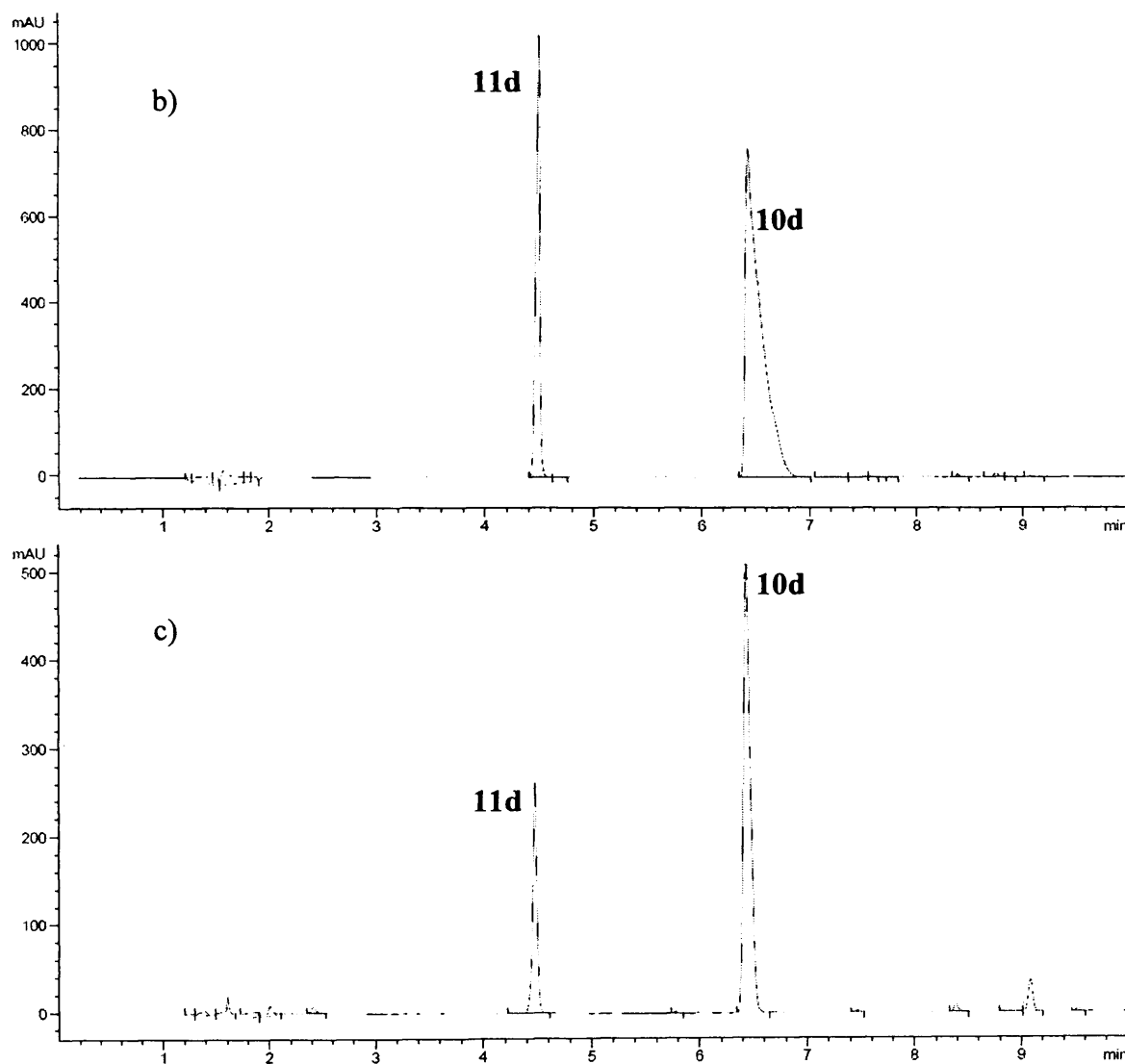
Figure S12. HPLC chromatograms for a) 0.05 mM, b) 0.1 mM of authentic 4-carboxyphenol (**11d**) and 4,4'-dicarboxybiphenyl (**10d**) in 10 mM CTAB and borate buffer pH 8.4, and c) reaction mixture of 0.1 mM **2d** in 10 mM CTAB and borate buffer buffer using 10 μM of **3** as catalyst at 30 °C at pH 8.4.
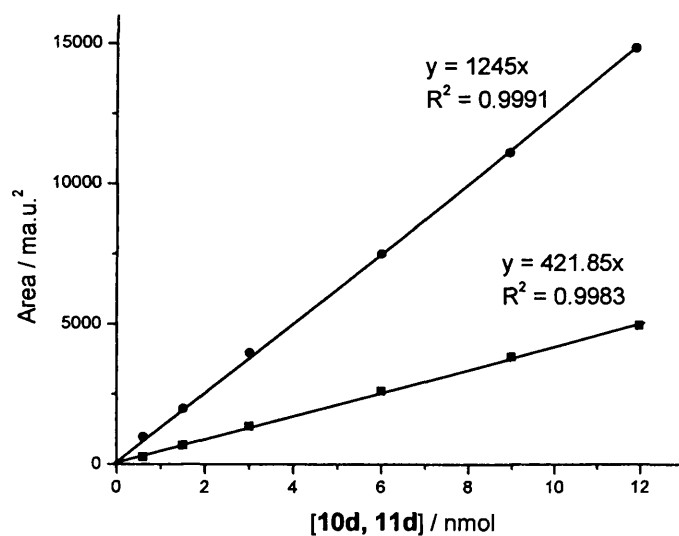
Figure S13. Calibration graph of **10d** (●) and **11d** (■) in CTAB and borate buffer pH 8.4, based on the related area under the peak of the related HPLC chromatogram.
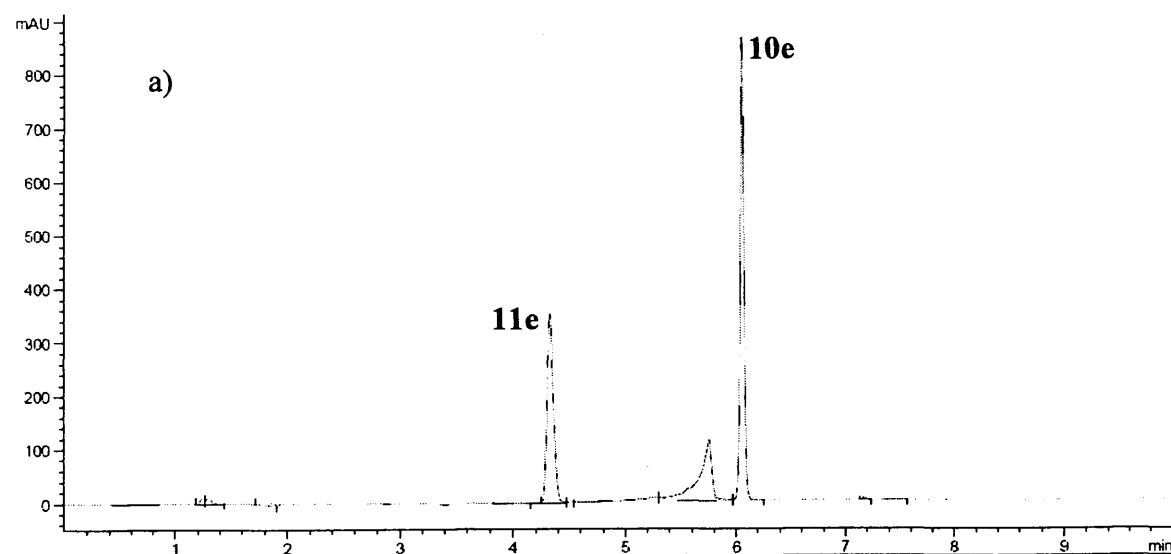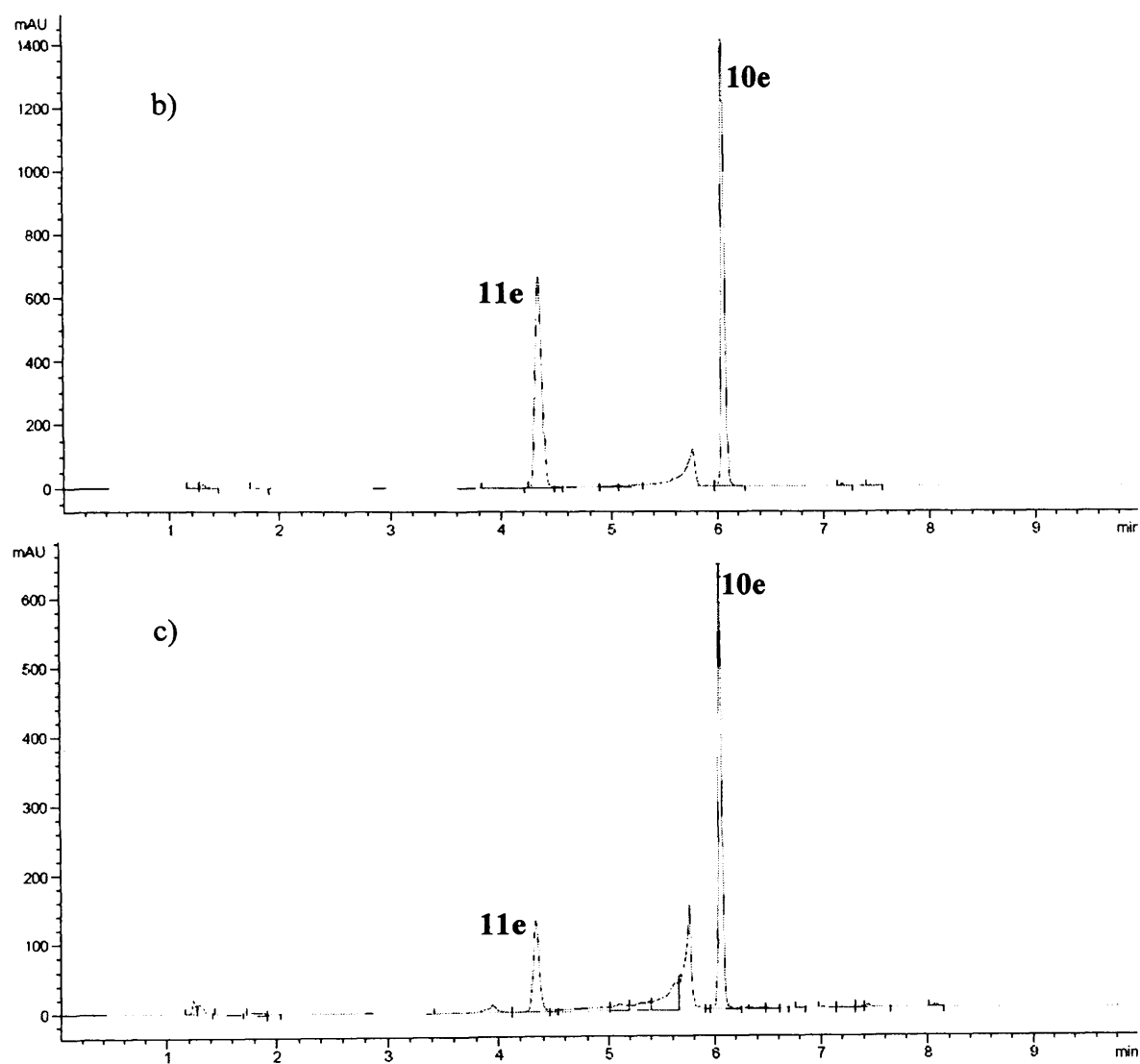
Figure S14. HPLC chromatograms for a) 0.05 mM, b) 0.1 mM of authentic 4-acetylphenol (**11e**) and 4,4'-diacetylbiphenyl (**10e**) in 10 mM CTAB and borate buffer pH 8.2, and c) reaction mixture of 0.1 mM **2e** in 10 mM CTAB and borate buffer buffer using 10 μM of **3** as catalyst at 30 °C at pH 8.2.
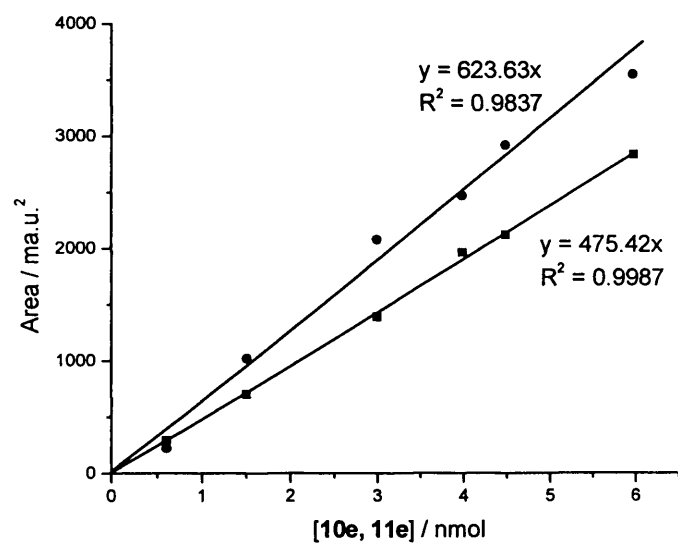
Figure S15. Calibration graph of **10e** (•) and **11e** (■) in CTAB and borate buffer pH 8.4, based on the related area under the peak of the related HPLC chromatogram.
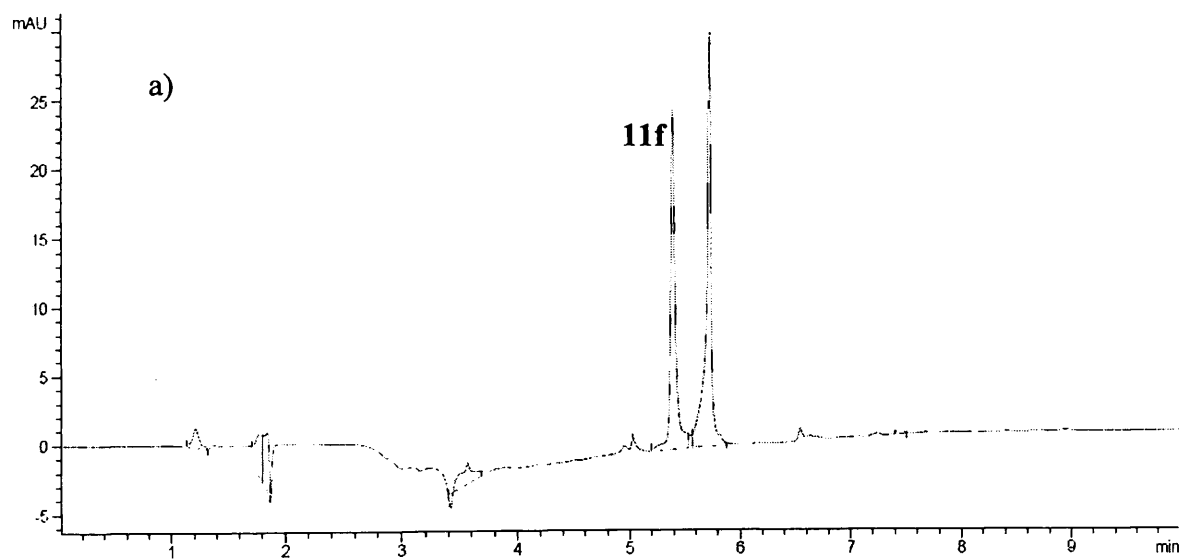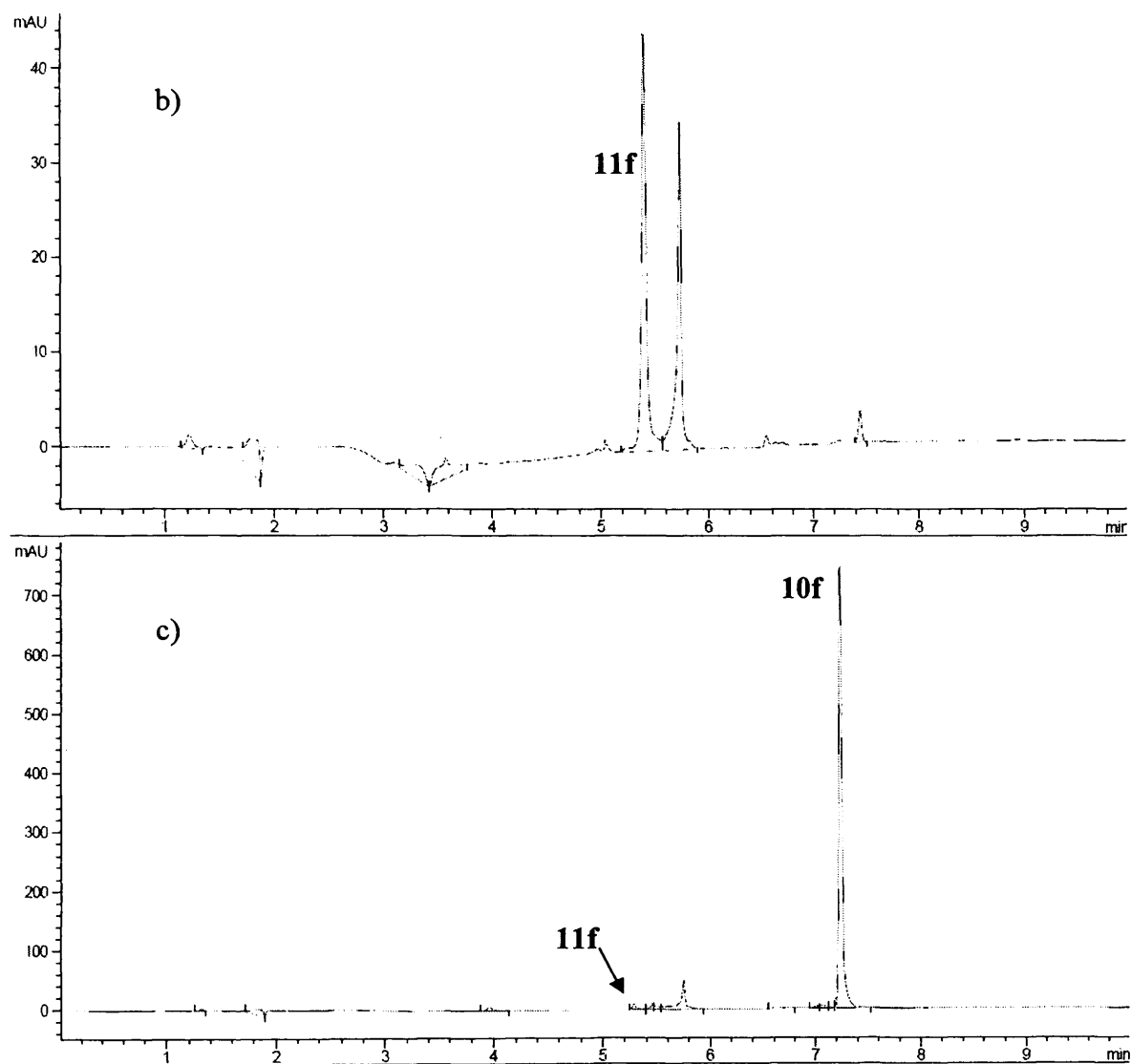
Figure S16. HPLC chromatograms for a) 0.05 mM, b) 0.1 mM of authentic 4-acetylphenol (**11e**) and 4,4'-diacetylbiphenyl (**10e**) in 10 mM CTAB and borate buffer pH 8.2, and c) reaction mixture of 0.1 mM **2e** in 10 mM CTAB and borate buffer buffer using 10 μM of **3** as catalyst at 30 °C at pH 8.2.

$$y = 25.313x$$
$$R^2 = 0.9875$$
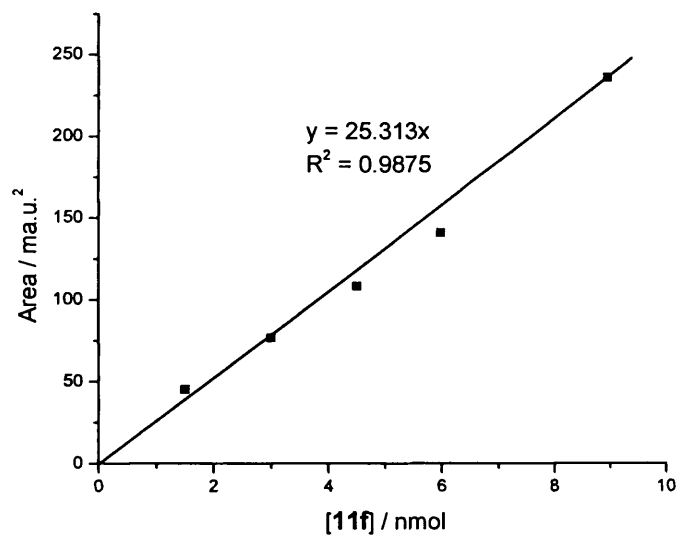
Figure S17. Calibration graph of **11e** (■) in CTAB and borate buffer pH 7.8, based on the related area under the peak of the related HPLC chromatogram of known concentrations in nanomoles of authentic **11f.**
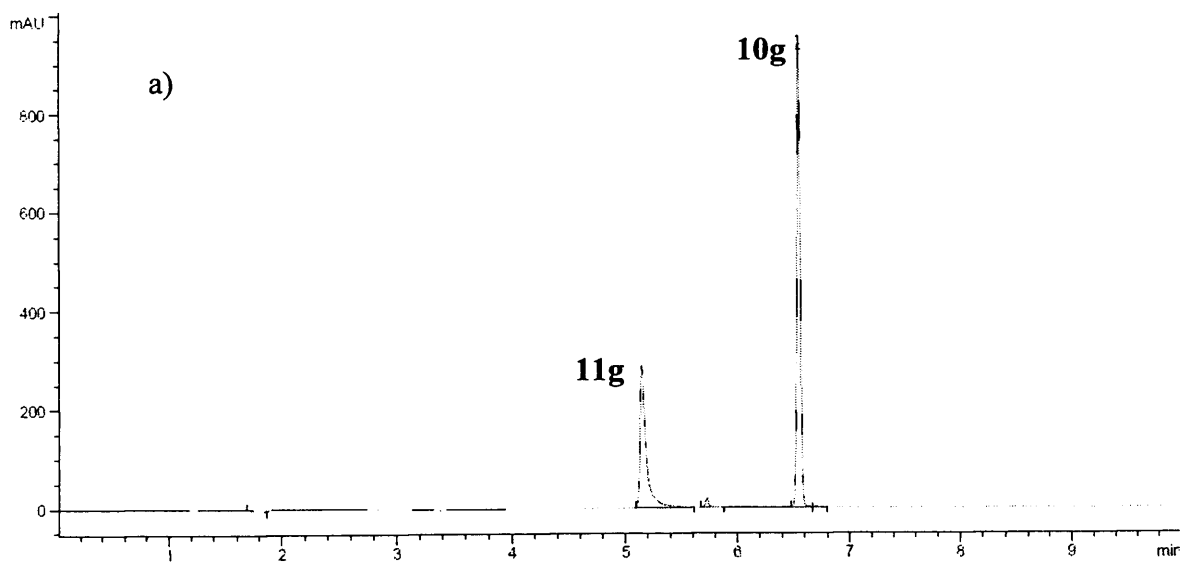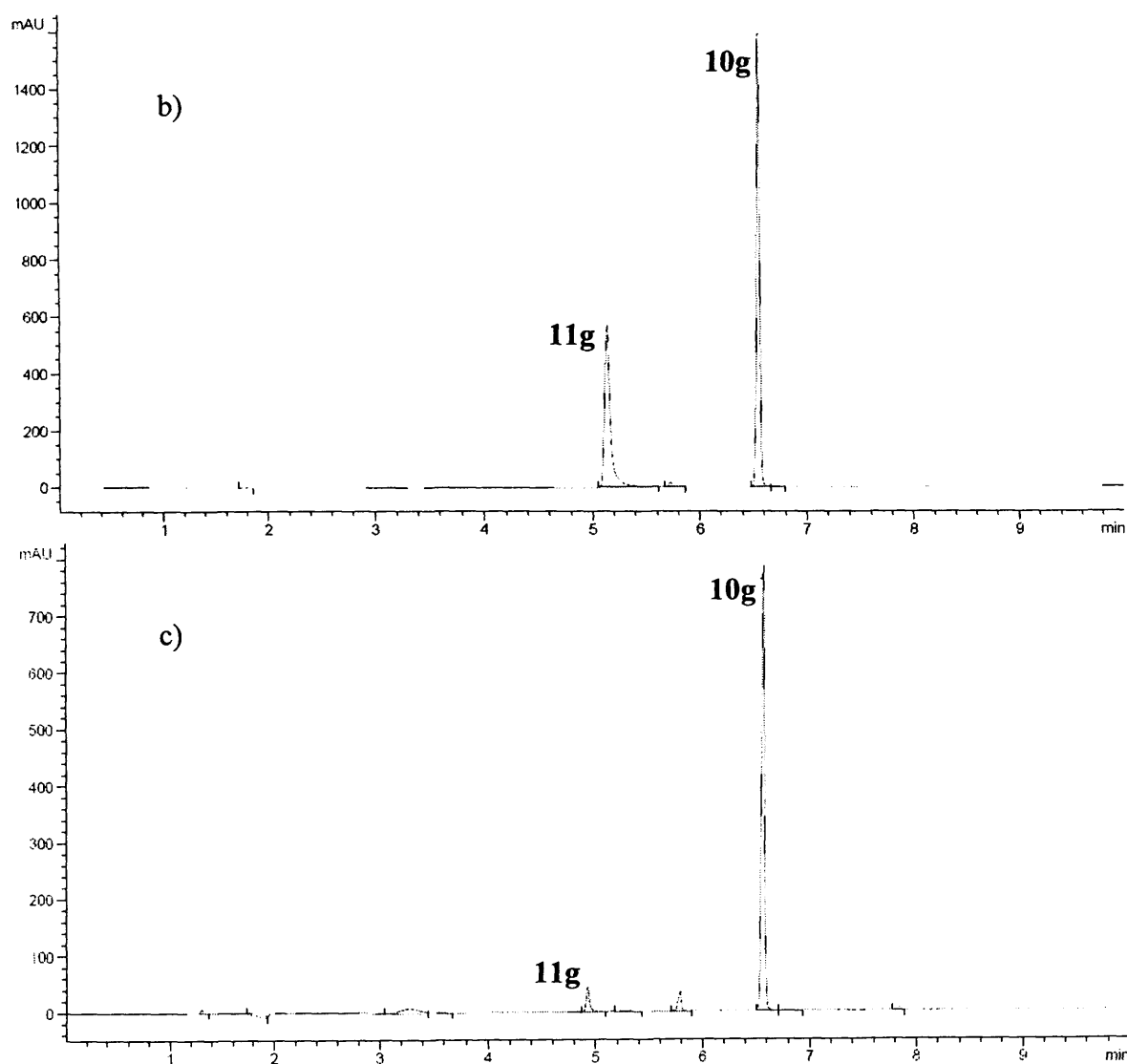
Figure S18. HPLC chromatograms for a) 0.05 mM, b) 0.1 mM of authentic 4-nitrophenol (**11g**) and 4,4'-dinitrobiphenyl (**10g**) in 10 mM CTAB and borate buffer pH 8.2, and c) reaction mixture of 0.1 mM **2g** in 10 mM CTAB and borate buffer buffer using 10 μM of **3** as catalyst at 30 °C at pH 8.2.
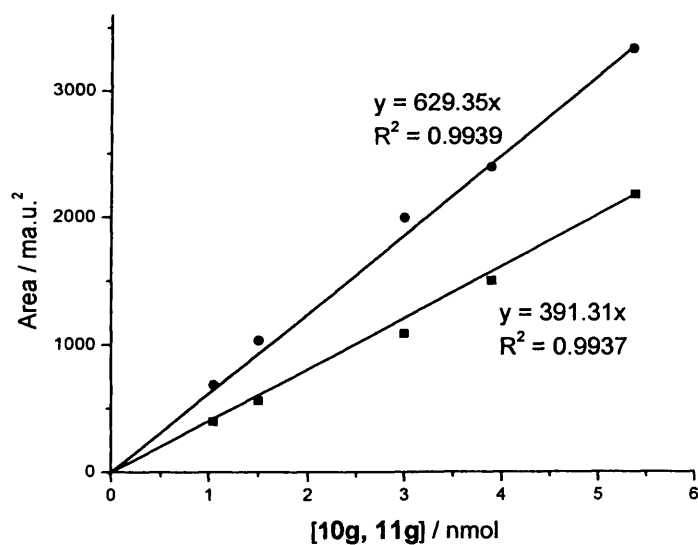
Figure S19. Calibration graph of **10g** (●) and **11g** (■) in CTAB and borate buffer pH 8.4, based on the related area under the peak of the related HPLC chromatogram
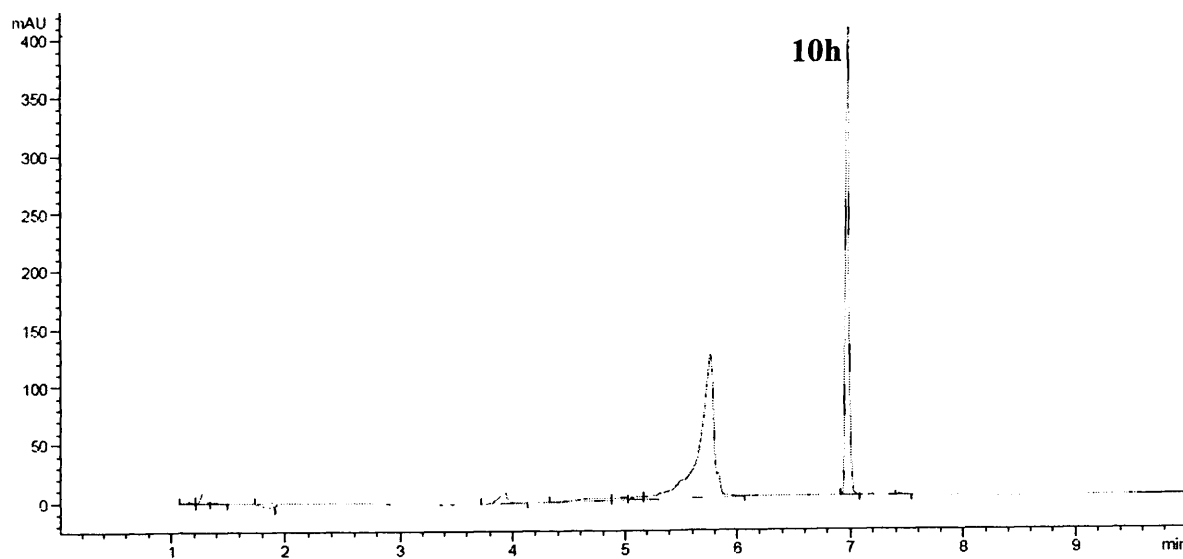
Figure S20. HPLC chromatograms for the products of the reaction mixture of 0.1 mM **2h** in 10 mM CTAB and borate buffer using 10 μM of **3** as catalyst at 30 °C at pH 8.0. Indicating the formation of the 2,2'-bithiophene **10h.**

A1.7. pH-rate profile after 2nd addition of 0.05 mM **2a-g** and fitting to kinetic equation 2.4.

e2)

f2)

g)
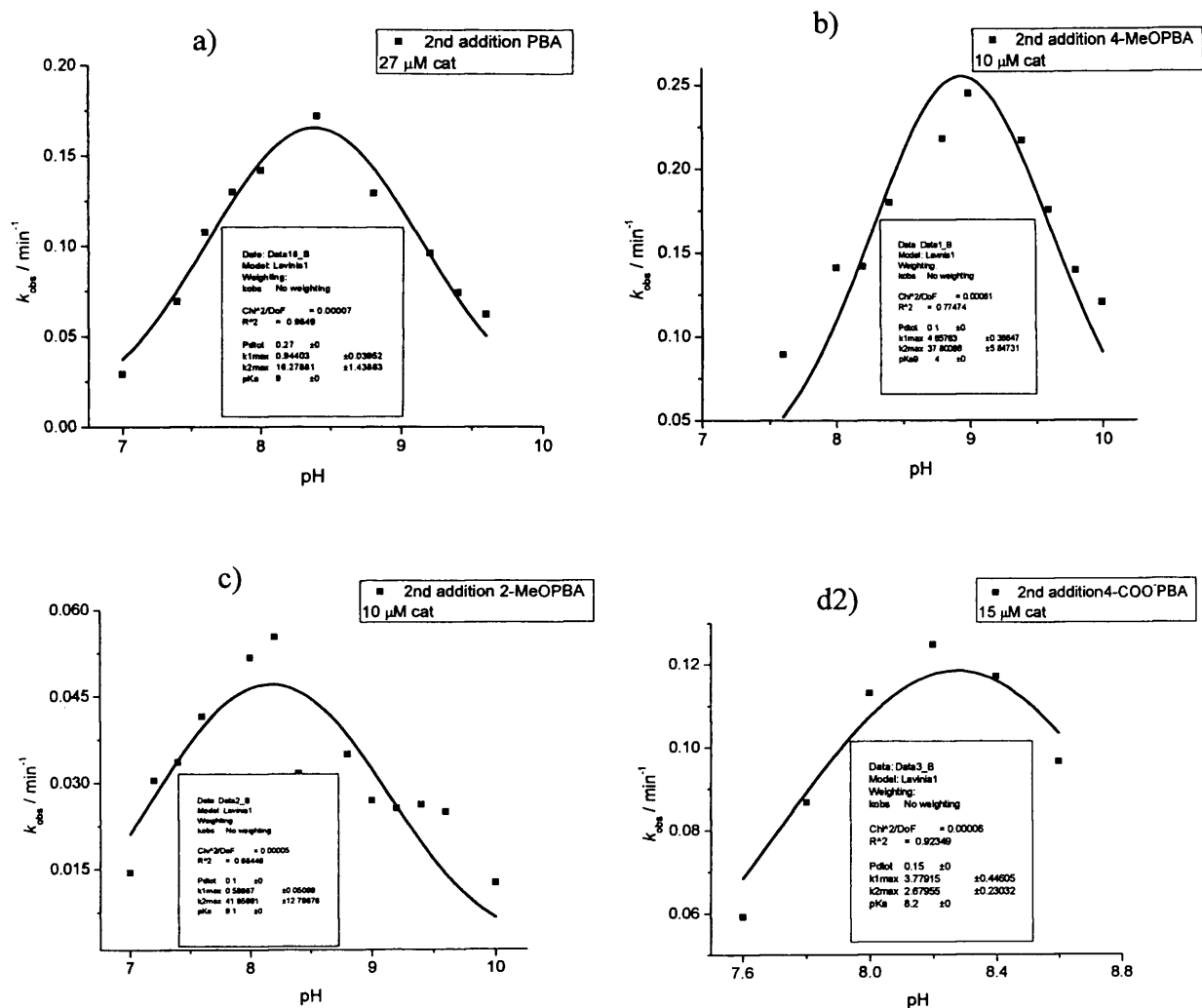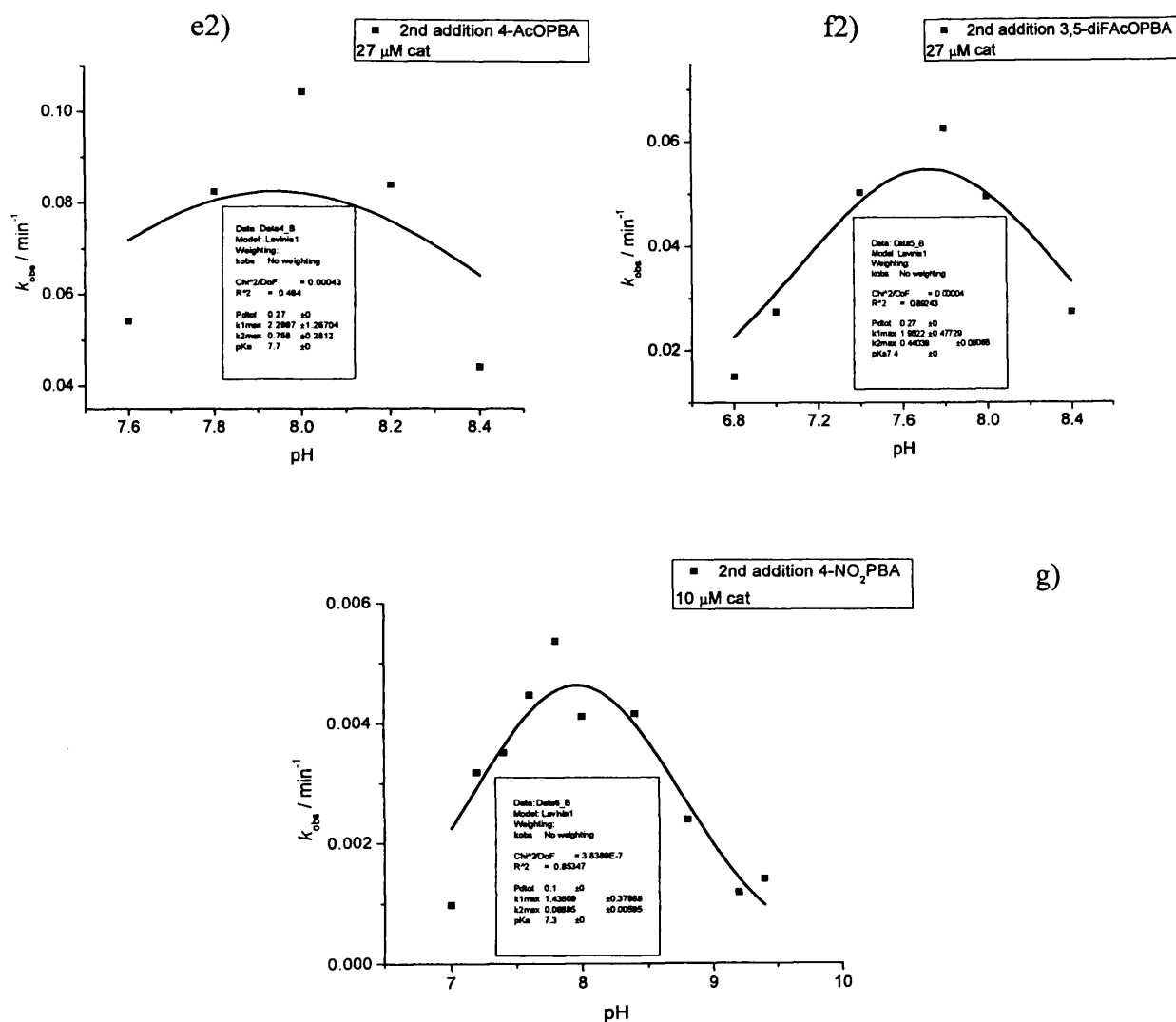
Figure S21a-h: Effect of pH on k_{obs} for the reaction involving 2nd addition of an additional 0.05 mM **2a-h** (■), (a) 27 μM of **3** (b) 10 μM of **3**, (c) 10 μM of **3**, (d2) 15 μM of **3**, (e2) 27 μM of **3**, (f2) 27 μM of **3**, and (g) 10 μM of **3**, and (h) 10 μM of **3**, all at 30 °C, solid lines are fits to equation 2.5.

A1.8. Derivation of equation 5.2

The kinetic data in figure S6.2 for the oxidative homocoupling reaction of PBA with the pre-activated catalyst, generated by the reduction $Pd^{II}\text{-}Pd^0$, can be analysed by a mathematical model formed by two consecutive steps:

$$Pd^0 + PBA_a \xrightarrow{\;k_{1,max}\;} I \tag{S1.1}$$

$$I + PBA_b \xrightarrow{\;k_{2,max}\;} Pd^0 + PhPh \tag{S1.2}$$

Here the first step (S1.1) describes the reaction of Pd^0-catalyst with the acidic form of PBA, PBA_a ("acidic PBA"), that occurs in the first part of the catalytic cycle. In the second step (S1.2) the intermediate I formed by (S1.1) reacts with PBA in the basic form, PBA_b ("basic PBA"), regenerating Pd^0-catalyst and producing biphenyl (PhPh). $k_{1,max}$ and $k_{2,max}$ denote the second-order rate constants for the two processes.

The above model, together with the mass law written in terms of molar concentrations:

$$[Pd^0] + [I] = [Pd_{tot}] \tag{S1.3}$$

Where $[Pd_{tot}]$ represents the total concentration of palladium in the catalytic cycle, which equals the initial concentration of Pd^0-catalyst, leads rapidly to a steady state for Pd^0-catalyst and its intermediate I. For every pH given by the buffer the two reaction rates, for (S1.1) and (S2.2), are equal:

$$k_{1,max}[Pd^0]f_a[PBA_{tot}] = k_{2,max}[I]f_b[PBA_{tot}] \tag{S1.4}$$

Here f_a and f_b are the fraction of PBA in acidic form ("fraction acidic") and the fraction of its conjugated base ("fraction basic"), respectively. Assuming equilibrium between PBA_a and PBA_b all over the homocoupling reaction, we obtain:

$$f_a = \frac{[PBA_a]}{[PBA_{tot}]} = \frac{1}{1 + 10^{pH - pKa}} \tag{S1.5.1}$$

$$f_b = \frac{[PBA_b]}{[PBA_{tot}]} = \frac{1}{1 + 10^{pKa - pH}} \tag{S1.5.2}$$

In conformity with eq. (S1.4) at every pH the observed rate constant is:

$$k_{obs} = k_{1,max}[Pd^0]f_a = k_{2,max}[I]f_b \tag{S1.6}$$

While $k_{1,max}$ and $k_{2,max}$ have the same value at any pH, the combinations $[Pd^0]f_a$ and $[I]f_b$ vary with pH, so that k_{obs} changes with pH.

In order to find the equation for fitting the kinetic data in Figure 2.19 in Chapter 2 we derive the expression of $[Pd^0]$ by using eqs. (S1.3) and (S1.6):

$$k_{obs} = k_{1,max}[Pd^0]f_a = k_{2,max}([Pd_{tot}] - [Pd^0])f_b \qquad (S1.7)$$

Therefore:

$$[Pd^0] = \frac{k_{2,max}f_b}{k_{1,max}f_a + k_{2,max}f_b}[Pd_{tot}] \qquad (S1.8)$$

The back substitution of eq. (S1.8) in eq. (S1.6) gives:

$$k_{obs} = \frac{k_{1,max}k_{2,max}f_af_b}{k_{1,max}f_a + k_{2,max}f_b}[Pd_{tot}] \qquad (S1.9)$$

By using the eqs. (S1.5.1) and (S1.5.2) the expression of k_{obs} as a function of pH is computed:

$$k_{obs} = \frac{k_{1,max}k_{2,max}}{k_{1,max}(1+10^{pK_a-pH}) + k_{2,max}(1+10^{pH-pK_a})}[Pd_{tot}] \qquad (2.5)$$

A1.9. pH-rate profile after 2nd addition of 0.05 mM **2a-g** and fitting to kinetic equation 2.8a.
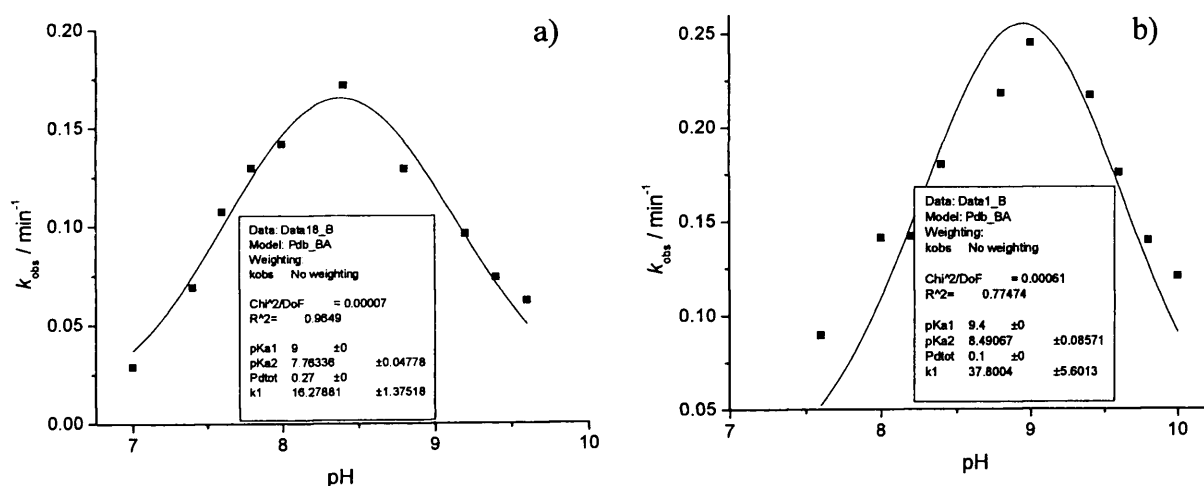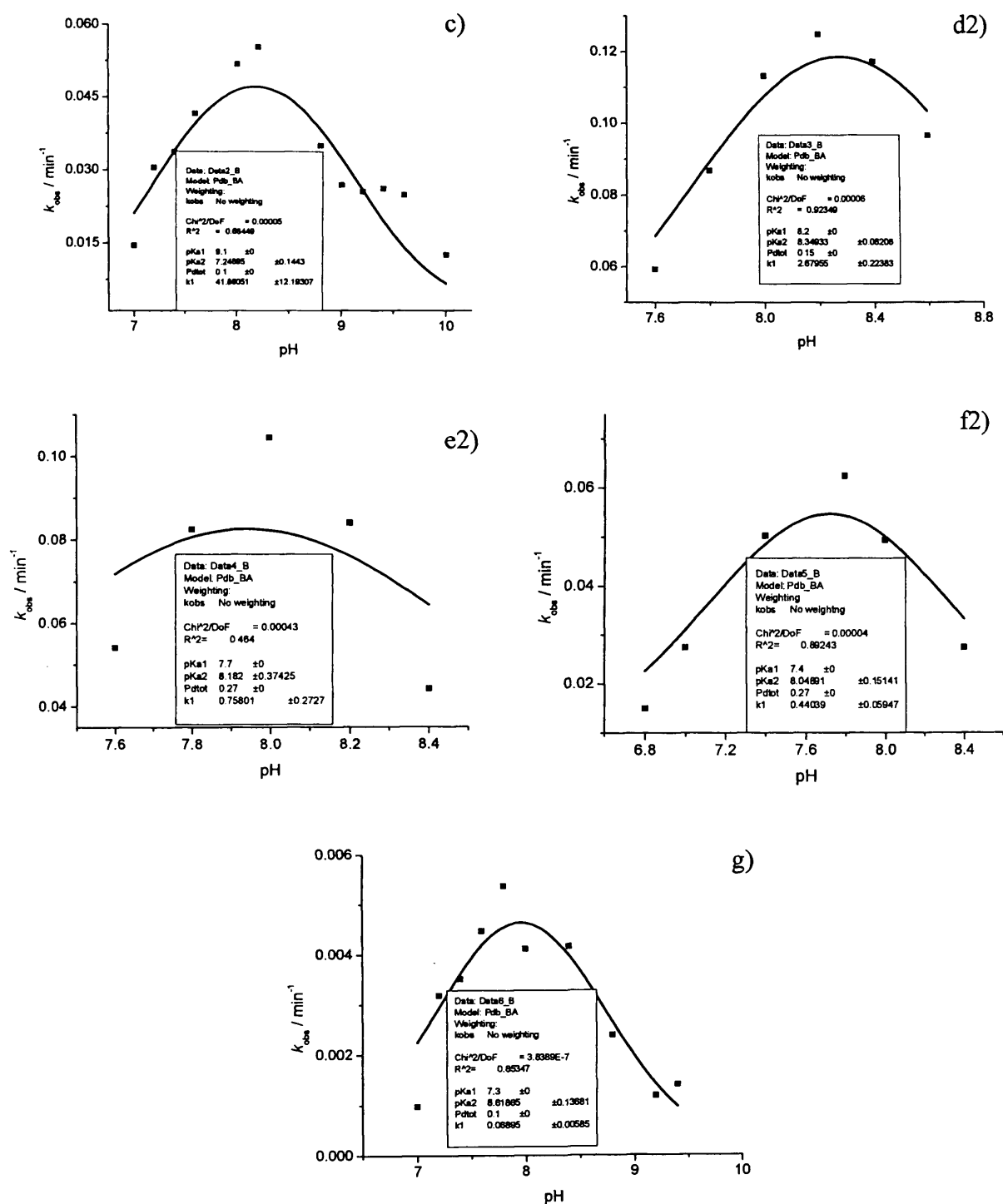
Figure S22a-g: Effect of pH on k_{obs} for the reaction involving 2nd addition of an additional 0.05 mM **2a-g** (■), (a) 27 μM of **3** (b) 10 μM of **3**, (c) 10 μM of **3**, (d2) 15 μM of **3**, (e2) 27 μM of **3**, (f2) 27 μM of **3**, and (g) 10 μM of **3**, and (h) 10 μM of **3** all at 30 °C, solid lines are fits to equation 2.8a.

A1.10. pH-rate profile after 2nd addition of 0.05 mM **2a-g** and fitting to kinetic equation 2.8b.
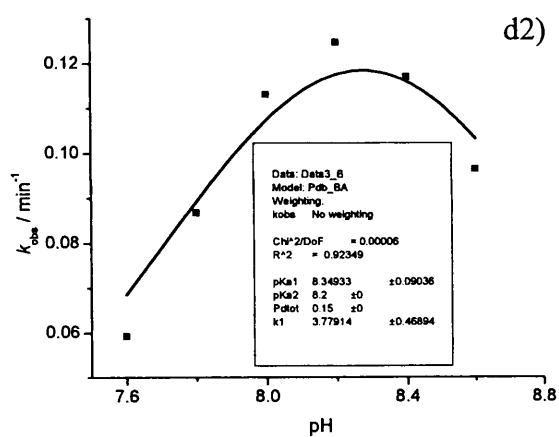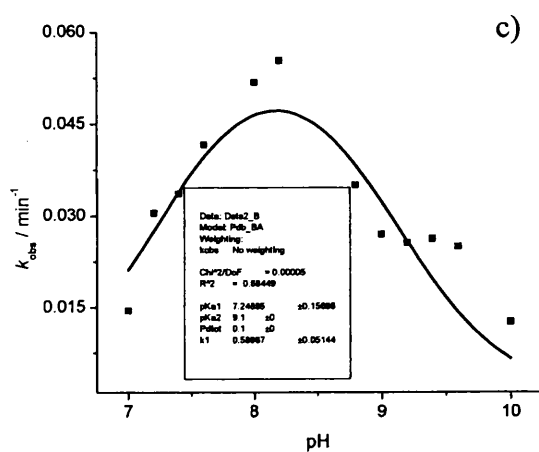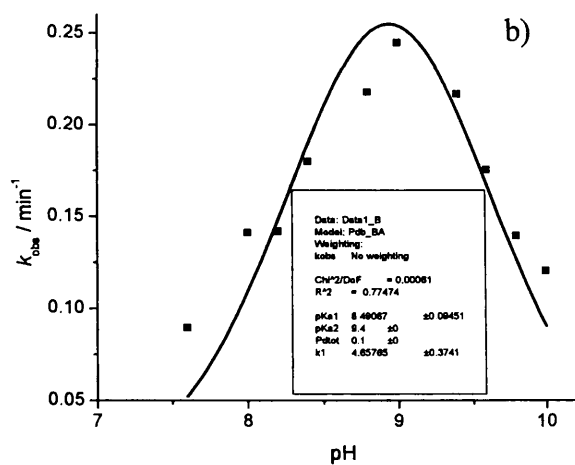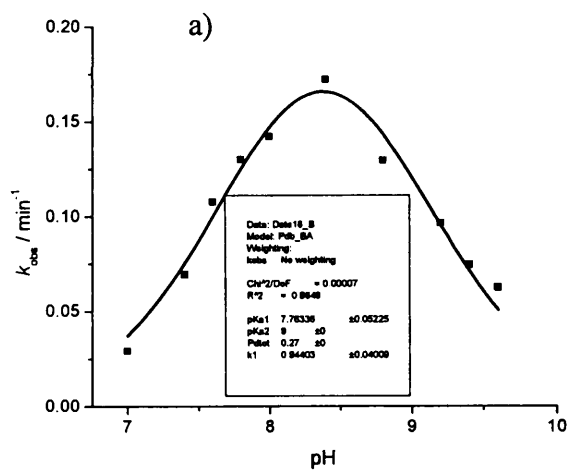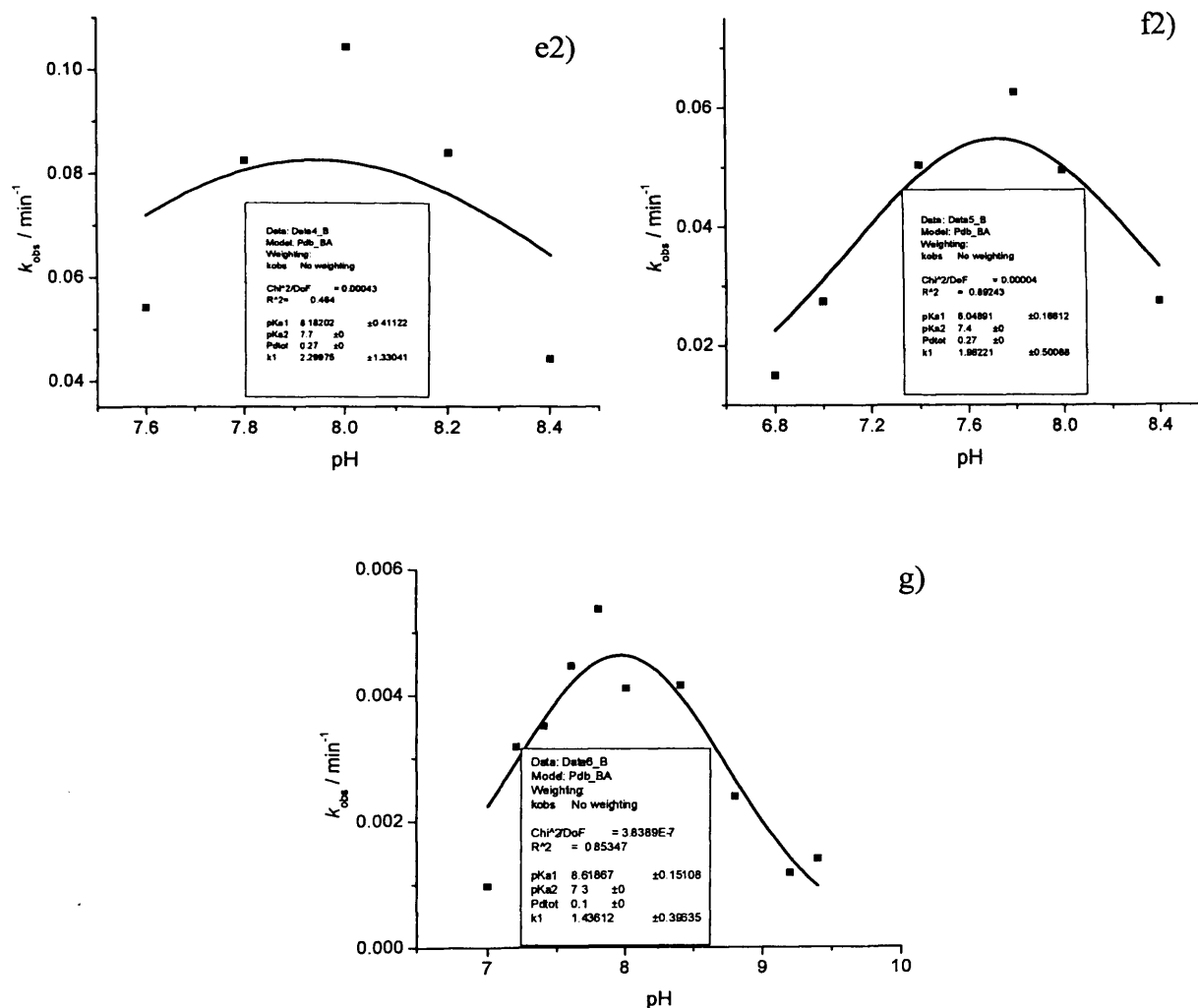
Figure S23a-g: Effect of pH on k_{obs} for the reaction involving 2nd addition of an additional 0.05 mM 2a-g (■), (a) 27 μM of 3 (b) 10 μM of 3, (c) 10 μM of 3, (d2) 15 μM of 3, (e2) 27 μM of 3, (f2) 27 μM of 3, and (g) 10 μM of 3, and (h) 10 μM of 3 all at 30 °C, solid line are fits to equation 2.8b.

Appendix 2

This Appendix is for Chapter 3

Homocoupling of phenylboronic acid using Pd-CTAB NPs as a catalyst

A2.1. HPLC chromatogram of the reaction of the homocoupling reaction of 0.1 mM PBA using 0.115 mM Pd-content (in Pd-CTAB NPs), 8.0 mM CTAB and to mM borate buffer at pH 8.8 and 30 °C.
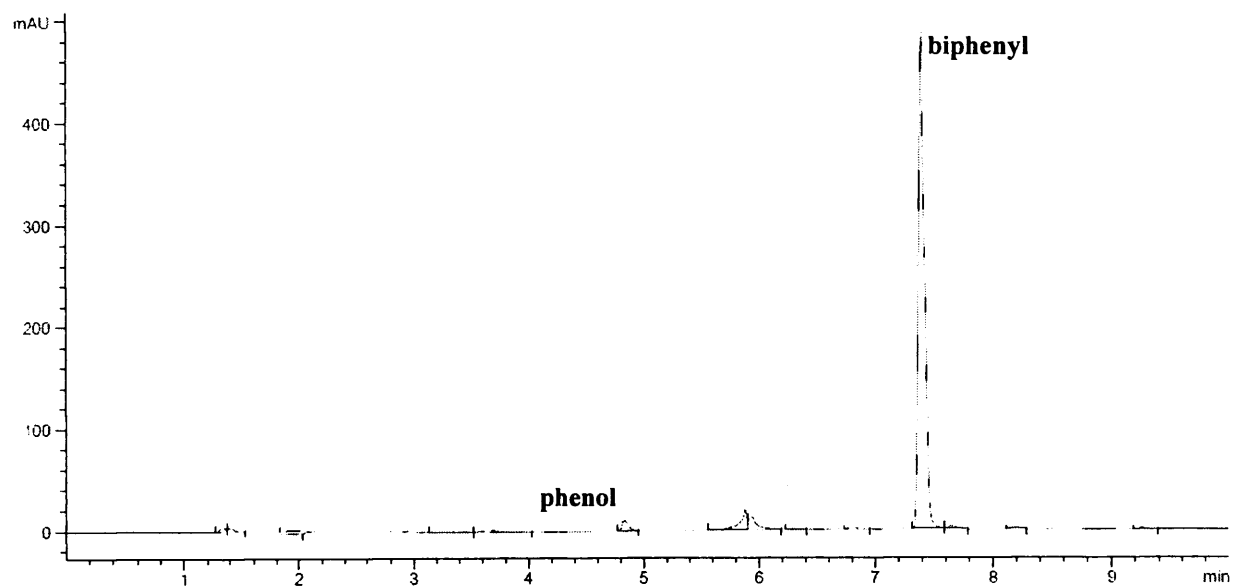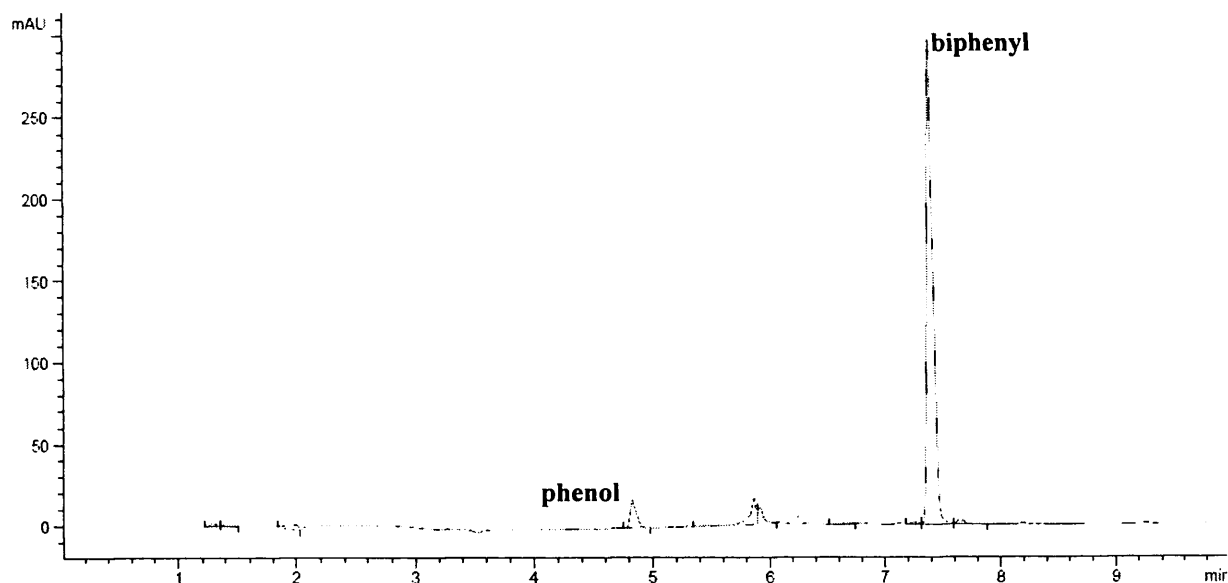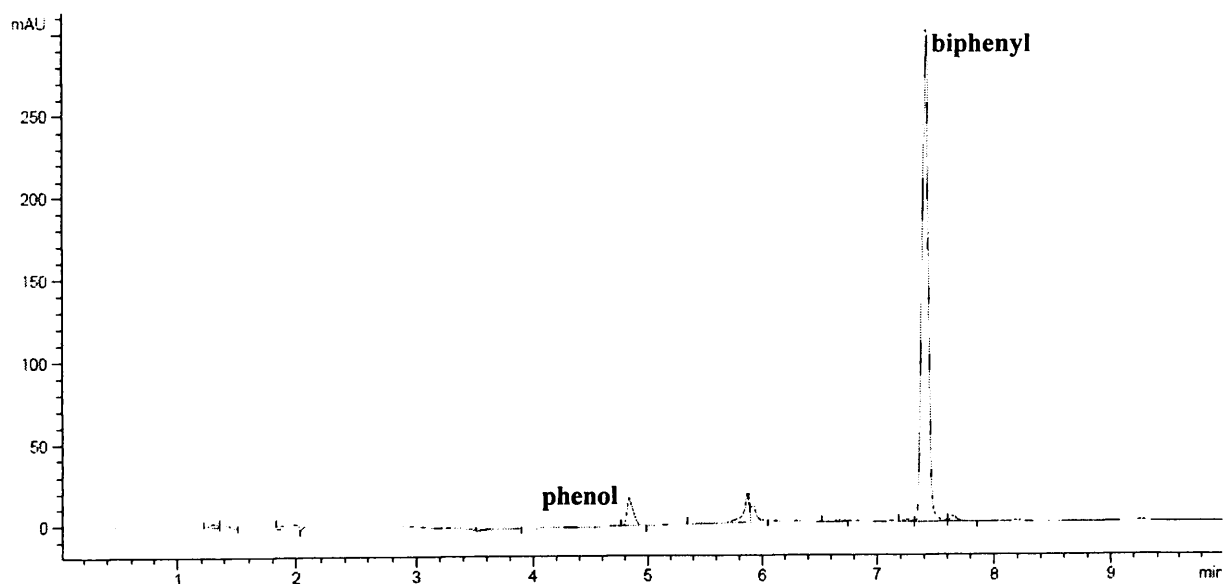

Figure S2.1. HPLC chromatograms for the products of the reaction mixture of 0.1 mM PBA in 8.0 mM CTAB and 10 mM borate buffer pH 8.8 using 0.1 mM of Pd content in Pd-CTAB NPs as catalyst at 30 °C, Indicating the formation of the biphenyl and phenol in a 2.5:1 ratio.

A2.2. Absorbance at 250 nm as a function of time for the reaction mixture of different concentration of 2a using Pd-CTAB NPs as a catalyst in CTAB and borate buffer at pH 8.8 and 30 °C.
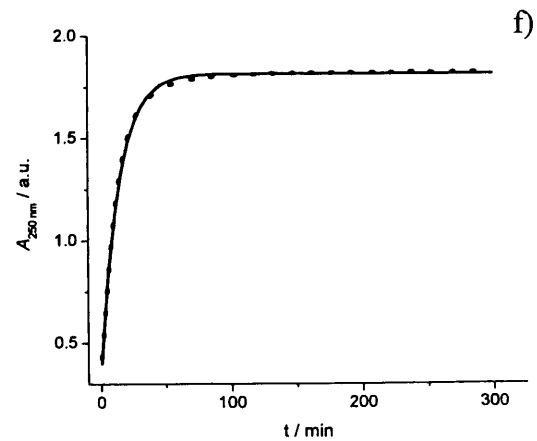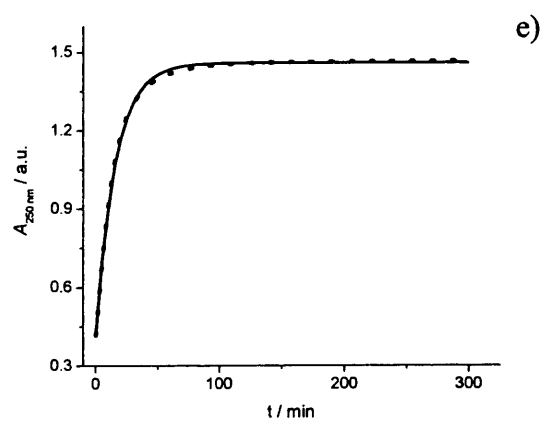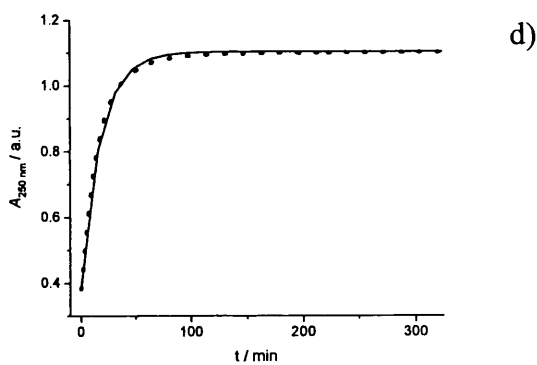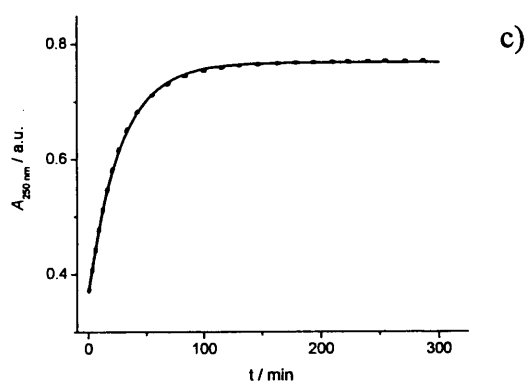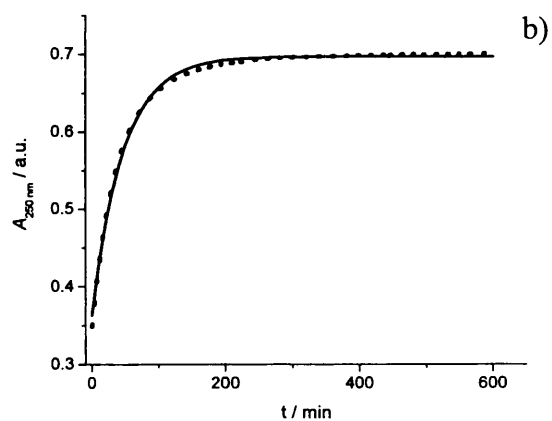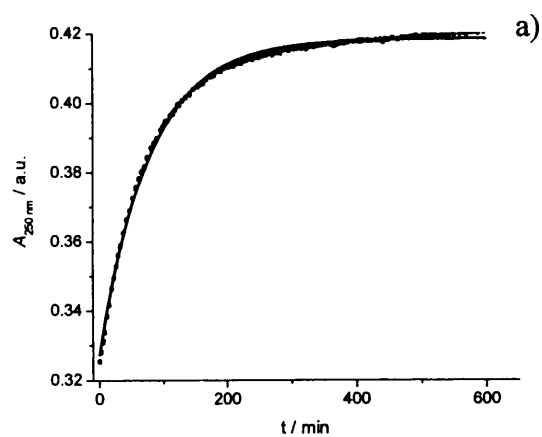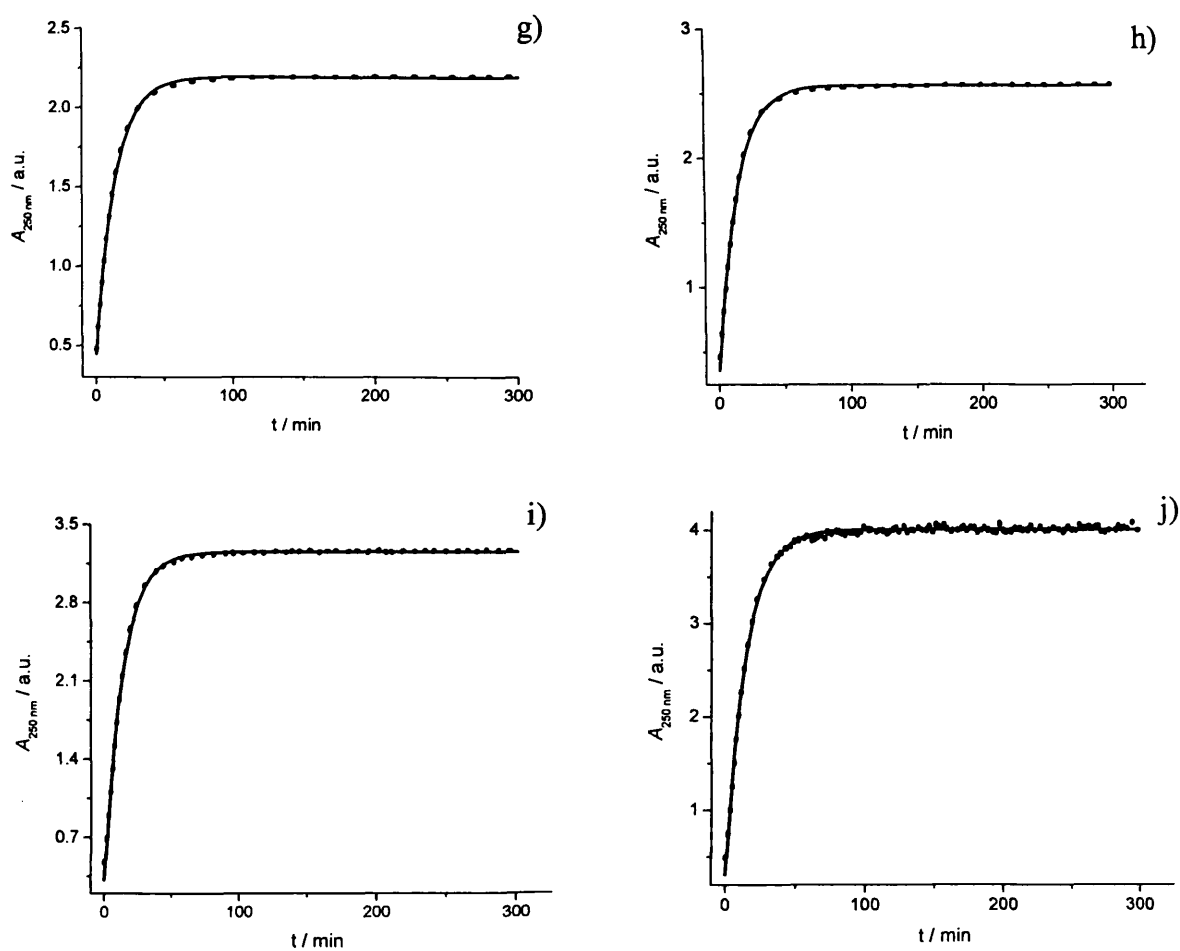
Figure S2.2. Absorbance at 250 nm versus time for the reaction mixture of a) 0.01mM **2a**, b) 0.025 mM, c) 0.05 mM **2a**, d) 0.01 mM **2a**, e) 0.015 mM **2a**, f) 0.02 mM **2a**, g) 0.25 mM **2a**, h) 0.3 mM **2a**, i) 0.4 mM **2a** and j) 0.5 mM **2a**, using 0.115 Pd-content (in Pd-CTAB), 8.0 mM CTAB, and 10 mM borate buffer at pH 8.8 and 30 °C. (dotted line) experimental data, solid line is the fit to eq. 2.1.

A2.3. Effect of [PBA] on the reaction rate, derivation of the kinetic equation.
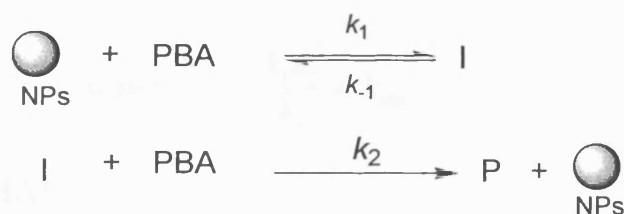
Scheme 3.6

$$\frac{d[I]}{dt} = k_1[PBA] - k_{-1}[I] - k_2[PBA][I] \tag{2.3.1}$$

Applying steady state approximation on equation 2.3.1

$$\frac{d[I]}{dt} = 0 = k_1[PBA] - k_{-1}[I] - k_2[PBA][I]$$

then, $[I] = \dfrac{k_1[PBA]}{k_{-1} + k_2[PBA]}$ \hfill (2.3.2)

Also,

$$\frac{d[P]}{dt} = k_2[I][PBA] \tag{2.3.3}$$

Substituting equation 2.3.2 in equation 2.3.3 leads to

$$\frac{d[P]}{dt} = \frac{k_1 k_2[PBA]^2}{k_{-1} + k_2[PBA]} \tag{3.1}$$

At low PBA concentration the $k_2[PBA]$ in the denominator is much less than k_{-1} therefore the

term $k_2[PBA]$ is negligible and equation 3.1 becomes as follows:

$$\frac{d[P]}{dt} = \frac{k_1 k_2[PBA]^2}{k_{-1}} \qquad \text{where} \qquad \frac{k_1 k_2}{k_{-1}} = k_{obs}$$

then $\dfrac{d[P]}{dt} = k_{obs}[PBA]^2$ \hfill (3.2)

Equation 3.2 shows that at low [PBA] the reaction is second-order in PBA.

However, at high PBA concentration k-1 in the denominator is much less than k2[PBA], therefore k-1 is negligible and equation 3.1 becomes:

$$\frac{d[P]}{dt} = \frac{k_1 k_2 [PBA]^2}{k_2 [PBA]} \qquad \text{where} \qquad \frac{k_1 k_2}{k_2} = k_{obs}$$

then $\dfrac{d[P]}{dt} = k_{obs}[PBA]$ (3.3)

Equation 3.3 shows that at high [PBA] the reaction is first-order in PBA.

Note: the concentration of the NPs is assumed to be constant during the course of the reaction. Therefore, the observed rate constant includes the NP concentration as well.

Appendix 3

This Appendix is for Chapter 4

Homocoupling of phenylboronic acid using Au@Pd@pNIPAM

nanoparticles and Pd-pNIPAM nanocomposites

A3.1. HPLC chromatogram of the reaction of the homocoupling reaction of 0.1 mM PBA using 132 µM (Au content) in Au-sphere(64 nm)@Pd(10.9 nm)@pNIPAM NPs, 10.0 mM CTAB and 10 mM borate buffer at pH 8.2 and 30 °C.
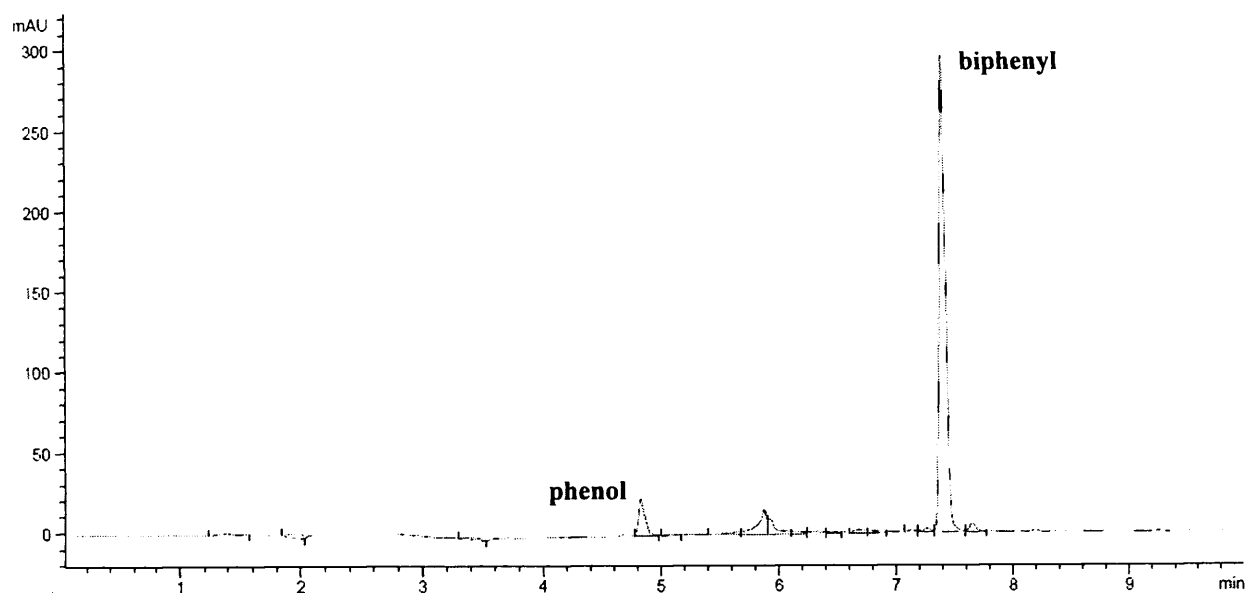
Figure S3.1. HPLC chromatograms for the products of the reaction mixture of 0.1 mM PBA in 8.0 mM CTAB and 10 mM borate buffer pH 8.2 using 152 µM (Au content) in Au@Pd@pNIPAM NPs, as catalyst at 30 °C, indicating the formation of the biphenyl and phenol in a 1.25:1 ratio.

A3.2. HPLC chromatogram of the reaction of the homocoupling reaction of 0.1 mM PBA using 100 µL Pd-pNIPAM (–ve) nanocomposite, 10.0 mM CTAB and 10 mM borate buffer at pH 8.8 and 30 °C.

Figure S3.2. HPLC chromatograms for the products of the reaction mixture of 0.1 mM PBA in 8.0 mM CTAB and 10 mM borate buffer pH 8.8 using 100 μL Pd-pNIPAM nanocomposites as catalyst at 30 °C, indicating the formation of the biphenyl and phenol in a 1.25:1 ratio.

A3.3. HPLC chromatogram of the reaction of the homocoupling reaction of 0.1 mM PBA using 100 μL Pd-pNIPAM (+ve) nanocomposite, 10.0 mM CTAB and 10 mM borate buffer at pH 8.4 and 30 °C.

Figure S3.3. HPLC chromatograms for the products of the reaction mixture of 0.1 mM PBA in 8.0 mM CTAB and 10 mM borate buffer pH 8.4 using 100 μL Pd-pNIPAM nanocomposites as catalyst at 30 °C, indicating the formation of the biphenyl and phenol in a 1.2:1 ratio.

A3.4. Absorbance at 250 nm as a function of time for the reaction mixture of 0.1 mM PBA using Au-sphere(64 nm)@Pd(10.9 nm)@pNIPAM NPs as a catalyst in CTAB and borate buffer at different pH and 30 °C.
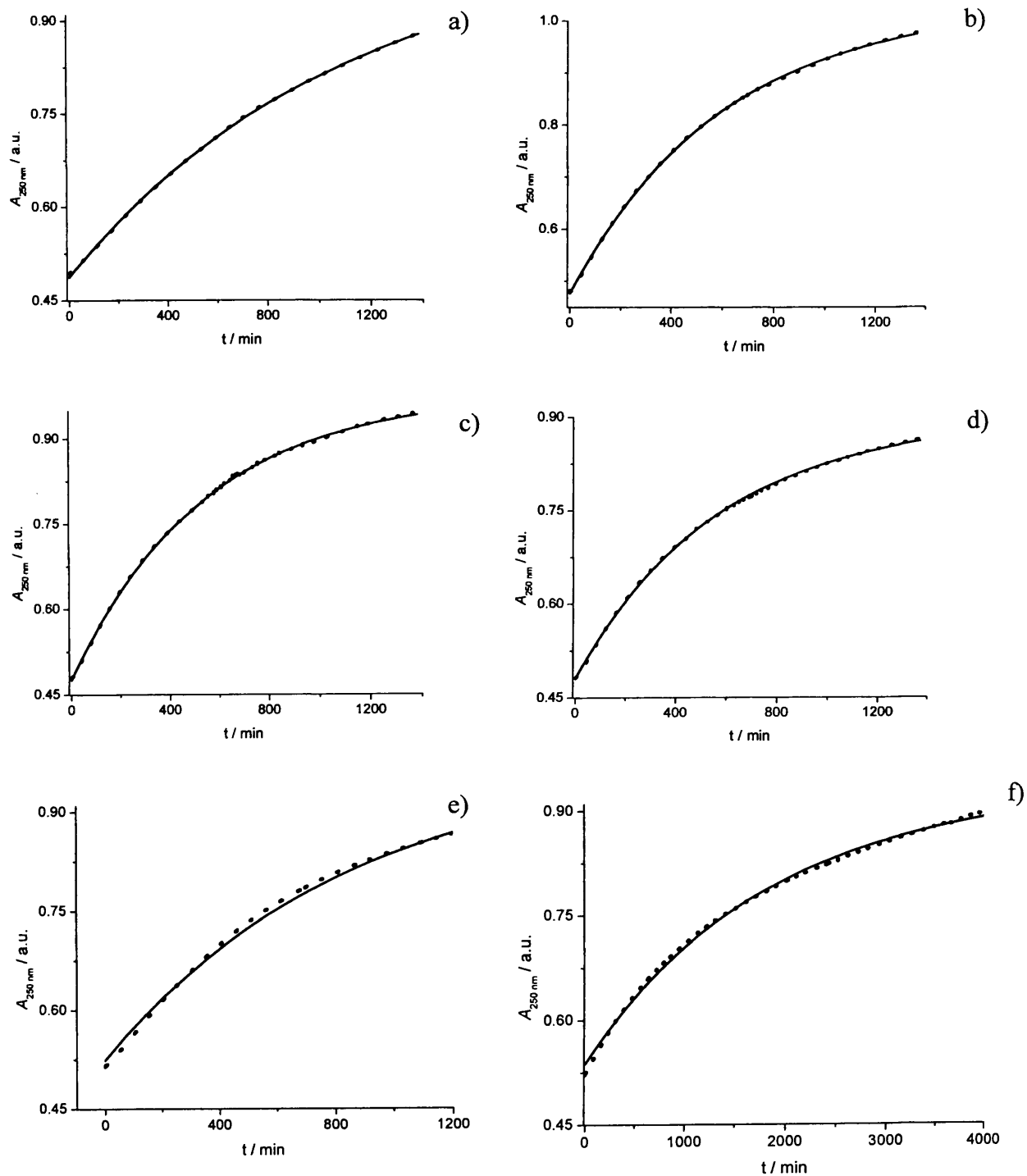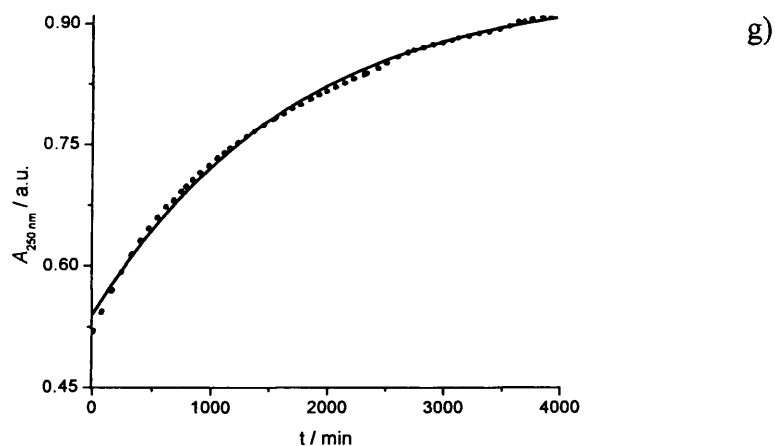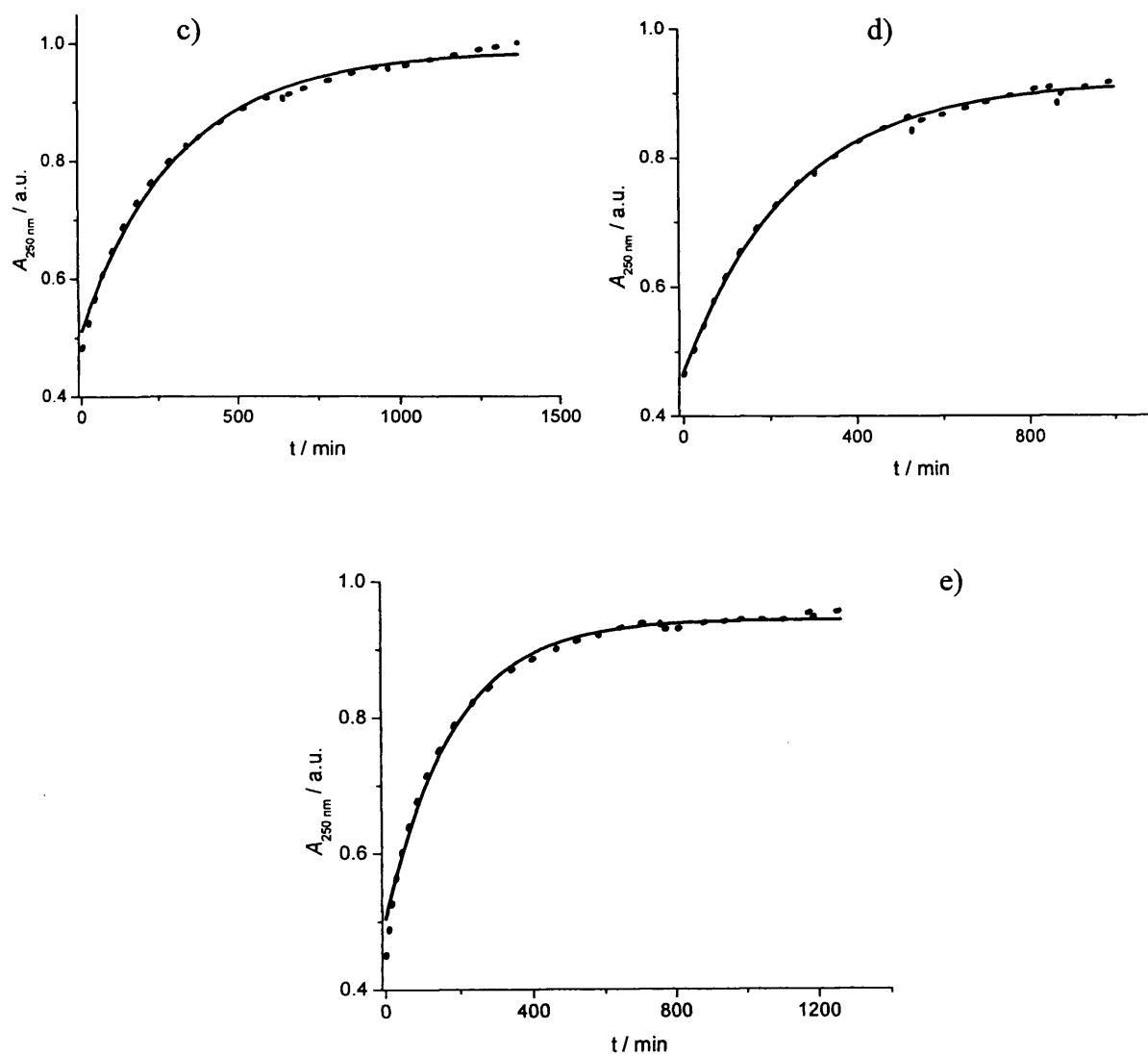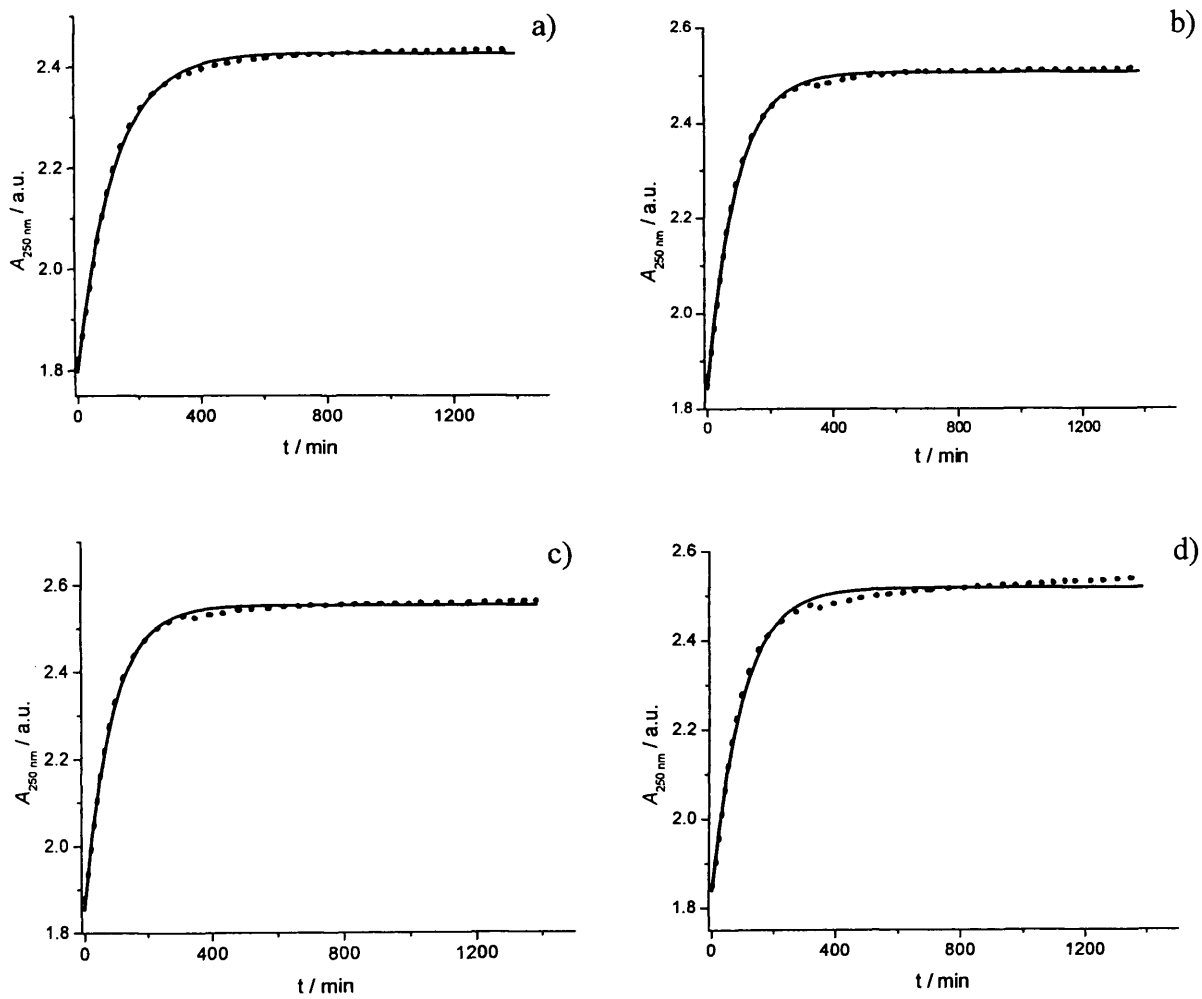
Figure S3.4. Absorbance at 250 nm versus time for the reaction mixture of 0.01mM **PBA**, using 182.4 µM (Au content) Au-sphere(64 nm)@Pd(10.9 nm)@pNIPAM NPs, 10.0 mM CTAB, and 10 mM borate buffer a) pH 7.4, b) pH 7.8, c) pH 8.2. d) pH 8.4, e) pH 8.8, f) pH 9.2, and g) pH 9.6, at 30 °C. (dotted line) experimental data and fit to eq 2.1 (solid line).

A3.5. Kinetic traces of the reaction mixture at different PBA concentrations using 152 mM (Au content) Au-sphere(64 nm)@Pd(10.9 nm)@pNIPAM NPs concentration in CTAB and borate buffer at 30 °C.
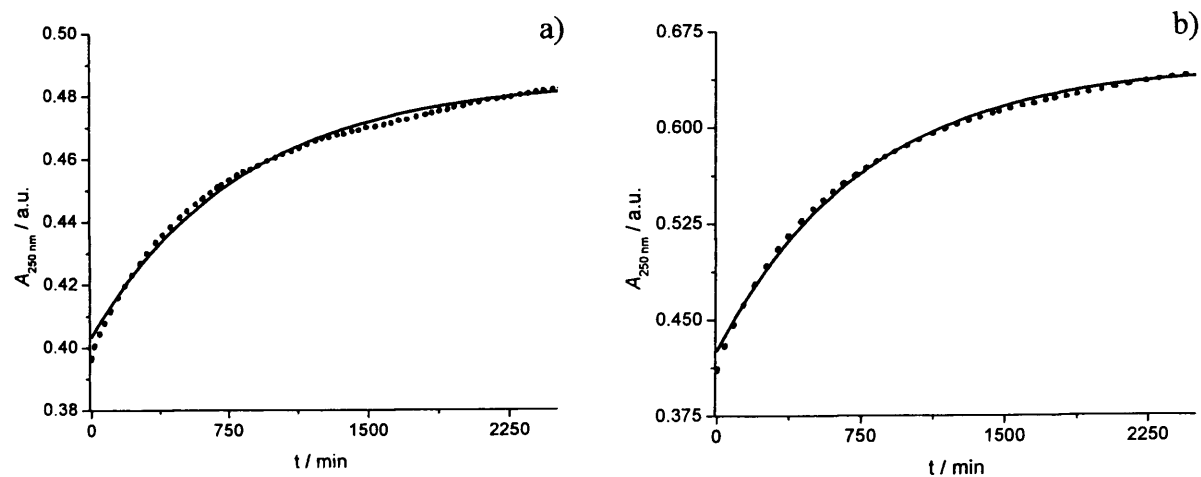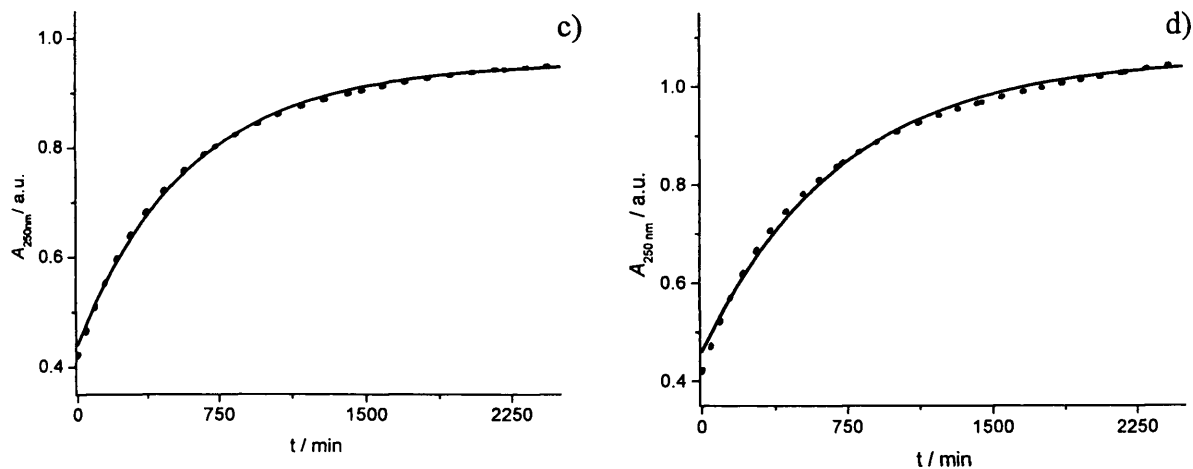
Figure S3.5. Absorbance at 250 nm versus time for the reaction mixture of a) 0.025 mM PBA, b) 0.05 mM PBA, c) 0.1 mM PBA. d) 0.125 mM PBA, using 152 μM (Au content) Au-sphere(64 nm)@Pd(10.9 nm)@pNIPAM NPs, 10.0 mM CTAB, and 10 mM borate buffer at pH 8.2 and 30 °C. (dotted line) experimental data and fit to eq 2.1 (solid line).

A3.6. Kinetic traces of the reaction mixture of 0.1 mM PBA using different concentrations of Au-sphere(64 nm)@Pd(10.9 nm)@pNIPAM NPs in CTAB and borate buffer at 30 °C.
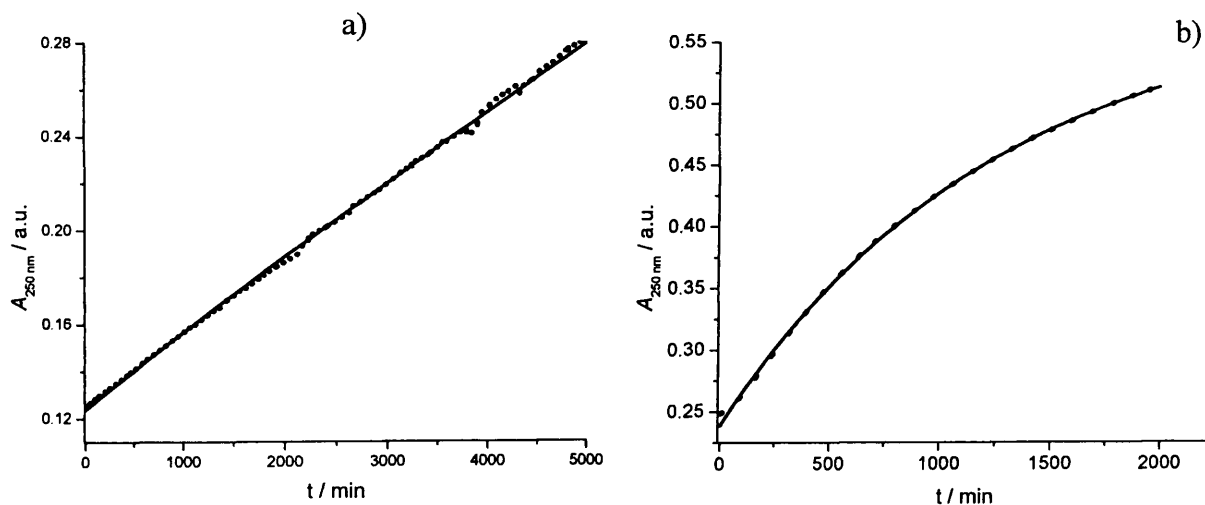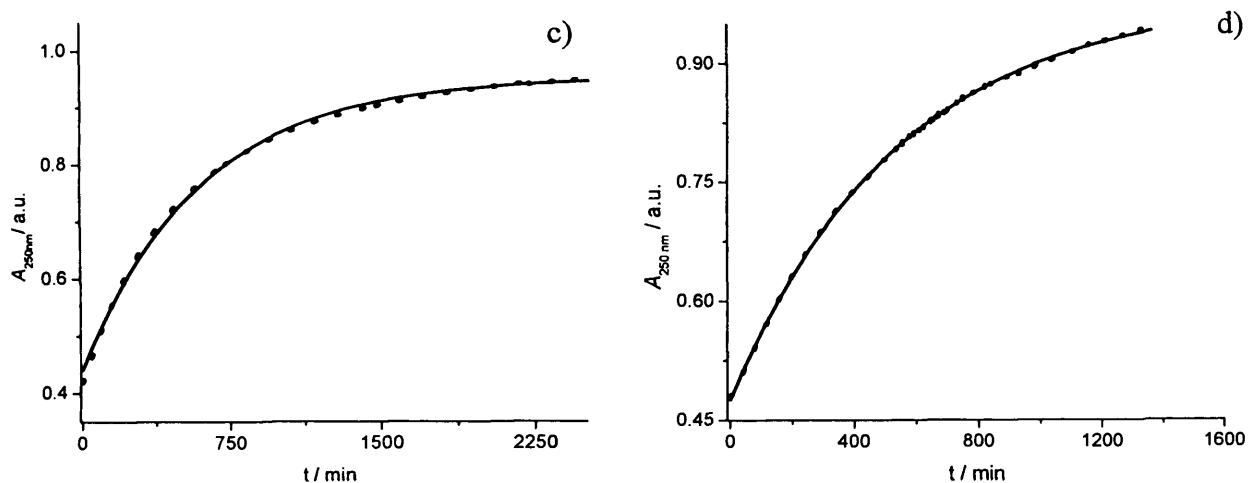
Figure S3.6. Absorbance at 250 nm versus time for the reaction mixture 0.1 mM PBA using a) 15.2 µM, b) 60.8 µM, c) 152 µM and d) 182.4 µM (Au content) Au-sphere(64 nm)@Pd(10.9 nm)@pNIPAM NPs, 10.0 mM CTAB, and 10 mM borate buffer at pH 8.2 and 30 °C. (dotted line) experimental data, and fit to eq 2.1 (solid line).

A3.7. Absorbance at 250 nm of the reaction mixture of the homocoupling of PBA using Au-sphere(64 nm)@Pd(10.9 nm)@pNIPAM NPs in CTAB and borate buffer at pH 8.2 and different temperature.
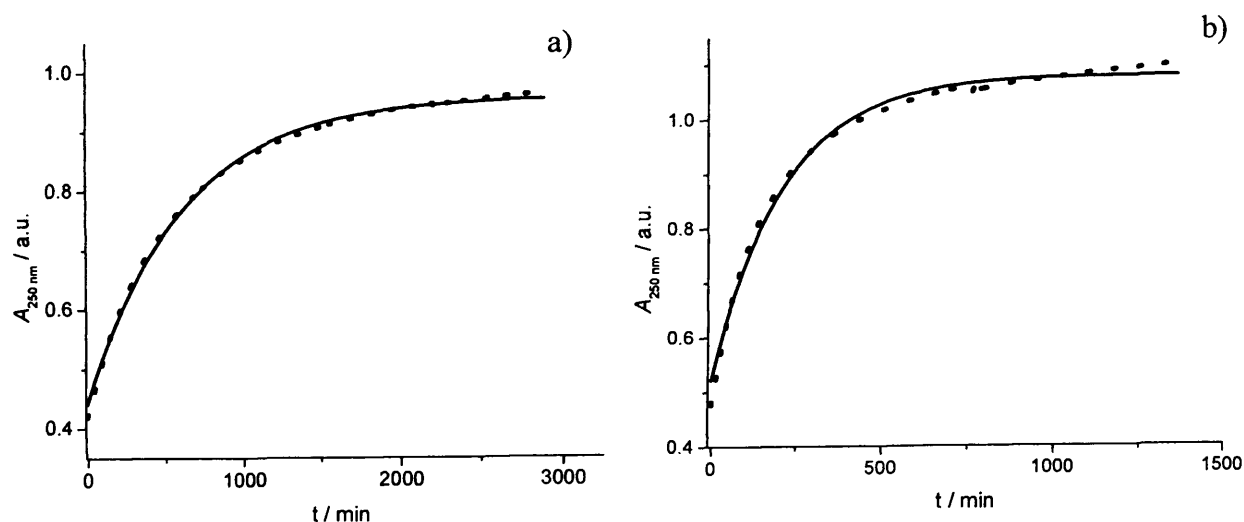
Figure S3.7. Absorbance at 250 nm versus time for the reaction mixture 0.1 mM PBA using 152 μM (Au content) Au-sphere(64 nm)@Pd(10.9 nm)@pNIPAM NPs, 10.0 mM CTAB, and 10 mM borate buffer pH 8.2 at;. a) 30 °C, b) 40 °C, c) 50 °C and d) 50 °C and e) 60 °C. (dotted line) experimental data and fit to eq 2.1 (solid line).

A3.8. Absorbance at 250 nm as a function of time for the reaction mixture of different concentration of PBA using Pd-pNIPAM (+ve) Ncomp as a catalyst in CTAB and borate buffer at different pH and 30 °C.

e)

f)
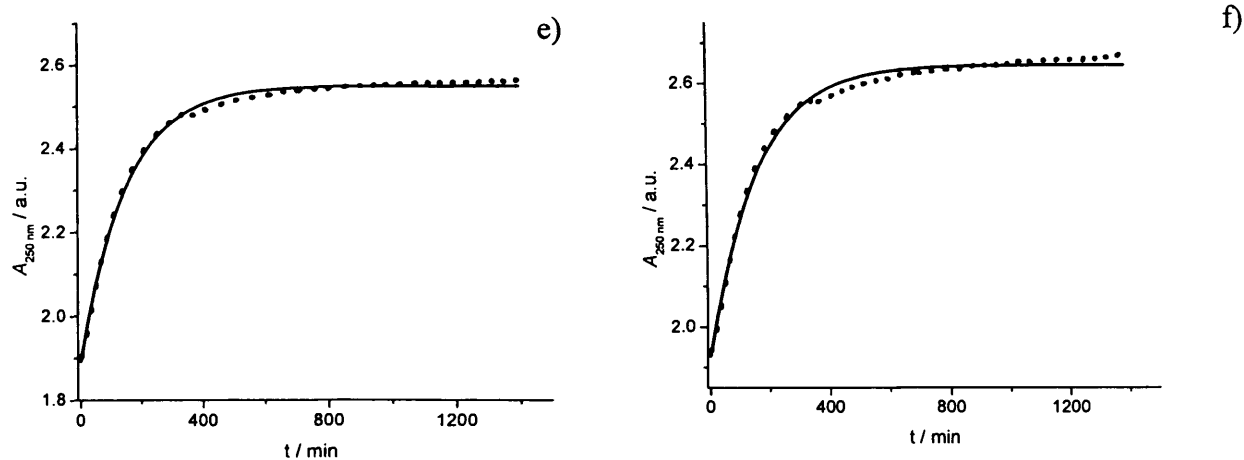
Figure S3.8. Absorbance at 250 nm versus time for the reaction mixture of 0.1mM PBA, using 200 µL Pd-pNIPAM (+ve) Ncomp, 10.0 mM CTAB, and 10 mM borate buffer a) pH 7.8, b) pH 8.2, c) pH 8.4. d) pH 8.8, e) pH 9.2 and f) pH 9.6, at 30 °C. (dotted line) experimental data, and fit to eq 2.1 (solid line).

A3.9. Absorbance at 250 nm as a function of time for the reaction mixture of different concentration of PBA using Pd-pNIPAM (-ve) Ncomp as a catalyst in CTAB and borate buffer at different pH and 30 °C.

a)

b)
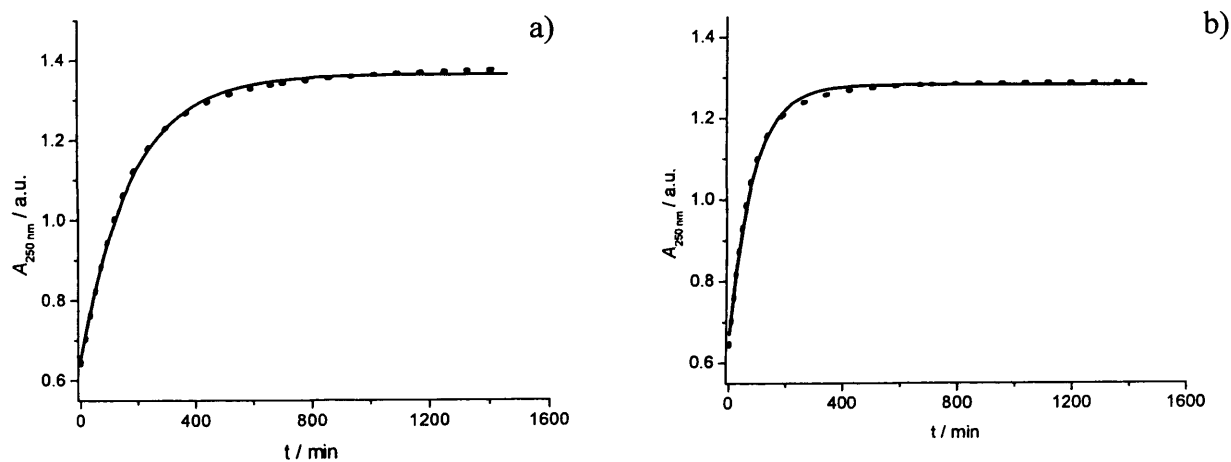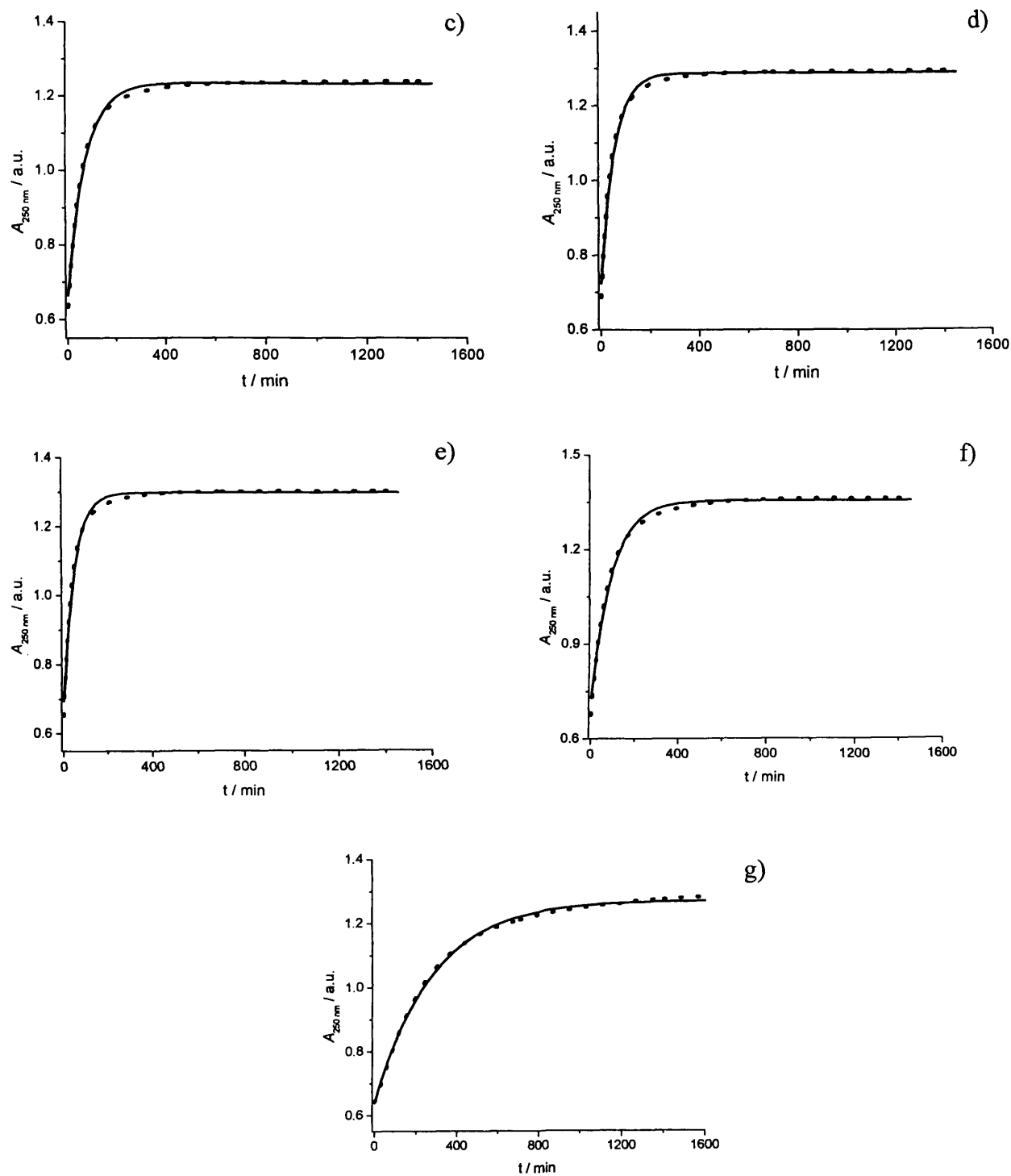
Figure S3.9. Absorbance at 250 nm versus time for the reaction mixture of 0.1mM PBA, using 200 µL Pd-pNIPAM (-ve) nanocomposites, 10.0 mM CTAB, and 10 mM borate buffer a) pH 7.4, b) pH 7.8, c) pH 8.2. d) pH 8.4, e) pH 8.8, f) pH 9.2 and g) pH 9.6, at 30 °C. (dotted line) experimental data, and fit to eq 2.1 (solid line).

**A3.10.** Kinetic traces of the reaction mixture using different PBA concentration. Pd-pNIPAM (-ve) Ncomp is used as catalyst.
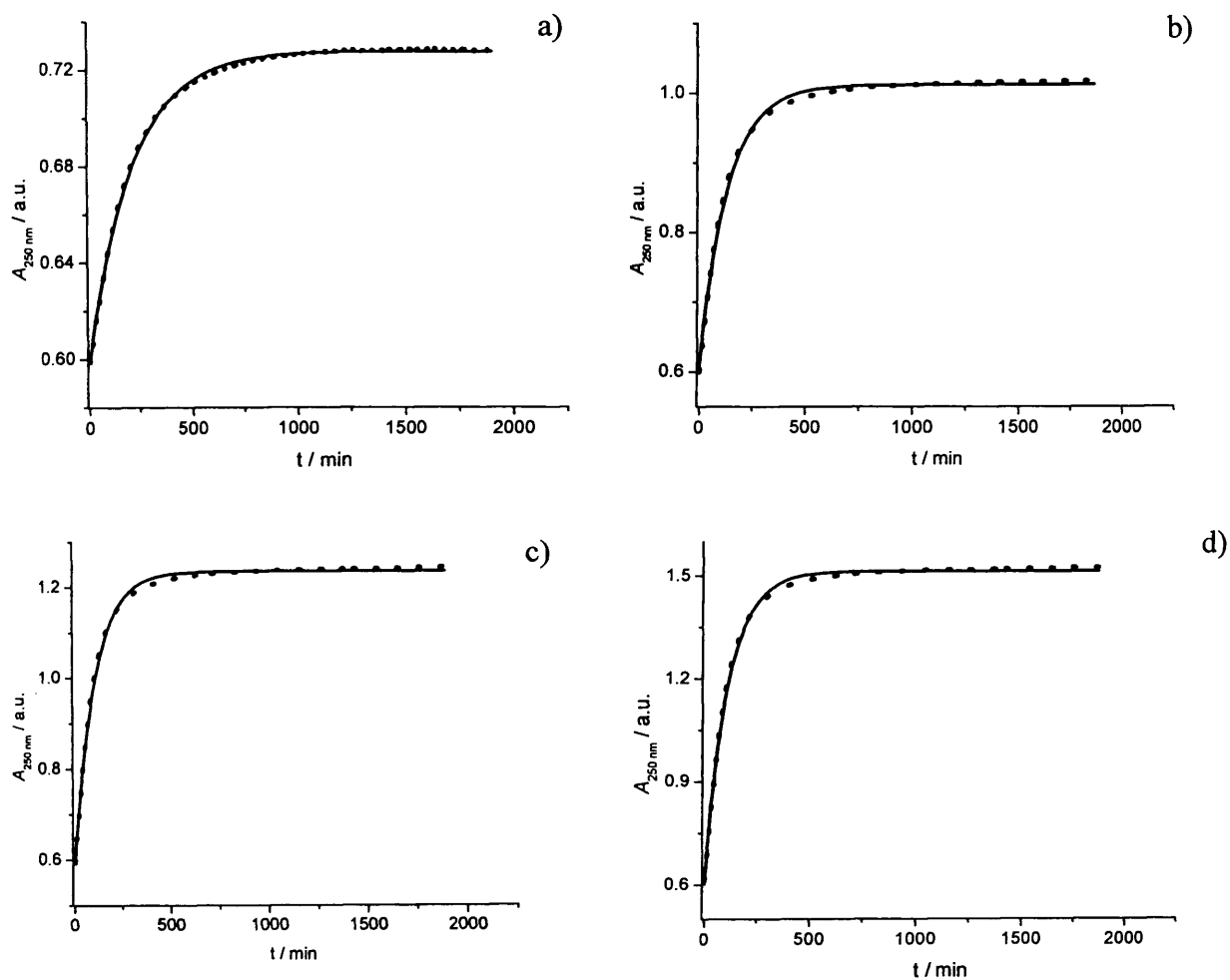
Figure S3.10. Absorbance at 250 nm versus time for the reaction mixture of a) 0.025 mM PBA, b) 0.05 mM PBA, c) 0.1 mM PBA and d) 0.15 mM PBA using 100 μL Pd-pNIPAM (-ve) Ncomp, in 10.0 mM CTAB, and 10 mM borate buffer at pH 8.8 and 30 °C. (dotted line) experimental data and fit to eq 2.1 (solid line).

A3.11. Kinetic traces of the reaction mixture of PBA using different concentration of Pd_pNIPAM (-ve) Ncomp catalyst.
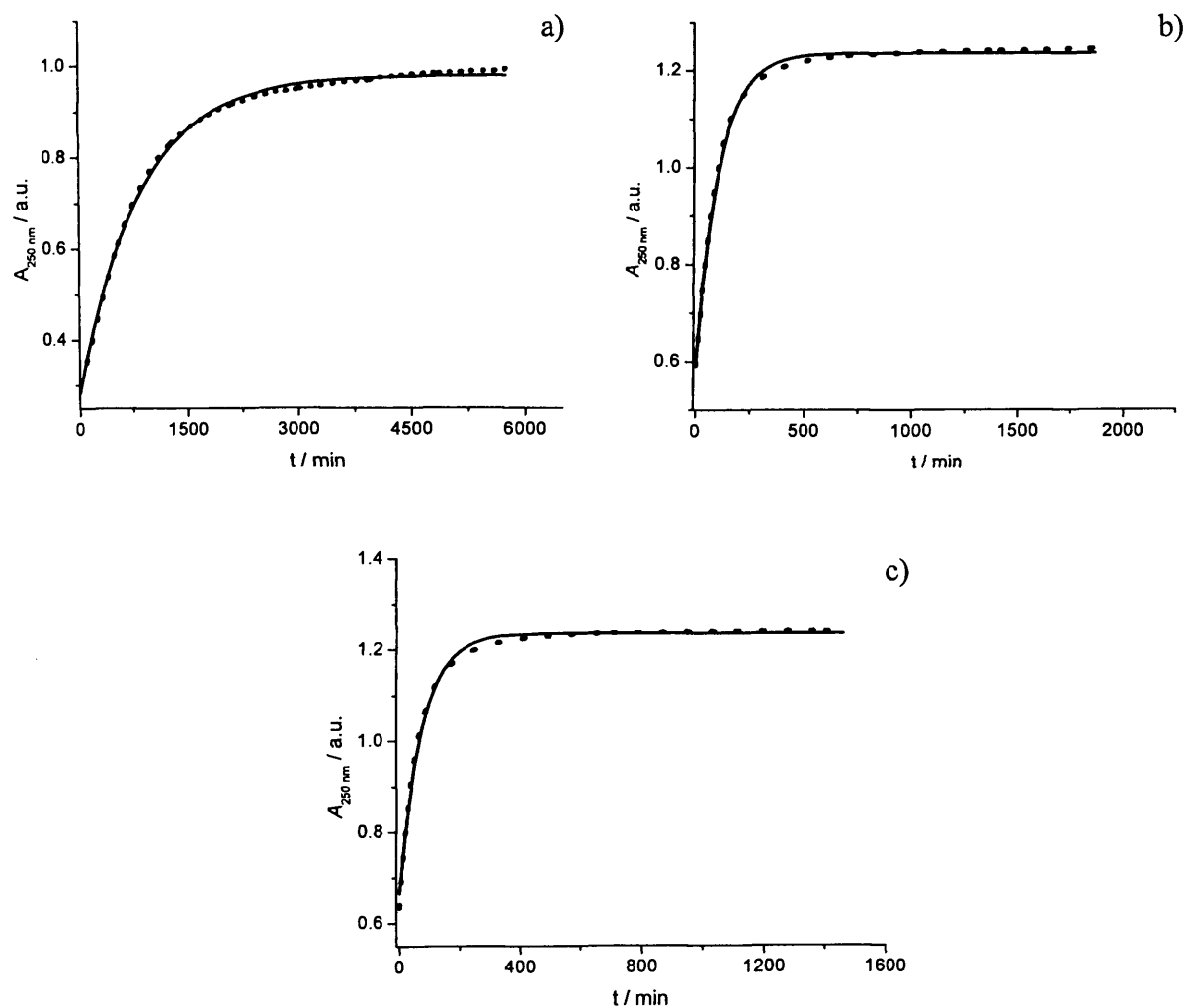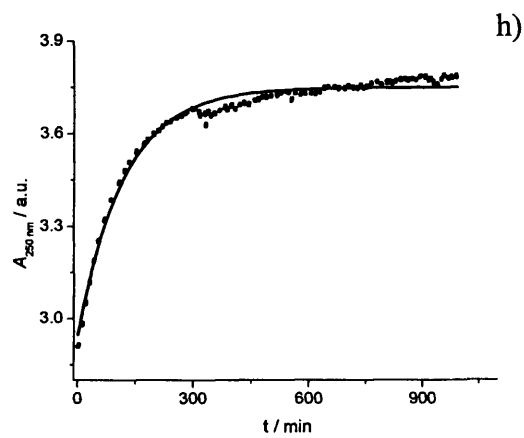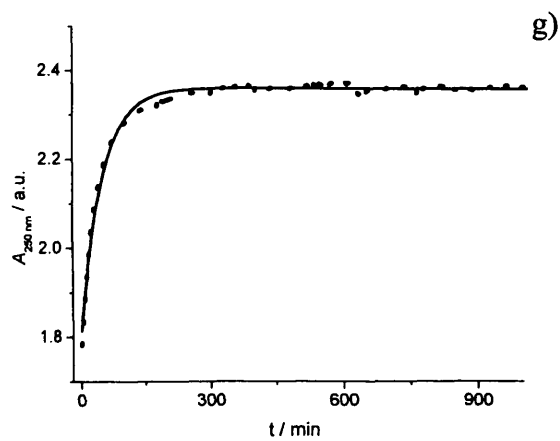

Figure S3.11. Absorbance at 250 nm versus time for the reaction mixture of 0.01 mM PBA a) 30 μL, b) 100 μL, and c) 200 μL Pd-pNIPAM (-ve) Ncomp, in 10.0 mM CTAB, and 10 mM borate buffer at pH 8.8 and 30 °C. (dotted line) experimental data and fit to eq 2.1 (solid line).

A3.12. Absorbance at 250 nm of the reaction mixture of the homocoupling of PBA using Au-Pd-pNIPAM (-ve) and (+ve) Ncomp in CTAB and borate buffer at pH 8.4 and 8.8 respectively, and at different temperature.
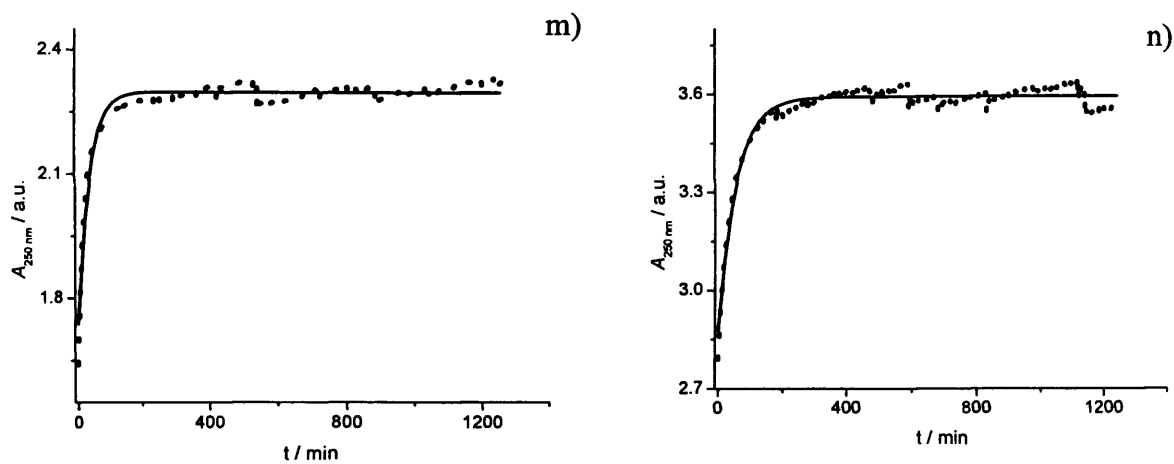
237
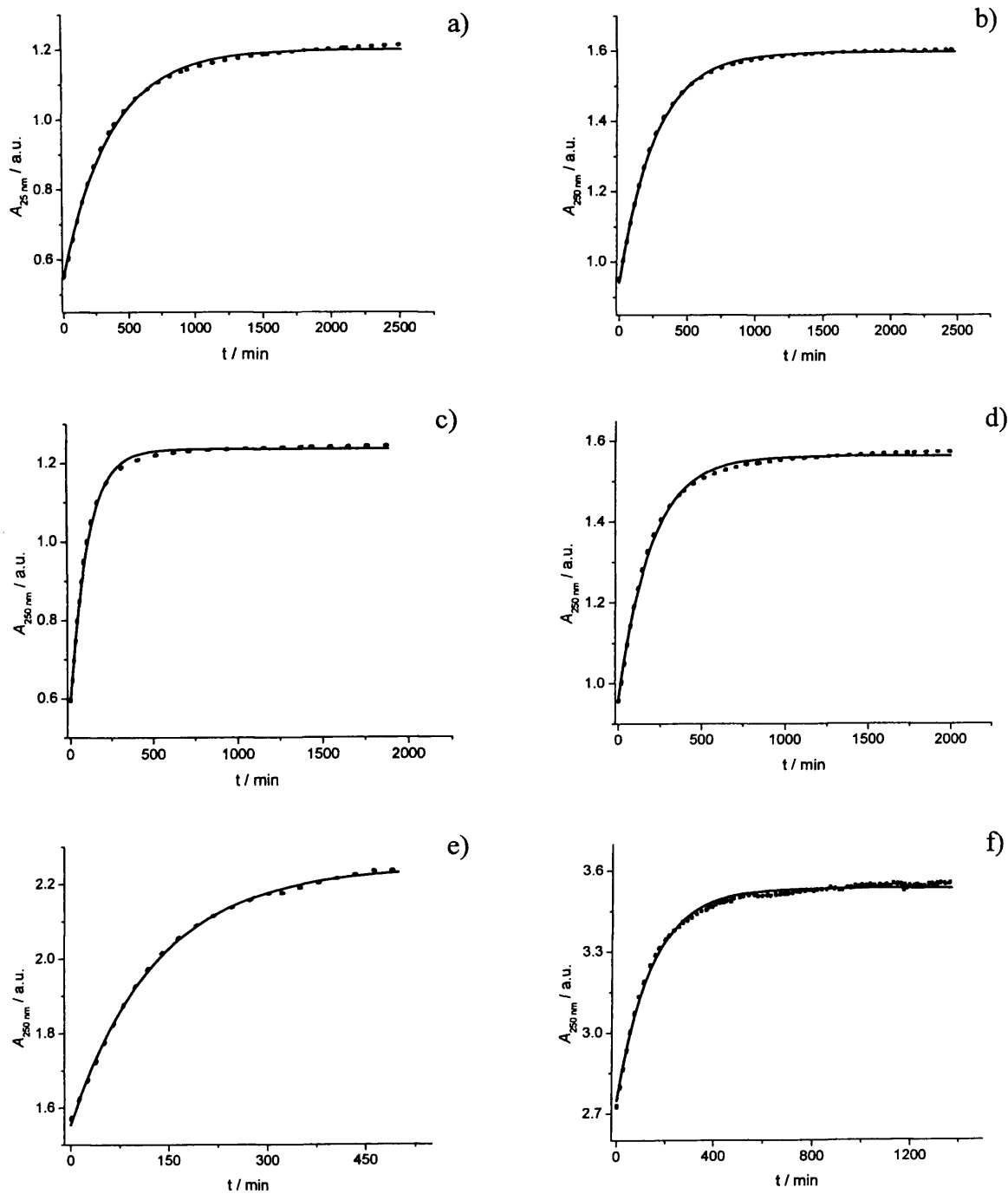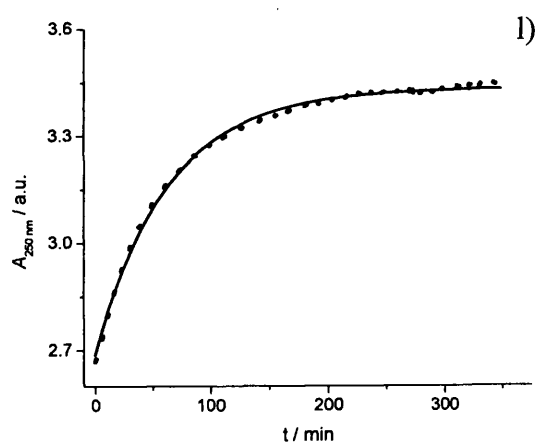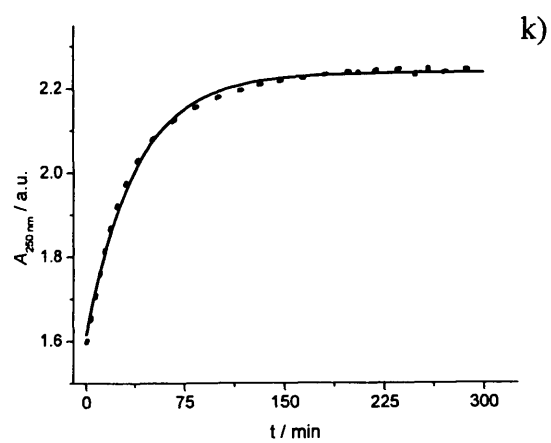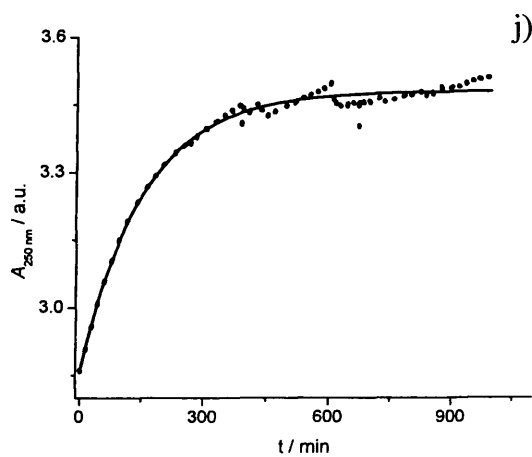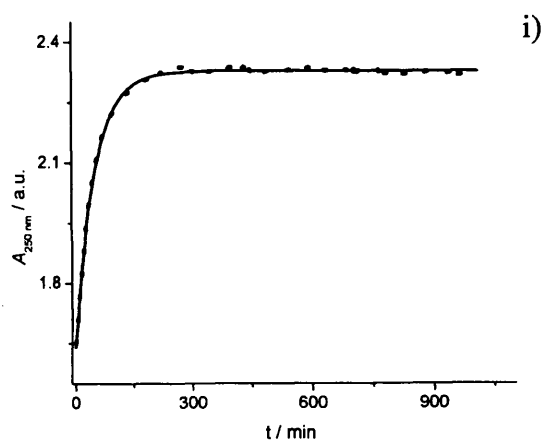
Figure S3.12. Absorbance at 250 nm versus time for the reaction mixture 0.1 mM PBA using 100 µL of Pd-pNIPAM nanocomposites (-ve or +ve), 10.0 mM CTAB, and 10 mM borate buffer pH 8.4 (+ve) and 8.8 (-ve), at; a) 25 °C (-ve), b) 25 °C (+ve), c) 30 °C (-ve), d) 30 °C (+ve), e) 40 °C (-ve), f) 40 °C (+ve), g) 50 °C (-ve), h) 50 °C (+ve), i) 50 °C (-ve), j) 50 °C (+ve), k) 55 °C (-ve), l) 55 °C (+ve), m) 60 °C (-ve), and n) 60 °C (+ve). (dotted line) experimental data and fit to eq 2.1 (solid line).

238